AD-A241 243

SC5498.FR

Copy No. 4

THEORETICAL AND EXPERIMENTAL INVESTIGATION OF HETEROJUNCTION INTERFACES

FINAL REPORT FOR THE PERIOD
December 1, 1984 through December 31, 1990

CONTRACT NO. N00014-85-C-0135

Prepared for

Office of Naval Research
800 N. Quincy Street
Arlington, VA 22217

E. Kraut
Principal Investigator

DTIC
ELECTE
OCT 0 3 1991
S B D

FEBRUARY 1991

Approved for public release; distribution unlimited

91-12263

Rockwell International
Science Center

91 10 3 003

DISCLAIMER NOTICE

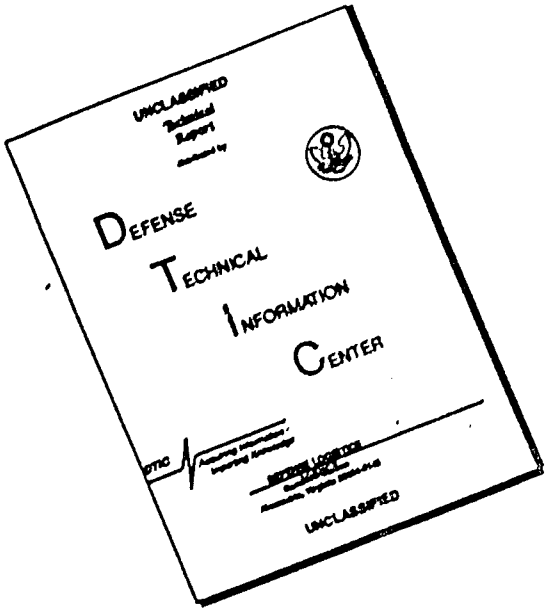

THIS DOCUMENT IS BEST QUALITY AVAILABLE. THE COPY FURNISHED TO DTIC CONTAINED A SIGNIFICANT NUMBER OF PAGES WHICH DO NOT REPRODUCE LEGIBLY.

UNCLASSIFIED

SECURITY CLASSIFICATION OF THIS PAGE

REPORT DOCUMENTATION PAGE

FORM APPROVED
OMB No. 0704-0188

1a. REPORT SECURITY CLASSIFICATION
UNCLASSIFIED

1b. RESTRICTIVE MARKINGS

2a. SECURITY CLASSIFICATION AUTHORITY

3. DISTRIBUTION/AVAILABILITY OF REPORT
Approved for public release, Distribution Unlimited

2b. CLASSIFICATION/DOWNGRADING SCHEDULE

4. PERFORMING ORGANIZATION REPORT NUMBER(S)
SC5498.FR

5. MONITORING ORGANIZATION REPORT NUMBER(S)

6a. NAME OF PERFORMING ORGANIZATION
ROCKWELL INTERNATIONAL
Science Center

6b. OFFICE SYMBOL (If Applicable)

7a. NAME OF MONITORING ORGANIZATION

6c. ADDRESS (City, State and ZIP Code)
1049 Camino Dos Rios
Thousand Oaks , CA 91360

7b. ADDRESS (City, State and ZIP Code)

8a. NAME OF FUNDING/SPONSORING ORGANIZATION
Scientific Officer
Office of Naval Research

8b. OFFICE SYMBOL (If Applicable)

9. PROCUREMENT INSTRUMENT IDENTIFICATION NUMBER
N0O014-85-C-0135

8C. ADDRESS (City, State and ZIP Code)
800 North Quincy St.
Arlington, VA 22217-5000

10. SOURCE OF FUNDING NOS.

PROGRAM ELEMENT NO.	PROJECT NO.	TASK NO.	WORK UNIT ACCESSION NO.

11. TITLE (Include Security Classification)
THEORETICAL AND EXPERIMENTAL INVESTIGATION OF HETEROJUNCTION INTERFACES

12. PERSONAL AUTHOR(S)
Kraut, E.A., Grant, R.W., and Waldrop, J.R.

13a. TYPE OF REPORT	13b. TIME COVERED	14. DATE OF REPORT (Year, Month, Day)	15. PAGE COUNT
FINAL REPORT	FROM 12/01/84 TO 12/31/90	1991, FEBRUARY	

16. SUPPLEMENTARY NOTATION

17. COSATI CODES			18. SUBJECT TERMS (Continue on reverse if necessary and identify by block number)
FIELD	GROUP	SUB-GROUP	
20	12		*heterojunction band discontinuities, SiC Schottky Barriers, semiconductor interfaces, interface dipole layers*
09	01		

19. ABSTRACT (Continue on reverse if necessary and identify by block number)

Heterojunction band discontinuities were investigated by the x-ray photoemission spectroscopy (XPS) technique. Interface dipole formation and dipole effects on band offsets were studied both theoretically and experimentally. Tight binding calculations of atom interchange across interfaces between dissimilar semiconductors suggest that interfaces will tend to reconstruct in a manner that minimizes the number of polar bonds. The effect of interface geometry on dipoles at the Ge/GaAs interface was shown to predict a relative ordering of crystallographic dipole shifts in agreement with experiment. A model was developed to explain why incorporation of an Al monolayer at the Ge/GaAs(100) interface does not change the band discontinuity. A scaling relationship was observed for the (110) heterojunctions Ge/GaAs, GaAs/ZnSe and Ge/ZnSe which is consistent with the idea that (110) band offsets for these materials are determined by bulk properties.

20. DISTRIBUTION/AVAILABILITY OF ABSTRACT
UNCLASSIFIED/UNLIMITED ☐ SAME AS RPT. ☒ DTIC USERS ☐

21. ABSTRACT SECURITY CLASSIFICATION
UNCLASSIFIED

22a. NAME OF RESPONSIBLE INDIVIDUAL
Dr. L.R. Cooper

22b. TELEPHONE NUMBER (INCLUDE AREA CODE)
703-696-4214

22c. OFFICE SYMBOL
Code 414

DD FORM 1473 Previous editions are obsolete.

UNCLASSIFIED

SECURITY CLASSIFICATION OF THIS PAGE

19. ABSTRACT (continued)

The valance band discontinuity (ΔE_v) for both (110) and (100) GaAs/Ge heterojunctions was observed to decrease with time (~ 100 hrs) at room temperature by more than 0.2 eV relative to the stable Ge/GaAs (110) interface. Annealing and As overpressure control could cycle the interface dipole which may be associated with antiphase disorder at the GaAs/Ge interface. Dipoles were observed at the AlAs/GaAs interface where they can alter ΔE_v by ~ 0.1 eV, depending on growth sequence and crystallographic orientation. Band discontinuities were determined for (100) InP lattice matched heterojunctions and are: ΔE_v ($InP/In_{0.52}Al_{0.48}As$) = 0.16 eV, ΔE_v ($InP/In_{0.53}Ga_{0.47}As$) = 0.34 eV, and ΔE_v ($In_{0.53}Ga_{0.47}As/In_{0.52}Al_{0.48}As$) = 0.22 eV.

Values of ΔE_v characteristic of unstrained lattice mismatched systems were determined to be: ΔE_v(AlAs/InP) = -0.27 eV, ΔE_v(InAs/InP) = 0.46 eV, and ΔE_v(GaAs/InP) = 0.34 eV. Relative core level deformation potentials were measured in strained Ge and GaAs. The comparison of these deformation potentials with theoretical calculations suggests caution when deriving ΔE_v by combining calculated deformation potentials with XPS data on strained layer heterojunctions.

The formation of Schottky barriers to well characterized n-type β-SiC(100) epitaxial layer (on Si(100)) surfaces in ultrahigh vacuum was investigated for several metals. Interface chemistry and Schottky barrier height were determined by XPS, current-voltage and capacitance-voltage methods. A wide range of barrier heights was observed and found to depend on metal work function in general accord with the Schottky-Mott limit.

DTIC
COPY
INSPECTED
4

Accession For
NTIS GRA&I ☑
DTIC TAB ☐
Unannounced ☐
Justification
By
Distribution/
Availability Codes
Dist | Avail and/or Special
A-1

1.0 INTRODUCTION

This is the final report for Contract No. N00014-85-C-0135 entitled "Theoretical and Experimental Investigation of Heterojunction Interfaces", covering the performance period December 1, 1984 to December 31, 1990.

Heterojunction energy-band discontinuities afford the device designer additional control over electron and hole transport near p-n junctions. Heterojunctions have been employed to realize new types of solid-state electron devices with properties not available from homojunction based technology. Central to the effective design and development of heterojunction devices is an accurate knowledge of how the bandgap discontinuity ΔE_g between adjoining semiconductors is distributed between the valence and conduction band offsets ΔE_v and ΔE_c subject to the requirement that $\Delta E_g = \Delta E_v + \Delta E_c$. We have developed an experimental technique, based on the use of x-ray photoelectron spectroscopy (XPS), that enables us to measure band offsets to a precision of ±0.04 eV and to measure changes in band offsets to a precision of ±0.01 eV. With the aid of this powerful experimental approach, we have been able to uncover much new heterojunction physics including crystallographic orientation dependence of band offsets, growth sequence variation, nontransitivity and time dependent shifts in band offsets. From these new data, an improved theoretical understanding of heterojunction band offsets has emerged, one in which there can be both bulk and interface specific contributions to band offsets so that $\Delta E_v = (\Delta E_v)_{bulk} + (\Delta E_v)_{interface}$. The interface specific contributions are modeled in terms of interface dipoles which shift the band offsets away from values determined purely by bulk semiconductor properties.

A major portion of the effort during the performance period reported herein, has been devoted to experimentally and theoretically characterizing interface dipole formation and dipole effects on band offsets to contribute to the improved understanding of real heterojunctions that technology advancement requires.

We have also used our XPS technique to measure band offsets in several technologically important heterojunction systems.

The accomplishments of this research program were reported in 16 publications.[1-16] Section 2.0 of this final report briefly summarizes the primary program accomplishments. The Appendix (Sect. 3.0) reproduces the publications supported by this contract.

2.0 SUMMARY OF ACCOMPLISHMENTS

Early in this program, we recognized that dipoles which can strongly affect heterojunction band offsets could be formed at polar heterojunction interfaces and that such dipoles might be eliminated by reconstructions involving atom interchanges across heterojunction interfaces. Clearly, the energetics of such atom interchanges affects the likelihood of their occurrence. To model the energetics of atom interchange across interfaces between dissimilar semiconductors, a theoretical tight-binding study was performed in collaboration with Professor Walter Harrison of Stanford University. This work[2,9] showed that the energy required to substitute a homovalent atom for a native atom in a semiconductor is primarily elastic misfit energy and is much smaller than the corresponding heterovalent atom exchange energy which is dominated by a redistribution of bond polarity. These calculations suggest that interfaces will tend to reconstruct so as to minimize the number of polar bonds at a heterojunction interface. This can in turn contribute to determining the resultant interface dipole and band offset.

The Ge/GaAs heterojunction ΔE_v is observed experimentally to depend on crystallographic orientation. The effect of interface geometry on interface dipoles was explored theoretically.[10] Interbond interactions yield different energies for geometries with unequal interface dipoles. A statistical average of interface cells at the Ge/GaAs growth temperature predicts a relative ordering of crystallographic orientation dipole shifts in agreement with experiment.[10]

A question of interest in heterojunction physics is the possibility of tailoring band offsets by artificially inserting a dipole layer at a heterojunction interface. By starting from a model of a three-layer Ge/Si/Ge polar heterojunction, we were able to explain why the incorporation of a monolayer of aluminum at the Ge/GaAs(100) interface does not change the measured band offset.[3]

Interface dipoles are most readily associated with polar heterojunction interfaces. For some nonpolar (110) interfaces, it may be possible that heterojunction band offsets are completely determined by bulk properties of the constituent semiconductors. A currently popular theoretical model establishes a universal charge neutrality level determined by the bulk band structure of each semiconductor; these

charge neutrality levels line up when a heterojunction is formed. One consequence of the existence of a charge neutrality level is that the band offsets for a family of heterojunctions such as those formed from Ge, GaAs, and ZnSe should scale with energy bandgap difference. Using our experimental data for Ge/GaAs(110), GaAs/ZnSe(110), and Ge/ZnSe(110) we showed that $\Delta E_v/\Delta E_g = 3/4$ within experimental error, consistent with the idea that for (110) heterojunctions, bulk properties determine the band offsets in the Ge, GaAs, ZnSe system.[7]

A major strength of the XPS technique for determining band discontinuities is the ability to measure changes in band discontinuities with very high precision and thus to detect the presence of interface dipoles.[8] With this technique, time variations in interface dipoles were observed at GaAs/Ge heterojunctions for both (110) and (100) crystallographic orientations.[1,4,5] At room temperature, the ΔE_v decreases for $\approx$100 hr after interface formation to a value > 0.2 eV lower than the ~ 0.56 eV value for the stable Ge/GaAs (110) interface. Annealing and control of As overpressure can be used to cycle the interface dipole by more than 0.2 eV. The dipole formation mechanism may require the presence of antiphase disorder that is expected at the GaAs/Ge interface. Interface dipoles have also been observed at the AlAs-GaAs interface where they can alter ΔE_v by ~ 0.1 eV, depending on growth sequence and crystallographic orientation.[6] This observation suggests an inherent asymmetry in potential wells associated with AlAs-GaAs quantum well and superlattice structures.

Heterojunction devices that employ the lattice-matched semiconductors InP, $In_{0.53}Ga_{0.47}As$ and $In_{0.52}Al_{0.48}As$ are of high current interest for a wide variety of optoelectronic and high-speed electronic applications. A knowledge of the band discontinuities in this system is important to understanding the operation of the devices. The XPS technique was used to determine $\Delta E_v(InP/In_{0.52}Al_{0.48}As) = 0.16$ eV, $\Delta E_v(InP/In_{0.53}Ga_{0.47}As) = 0.34$ eV and $\Delta E_v(In_{0.53}Ga_{0.47}As/In_{0.52}Al_{0.48}As) = 0.22$ eV for the (100) interfaces.[14,16] Core level binding energy difference measurements showed that band offset transitivity in this system was satisfied to within experimental uncertainty (±0.04 eV) and therefore interfaces formed between these semiconductors are not influenced by interface specific effects.

In conjunction with the investigation of InP lattice-matched semiconductors, values of ΔE_V for pseudomorphic InAs/InP, GaAs/InP and AlAs/InP were determined,[11,12,14,16] With the assumption that ΔE_{CL} (the difference in core level binding energies) is independent of strain at a pseudomorphic interface, ΔE_V values characteristic of the unstrained interfaces were derived and are ΔE_V(AlAs/InP) = -0.27 eV, ΔE_V(InAs/InP) = 0.46 eV and ΔE_V(GaAs/InP) = 0.34 eV. Strain has two components, a hydrostatic strain associated with volume change and a shear strain associated with tetragonal distortion of the overlayer. The effect of these strains on ΔE_V at the pseudomorphic interface has been estimated from deformation potentials.

The use of pseudomorphic semiconductor layers in device structures is very attractive because an important new parameter (strain) is available to alter material electronic properties. The extension of XPS methods to measure band discontinuities at pseudomorphic heterojunction interfaces is a nontrivial task. One approach reported in the literature involves the calculation of core level deformation potentials by using a self-consistent linear combination of muffin-tin orbitals method and the local density functional approximation. The results of this calculation suggests that core levels may have different hydrostatic deformation potentials that depend on orbital character and binding energy. We performed measurements to determine 3d, 3p and 3s intra-atomic relative core level binding energy deformation potentials in strained Ge and As3d-Ga3d interatomic relative core level binding energy deformation potentials in strained GaAs.[13] For the intra-atomic deformation potentials, no measurable core level shifts with strain were observed consistent with theoretical core term value calculations. However, for the interatomic deformation potentials, comparison between calculation and experiment was not good. This discrepancy needs to be resolved and alternative approaches need to be explored before XPS methods can be reliably applied to measure band discontinuities at pseudomorphic strained heterojunction interfaces.

During the course of this contract, the scope of work was expanded to include studies of SiC Schottky barriers. This resulted in part from the recent availability of large area epitaxial β-SiC films grown on Si(100) and the associated device development acitivities. The formation of Schottky barrier contacts to well-characterized n-type β-SiC(100) surfaces in ultrahigh vacuum was systematically investigated for several

metals.[15] The metals were deposited onto oxygen terminated (~ 1 monolayer) surfaces. Interface chemistry and Schottky barrier height during contact formation were obtained by XPS; the corresponding electrical properties of thick contacts were characterized by capacitance-voltage and current-voltage methods. The metal contacts exhibited a wide range (0.95 to 0.16 eV) of barrier heights; within this range, the barrier heights were observed to depend strongly on the metal work function in general accord with the Schottky-Mott limit.

3.0 APPENDIX

This Appendix reproduces publications supported by Contract No. N00014-85-C-0135 in chronological order. These publications (which are referenced in this final report) are:

1. "Heterojunction Band Discontinuity Growth Sequence Variation at Compound Semiconductor-Germanium (110) Interfaces: Possible Role of Antiphase Disorder," R.W. Grant, J.R. Waldrop, S.P. Kowalczyk and E.A. Kraut, J. Vac. Sci. Technol. B 3, 1295 (1985).

2. "Lattice Distortions and Energies of Atomic Substitution," E.A. Kraut and W.A. Harrison, J. Vac. Sci. Technol. B 3, 1267 (1985).

3. "Polar Heterojunction Interfaces: Isovalent Interlayers," E.A. Kraut, Phys. Rev. B 31, 6875 (1985).

4. "Heterojunction Band Discontinuities for GaAs Grown on Ge(110): Time Variation," R.W. Grant, J.R. Waldrop, S.P. Kowalczyk and E.A. Kraut, Surface Sci. 168, 498 (1986).

5. "GaAs-Ge Heterojunction Interfaces: Cyclical Behavior of Band Discontinuities," J.R. Waldrop, R.W. Grant, and E.A. Kraut, J. Vac. Sci. Tecnol. B 4, 1060 (1986).

6. "Effect of Growth Sequence on the Band Discontinuities at AlAs/GaAs(100) and (110) Heterojunction Interfaces," J.R. Waldrop, R.W. Grant and E.A. Kraut, J. Vac. Sci. Technol. B 5, 1209 (1987).

7. "Heterojunction Band Offsets and Scaling," E.A. Kraut, J. Vac. Sci. Technol. B 5, 1246 (1987).

8. "Interface Contributions to Heterojunction Band Discontinuities: X-Ray Photoemission Spectroscopy Investigations," R.W. Grant, E.A. Kraut, J.R. Waldrop and S.P. Kowalczyk, in Heterojunction Band Discontinuities: Physics and Device Applications, pp. 167 (North-Holland, Amsterdam, 1987), edited by F. Capasso and G. Margaritondo.

9. "Energies of Substitution and Solution in Semiconductors," W.A. Harrison and E.A. Kraut, Phys. Rev. B 37, 8244 (1988).

10. "Dipoles at Polar Heterojunction Interfaces," R.W. Grant and W.A. Harrison, J. Vac. Sci. Technol. B 6, 1295 (1988).

11. "GaAs/InP and InAs/InP Heterojunction Band Offsets Measured by X-Ray Photoemission Spectroscopy," J.R. Waldrop, R.W. Grant and E.A. Kraut, J. Vac. Sci. Technol. B 7, 815 (1989).

12. "Measurement of GaAs/InP and InAs/InP Heterojunction Band Offsets by X-Ray Photoemission Spectroscopy," J.R. Waldrop, R.W. Grant and E.A. Kraut, Appl. Phys. Lett. 54, 1878 (1989).

13. "Relative Core Level Deformation Potentials in Strained Layer Heterojunctions," R.W. Grant, J.R. Waldrop, E.A. Kraut, and W.A. Harrison, J. Vac. Sci. Technol. B 8, 736 (1990).

14. "Measurement of AlAs/InP and InP/$In_{0.52}Al_{0.48}As$ Heterojunction Band Offsets by X-Ray Photoemission Spectroscopy," J.R. Waldrop, E.A. Kraut, C.W. Farley and R.W. Grant, J. Vac. Sci. Technol. B 8, 768 (1990).

15. "Formation and Schottky Barrier Height of Metal Contacts to β-SiC," J.R. Waldrop and R.W. Grant, Appl. Phys. Lett. 56, 557 (1990).

16. "Measurement of InP/$In_{0.53}Ga_{0.47}As$ and $In_{0.53}Ga_{0.47}As/In_{0.52}Al_{0.48}As$ Heterojunction Band Offsets by X-Ray Photoemission Spectroscopy," J.R. Waldrop, E.A. Kraut, C.W. Farley and R.W. Grant, J. Appl. Phys. 69, 372 (1991).

Heterojunction band discontinuity growth sequence variation at compound semiconductor-germanium (110) interfaces: Possible role of antiphase disorder

R. W. Grant, J. R. Waldrop, S. P. Kowalczyk, and E. A. Kraut
Rockwell International Corporation, Microelectronics Research and Development Center, Thousand Oaks, California 91360

(Received 4 April 1985; accepted 15 April 1985)

The valence-band discontinuity (ΔE_v) at heterojunctions formed by growing GaAs epitaxially on Ge(110) substrates has been studied by using x-ray photoelectron spectroscopy. The GaAs grown on Ge (110) interface is observed to exhibit a time dependent variation in ΔE_v that is as much as $\sim$0.2 eV. For GaAs/Ge(110) heterojunctions grown at 350 °C and kept at room temperature for $>$ 100 h, $\Delta E_v \sim 0.3$ eV; this is $\sim$0.25 eV less than the ΔE_v measured for the stable interface formed by growing Ge epitaxially on GaAs (110). It is observed that ΔE_v for growth of a lattice matched compound semiconductor (AB) on Ge(110) is substantially smaller than for the reverse growth sequence, i.e., ΔE_v [AB/Ge(110)] $< \Delta E_v$[Ge/AB(110)]. A possible mechanism for this growth sequence effect which involves antiphase disorder at AB/Ge(110) interfaces is suggested.

I. INTRODUCTION

The development of photoemission techniques for measuring heterojunction band discontinuities has substantially improved the ability to determine these quantities with accuracy. Measurements which utilize photoemission techniques have established that heterojunction band discontinuities are markedly influenced by microscopic details of interface structure.[1,2] The nature of the microscopic effects is uncertain; indeed, the most utilized predictive theories[3–5] of heterojunction band alignment do not account for variations due to microscopic structure. Heterojunction formation between compound and elemental semiconductors on polar surfaces is influenced by atomic exchange across the interface to satisfy electrostatic considerations[6]; thus, technology dependent interface dipoles are expected to influence band discontinuities measured on polar interfaces.[7,8] However, a growth sequence dependence of the valence-band discontinuity (ΔE_v) for nonpolar (110) Ge–ZnSe and Ge–GaAs heterojunctions that has been observed,[9,10] also may be caused by microscopic interface structural effects. In this paper, systematics of the ΔE_v growth sequence dependence for compound semiconductor-germanium (110) interfaces are reviewed; a possible explanation for this growth sequence phenomenon which involves the role of antiphase domain disorder at interfaces is offered, and new data for the GaAs epitaxially grown on Ge(110) interface are presented. These data report a previously unobserved time dependence of ΔE_v that is attributed to interface instability.

II. SYSTEMATICS OF ΔE_v GROWTH SEQUENCE VARIATION FOR AB–Ge(110) INTERFACES

A growth sequence variation of ΔE_v for a compound semiconductor (AB)–Ge(110) interface was first reported for the ZnSe–Ge semiconductor pair.[9] It was observed that ΔE_v for Ge grown epitaxially on ZnSe(Ge/ZnSe) was 1.52 ± 0.04 eV, while ΔE_v for ZnSe grown epitaxially on Ge (ZnSe/Ge) was 1.29 ± 0.04 eV. A similar growth sequence variation for the GaAs–Ge(110) interface has been reported[10] where ΔE_v(Ge/GaAs) $> \Delta E_v$(GaAs/Ge) by about 0.2 eV; this result is confirmed by independent measurements reported in Sec. IV.

A third AB–Ge(110) interface for which a growth sequence can be inferred involves the CuBr–Ge semiconductor pair. As a test for the transitive nature of heterojunction band discontinuities, it was found[2,11] that the difference between $\{\Delta E_v$[Ge/GaAs(110)] + ΔE_v[CuBr/GaAs(110)]$\}$ and ΔE_v[CuBr/Ge(110)] was $+0.70 \pm 0.05$ eV rather than the zero difference implied by transitivity. It has been suggested that antiphase domain disorder may affect the magnitude of ΔE_v at the CuBr–Ge(110) interface[12] and thus account for this reported[2,11] nontransitive ΔE_v result. This view is supported by recent results[11] for transitivity test sequences of heterojunctions specifically chosen to avoid antiphase domain disorder (further discussion of this point is given in Sec. III). Unfortunately, it is not possible to prepare the Ge/CuBr(110) interface due to a strong chemical reaction which occurs between Ge and a CuBr substrate[11] [this reaction does not occur at the abrupt CuBr/Ge(110) interface]. If the large nontransitive ΔE_v result mentioned above is assumed to be associated primarily with the CuBr/Ge(110) interface, it follows that ΔE_v[CuBr/Ge(110)] is less than ΔE_v[Ge/CuBr(110)].

It is thus observed that ΔE_v[AB/Ge(110)] is systematically smaller than ΔE_v[Ge/AB(110)] for AB = GaAs, ZnSe, and CuBr. These three interfaces involve band alignments in which the band gap of Ge is completely contained within the AB semiconductor band gap. The systematic variation of this growth sequence effect suggests that a similar mechanism may be involved in each case. A possible mechanism is offered in the next section.

III. POSSIBLE EFFECT OF ANTIPHASE DISORDER ON ΔE_v

As pointed out in Sec. II, an apparently general experimental result is that ΔE_v for growth of a lattice matched compound semiconductor on Ge(110) is smaller than for the

 0734-211X/85/041295-05$01.00 © 1985 American Vacuum Society

opposite growth sequence. Recent studies[11] of ΔE_v transitivity have observed that $\{\Delta E_v[\text{Ge/GaAs(110)}] + \Delta E_v[\text{ZnSe/GaAs(110)}]\} - \{\Delta E_v[\text{Ge/ZnSe(110)}]\} = -0.03 \pm 0.03$ eV and $\{\Delta E_v[\text{Ge/GaAs(110)}] + \Delta E_v[\text{GaAs/AlAs(110)}]\} - \{\Delta E_v[\text{Ge/AlAs(110)}]\} = +0.07 \pm 0.1$ eV; i.e., ΔE_v appears to be transitive in these two cases because the differences are approximately zero. A common feature of the heterojunctions used in these two transitivity tests is the absence of AB/Ge(110) interfaces. It appears, therefore, that the growth sequence effect and deviations from transitivity may be associated with an AB/Ge(110) interface dipole. The relative magnitude of the growth sequence effect {i.e., $\Delta E_v[\text{AB/Ge(110)}] < \Delta E_v[\text{Ge/AB(110)}]$} can be used to infer that at an AB/Ge(110) interface, positive charge is transferred into the Ge and negative charge into the AB overlayer.

The growth of a compound semiconductor on Ge(110) involves an ambiguity in nucleation site which may produce antiphase domain disorder; Kroemer[7,8,13] has emphasized the importance of solving this site allocation problem for producing device quality heterojunctions from compound on elemental semiconductor growth. Antiphase domains have been directly observed at the GaAs/Ge(100) interface.[14] The presence of antiphase domain disorder at an interface would not affect the observed ΔE_v *per se* unless this disorder causes charge transfer across the interface to create an interface dipole. Atom transfer across a heterojunction interface, which involves atoms from different columns of the periodic table, has been shown to produce large interface dipoles.[6,8] If the AB–Ge(110) growth sequence effect in ΔE_v is caused by this atom transfer, the electrostatic model of heterojunction interfaces[6] can be used to infer that anions (i.e., As, Se, and Br) rather than cations preferentially interchange with Ge at a compound semiconductor/Ge(110) interface.

A large number of possible antiphase domain walls can be imagined. However, the crystallographic planes associated with these domain walls may be characterized by whether one, two, or three A–A (or B–B) bonds per atom exist at the domain boundary. If attention is restricted to only those cases where the A–A (or B–B) bonds involve atoms in the A–B plane, which is immediately adjacent to the last Ge plane, only three nearest-neighbor, bonding arrangements are possible for the abrupt interface. These possibilities are shown in Fig. 1 and are listed in Table I.

The energetics of atomic exchange across an interface are associated primarily with bonds formed or broken during the exchange. For example, exchange of a Ge atom in bulk Ge with an As atom in bulk GaAs would require that 4 Ge–Ge and 4 Ga–As bonds be broken and that 4 Ge–As and 4 Ga–Ge bonds be formed. Kraut and Harrison[15,16] have calculated energies of atomic substitution by tight binding theory and have shown that atomic exchange at an ideal AB/Ge interface is not favored. A bond formation energy $E_b = 2(V_2^2 + V_3^2)^{1/2}$ is associated with each bond where V_2 is a covalent energy which depends on bond length and thus is a constant (4.12 eV) for all bonds considered here. The polar energy V_3 is $(\epsilon_{h\,A} - \epsilon_{h\,B})/2$, where values of the hybrid energies (ϵ_h) are tabulated in Ref. 17. Interchange of atoms across the interface changes the V_3's and therefore the total energy. It is this change which makes atomic exchange at an ideal AB/Ge interface unfavorable. However, at an antiphase domain boundary there are bonds between like atoms; these atoms may favor exchange.

To investigate the possible exchange of atoms at the intersection of an antiphase domain boundary with a Ge(110) plane, the above expression for E_b was used to calculate the sum of the bond formation energies associated with both the abrupt and the interchanged domain boundary bonding arrangements listed in Table I. Cation (A) antiphase domain boundary bonding arrangements (instead of the anion domain boundaries shown) are simply obtained by interchanging A and B everywhere in Table I. The result of this simple calculation shows that a bonding arrangement which involves only *one* B–B(or A–A) bond is *stable* with respect to B⇄Ge (or A⇄Ge) exchange, while interfaces which involve *two* or *three* B–B (or A–A) bonds *favor* the exchange indicated by arrows in Fig. 1. As an example, the sum of the bond formation energies for the 2 B–B and 2 A–A bonding arrangements is shown in Table II. The results indicate that bond energy will be gained by interchanging Ge with either anions or cations for this bonding arrangement.

The above calculation thus suggests that atomic exchange across the AB/Ge(110) interface at an antiphase domain

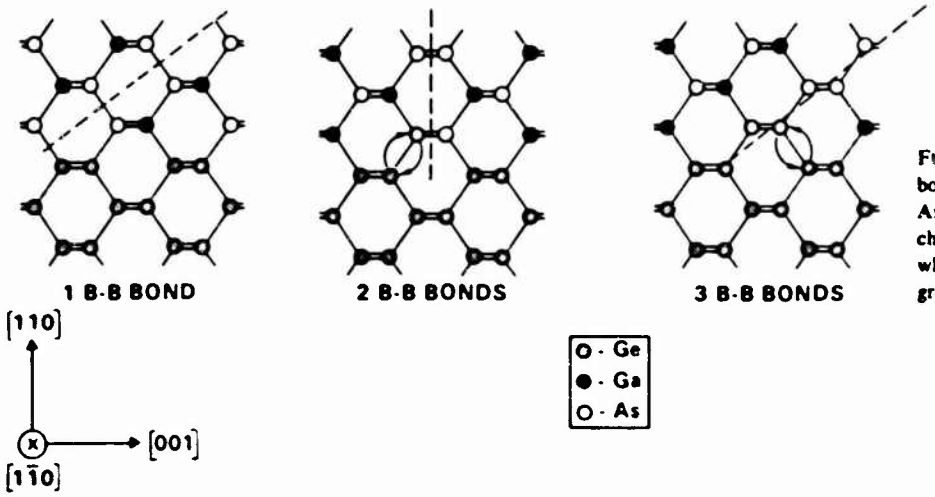

FIG. 1. Examples of arsenic antiphase domain boundaries (- - - - -) with one, two, or three As–As bonds. The arrows suggest an atomic exchange across the GaAs/Ge (110) interface which could account for the observed ΔE_v growth sequence effect.

TABLE I. Nearest neighbor bonding arrangement for a B antiphase domain at an AB/Ge(110) interface.

Interface with 1 B–B bond		Interface with 2 B–B bonds		Interface with 3 B–B bonds	
Abrupt	Interchanged	Abrupt	Interchanged	Abrupt	Interchanged
1 B–B	2 Ge–A	2 B–B	1 Ge–A	3 B–B	7 Ge–B
2 A–B	5 Ge–B	1 A–B	6 Ge–B	1 Ge–B	
1 Ge–B		1 Ge–B		3 Ge–Ge	
3 Ge–Ge		3 Ge–Ge			

boundary will be favored whenever 2 or 3 B–B (or A–A) bonds can be eliminated. Within the accuracy of the theory, a preference for anion or cation exchange is not specified; although, as indicated above, the systematic experimental observations are consistent with preferential B–Ge exchange. Although no attempt is made here to specify the bonding arrangements for all possible intersections of antiphase domain boundaries with a Ge(110) plane, it is likely that all antiphase domain boundaries which involve 2 or 3 B–B (or A–A) bonds will be unstable with respect to Ge exchange. The key point to be made is the identification of a plausible microstructural explanation for the observed ΔE_v growth sequence variation at AB–Ge (110) interfaces.

IV. EXPERIMENTAL INVESTIGATION OF GaAs/Ge(110) INTERFACES

X-ray photoemission spectroscopy (XPS) was used to measure ΔE_v for several GaAs/Ge (110) interfaces. This technique has been described in detail previously.[18,19] A HP5950A XPS system, which employs monochromatic AlKα (1486.6 eV) radiation, was used both for the measurements and the heterojunction growths. Germanium (110) single crystals cut and polished to 0.02 in. thickness were purchased from Eagle–Picher Industries, Inc. Immediately prior to insertion into the XPS sample preparation chamber, the Ge(110) substrate was etched in 3:5:3, HNO_3:CH_3COOH:HF to remove polishing damage. A clean ordered Ge(110) substrate was obtained by sputtering with 2 keV Ar^+ and annealing at 600 °C. The room temperature low energy electron diffraction (LEED) pattern associated with this substrate was complex and resembled the $c(8\times 10)$ pattern reported by Olshanetsky.[20] No oxygen or carbon impurities were detectable by XPS analysis.

The clean Ge(110) substrate was dosed initially with As by exposing the surface (heated to 350 °C) to an As_4 beam. Typically, the exposure of about 30 L done prior to GaAs growth produced an As surface coverage of ~0.6 monolayer (as estimated by XPS). Thin epitaxial layers of GaAs were grown *in situ* on the Ge(110) substrates by molecular beam epitaxy. The growth temperature was 350 °C and the As/Ga flux ratio was ~5:1. Four GaAs/Ge (110) samples labeled A–D were studied. The thicknesses of the GaAs layers for samples A–D (as estimated from the XPS measurements) were 23, 23, 25, and 29 Å, respectively. In general, the GaAs layer was grown immediately following the substrate As exposure; sample A was an unintentional exception in which the As dosed Ge(110) substrate was stored in vacuum ($\sim 1\times 10^{-9}$ Torr) for 51 h prior to GaAs growth. Following GaAs growth, epitaxy was confirmed by LEED and surface cleanliness (no detectable carbon or oxygen) was assessed by XPS. The ΔE_v measurements were initiated as soon as possible thereafter.

A typical GaAs/Ge (110) XPS spectrum in the binding energy region which contains Ga3*d*, Ge3*d*, and As3*d* core levels is shown in Fig. 2. As with previous studies[18,21] that involved the reverse growth sequence [i.e., Ge/GaAs (110)], the Ga3*d* to Ge3*d* core-level binding energy difference ($E^{Ge}_{Ge3d} - E^{GaAs}_{Ga3d}$) was utilized to determine ΔE_v. A plot of $E^{Ge}_{Ge3d} - E^{GaAs}_{Ga3d}$ vs time after GaAs growth (t) is shown in Fig. 3. The corresponding ΔE_v is shown on the right-hand scale in this figure. The ΔE_v measurements for samples A–C were obtained at room temperature. The ΔE_v measurements for sample D were obtained with the sample held at 200 °C. As can be seen from the figure, the four GaAs/Ge (110) interfaces appear to be initially unstable with respect to ΔE_v. For

TABLE II. Sum of bond formation energies (eV) associated with nearest neighbor bond arrangement at the intersection of an antiphase domain boundary with a Ge(110) plane. The abrupt interface has 2 A–A or 2 B–B bonds.

Domain boundary	Abrupt	Interchanged
As–As	59.02	59.64
Ga–Ga	59.02	59.64
Se–Se	62.56	65.45
Zn–Zn	62.49	65.10
Br–Br	66.72	73.97
Cu–Cu	66.00	70.37

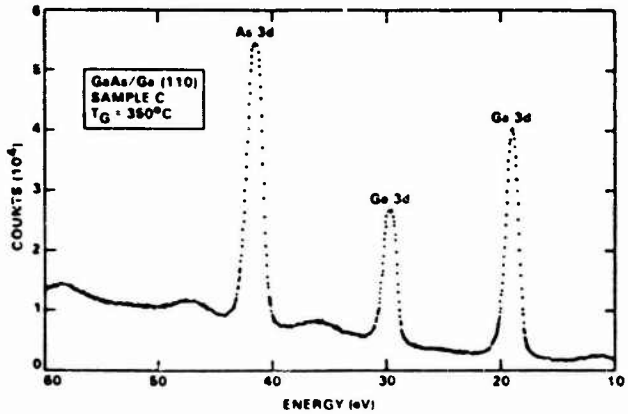

FIG. 2. Typical XPS spectrum of a GaAs/Ge (110) sample.

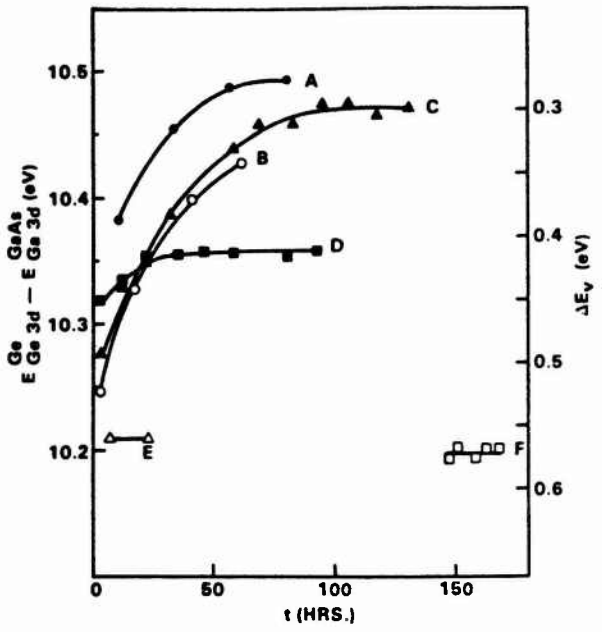

FIG. 3. Variation of $E^{Ge}_{Ge3d} - E^{GaAs}_{Ga3d}$ and of ΔE_v vs time after interface formation for four GaAs/Ge samples and two Ge/GaAs samples.

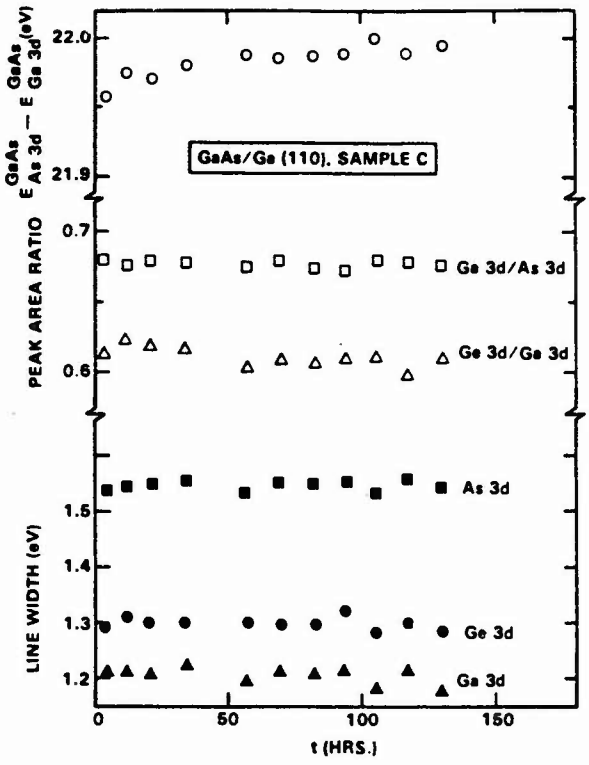

FIG. 4. XPS data for sample C. (Top) Variation of $E^{GaAs}_{As3d} - E^{GaAs}_{Ga3d}$ vs t (time after interface formation). (Middle) Ga3*d* /As3*d* and Ge3*d* /Ga3*d* peak area ratios vs t. (Bottom) As3*d*, Ge3*d*, and Ga3*d* linewidths vs t.

comparison, ΔE_v vs t data for two Ge/GaAs(110) samples (labeled E and F) are also shown in Fig. 3; these data were obtained from previously published work.[1,21] No time-dependent variation of ΔE_v is noted for the Ge/GaAs(110) interface.

For sample C, the Ga3*d*, Ge3*d*, and As3*d* linewidths (full width at half maximum intensity) vs t are shown at the bottom of Fig. 4. The Ga3*d* /As3*d* and Ge3*d* /Ga3*d* peak area ratios and the As3*d* to Ga3*d* core-level splitting in GaAs, $E^{GaAs}_{As3d} - E^{GaAs}_{Ga3d}$, as a function of t, are also shown in the figure. Except for a very small increase (~0.03 eV) in $E^{GaAs}_{As3d} - E^{GaAs}_{Ga3d}$ (which may be associated with a change in GaAs surface chemical shifts due to a slight carbon contamination accumulation for large t) there is no systematic variation in any of the parameters. The data in Fig. 4 rule out the possibility that substantial chemical reactions are occurring to cause the $E^{Ge}_{Ge3d} - E^{GaAs}_{Ga3d}$ vs t variation noted in Fig. 3.

A semilog plot of $\Delta E_v(t) - \Delta E_v(\infty)$ vs t is shown in Fig. 5 for samples C and D. The straight lines through the data are least-squares fits. The data appear to be well represented by an exponential function of the form

$$\Delta E_v(t) - \Delta E_v(\infty) = [\Delta E_v(0) - \Delta E_v(\infty)] \exp(-t/\tau_T), \quad (1)$$

where τ_T^{-1} is a rate constant. At 300 K $\tau_{300}^{-1} = 0.038\ h^{-1}$, while at 473 K, $\tau_{473}^{-1} = 0.087\ h^{-1}$. An atom transfer mechanism at antiphase domain boundaries (as proposed in Sec. III to explain the observed ΔE_v growth sequence effect) would be expected to have an exponential time dependence if the probability of atom exchange per unit time was constant and there were a fixed number of initial available sites at which the exchange could occur. The rate constant is observed to increase with temperature, which indicates that thermal energy increases the charge transfer rate.

V. SUMMARY

New XPS studies of ΔE_v for interfaces formed by growing GaAs epitaxially on Ge(110) at 350 °C have been reported. A variation of ΔE_v as a function of time after interface growth

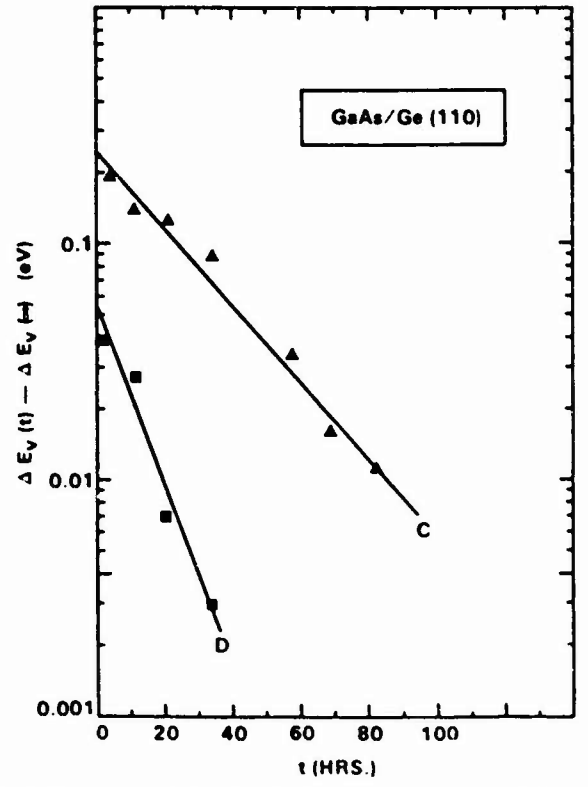

FIG. 5. Semilog plot of $\Delta E_v(t) - \Delta E_v(\infty)$ vs t for samples *C* and *D*.

is observed. This variation indicates interface dipole formation caused by structural instability. The time variation of ΔE_v has an exponential form and the associated rate constant appears to increase with sample temperature. The GaAs/Ge (110) interface reaches equilibrium at room temperature after about 100 h. The equilibrium ΔE_v is ~ 0.3 eV, which is ~ 0.25 eV less than ΔE_v observed for the reverse growth sequence [i.e., Ge grown epitaxially on GaAs(110)]. No instability of ΔE_v for the Ge/GaAs(110) interface is observed as a function of time.

Valence-band discontinuities for heterojunctions formed by growth of compound semiconductors (i.e., GaAs, ZnSe, and CuBr) on Ge(110) are observed to be smaller than the same quantities for the reverse growth sequence in all cases. Transitivity tests of ΔE_v for heterojunction sequences chosen specifically to avoid site nucleation problems suggest that antiphase disorder may be responsible for the growth sequence effect. If this growth sequence effect is associated with atomic exchange across the interface, an electrostatic model of heterojunction interfaces can be used to infer that anions (i.e., As, Se, and Br) preferentially interchange with Ge at a compound semiconductor/Ge (110) interface. Tight binding theory predicts that where certain antiphase domain boundaries intersect the Ge(110) interface, interchange of Ge and constituent atoms of the compound semiconductor is favored. If the atom interchange mechanism has a constant probability per unit time and there are a fixed number of available sites at which this interchange can occur, an exponential variation of ΔE_v with time would be expected. The time-dependent variation in ΔE_v, which is observed for the GaAs/Ge (110) interface, is consistent with this mechanism.

ACKNOWLEDGMENTS

Several helpful discussions with Professor W. A. Harrison are gratefully acknowledged. The work was supported by ONR Contract No. N00014-85-C-0135.

[1] R. W. Grant, J. R. Waldrop, and E. A. Kraut, Phys. Rev. Lett. **40**, 656 (1978).
[2] J. R. Waldrop and R. W. Grant, Phys. Rev. Lett. **43**, 1686 (1979).
[3] W. A. Harrison, *Electronic Structure and the Properties of Solids* (Freeman, San Francisco, 1980), p. 252.
[4] W. R. Frensley and H. Kroemer, Phys. Rev. B **16**, 2642 (1977).
[5] R. L. Anderson, Solid State Electron. **5**, 341 (1962).
[6] W. A. Harrison, E. A. Kraut, J. R. Waldrop, and R. W. Grant, Phys. Rev. B **18**, 4402 (1978).
[7] H. Kroemer, Surf. Sci. **132**, 543 (1983).
[8] H. Kroemer, in *Proceedings of the NATO Advanced Study Institute on Molecular Beam Epitaxy and Heterostructures, Erice, Sicily, 1983*, edited by L. L. Chang and K. Ploog (Martinus Nijhoff, The Netherlands, 1984).
[9] S. P. Kowalczyk, R. W. Grant, J. R. Waldrop, and E. A. Kraut, J. Vac. Sci. Technol. **21**, 482 (1982).
[10] P. Zurcher and R. S. Bauer, J. Vac. Sci. Technol. A **1**, 695 (1983).
[11] J. R. Waldrop, R. W. Grant, S. P. Kowalczyk, and E. A. Kraut, J. Vac. Sci. Technol. A **3**, 835 (1985).
[12] J. C. Phillips, J. Vac. Sci. Technol. **19**, 545 (1981).
[13] H. Kroemer, J. Vac. Sci. Technol. B **2**, 433 (1984).
[14] J. H. Neave, P. K. Larsen, B. A. Joyce, J. P. Gowers, and J. F. Van der Veen, J. Vac. Sci. Technol. B **1**, 668 (1983).
[15] E. A. Kraut and W. A. Harrison, J. Vac. Sci. Technol. B **2**, 409 (1984).
[16] E. A. Kraut and W. A. Harrison, J. Vac. Sci. Technol. B **3**, 1267 (1985).
[17] W. A. Harrison, Phys. Rev. B **24**, 5835 (1981).
[18] E. A. Kraut, R. W. Grant, J. R. Waldrop, and S. P. Kowalczyk, Phys. Rev. Lett. **44**, 1620 (1980); Phys. Rev. B **28**, 1965 (1983).
[19] R. W. Grant, E. A. Kraut, S. P. Kowalczyk, and J. R. Waldrop, J. Vac. Sci. Technol. B **1**, 320 (1983).
[20] B. Z. Olshanetsky, S. M. Repinsky, and A. A. Shklyaev, Surf. Sci. **64**, 224 (1977).
[21] J. R. Waldrop, E. A. Kraut, S. P. Kowalczyk, and R. W. Grant, Surf. Sci **132**, 513 (1983).

Lattice distortions and energies of atomic substitution

Edgar A. Kraut and Walter A. Harrison[a)]
Rockwell International Corporation, Microelectronics Research and Development Center, Thousand Oaks, California 91360

(Received 4 April 1985; accepted 15 April 1985)

The energies of atomic substitution and the associated excess enthalpies of mixing have been calculated with and without lattice relaxation for both isovalent and heterovalent substitutional impurities in tetrahedrally coordinated semiconductors by using the universal parameter tight binding theory of Harrison. For isovalent substitutional impurities, where experimental data and other theoretical predictions are available, agreement is good. Distortions around isovalent impurities such as indium in gallium arsenide can be readily calculated using the known natural bond lengths for indium arsenide and gallium arsenide. We define corresponding natural bond lengths for heterovalent substitutional impurities (those which come from a different column from that of the atom they replace) by minimizing the total bond energy with respect to interatomic separation. We have used the natural bond lengths calculated in this way to estimate the displacement of the neighbors to a number of impurity systems, and the corresponding reductions in the energy to substitute a free atom for a host atom. When two atoms are exchanged across an interface, relaxation around both atoms must be included and can be large. Such interchanges for heterovalent atoms affect heterojunction band lineups and are therefore of particular interest.

I. INTRODUCTION

During the past few years several, previously unanticipated, new experimental phenomena have been observed to occur at lattice-matched heterojunction interfaces. In some cases, the valence- and conduction-band edge discontinuities have been found to depend on crystallographic orientation,[1] on growth sequence,[2] and to be nontransitive.[3] We have speculated, on simple electrostatic grounds, that for the case of polar–nonpolar heterojunction interfaces, truly abrupt junctions cannot occur because they would produce a charge accumulation corresponding to an electric field in excess of a half an electron volt per angstrom.[4] We showed that reconstruction by compositional mixing over a few atomic planes near the interface is sufficient to eliminate this charge accumulation.[4] The mechanism by which the intermixing might occur during growth is unknown. Diffusion over a few atomic planes is one possibility[5] but the details remain elusive.

A first step towards a useful description of the atomic intermixing near heterojunction interfaces is to analyze the energetics of the solution of one bulk semiconductor in another. Van Vechten, Stringfellow, and more recently, Martins and Zunger, and also Fedders and Muller, have considered the isovalent solution of one III–V, II–VI, or column IV element or compound in another.[6–10] Experimentally, the heats of solution for this case tend to be small[8,11] and since there is no change in the valence of the atoms substituting for one another, the semiconducting properties are not strongly affected.

For example, the intersolution of GaAs and InAs crystals in contact with each other is simply the interchange of gallium and indium atoms. The number of gallium-arsenide and indium-arsenide bonds is the same before and after, so that to the extent that the total energy consists of independent bond energies, the heat of solution vanishes. There are two corrections to this.

First, the distance between atoms is different in GaAs and InAs, so that when an indium atom is placed in a GaAs crystal the resulting indium-arsenide bonds are distorted; in fact, the neighboring arsenic atoms will move, and to a lesser extent so will the more distant atoms. As a result, many bonds are distorted from their pure material state. To the extent that the total energy is a sum of bond energies, the change in energy is elastic energy of the bonds and can be reasonably estimated from any spring constant model of the bond energies.

Similarly, the lattice distortions themselves can be estimated by such models. They are plausible and successful theories.[9,10] Such elastic theories can even be applied to solutions of compounds such as InP in GaAs where new bonds (GaP and InAs) arise in the solution since the average of the undistorted bond energies will ordinarily change little and the elastic energy is still dominant.

Second, a bond energy does depend slightly on the neighboring bonds even in the absence of distortions, an effect called metallization. Thus the energy of an indium-phosphorous bond is shifted by its coupling to neighboring indium-arsenide antibonds and this shift is modified when those antibonds are replaced by gallium arsenide antibonds. However, when one III–V compound is dissolved in another the changes tend to average to zero and the elastic theory remains appropriate. The experiments of Mikkelsen and Boyce[12] show, and we will find from our theory, that a gallium-arsenic bond is only some 0.04 Å longer when it is embedded in an indium-arsenide crystal, though the host bond length is 0.16 Å longer.

When the two semiconductors are not isovalent, as when germanium is dissolved in gallium arsenide, these simple models do not apply. Germanium-arsenic bonds are formed which do not exist in pure zincblende-structure compounds. Thus the relaxed, natural bond length for such bonds is not known for use in the spring-constant models. Chemists may

 0734-211X/85/041267-07$01.00 © 1985 American Vacuum Society

approximate these bonds by germanium-arsenic bonds which occur in other structures, but they may be quite different. A further complication arises in that interchanging a gallium and a germanium atom is equivalent to moving a proton from one atom to the other. If the impurities are to be uncharged, an electron must be transferred also. It is this difficulty which in fact makes these heterovalent systems more interesting than the isovalent systems since the solution process dopes the semiconductor and therefore becomes important to the electrical properties, in contrast to the case of isovalent substitutions. This difficulty is avoided if we interchange both a germanium with a gallium and a germanium with an arsenic atom. Then the two charge transfers cancel and the system remains neutral, but then, of course there is also no doping.

Kraut and Harrison[13] calculated the heats of solution and the energies of substitution for such systems using the theory of the two-center bond[14] but neglecting any distortion of the host lattice. When they substituted atoms of different valence any extra electrons required for charge neutrality were placed at the top of the valence band of the host crystal. Similarly, any extra electrons required to retain the two center bond were obtained by removing electrons from the top of the valence band leaving holes behind, as would be appropriate for p-type materials. By dissolving III–V compounds in elemental semiconductors or II–VI's in III–V's (and vice versa) one electron is always added and subtracted from the top of the host valence band so no net charge is transferred. Here we shall treat the lattice distortions theoretically and shall also address the problem of charged impurities from heterovalent substitutions.

II. NATURAL BOND LENGTHS AND FORCE CONSTANTS

The energy of a semiconductor crystal can be written as a sum of bond energies, each containing four terms:

(1) its share of the promotion energy E_{pro} required to put free atom s and p electrons into sp^3 hybrid orbitals; it is independent of bond length and therefore is of no interest here;

(2) the energy gained in forming the bond $-2(V_2^2+V_3^2)^{1/2}$, with $V_2=-3.22\hbar^2/md^2$ the covalent energy, and $V_3=(\epsilon_{hA}-\epsilon_{hB})/2$ the polar energy equal half the difference between the two hybrid energies in an AB compound;

(3) the overlap interaction $V_0=2\eta_0V_2^2/|\epsilon_{hA}+\epsilon_{hB}|$ arising from the nonorthogonality of the orbitals on neighboring atoms and,

(4) the metallization energy from the coupling (proportional to V_{1A} or V_{1B}, each equal to $(\epsilon_s-\epsilon_p)/4$ for the A or B atom) between the bond and neighboring antibonds through the hybrids sharing the end atoms of the bond. The total energy per bond may be written explicitly as

$$E_{bond}=E_{pro}-2(V_2^2+V_3^2)^{1/2}+2\eta_0V_2^2/|\epsilon_{hA}+\epsilon_{hB}| -(3/4)(V_{1A}^2+V_{1B}^2)V_2^2/(V_2^2+V_3^2)^{3/2}. \quad (1)$$

This equation predicts the cohesive energy and, in principle, the equilibrium bond length when minimized with respect to the nearest neighbor distance d. The value of η_0 is of order unity, but is not known from theory. It has been adjusted to give the correct equilibrium spacing for the homopolar semiconductors and then taken to be the same for compounds from the same row of the periodic table; a geometric mean is used for skew compounds. This then provides predictions of the bond lengths for any tetrahedral compound.[14]

The only dependence upon d in Eq. (1) comes through V_2 so Eq. (1) can be minimized with respect to V_2 and then d can be found from V_2. In particular, Eq. (1) can be written for an elemental semiconductor ($V_3=0$) to obtain:

$$\partial E_{bond}/\partial V_2=2-2\eta_0V_2/\epsilon_h-3V_1^2/2V_2^2=0. \quad (2)$$

Note that V_2 and ϵ_h are negative. Given the equilibrium spacing for, say germanium, the covalent energy V_2 is determined and Eq. (2) can be solved for η_0. The same η_0 is then used for all the germanium row compounds such as GaAs, ZnSe, and CuBr.

Each term in the energy gives rise to tension in the bond,

$$T=-\partial E_{bond}/\partial d=-(2V_2/d)\partial E_{bond}/\partial V_2. \quad (3)$$

The first and third terms in Eq. (2) may be thought of as giving rise to a positive and negative tension, the sum being balanced by the overlap repulsion from the second term. In the compounds, the first term in Eq. (2) is reduced by a factor of $\alpha_c=|V_2|/(V_2^2+V_3^2)^{1/2}$, the covalency, which would tend to increase the equilibrium bond length considerably. However, the negative tension from the metallization contribution in the third term is also reduced by a comparable amount and the observed bond length remains essentially the same for GaAs, ZnSe, and CuBr. Actual evaluation of the derivatives of Eq. (1) showed this strong cancellation and gave predictions of $d=2.44$, 2.42, and 2.70 Å for Ge, GaAs, and CuBr. The observed values are 2.44, 2.45, and 2.45 Å the deviations arising from inaccuracy in the two large cancelling terms. Based on this observation, Eq. (1) is simplified using $2V_2+2\eta_0V_2^2/|\epsilon_{h-}+\epsilon_{h+}|$. The average of the values of the hybrid energies for two constituents from the same row of the periodic table in a III–V or II–VI compound is almost identical to the value for the column IV element in that row (and the geometric mean of the two column IV elements if two rows are involved), so this predicts nearly the same bond lengths for isoelectronic systems, in agreement with experiment.

We call these the *natural bond lengths* for these compounds; the procedure has been constructed to give values close to the observed internuclear distances in the pure compounds; that is systems where the average valence of the constituents is four. For isovalent impurities such as indium substituted for gallium in gallium phosphide, this natural bond length will be used in conjunction with the natural bond length of the host to obtain predictions of the actual bond length in the alloy.

This also suggests a procedure for obtaining natural bond lengths when the average valence of the elements forming the bond is not four; that is, for heterovalent substitutions, such as germanium substituted for gallium in gallium arsenide. Making such a substitution modifies the overlap interaction which is again taken into account by using an average hybrid energy; in this case the average is not approximately

equal to the column IV counterpart. (The geometric mean of the η_0 values is also used if the two elements come from different rows.) The substitution also modifies the polar energy V_3 which enters the second and fourth terms in Eq. (1). These two modifications nearly cancel so replacing the two terms by $2V_2$ is appropriate though V_3 has been modified. However the replacement also changes the average $(V_{1A}^2 + V_{1B}^2)/2$ which enters the metallization in Eq. (1); that average changed little in the III–V and II–VI compounds so the homopolar expression was adequate. Here it is necessary to add the effect of the change in $(V_{1A}^2 + V_{1B}^2)$, which is done by adding $-(3/4)[V_{1A}^2 + V_{1B}^2 - V_{11V}(A)^2 - V_{11V}(B)^2]V_2^2/(V_2^2 + V_3^2)^{3/2}$ where $V_{11V}(A)$ and $V_{11V}(B)$ are the V_1 values for the column IV element from the row of atoms A and B, respectively. This does not change the estimate appreciably for the bonds between atoms with an average valence of four, but will increase the estimated bond length for the arsenic–arsenic bond, for example, by 5%. We believe that this correction is real and it is large enough to be important.

This gives us a procedure for estimating natural bond lengths for any pair of elements in a tetrahedral compound, even if, as in the case of the germanium-arsenic bond, the bond can occur only when one of the atoms is present as an impurity. In such a case, two electrons are retained in each bond so the impurity is not neutral. Corrections for other charge states could also be made, but are not included here. The natural bond length is obtained by setting the partial derivative with respect to V_2 of the bond energy, obtained as described, equal to zero. That condition is now:

$$\begin{aligned}\partial E_{\text{bond}}/\partial V_2 = 2 + 4\eta_0 V_2/|\epsilon_{h-} + \epsilon_{h+}| - (3/2)\\ \times [V_{1A}^2 + V_{1B}^2 - V_{11V}(A)^2 - V_{11V}(B)^2]\\ \times [V_2/(V_2^2 + V_3^2)^{3/2}\\ - 3V_2^3/2(V_2^2 + V_3^2)^{5/2}] = 0 . \qquad (4)\end{aligned}$$

The value of η_0 is obtained from the column IV semiconductor for each row in the periodic table; the geometric mean is to be used when two rows are involved. The value for each row is obtained by noting that for a column IV semiconductor, A and B are identically the same column IV atom, so the metallization term in Eq. (4) vanishes. Thus the equilibrium condition for the homopolar system is $\eta_0 = \epsilon_h/V_2$. Both ϵ_h and V_2 are negative and take their values for the column IV element. Using this number for η_0 Eq. (4) is to be solved for V_2 and then the natural bond length is given by

$$d = (-mV_2/3.22\hbar^2)^{-1/2}, \qquad (5)$$

where $\hbar^2/m = 7.62$ eV (Å)^2. As an example, we evaluate germanium-arsenic natural bond length, with Ge entering as the + atom. We need first the η_0 for the Ge row since both Ge and As are from that row. With the Ge hybrid energy of $\epsilon_{h+} = -9.29$ eV obtained from the Hartree–Fock term values[14] and a $V_2 = -4.12$ eV for the 2.44 Å bond length of Ge, a value of $\eta_0 = 2.25$ is obtained. The arsenic hybrid energy is $\epsilon_{h-} = -11.46$ eV. For V_3, a value of 1.09 eV is obtained from the difference in the hybrid energies, and $V_{1+} = -1.96$ eV and $V_{1-} = -2.48$ eV are obtained as one-quarter of the difference between ϵ_s and ϵ_p from the Hartree–Fock term values; both $V_{11V}(A)$ and $V_{11V}(B)$ are given by V_{1+} for this case since both elements are in the germanium row. This provides all the parameters for Eq. (4), which is solved numerically to obtain the value of $V_2 = -4.44$ eV, or a d of 2.35 Å. We have evaluated natural bond lengths for all combinations of Cu, Zn, Ga, Ge, As, Se, and Br in Table I. It is interesting to observe that the natural bond length of ZnSe (2.417 Å) is not equal to the sum of half the natural bond length of a Zn–Zn bond (1.475 Å) and half the natural bond length of a Se–Se bond (1.091 Å).

TABLE I. Natural bond lengths (Å) between atoms of the germanium row of the periodic table. The natural bond length is defined as that of a perfect tetrahedral solid composed of the selected atoms and is determined by minimizing the total bond energy with respect to atomic separation independent of the existence of the particular solid. Natural bond lengths are useful for the prediction of the lattice relaxation around substitutional impurities in tetrahedral solids.

	Cu	Zn	Ga	Ge	As	Se	Br
Cu	3.358	3.212	3.195	2.941	2.697	2.498	2.333 (Å)
	Zn	2.950	2.871	2.776	2.594	2.417	2.266
		Ga	2.651	2.556	2.442	2.302	2.169
			Ge	2.440	2.348	2.227	2.102
				As	2.290	2.196	2.070
					Se	2.182	2.081
						Br	2.463

These natural bond lengths have been calculated as if all bonds in the system were of the same AB type and all AB pairs were tetrahedrally coordinated. It should be noted that there are corrections to the natural bond length due to a change in environment that have not been included here. For example, the metallization of an InAs bond in GaAs is modified because this interaction couples the InAs bond to a GaAs antibond, and vice versa, modifying the V_3 at appropriate places in Eq. (4). This complication is omitted here.

We may also evaluate the force constant k for the bond. It is given by

$$k = \partial^2 E_{\text{bond}}/\partial d^2 . \qquad (6)$$

We shall use Eq. (2) since these constants are found to be rather independent of the polarity of the bond and the small observed variations are not given well by the theory. The metallization term in Eq. (1) and Eq. (2) can also be omitted in calculating the force constant k, as was done in obtaining $\eta_0 = \epsilon_h/V_2$ above. The force constant is given by

$$\begin{aligned}k &= \partial^2 E_{\text{bond}}/\partial d^2\\ &= [12V_2 + 20\eta_0 V_2^2/|\epsilon_h|]/d^2 = -8V_2/d^2 , \qquad (7)\end{aligned}$$

equal to 5.54 eV/Å^2 for Ge, compared to an experimental value of 8.00 eV/Å^2 obtained from the bulk modulus. The discrepancy reflects inaccuracy of the theory and is not necessarily improved by switching to experimental values for k while using theoretical values for the other parts of the calculation.

III. DISTORTIONS AND RELAXATION ENERGY AT IMPURITY ATOMS

Shih *et al.*[16] have made a simple calculation of the relaxation of bonds in pseudobinary alloys, depending just upon the natural bond lengths (which are equal to the pure-compound bond lengths for their case) and an assumed radial force constant. They neglected relaxation of the second neighbors to an impurity; then there is a symmetric radial relaxation of the nearest neighbors. Treating each bond as a spring with the same force constant, but with a relaxed length equal to the natural bond length, one may allow a small relaxation for each neighbor such that the net force on it is zero, they find immediately that the nearest-neighbor distance becomes three fourths of the natural bond length for the impurity neighbor bond plus one fourth of the host bond length. We use exactly this result, but of course now have natural bond lengths for impurities other than those of a pseudobinary alloy. The calculation of the nearest neighbor relaxation is immediate. For example using Table I we see that a gallium atom substituted in germanium will have nearest-neighbor bond lengths of (3/4)2.56 Å + (1/4)2.44 Å = 2.53 Å, corresponding to nearest neighbors relaxing outwards by 0.09 Å. This would be slightly increased if we allowed the second neighbors to relax also and would be slightly decreased if we included angular force constants, but the multitude of small corrections are dropped here. Similarly, an arsenic atom substituted in silicon will have a nearest-neighbor bond length of 2.315 Å, corresponding to nearest neighbors relaxing inwards by 0.03 Å. In our earlier work[13] we did not allow relaxation of the neighbors. It is of interest to include the effect of this relaxation which we do here. Substituting an impurity introduces a net positive or negative tension in the bonds adjacent to it which we have described as a change in the length of a relaxed spring, but which we can equally well regard as a force F, leaving the springs the same as in the host material. The nearest neighbors then relax under this force until the force arising from the four springs surrounding each atom balances F, that is, the displacement δd will be such that $F = (4/3)k\delta d$. (Note that the change in length of the three outer bonds is only δd / 3 and the radial component of the corresponding force is only a third of the total, but there are three such springs for each nearest-neighbor atom.) Half of the work done by the force ($F\delta d$) is cancelled by the increase in the spring energy, $(2/3)k(\delta d)^2$ for each of the four nearest-neighbor bonds. Using the expression obtained above for the radial force constant, we obtain a relaxation energy of

$$E_{\text{relax}} = (64/3)V_2(\delta d/d)^2, \tag{8}$$

with V_2 the host covalent energy. This is a lowering in energy required to substitute the impurity. For a gallium atom substituted for germanium with $\delta d/d = 0.09/2.44$, this is -0.12 eV.

IV. RESULTS: COMPARISON WITH EXPERIMENT AND OTHER THEORIES

The systems which have been most thoroughly studied both experimentally and theoretically are those involving only isovalent substitutions as, for example, InAs in GaAs.

TABLE II. Comparison of predicted natural bond lengths for isovalent substitutional impurities: M–Z (Martins and Zunger Ref. 9) UPTB (relaxed universal parameter tight-binding theory).

System	R (Å) M–Z	R (Å) UPTB	System	R (Å) M–Z	R (Å) UPTB
AlP : In	2.480	2.466	InP : Al	2.414	2.385
GaP : In	2.474	2.473	InP : Ga	2.409	2.405
AlAs : In	2.553	2.542	InAs : Al	2.495	2.457
GaAs : In	2.556	2.549	InAs : Ga	2.495	2.478
AlSb : In	2.746	2.754	InSb : Al	2.693	2.656
GaSb : In	2.739	2.761	InSb : Ga	2.683	2.677
AlP : As	2.422	2.397	AlAs : P	2.395	2.362
AlP : Sb	2.542	2.541	AlSb : P	2.444	2.409
AlAs : Sb	2.574	2.559	AlSb : As	2.510	2.462
GaP : As	2.414	2.425	GaAs : P	2.387	2.389
GaP : Sb	2.519	2.569	GaSb : P	2.436	2.437
GaAs : Sb	2.564	2.587	GaSb : As	2.505	2.491
InP : As	2.595	2.565	InAs : P	2.562	2.526
InP : Sb	2.700	2.729	InSb : P	2.597	2.581
InAs : Sb	2.739	2.748	InSb : As	2.667	2.639
ZnS : Se	2.420	2.392	ZnSe : S	2.367	2.342
ZnS : Te	2.539	2.574	ZnTe : S	2.407	2.403
ZnSe : Te	2.584	2.599	ZnTe : Se	2.502	2.478
HgS : Se	2.611	2.477	HgSe : S	2.553	2.425
HgS : Te	2.716	2.667	HgTe : S	2.579	2.488
HgSe : Te	2.748	2.693	HgTe : Se	2.665	2.566
ZnS : Hg	2.482	2.379	HgS : Zn	2.380	2.337
ZnSe : Hg	2.587	2.482	HgSe : Zn	2.494	2.439
ZnTe : Cd	2.755	2.749	CdTe : Zn	2.674	2.690
ZnTe : Hg	2.748	2.732	HgTe : Zn	2.673	2.684
CuCl : Br	2.440	2.302	CuBr : Cl	2.367	2.240
CuCl : I	2.563	2.497	CuI : Cl	2.407	2.305
CuBr : I	2.585	2.528	CuI : Br	2.500	2.398
C : Si	1.665	1.802	Si : C	2.009	2.004
Si : Ge	2.380	2.383	Ge : Sn	2.419	2.406
Si : Sn	2.473	2.509	Sn : Si	2.645	2.622
Ge : Sn	2.549	2.569	Sn : Ge	2.688	2.659

There are two reasons for this. First, the natural bond lengths are associated with naturally occurring tetrahedrally coordinated compounds, and second, this class of substitutions is of interest in the formation of pseudobinary alloys. Recently, Martins and Zunger[9] used a valence force field model to predict the symmetric lattice distortions around isovalent impurities in 64 semiconductor impurity systems. In their model the force constants were obtained by fitting experimental elastic constants of tetrahedral compounds. For the five systems which they compared with experimental extended x-ray absorption fine-structure (EXAFS) data, GaAs : In, InAs : Ga, CdTe : Mn, ZnSe : Te, and ZnTe : Se, the predicted and observed impurity bond lengths agreed within the experimental error of 0.01 Å. In order to compare our theory with that of Martins and Zunger, we calculated the impurity host bond length for the same 64 systems by solving Eq. (4) for each type of tetrahedral bond. The natural bond length for the impurity substituted into the host was obtained as three quarters of the host-impurity bond length plus one-quarter of the host bond length, just as discussed above. The results are shown in Table II. The agreement is remarkable, especially since there are no adjustable parameters in our theory. Martins and Zunger also obtained the

TABLE III. Comparison of experimental excess heats of mixing for $(AB)_x(Cd)_{1-x}$ pseudobinary alloys tabulated by Stringfellow (Ref. 8) (for $x = 1/2$) with theoretical values: Martins and Zunger's model (1984) (Ref. 9); Fedders and Muller's model (1984) (Ref. 10); UPTB (unrelaxed universal parameter tight-binding model).

System	$8\Delta H^m$ Experiment	$8\Delta H^m$ MZ	$8\Delta H^m$ FM	$8\Delta H^m$ Unrelaxed UPTB
AlAs–GaAs	0.00	0.00	0.00	0.00 (eV)
AlAs–InAs	0.22	0.31	0.21	0.32
AlSb–GaSb	0.00	0.00	0.00	−0.01
AlSb–InSb	0.05	0.18	0.13	0.21
GaP–GaAs	0.03 0.09	0.10	0.06	0.05
GaP–GaSb	Misc. Gap	...	...	0.67
GaP–InP	0.30 0.28	0.39	0.28	0.43
GaAs–GaSb	0.35 0.39	0.40	0.24	0.33
GaAs–InAs	0.14 0.26 0.17	0.22	0.21	0.32
GaSb–InSb	0.13 0.16	0.22	0.16	0.20
InP–InAs	0.03	0.06	0.05	0.02
InP–InSb	Misc. Gap	...	...	0.46
InAs–InSb	0.20 0.25	0.25	0.19	0.29
Ge–Si	0.10	0.14	0.08	0.11
Si–Sn	1.69	2.38	1.48	0.36
Ge–Sn	0.65	1.33	0.78	−0.35

contribution of the deformation energy to the excess enthalpy of mixing ΔH_m. Kraut and Harrison[13] have related the excess enthalpy of mixing to the energies of substitution and heats of solution as obtained from the theory of the two-center bond.[14] This relation may be written as

$$8\Delta H_m(x = 1/2) = E_{AB}(C_A) + E_{AB}(D_B) + E_{CD}(A_C) + E_{CD}(B_D) = 2\Omega' \quad (9)$$

for the alloy $(AB)_x(CD)_{1-x}$. Here $E_{AB}(C_A)$ is the energy required to substitute a C atom on an A site in compound AB and Ω' is the interaction parameter of regular solution theory discussed in Ref. 13. Our previous calculations,[13] without lattice distortions, showed that the heats of solution for isovalent substitutions such as AlAs in GaAs or InAs in GaAs are roughly an order of magnitude smaller than the heats of solution for heterovalent substitutions such as Ge in GaAs or ZnSe in GaAs. When the unrelaxed heat of solution (meaning the heat of solution not including lattice distortion) is already near zero, then one does not expect the addition of an equally small negative contribution to the heat of solution, calculated in a different way, to make the number more accurate or meaningful. Consequently we have compared experimental excess enthalpies of mixing for isovalent substitution, from the tabulation of Stringfellow,[8] with our unrelaxed tight-binding predictions[13] in Table III. Table III also gives results of Martins and Zunger.[9] The elastic model of Fedders and Muller,[10] Stringfellow's 1972 calculations[7] using Van Vechten's dielectric-spectroscopic model,[6] and Stringfellow's 1973 modification thereof,[8] taking into account an average band gap, give similar results. The agreement between experiment and the tight-binding results is encouraging, particularly since, unlike the other theories, the tight-binding calculation contains no adjustable parameters. Adding the relaxation energy, calculated as indicated here, reduces the predicted values considerably and worsens agreement with experiment.

For the case of heterovalent substitutions such as Ge in GaAs, where the heats of solution are an order of magnitude greater than the small negative corrections associated with lattice distortions, we do not have this problem. Because of the relative insolubility of heterovalent semiconductors in one another and the associated large positive heats of solution, only limited experimental data is available.[6–8] However, these systems are of significant interest because they form lattice-matched heterojunctions. Table IV gives the energy of substitution and excess enthalpy of mixing with and without including relaxation. Direct comparison with experiment is difficult, but the theory is the same as for the isovalent systems where agreement with experiment is good. For heterovalent systems, solid state core-level shifts can be calculated with the aid of the Born–Haber cycle and the energies of substitution listed in Table IV, as Enderlein and Harrison[17] and Kraut and Harrison have done.[13] Unfortunately,

TABLE IV. The first five columns give unrelaxed energies of substitution and associated excess heat of mixing for elements and compounds. For example, $E_{AB}(C_A)$ is the energy in eV required to substitute a C atom on an A site in compound AB as computed by the universal parameter tight-binding method (UPTB). The final column includes the reduction due to relaxation.

AB/CD	$E_{AB}(C_A)$	$E_{AB}(D_B)$	$E_{CD}(A_C)$	$E_{CD}(B_D)$	$4\Delta H^m$ unrelaxed	$4\Delta H^m$ relaxed
Si/GaP	3.79	−1.78	−3.21	4.14	1.47	1.11 (eV)
Ge/AlAs	2.20	−1.55	−2.07	3.55	1.07	0.92
InAs/ZnTe	3.06	0.51	−3.26	0.27	0.29	0.26
Si/AlP	3.14	−1.78	−2.42	4.46	1.70	1.40
Ge/GaAs	2.84	−1.55	−2.79	3.26	0.88	0.70
Ge/ZnSe	6.81	−1.14	−6.33	10.59	4.96	3.60
Ge/CuBr	16.42	1.83	−17.58	18.51	9.59	5.97
GaAs/ZnSe	3.53	−0.96	−3.60	3.91	1.44	1.07
GaAs/CuBr	13.22	0.70	−15.27	9.31	3.98	2.61
ZnSe/CuBr	10.47	−0.90	−11.47	3.67	0.59	0.30
Sn/InSb	2.07	−1.12	−2.19	2.46	0.61	0.50
Sn/CdTe	4.83	−0.64	−4.77	8.43	3.93	3.05
InSb/CdTe	2.56	−0.66	−2.69	3.11	1.15	0.91

such calculations do not appear to be accurate enough to provide a good test of the contribution of lattice relaxation to the energies of substitution.

V. HETEROVALENT MIXING WITH CHARGE TRANSFER

As an example of the application of the energies of substitution listed in Table IV and the importance of the small corrections for lattice distortions, consider the germanium-gallium arsenide system. The heterojunction interface can be thought of as a crystalline layer serving as a transition region between the dissimilar bulk semiconductors which it separates. For polar interfaces, an important function of this transition region is to minimize the difference in the average potential and average potential gradient across the interface by an appropriate exchange of atoms between the bulk semiconductors, forming a transition region of intermediate atomic composition.[4] For a (110) interface between bulk germanium and bulk gallium arsenide, simple electrostatic arguments do not constrain the atomic composition of the interface region. The potential is already flat there, since both Ge(110) and GaAs(110) planes are charge neutral. However, atom exchanges may still occur. The energies of substitution can be used to obtain information concerning such exchanges and the ones across polar interfaces as well. The energy to interchange an As and a Ge atom across a Ge–GaAs interface is $3.26 - 1.55 = 1.71$ eV from Table IV neglecting lattice distortion, and 1.53 eV when it is included. Interchanging a Ge and an As atom across a Ge–GaAs interface, increases the nuclear charge on the Ge side by one unit and decreases it by one unit on the GaAs side. To maintain charge neutrality, the change in nuclear charge must be balanced by addition of an electron at the valence-band maximum of Ge and subtraction of an electron from the valence-band maximum of GaAs. In this process, no net charge has been transferred across the interface since the nuclear and electronic charges have been balanced. Since the Fermi energy is continuous across the interface, and can therefore be taken constant in the region of interest, the electron transferred across the interface to maintain charge neutrality must be transferred back. Removing an electron from the valence-band maximum of Ge costs an energy of 8.97 eV and removing an electron from the valence-band maximum of GaAs costs an energy of 9.64 eV.[18] The difference (-0.67 eV) must be added to the energy required to interchange the arsenic and germanium atoms, in this case 1.71 or 1.53 eV, depending on whether or not lattice distortion is taken into account, to obtain the energy of interchange for charged As and Ge impurities. This conclusion is valid for both intrinsic and doped starting heterojunctions. For interchange of a Ge and a Ga atom across a Ge–GaAs interface, the energy from Table IV neglecting lattice relaxation is $2.84 - 2.79 = 0.05$ eV and is $2.73 - 2.87 = -0.14$ eV including lattice relaxation. The interchange of a Ge and a Ga atom decreases the nuclear charge on the germanium side by one and increases it on the gallium arsenide side by one, again compensated by removing an electron from the top of the germanium valence band and adding it to the top of the gallium arsenide valence band. To put this electron back costs, 9.64 eV to remove it from the GaAs and gains 8.97 eV in returning it to the Ge,[18] for a net change of 0.67 eV which must be added to the energy of interchange (0.05 or -0.14 eV). These may be immediately estimated for any other combination of lattice matched heterojunction systems using the results of Tables IV and the Hartree–Fock valence-band maxima from Ref. 18.

It is interesting and important that putting either Ga or As atoms into germanium is energetically expensive. Such a transfer would be important to the electrical properties because it produces dipole fields and doping. If one of the interchange energies is small or negative, spontaneous interchanges might be expected and an associated dipole would be created determined by the substitution energies. This dipole might grow in strength until it just balanced the small substitution energies. Our results would suggest that the interchange energies are too large to allow this. However, our calculations have been performed for impurities in bulk semiconductors and we have not explicitly taken into account the effects of a real adjacent interface and the perturbations that it would produce in the electronic states.

VI. SUMMARY AND CONCLUSIONS

We have defined a natural bond length for any binary tetrahedrally coordinated solid, whether or not it actually occurs in nature, by minimizing its bond energy. For solids containing three or more kinds of atoms, these natural bond lengths have been used together with a simple spring model of lattice distortion to calculate the corresponding alloy bond lengths. We find that these bond lengths are given by three-quarters of the host-impurity bond length, computed from energy minimization, plus one-quarter of the host's natural bond length. Calculations have been performed for both isovalent and heterovalent impurities in tetrahedral semiconductors. For isovalent impurities, our results are in reasonably good agreement with experimental EXAFS bond lengths, and with experimental excess enthalpies of mixing, as well as with other theories. For heterovalent impurities, the impurities may become charged, and when atoms are interchanged across lattice matched heterojunction interfaces, this may create interface dipoles. Such interface dipoles would cause the heterojunction band lineups to deviate from predictions based on simple differences between the bulk properties of the constituent semiconductors, in agreement with experiment. The present energies of interchange at heterojunction interfaces seem too large to be associated with spontaneous interchanges and other processes may be involved. These processes are as yet unidentified and may be interface related.

ACKNOWLEDGMENT

This research was supported, in part, by the Office of Naval Research of the United States Navy under Contract No. N00014-85-C-0135.

[a]Stanford University, Department of Applied Physics, Stanford, California 94305.

[1]R. W. Grant, J. R. Waldrop, and E. A. Kraut, Phys. Rev. Lett. 40, 656 (1978).
[2]J. R. Waldrop, S. P. Kowalczyk, R. W. Grant, E. A. Kraut, and D. L. Miller, J. Vac. Sci. Technol. 19, 573 (1981).
[3]J. R. Waldrop and R. W. Grant, Phys. Rev. Lett. 43, 1686 (1979).
[4]W. A. Harrison, E. A. Kraut, J. R. Waldrop, and R. W. Grant, Phys. Rev. B 18, 4402 (1978).
[5]E. A. Kraut, J. Vac. Sci. Technol. B 1, 643 (1983).
[6]J. A. Van Vechten, in *Semiconductor Handbook*, edited by S. P. Keller (North-Holland, Amsterdam, 1980), Vol. 3, p. 1.
[7]G. B. Stringfellow, J. Phys. Chem. Solids 33, 665 (1972).
[8]G. B. Stringfellow, J. Phys. Chem. Solids 34, 1749 (1973).
[9]J. L. Martins and A. Zunger, Phys. Rev. B 30, 6217 (1984).
[10]P. A. Fedders and M. W. Muller, J. Phys. Chem. Solids 45, 685 (1984).
[11]M. B. Panish and M. Ilegems, Prog. Solid State Chem. 7, 39 (1972); A. Laugier, Rev. Phys. Appl. 8, 259 (1973); G. B. Stringfellow, J. Cryst. Growth 27, 21 (1974); 58, 194 (1982).
[12]J. C. Mikkelsen and J. B. Boyce, Phys. Rev. Lett. 49, 1412 (1982); Phys. Rev. B 28, 7130 (1983).
[13]E. A. Kraut and W. A. Harrison, J. Vac. Sci. Technol. B 2, 409 (1984).
[14]W. A. Harrison, Phys. Rev. B 27, 3592 (1983).
[15]W. A. Harrison, Phys. Rev. B 24, 5835 (1981).
[16]C. K. Shih, W. E. Spicer, W. A. Harrison, and A. Sher, Phys. Rev. B 31, 1139 (1985).
[17]R. Enderlein and W. A. Harrison, Phys. Rev. B 30, 1867 (1984).
[18]E. A. Kraut, J. Vac. Sci. Technol. B 2, 486 (1984).

Polar heterojunction interfaces: Isovalent interlayers

Edgar A. Kraut
Rockwell International Corporation, Microelectronics Research and Development Center, Thousand Oaks, California 91360
(Received 4 March 1985)

Starting from nonpolar heterostructures, such as Ge/Si/Ge, polar heterojunction interfaces with isovalent interlayers are constructed by transferring protons between nuclei (Harrison *et al.*). The relation between isovalent interlayers and interface dipoles is explained and it is shown that, despite the chemical inhomogeneity represented by an isovalent interlayer, the valence-band discontinuity between the adjacent semiconductors may depend only on their bulk properties.

The purpose of this Rapid Communication is to show how three-layer heterostructures composed entirely of semiconductors can be used to form polar heterojunction interfaces having isovalent interlayers and to explain the relationship of these interlayers to interface dipoles. We shall see that by an appropriate interface reconstruction, the interface dipoles can always be eliminated with the result that the band discontinuities between the adjacent semiconductors may be determined by their bulk properties alone. Recent experimental evidence[1] that the incorporation of a monolayer of aluminum at the Ge/GaAs(100) interface does not change the measured valence-band offset supports these ideas and suggests that interfaces may reconstruct to minimize the change in the average potential and average potential gradient across the interface. To the degree that reconstruction processes may be governed by irreversible thermodynamics, the reconstruction may be incomplete and a remanent dipole may remain. Such remanent dipoles might be responsible for the crystallographic orientation dependence,[2] nontransitivity,[3] and growth sequence dependence[4] observed in experiments. From a technological point of view, a remanent dipole as large as 0.2 eV would correspond to $8kT$ in units of room-temperature thermal energy and could not be ignored in practical applications.

In what follows, we shall focus our attention on the Ge/Al/GaAs(100) system because that is the one which has been experimentally investigated[1] but the methods and conclusions apply equally well to the Ge/In/GaAs(100), Si/Ga/AlP(100), and α-Sn/Ga/InSb(100) heterostructures and to their (111) orientations as well. To construct the Ge/Al/GaAs(100) system, we start from an infinite Ge crystal and imagine a single (100) plane of Ge atoms to be replaced by an equivalent (100) plane of Si atoms forming a Ge/Si/Ge heterostructure. Since the atom planes are uncharged, there is no variation in the bulk electrostatic potential normal to the Si plane. Following Harrison, Kraut, Waldrop, and Grant,[5] we imagine removing a proton from each Si nucleus and transferring these protons to the nearest-neighbor Ge atoms on one side of the Si plane. At the same time, we imagine the electronic structure to be unchanged from that of the Ge/Si/Ge heterostructure. Electronic relaxation can be included by allowing the bonds to become polar in a later step. As a result of the proton transfers, the neutral Si atoms have become negatively charged Al atoms with a charge of -1 and the Ge atoms have become positively charged As atoms with a charge of $+1$.

The process is now repeated, starting with the row of Ge atoms adjacent to the positively charged As atoms. A proton is removed from each Ge atom, converting it to a negatively charged Ga atom. These protons are then inserted into the adjacent Ge atoms to obtain positively charged As atoms and so on *ad infinitum*. The resulting Ge/Al/GaAs(100) heterostructure and its associated electrostatic potential, obtained by solving Poisson's equation, is shown in Fig. 1. Although the bonds will polarize in the electrostatic field produced by the proton transfers, only the center

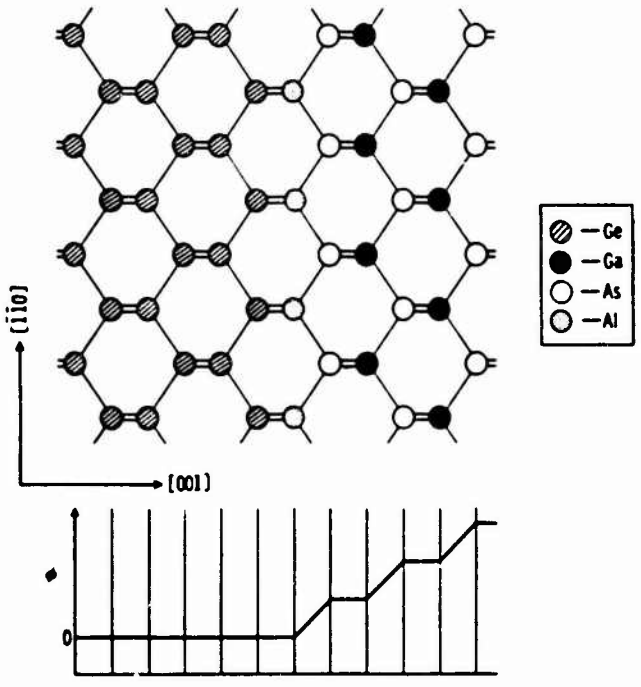

FIG. 1. Starting from a Ge/Si/Ge heterostructure, a Ge/Al/GaAs(100) heterostructure is produced by transferring protons to the right beginning with the Si plane. The potential ϕ averaged over planes parallel to the interface is obtained by integrating Poisson's equation from left to right. The first atomic plane to the right of the junction is composed entirely of aluminum atoms and is negatively charged in the absence of bond polarization. A nonzero average electric field has arisen to the right of the junction due to charge accumulation. It is not eliminated by bond polarization (Ref. 5), although the latter will change the sign of the effective charge on the aluminum atoms.

 ©1985 The American Physical Society

of gravity of the two electrons in each bond will be affected and it follows that the charge redistribution in the bonds at the interface cannot remove the charge accumulation arising from the proton transfers.[5] The potential for the structure of Fig. 1 increases at a rate of about 0.5 eV per Å [see Eq. (1) of Ref. 5]. This corresponds to a huge electric field for which there is no experimental evidence. Consequently, it is likely that the interface reconstructs so as to eliminate the large electric field associated with the abrupt interface. The simplest reconstruction is shown in Fig. 2. It eliminates the charge accumulation but not the interface dipole and corresponds to two transition planes, each containing half a monolayer of Al, separating bulk Ge from bulk GaAs. The change δ in the average potential between bulk Ge and bulk GaAs is $\delta = \pi e^2/2\epsilon a$ for this case, where $\epsilon = 12$ and $a = 5.65$ Å for GaAs, giving $\delta = 0.34$ eV. The experimental data[1] do not support a dipole of this magnitude at the Ge/Al/GaAs(100) interface. The next simplest reconstruction eliminates both the change in the average potential and the change in the average potential gradient in the direction normal to the interface by using three transition planes separating bulk Ge and bulk GaAs. The plane nearest the bulk Ge consists of $\frac{3}{4}$ Ge atoms and $\frac{1}{4}$ As atoms. The next plane consists of $\frac{1}{4}$ Ge atoms and $\frac{3}{4}$ Al atoms followed by an As(100) plane and a Ga(100) plane containing $\frac{1}{4}$ Al atoms as shown in Fig. 3. Since there is no interface dipole, the valence-band discontinuity for the reconstruction of Fig. 3 should be determined entirely by the properties of bulk Ge and bulk GaAs despite the presence of Al atoms at the interface. For this case, one might predict that photoemission experiments would show chemical shifts and line broadening associated with the presence of Al at the interface without there being any effect on the valence-band offset between Ge and GaAs.

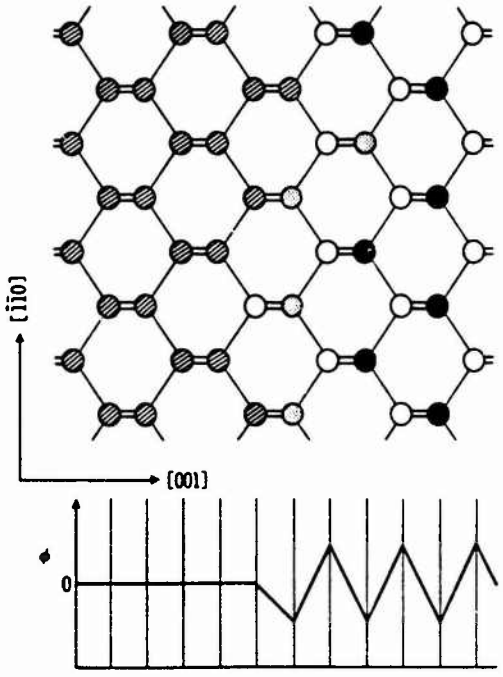

FIG. 3. A (001) heterojunction as in Figs. 1 and 2 but with three transition planes. The first is $\frac{1}{4}$ As and $\frac{3}{4}$ Ge. The second is $\frac{3}{4}$ Al and $\frac{1}{4}$ Ge, and the third is $\frac{3}{4}$ Ga and $\frac{1}{4}$ Al. This is the simplest junction geometry which eliminates both the interface dipole and the charge accumulation. The valence-band offset for this reconstruction depends only on the bulk properties of Ge and GaAs.

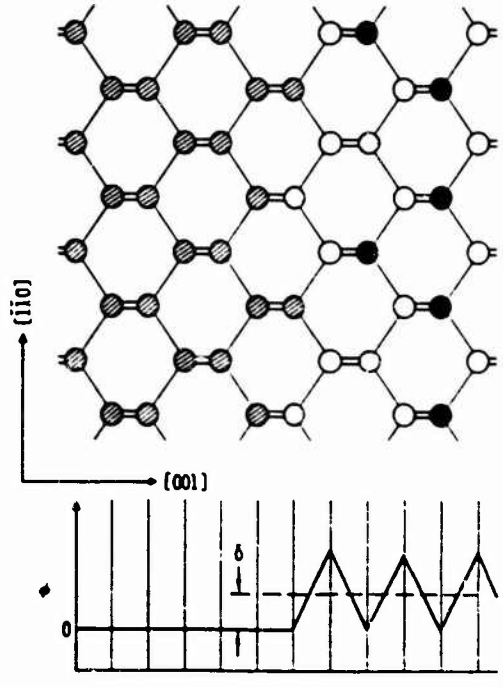

FIG. 2. A (001) heterostructure as in Fig. 1 but with $\frac{1}{2}$ of the Al atoms replaced by Ge atoms and a $\frac{1}{2}$ monolayer of Al on the next Ga plane. The average electric field in the GaAs has been eliminated but there is still a dipole shift δ much larger than is experimentally observed (Ref. 1). The dipole shift is not eliminated by bond polarization (Ref. 5).

It is clear that by varying the Al, Ga, and As atomic composition over a few interface planes separating bulk Ge from bulk GaAs, different interface dipoles, including zero, can be obtained. Therefore, an experimental observation[1] that the valence-band offset at a polar heterojunction interface is not affected by the presence of a monolayer or more of an isovalent impurity does not prove that band offsets are interface-independent bulk semiconductor properties in general. Crystallographic orientation dependence,[2] growth sequence dependence,[4] and nontransitivity[3] remain important interface-dependent phenomena affecting the magnitudes of heterojunction band discontinuities and providing important information about the interface. Although these phenomena may not occur at all heterojunction interfaces, they are likely to be important in systems involving an interface which involves growth of a compound semiconductor on an elemental semiconductor such as CuBr on Ge[3] or GaAs on Ge.[6,7] A theory of heterojunction band discontinuities should be broad enough to include these phenomena even though they may not occur in every case. The conclusions reached here also apply to the Ge/In/GaAs(100), Si/Ga/AlP(100), and α-Sn/Ga/InSb(100) interfaces, and their (111) equivalents, obtained by starting from Ge/α-Sn/Ge, Si/Ge/Si, and α-Sn/Ge/α-Sn covalent heterostructures.

In summary, a method has been presented for obtaining polar heterojunction interfaces with an isovalent interlayer

by starting from a semiconductor heterostructure and transferring protons between adjacent atomic planes. It has been shown that the resulting interface dipole can be eliminated by a reconstruction involving as few as three atomic planes. Finally, the absence of any experimentally detectable effect of an isovalent interlayer on a heterojunction band lineup suggests that such a dipole-reducing reconstruction may have occurred and is not necessarily an indication that polar heterojunction band lineups are interface independent.

This work was supported by the U.S. Office of Naval Research under Contract No. N00014-85-C-0135.

[1]A. D. Katnani and R. S. Bauer, in *Proceedings of the 12th Annual Conference on the Physics and Chemistry of Semiconductor Interfaces, Tempe, AZ, 1985,* edited by R. S. Bauer [J. Vac. Sci. Technol. B (to be published)].

[2]R. W. Grant, J. R. Waldrop, and E. A. Kraut, Phys. Rev. Lett. 40, 656 (1978).

[3]J. R. Waldrop and R. W. Grant, Phys. Rev. Lett. 43, 1686 (1979).

[4]J. R. Waldrop, S. P. Kowalczyk, R. W. Grant, E. A. Kraut, and D. L. Miller, J. Vac. Sci. Technol. 19, 573 (1981).

[5]W. A. Harrison, E. A. Kraut, J. R. Waldrop, and R. W. Grant, Phys. Rev. B 18, 4402 (1978).

[6]P. Zurcher and R. S. Bauer, J. Vac. Sci. Technol. A 1, 695 (1983).

[7]R. W. Grant, J. R. Waldrop, S. P. Kowalczyk, and E. A. Kraut, in *Proceedings of the 12th Annual Conference on the Physics and Chemistry of Semiconductor Interfaces, Tempe, AZ, 1985,* edited by R. S. Bauer [J. Vac. Sci. Technol. B (to be published)].

Surface Science 168 (1986) 498–506
North-Holland, Amsterdam

HETEROJUNCTION BAND DISCONTINUITIES FOR GaAs GROWN ON Ge(110): TIME VARIATION

R.W. GRANT, J.R. WALDROP, S.P. KOWALCZYK and E.A. KRAUT

Rockwell International Corporation, Microelectronics Research and Development Center, Thousand Oaks, California 91360, USA

Received 10 June 1985; accepted for publication 3 July 1985

The valence-band discontinuity, ΔE_v, for heterojunctions formed by growing GaAs on epitaxial Ge(110) layers has been observed to exhibit a continuous decrease with time for ≈100 h after interface formation. These new results are compared with previous measurements for heterojunctions formed by growing GaAs on sputter-annealed Ge(110) substrates. It is found that the magnitude of the ΔE_v variation and the associated time constant depend somewhat on interface preparation variables. Because the time-dependent ΔE_v variation is observed for GaAs grown on both epitaxial Ge(110) layers and on Ge(110) substrates, it appears to be a characteristic feature of GaAs grown on Ge interfaces.

1. Introduction

The band discontinuities between epitaxial Ge and GaAs have been the subject of considerable experimental study [1–16], due, at least in part, to the possibility of utilizing Ge–GaAs heterojunctions and superlattices in semiconductor device applications. It has been observed [12,13,16] that the valence-band discontinuity, ΔE_v, for GaAs grown epitaxially on Ge(110) is substantially smaller than for the reverse growth sequence*, i.e.

$$\Delta E_v[\text{GaAs/Ge(110)}] < \Delta E_v[\text{Ge/GaAs(110)}].$$

The growth of a compound semiconductor (e.g., GaAs) on an elemental semiconductor (e.g., Ge) involves an ambiguity in nucleation site which may produce antiphase disorder; it may be necessary to eliminate this disorder if device quality GaAs/Ge interfaces are to be prepared [17,18]. Heterojunction formation between GaAs and Ge on polar surfaces is influenced by atomic exchange across the interface to satisfy electrostatic considerations [19]. However, on non-polar surfaces (i.e. (110)), the energetics of atomic exchange

* In this paper, A/B refers to a heterojunction formed by growing A on B, while A–B refers to a heterojunction without specifying the growth sequence.

0039-6028/86/$03.50 © Elsevier Science Publishers B.V.
(North-Holland Physics Publishing Division)

across an interface is associated primarily with bonds formed or broken during the exchange. Tight-binding theory has been used [20] to calculate energies of atomic substitutions; these calculations indicate that atomic exchange is not favored at an ideal Ge–GaAs interface. However, at a GaAs/Ge(110) interface, where antiphase domain disorder exists, there are bonds between like atoms and these atoms may favor exchange. It has been suggested that atomic exchange of Ge and As atoms at the intersection of As antiphase domain boundaries with the Ge(110) substrate may be responsible for the observed Ge–GaAs(110) ΔE_v growth sequence effect [16].

A new phenomenon was observed recently [16] in a study of GaAs grown epitaxially on Ge(110). It was found that ΔE_v decreased with time for ≈100 h after interface formation. This time variation had an exponential form and the associated rate constant appeared to increase with temperature. No time-dependent variation of ΔE_v has been noted for the Ge/GaAs(110) interface. The time-dependent ΔE_v variation for the GaAs/Ge(110) interface may be a direct result of the Ge and As atomic exchange mechanism proposed to account for the ΔE_v growth sequence effect. The initial study only involved growth of GaAs on sputter-annealed Ge(110) surfaces. To investigate the possibility that the sputter–anneal cycle may be related to the GaAs/Ge(110) interface instability, new measurements have been performed for GaAs grown on epitaxial Ge(110) layers. These new results show that the time-dependent ΔE_v variation is observed for GaAs/Ge(110) heterojunctions formed by growing GaAs on surfaces of either epitaxial or sputter-annealed Ge(110).

2. Experimental

An X-ray photoelectron spectroscopy (XPS) technique was used for the ΔE_v measurements. This technique has been described previously in detail [21,22]. A HP5950A XPS spectrometer was used which employs monochromatic Al Kα (1486.6 eV) radiation. The GaAs/Ge(110) heterojunctions were prepared in a UHV sample preparation chamber which is attached to the spectrometer.

A schematic of the heterojunction samples is shown in fig. 1. The Ge(110) substrates were purchased from Eagle-Picher Industries, Inc. To remove polishing damage, the substrates were etched in $3HNO_3$:$5CH_3COOH$:3HF for a few minutes immediately before insertion into the XPS spectrometer. A clean and ordered Ge(110) substrate was prepared by sputtering with 1 keV Ar^+ ions and annealing at 600°C for ≈30 s. The room-temperature low-energy electron diffraction (LEED) pattern associated with this substrate was complex and resembled the c(8×10) pattern reported by Olshanetsky et al. [23]. No oxygen or carbon contamination was detectable by XPS. Epitaxial Ge layers were grown in situ at a deposition rate of ≈15 Å/min with the

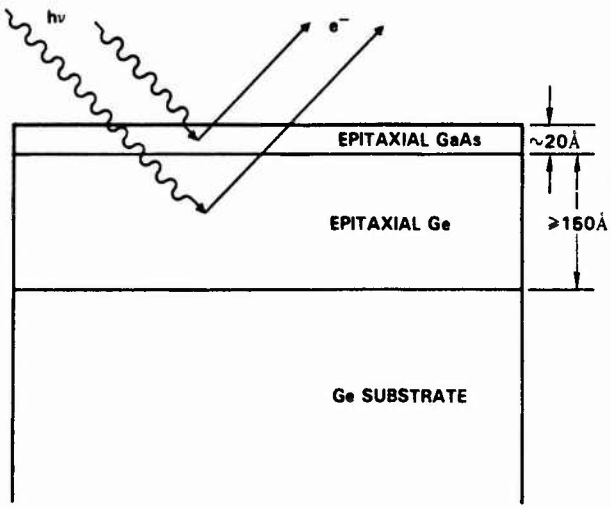

Fig. 1. Schematic illustration of GaAs/Ge(110) sample geometry.

substrate held at ≈450°C. For samples A and B, the epitaxial Ge layers were ≈500 and ≈150 Å thick, respectively, as estimated by using a quartz crystal deposition monitor. The escape depth of Ge 3d photoelectrons (kinetic energy ≈1450 eV) is ≈25 Å; as suggested in fig. 1, only the epitaxial Ge layer was sampled during the XPS ΔE_v measurements.

Following Ge epitaxial growth, sample A was immediately (in a few minutes) cooled to room temperature. Sample B was annealed at 600°C for ≈30 s before cooling to room temperature to reproduce the same annealing conditions used to prepare the sputter-annealed Ge(110) surfaces employed in the previous [16] GaAs/Ge(110) heterojunction studies. The LEED patterns for both epitaxial Ge(110) surfaces were complex; although the integral-order spots were sharp, the fractional-order spots were not as clearly resolved as for the sputter-annealed surfaces. No carbon or oxygen impurities were detected by XPS.

The epitaxial Ge(110) surfaces were dosed initially with As by exposing the heated (≈350°C) surface to an As_4 beam; the exposure was ≈30 L. Thin epitaxial layers of GaAs were grown on these As-dosed surfaces by molecular beam epitaxy. The GaAs growth temperature was ≈350°C and the As_4/Ga flux ratio was ≈ 5:1. The GaAs layer thicknesses for samples A and B were ≈22 and ≈24 Å, respectively, as measured by XPS. Following growth, LEED was used to confirm epitaxy and surface cleanliness (no detectable carbon or oxygen) was assessed by XPS. The ΔE_v measurements were initiated as soon as possible thereafter.

To facilitate comparison of results obtained with GaAs/epitaxial Ge(110)

and with GaAs/sputter-annealed Ge(110) heterojunctions, a set of data for the latter case (sample C) is reproduced from ref. [16]. The Ge(110) surface for sample C was sputtered with 2 keV Ar^+ ions, annealed at ≈600°C for ≈30 s, and was dosed with As prior to GaAs growth in the same manner as the epitaxial Ge layers. The GaAs growth conditions were the same as for samples A and B; the GaAs layer thickness for sample C was ≈25 Å.

Fig. 2 shows a typical XPS spectrum (obtained from sample A) in the binding-energy region which contains the Ga 3d, Ge 3d and As 3d core levels. Spectra similar to that shown in fig. 2 were recorded at several times (t) following interface formation. The accumulation of data with counting statistics similar to that shown in fig. 2 required several (4–12) hours. The 10–60 eV binding-energy region data were obtained by repeatedly scanning (several hundred times) this spectral region during the data accumulation period.

Fig. 3 shows XPS data (for sample A) at (a) t = 3 h and (b) t = 249.5 h. Because data collection required several hours, t was taken as the midpoint of the data accumulation period. The data in fig. 3 are plotted relative to the center of the Ga 3d photoelectron line (note breaks in the energy scale). For ease of comparison, each peak has been normalized to equal intensity. The peak center is defined as the half width at half height. The solid lines in fig. 3 define the peak centers at t = 3 h, while the dashed lines are peak centers at t = 249.5 h. A large increase (0.30 eV) is observed in the Ge 3d to Ga 3d core-level binding-energy difference $E^{Ge}_{Ge\,3d} - E^{GaAs}_{Ga\,3d}$ for the t = 249.5 h data as

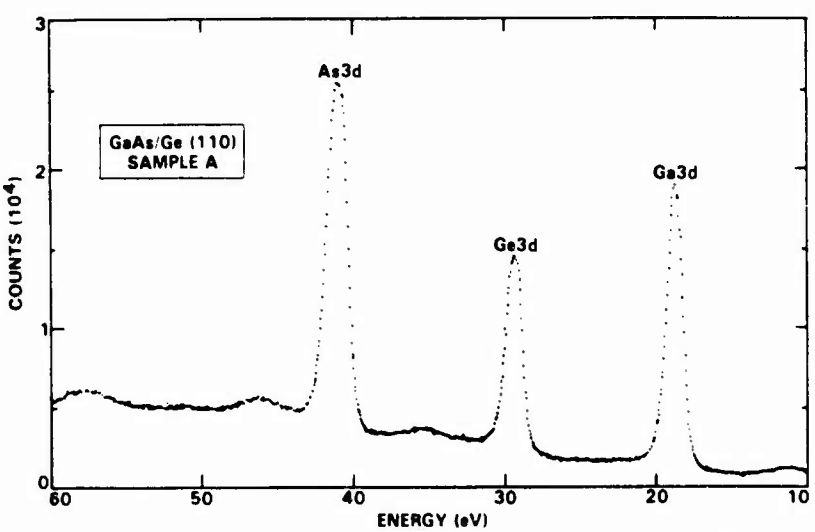

Fig. 2. Typical XPS spectrum of a GaAs/epitaxial Ge(110) sample in the Ga 3d, Ge 3d and As 3d core-level region

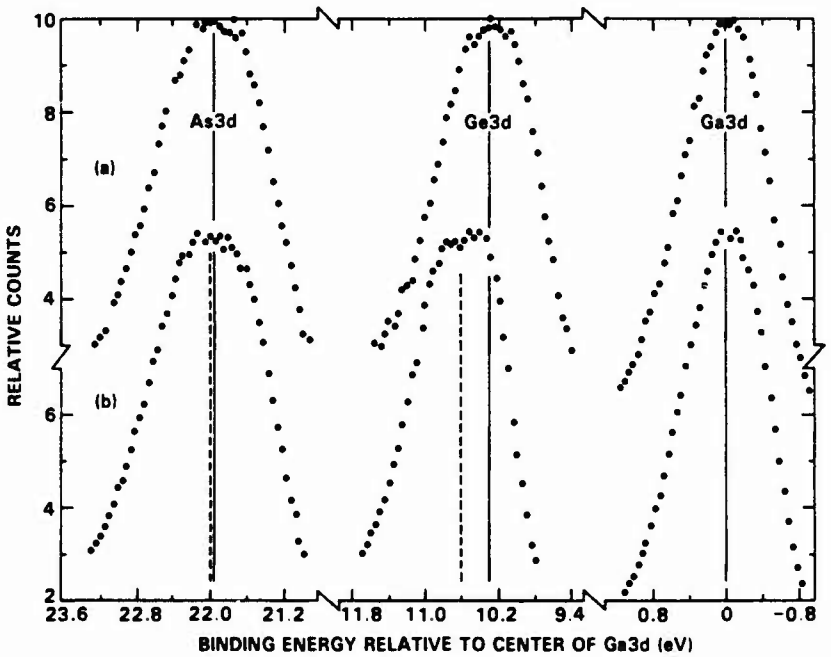

Fig. 3. XPS spectrum in the region of the Ga 3d, Ge 3d and As 3d core levels obtained for sample A at (a) t = 3 h and (b) t = 249.5 h. The binding-energy scale is relative to the Ga 3d core level. The solid vertical lines are the peak centers at t = 3 h; the dashed vertical lines are the peak centers at t = 249.5 h.

compared to the t = 3 h data. (A much smaller increase (0.05 eV) in the As 3d to Ga 3d core-level binding-energy difference $E^{GaAs}_{As\,3d} - E^{GaAs}_{Ga\,3d}$ is also noted.)

3. Results and conclusions

The core-level binding-energy difference, $E^{Ge}_{Ge\,3d} - E^{GaAs}_{Ga\,3d}$, measured as a function of t for samples A, B and C is plotted in fig. 4. This binding-energy difference is related [10] to ΔE_v (in eV) by

$$\Delta E_v = (E^{Ge}_{Ge\,3d} - E^{Ge}_v) - (E^{GaAs}_{Ga\,3d} - E^{GaAs}_v) - (E^{Ge}_{Ge\,3d} - E^{GaAs}_{Ga\,3d}), \quad (1)$$

where $E^{Ge}_{Ge\,3d} - E^{Ge}_v$ and $E^{GaAs}_{Ga\,3d} - E^{GaAs}_v$ are the Ge 3d and Ga 3d core-level binding energies relative to the valence-band maximum in bulk Ge and GaAs, respectively. Values of these quantities are $E^{Ge}_{Ge\,3d} - E^{Ge}_v = 29.57 \pm 0.03$ eV and $E^{GaAs}_{Ga\,3d} - E^{GaAs}_v = 18.80 \pm 0.03$ eV [21]. Thus, ΔE_v (in eV) for GaAs/Ge heterojunctions is

$$\Delta E_v = 10.77 - (E^{Ge}_{Ge\,3d} - E^{GaAs}_{Ga\,3d}) \quad (2)$$

and a change in $E^{Ge}_{Ge\,3d} - E^{GaAs}_{Ga\,3d}$ directly represents an equal change in ΔE_v. The right-hand scale in fig. 4 shows the value of ΔE_v.

The photoelectron peak linewidths, peak area ratios, and $E^{GaAs}_{As\,3d} - E^{GaAs}_{Ga\,3d}$ were also determined as a function of t. The small increase observed in $E^{GaAs}_{As\,3d} - E^{GaAs}_{Ga\,3d}$ (see fig. 3) most likely is associated with a change in GaAs surface chemical shifts due to a slight surface carbon accumulation for large t. A slight decrease in the Ge 3d linewidth with t was also suggested which might be associated with the long data accumulation period and rapid initial variation in ΔE_v. No other time-dependent change in the spectral parameters was observed.

A semilog plot of $\Delta E_v(t) - \Delta E_v(\infty)$ is shown in fig. 5 for samples A, B and C. The straight lines through the data were obtained by a least-squares

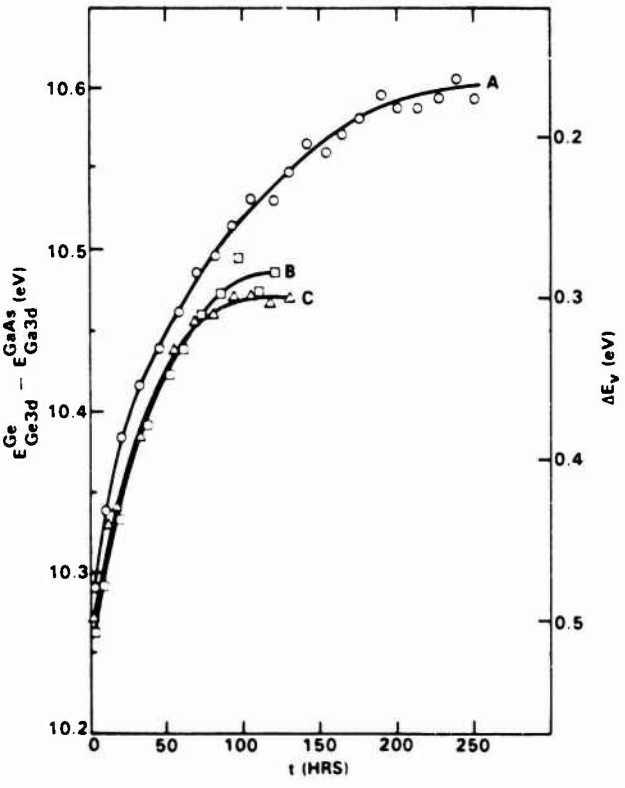

Fig. 4. Variation of $E^{Ge}_{Ge\,3d} - E^{GaAs}_{Ga\,3d}$ and of ΔE_v versus time after interface formation for GaAs/Ge(110) samples. The GaAs was grown on epitaxial Ge layers for samples A and B, and on a sputter-annealed Ge surface for sample C.

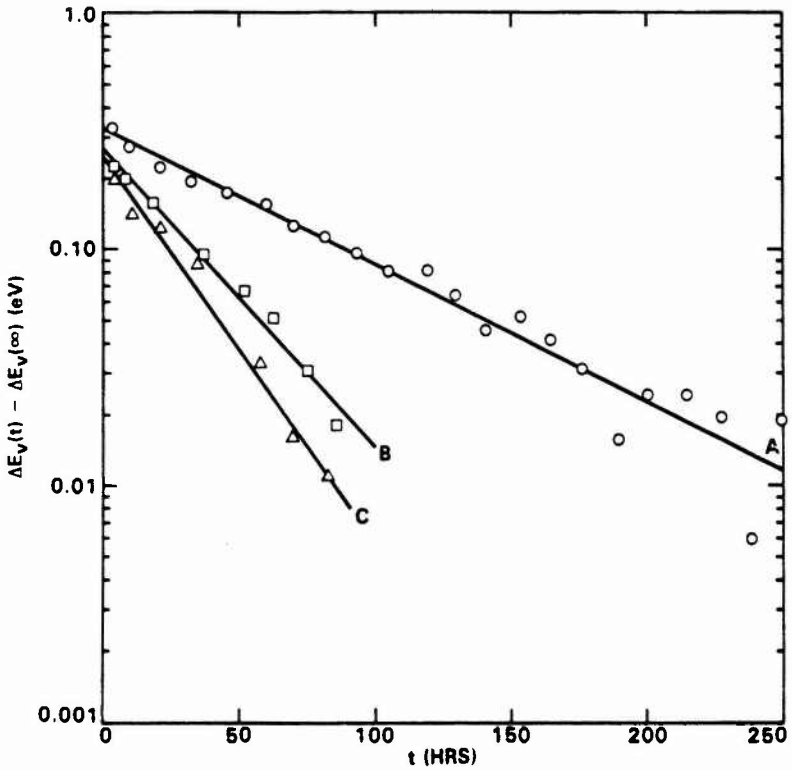

Fig. 5. Semilog plot of $\Delta E_v(t) - \Delta E_v(\infty)$ versus t for samples A, B and C.

fit. To a good approximation, the data have an exponential behavior of the form

$$\Delta E_v(t) - \Delta E_v(\infty) = [\Delta E_v(0) - \Delta E_v(\infty)] \exp(-t/\tau), \tag{3}$$

where τ^{-1} is a rate constant. The values of τ^{-1} for samples A, B and C are 0.013 h^{-1}, 0.029 h^{-1} and 0.038 h^{-1}, respectively. The data for samples B and C are similar. A common feature of these two samples was the brief ($\approx$30 s) 600°C anneal which followed either the expitaxial Ge growth (sample B) or the sputter–anneal Ge surface preparation (sample C) and preceded the GaAs epitaxial growth. For sample A, both τ and $\Delta E_v(\infty)$ are substantially larger than for the other two samples. This may suggest a dependence of interface structure on the Ge annealing temperature (450°C versus 600°C) used prior to GaAs growth.

The primary conclusion from these experiments is that the previously reported [16] GaAs/Ge(110) interface instability is observed for heterojunctions prepared both on sputter-annealed Ge(110) substrates and on epitaxial

Ge(110) layers. The magnitude of $\Delta E_v(\infty)$ and the time constant which approximates the ΔE_v versus t behavior may depend on variations in the antiphase disorder, as determined by variations in the Ge(110) surface prior to interface formation. The time-dependent variation of ΔE_v is consistent with the model that atomic exchange of As and Ge atoms occurs as a result of antiphase domain disorder at GaAs/Ge(110) heterojunctions. The variation of ΔE_v with time after interface formation may be observable at other heterojunction interfaces where antiphase domain disorder is expected (e.g., ZnSe/Ge(110)), and where ΔE_v growth sequence dependence has been reported [24].

Acknowledgement

This work was supported by the Office of Naval Research, Contract No. N00014-85-C-0135.

References

[1] R.L. Anderson, Solid State Electron. 5 (1962) 341.
[2] F.F. Fang and W.E. Howard, J. Appl. Phys. 35 (1964) 612.
[3] R.W. Grant, J.R. Waldrop and E.A. Kraut, Phys. Rev. Letters 40 (1978) 656; J. Vacuum Sci. Technol. 15 (1978) 1451.
[4] R.S. Bauer and J.C. McMenamin, J. Vacuum Sci. Technol. 15 (1978) 1444.
[5] P. Perfetti, D. Denley, K.A. Mills and D.A. Shirley, Appl. Phys. Letters 33 (1978) 667.
[6] E.A. Kraut, R.W. Grant, J.R. Waldrop and S.P. Kowalczyk, Phys. Rev. Letters 44 (1980) 1620.
[7] W. Mönch, R.S. Bauer, H. Gant and R. Murschall, J. Vacuum Sci. Technol. 21 (1982) 498.
[8] R.S. Bauer and J.C. Mikkelsen, Jr., J. Vacuum Sci. Technol. 21 (1982) 491.
[9] P. Chen, D. Bolmont and C.A. Sébenne, J. Phys. C15 (1982) 6101.
[10] J.R. Waldrop, E.A. Kraut, S.P. Kowalczyk and R.W. Grant, Surface Sci. 132 (1983) 513.
[11] S.P. Kowalczyk, R.W. Grant, J.R. Waldrop and E.A. Kraut, J. Vacuum Sci. Technol. B1 (1983) 684.
[12] P. Zurcher and R.S. Bauer, J. Vacuum Sci. Technol. A1 (1983) 695.
[13] R.S. Bauer, P. Zurcher and H.W. Sang, Jr., Appl. Phys. Letters 43 (1983) 663.
[14] P. Chiaradia, A.D. Katnani, H.W. Sang, Jr. and R.S. Bauer, Phys. Rev. Letters 52 (1984) 1246.
[15] A.D. Katnani, P. Chiaradia, H.W. Sang, Jr. and R.S. Bauer, J. Vacuum Sci. Technol. B2 (1984) 471; J. Electron. Mater. 14 (1985) 25.
[16] R.W. Grant, J.R. Waldrop, S.P. Kowalczyk and E.A. Kraut, J. Vacuum Sci. Technol. B3 (1985) 1295.
[17] H. Kroemer, Surface Sci. 132 (1983) 543.
[18] H. Kroemer, in: Proc. of the NATO Advanced Study Institute on Molecular Beam Epitaxy and Heterostructures, Erice, Sicily, 1983, Eds. L.L. Chang and K. Ploog (Nijhoff, The Hague, 1984).
[19] W.A. Harrison, E.A. Kraut, J.R. Waldrop and R.W. Grant, Phys. Rev. B18 (1978) 4402.

[20] E.A. Kraut and W.A. Harrison, J. Vacuum Sci. Technol. B2 (1984) 409; B3 (1985) 1267.
[21] E.A. Kraut, R.W. Grant, J.R. Waldrop and S.P. Kowalczyk, Phys. Rev. B28 (1983) 1965.
[22] R.W. Grant, E.A. Kraut, S.P. Kowalczyk and J.R. Waldrop, J. Vacuum Sci. Technol. B1 (1983) 320.
[23] B.Z. Olshanetsky, S.M. Repinsky and A.A. Shklyaev, Surface Sci. 64 (1977) 224.
[24] S.P. Kowalczyk, E.A. Kraut, J.R. Waldrop and R.W. Grant, J. Vacuum Sci. Technol. 21 (1982) 482.

GaAs–Ge heterojunction interfaces: Cyclical behavior of band discontinuities

J. R. Waldrop, R. W. Grant, and E. A. Kraut
Rockwell International Corporation, Thousand Oaks, California 91360

(Received 29 January 1986; accepted 7 April 1986)

The valence band discontinuity ΔE_v of (110) and (100) oriented heterojunctions made by growth of GaAs onto Ge (GaAs–Ge) is found to decrease with time after interface formation (on a scale of tens of hours). The thin, abrupt heterojunction samples were prepared by molecular beam epitaxy techniques and characterized by x-ray photoemission spectroscopy. The final room temperature value of ΔE_v (GaAs-) is >0.2 eV lower than the ~ 0.56 eV value for the stable Ge–GaAs (reverse growth sequence) interface. Annealing a sample for several minutes in vacuum at the growth temperature increases ΔE_v (GaAs–Ge) to approximately the Ge–GaAs value. By control of anneal time and an accompanying As overpressure, ΔE_v (GaAs–Ge) can be cycled by >0.2 eV. This variation in an interface electrostatic dipole is apparently related to a variable amount of electrically active As that is located at the heterojunction interface. The dipole formation mechanism involved may require the presence of the antiphase disorder that is expected for growth of GaAs on Ge.

I. INTRODUCTION

Knowledge of the factors that control and influence heterojunction band discontinuities is both of fundamental interest and of use in practical applications. A customary assumption to simplify the formulation of models[1–4] to predict the magnitude of band offsets is to ignore the contribution of interface effects. Experimental investigation of the size and origin of interface contributions to band discontinuities can thus help determine the cases when a refined model that incorporates such effects is appropriate. An example of a sizable interface effect is the growth sequence dependence of the valence band discontinuity ΔE_v for the (110) oriented Ge/GaAs heterojunction pair, where ΔE_v for the Ge grown on GaAs interface [designated ΔE_v (Ge–GaAs)] is substantially larger than ΔE_v (GaAs–Ge) for the reverse grown interface.[5–7] Another effect that is associated with the growth sequence of the (110) interface has recently been observed,[7] whereby ΔE_v (GaAs-Ge) has a remarkable change (>0.2 eV) with time after interface formation (no time dependence has been observed for the Ge–GaAs interface); over 100 h were required for ΔE_v (GaAs–Ge) to obtain a constant value.

In this paper the time dependent nature of ΔE_v is further investigated for both (110) and (100) oriented GaAs–Ge heterojunction interfaces. The samples were prepared by molecular beam epitaxy (MBE) techniques and characterized by x-ray photoemission spectroscopy (XPS). For both (110) and (100) crystallographic orientations, ΔE_v was found to have a cyclical variation in magnitude as a function of time, temperature, and sample exposure to elemental As.

II. EXPERIMENTAL

The method of using XPS to measure heterojunction band discontinuities has been discussed in detail elsewhere.[8] The XPS system is a HP5950A electron spectrometer ($h\nu = 1486.6$ eV monochromatic x-ray source) that is coupled to a custom ultrahigh vacuum (10^{-10} Torr range) sample preparation chamber. The photoelectron escape depth for the photoelectron kinetic energies analyzed and emission angle used is ~ 16 Å. The structure of the heterojunction samples is illustrated in Fig. 1(a). To prepare a sample, an $\sim 8 \times 8$ mm piece of bulk Ge wafer, either (110) or (100) orientation, is etched for several minutes in 3:5:3 HNO_3:CH_3COOH:HF to remove polishing damage, quenched in H_2O, dried, then put into the XPS system. Sputtering with 1 keV Ar^+ ions followed by annealing at 600 °C for 30 s produced a clean and ordered Ge surface. The low energy elec-

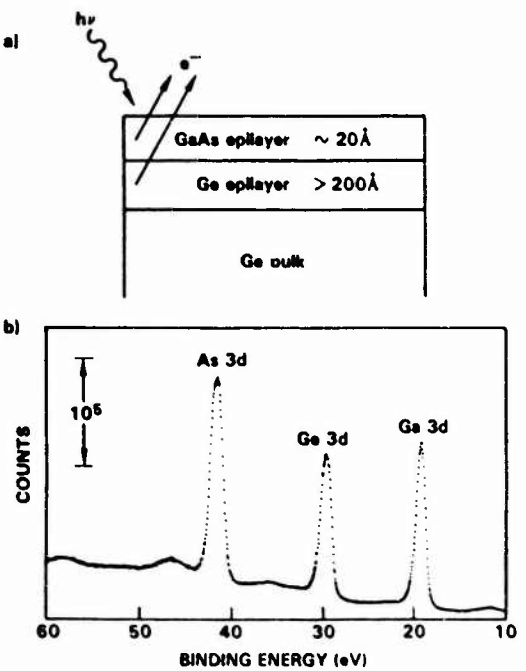

FIG. 1. (a) Structure of the GaAs–Ge heterojunction samples. (b) Representative XPS binding energy spectrum of a GaAs–Ge (110) sample in the region of the Ga 3*d*, Ge 3*d*, and As 3*d* core levels.

 0734-211X/86/041060-04$01.00 © 1986 American Vacuum Society

tron diffraction (LEED) pattern for the (110) surface was complex and resembled a $c(8\times10)$ pattern[9]; the (100) surface LEED pattern[9] was $c(4\times2)$. A >200 Å thick Ge epitaxial layer was grown onto the Ge bulk material at a substrate temperature of ~450 °C and a 0.5–1 Å/s growth rate. The LEED patterns from the epitaxial Ge layer surfaces were the same as those of the starting substrate surfaces.

Each sample had a thin, ~20 Å thickness, GaAs epitaxial layer grown onto the Ge epilayer by MBE at a substrate temperature of ~325 °C. The Ge surfaces were exposed to ~10 L of As_4 at the growth temperature prior to GaAs growth, which then proceeded with a As_4/Ga flux ratio of $\sim5{:}1$ and ~5 Å/min rate. LEED was used to confirm epitaxial growth of the GaAs; no C or O in the samples was detectable by XPS.

For a thin, abrupt heterojunction sample in which the interface is at a distance comparable to the XPS photoelectron escape depth from the surface, as in the present case, photoelectrons that originate from each side of the interface will be observed in the same XPS spectrum. For example, Fig. 1(b) is a representative 10–60 eV binding energy spectrum from a GaAs–Ge (110) sample that contains the Ga 3*d* and As 3*d* core level peaks from the GaAs epilayer and the Ge 3*d* core level peak from the underlying Ge epilayer.

Figure 2(a) is a schematic energy band diagram of the interface region of a GaAs–Ge (or Ge–GaAs) heterojunction, where E_c and E_v are conduction and valence bands, respectively, and $\Delta E_{CL} = (E^{Ge}_{Ge\,3d} - E^{GaAs}_{Ga\,3d})$ is the binding energy difference across the interface between the Ge 3*d* core level in the Ge and the Ga 3*d* core level in the GaAs. By inspection, $\Delta E_v = (E^{Ge}_{Ge\,3d} - E^{Ge}_v) - (E^{GaAs}_{Ga\,3d} - E^{GaAs}_v) - \Delta E_{CL}$, where the $(E^{Ge}_{Ge\,3d} - E^{Ge}_v)$ and $(E^{GaAs}_{Ga\,3d} - E^{GaAs}_v)$ terms are Ge and GaAs bulk material constants that have previously been determined[10] to be 29.57 ± 0.03 and 18.80 ± 0.03 eV, respectively. Thus, $\Delta E_v = 10.77 - \Delta E_{CL}$ eV. This relation also indicates that a change observed in ΔE_{CL}, as a result of some sample treatment for example, is a direct measure of the change that also has occurred in ΔE_v [i.e., $\delta(\Delta E_v) = -\delta(\Delta E_{CL})$]. Figure 2(b) illustrates the precision measurement of ΔE_{CL}, which for this example is the data in Fig. 1(b). A background function that is proportional to the integrated photoelectron peak intensity is first subtracted from each core level peak. The binding energy of a core level peak is then measured at the half-width point at half-height. The peak height and width are consistently determined by using a computerized algorithm that involves a third order least square fit to segments at the sides and top of the discrete peak data. With this method ΔE_{CL} is reproducibly measured to ±0.01 eV. Thus, although the measurement uncertainty of an absolute ΔE_v value is ±0.04 eV because of the uncertainty in the $(E_{CL} - E_v)$ values, the relative changes in ΔE_v for a given sample (and the sample-to-sample comparison of ΔE_v differences) are measured to ±0.01 eV.

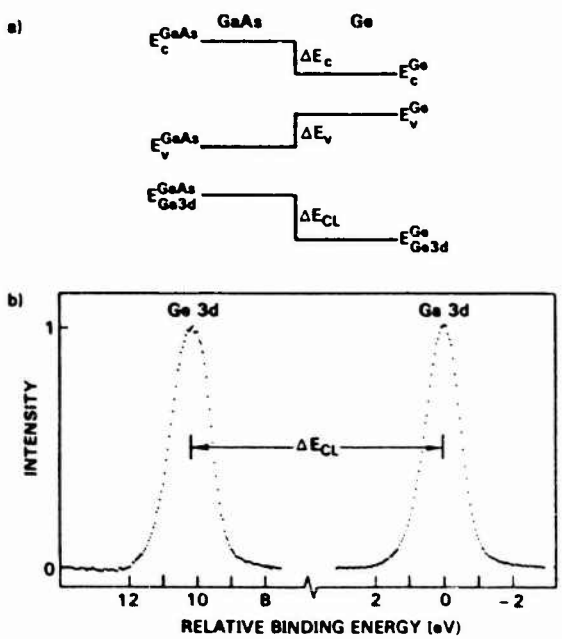

FIG. 2. (a) Schematic energy band diagram of the GaAs–Ge interface. (b) Measurement of $\Delta E_{CL} = (E^{Ge}_{Ge\,3d} - E^{GaAs}_{Ga\,3d})$ (data from spectrum in Fig. 1).

The $(E^{GaAs}_{As\,3d} - E^{GaAs}_{Ga\,3d})$ difference, As 3*d* linewidth, and the Ga 3*d*/As 3*d* and Ga 3*d*/Ge 3*d* peak area ratios were also measured in each 10–60 eV spectrum. These data and the Ga 3*d* and Ge 3*d* linewidth data showed no evidence of interface chemical effects. The attenuation of the Ge 3*d* peak intensity after GaAs growth relative to that of the initial Ge substrate was used to evaluate the GaAs thickness. This peak attenuation data and the absence of a detectable characteristic Ge LEED pattern after GaAs overlayer coverage were both consistent with a uniform growth mode. Recent, more direct, data relating to the morphology of GaAs on Ge in the initial epitaxial growth regime indicate that island growth can occur.[11] The relatively low growth temperature used to prepare our XPS samples may have helped, however, to minimize island formation.

Two (110) oriented samples and one (100) oriented sample were prepared. A sequence of XPS spectra such as shown in Fig. 1 was collected at intervals during the time t after GaAs–Ge interface formation. Each spectrum required several hours of data accumulation time. Hence, the t for a ΔE_{CL} (ΔE_v) data point is measured to the midpoint of each spectrum accumulation period. In the course of a ΔE_{CL} vs t measurement sequence, which in each case lasted longer than 100 h, a sample was at times cycled to the GaAs epilayer growth temperature (~325 °C), either with or without an As overpressure, for a duration of several minutes (XPS data were always obtained at room temperature). The 10^{-6} Torr As overpressure and the ~325 °C anneal temperature were used to reproduce the initial MBE GaAs growth conditions. These short temperature and As exposure cycles tested the stability of the interface with respect to ΔE_v.

III. RESULTS

Figure 3 is a plot of $\Delta E_{CL} = (E^{Ge}_{Ge\,3d} - E^{GaAs}_{Ga\,3d})$ vs t (and corresponding ΔE_v) for one of the (110) samples. Interval I is the initial period after growth. At $t = 41.9$ h the sample was annealed in vacuum at the growth temperature (~325 °C) for 10 min. Interval II is the period subsequent to this anneal.

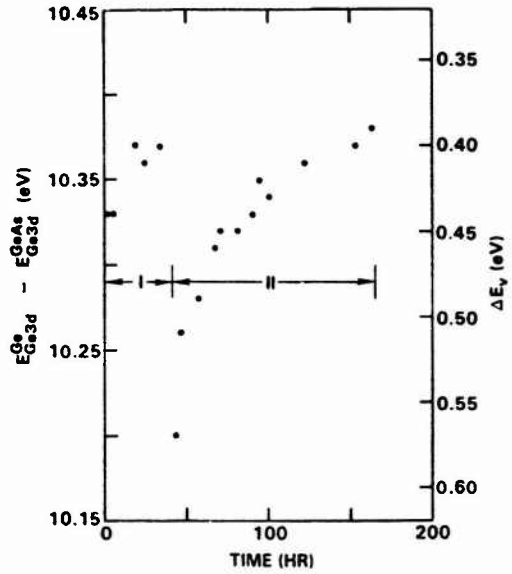

FIG. 3. Plot of ΔE_{CL} and of the corresponding ΔE_v vs time after interface formation for a GaAs grown on Ge (110) interface. Interval I: as grown; Interval II: after 10 min vacuum anneal (details in text).

The other (110) sample was subjected to several anneal and As exposure treatments after interface formation. In the ΔE_{CL} (ΔE_v) plot shown in Fig. 4 interval I is after growth. A 10 min vacuum anneal was given at $t = 65.4$ h (the data point at the boundary of intervals I and II is the result). This anneal was followed by an additional 20 min vacuum anneal. Interval II is thus after a 30 min total vacuum anneal. Between II and III, at $t = 158.9$ h, the sample was annealed 5 min with As overpressure. Interval IV is after a 20 min vacuum anneal at $t = 230.8$ h. At the start of interval V, $t = 277.8$ h, the sample was again annealed for 5 min with As overpressure. To summarize, intervals I, III, and V are after the sample was at the GaAs growth temperature in an As overpressure; intervals II and IV are after a vacuum anneal at the growth temperature.

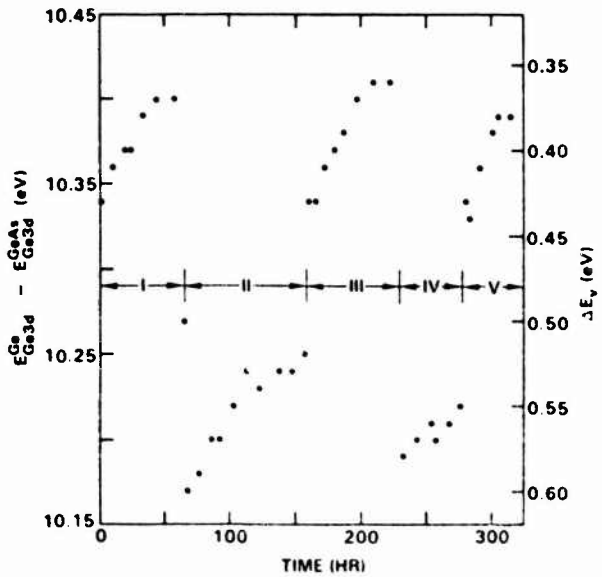

FIG. 4. Plot of ΔE_{CL} and of ΔE_v vs time after interface formation for another GaAs–Ge (110) interface. Interval I: as grown; Interval II: after 30 min vacuum anneal; Interval III: after 5 min As anneal; Interval IV: after 20 min vacuum anneal; Interval V: after 5 min As anneal.

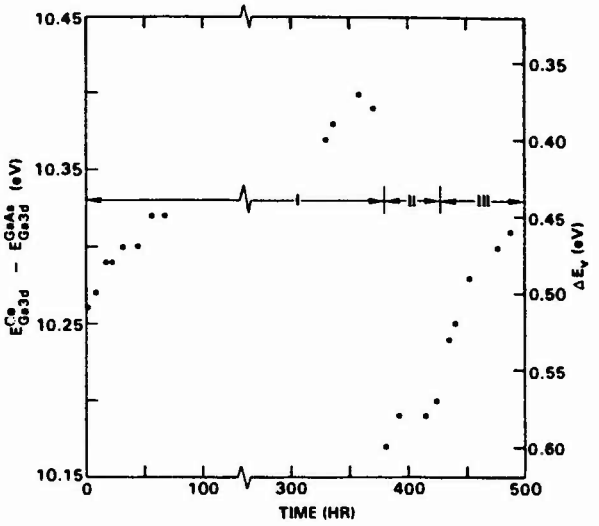

FIG. 5. Plot of ΔE_{CL} and of ΔE_v vs time after interface formation for a GaAs–Ge (100) interface. Interval I: as grown; Interval II: after 20 min vacuum anneal; Interval III: after 5 min As anneal.

The ΔE_{CL} vs t data for the (100) sample are shown in Fig. 5. Interval I extended to 380.4 h after growth, at which time there was a 20 min vacuum anneal prior to interval II. Between intervals II and III, at 426.1 h, the sample was annealed 5 min with As overpressure.

The range of ΔE_{CL} in Figs. 3–5 is > 0.2 eV for each sample. In comparison, the corresponding values of the ($E^{GaAs}_{As\,3d} - E^{GaAs}_{Ga\,3d}$) core level binding energy difference for a given sample showed in every instance only small $\sim \pm 0.02$ eV variations. Similarly, the Ga 3*d*, As 3*d*, and Ge 3*d* linewidths exhibited random fluctuations of $\sim \pm 0.03$ eV.

IV. DISCUSSION

The slow decrease in ΔE_v with time after initial interface formation observed in these (110) and (100) oriented samples is consistent with the time variation after growth previously reported[7] for several GaAs–Ge (110) heterojunction samples. If these other results are also considered, the sample-to-sample initial (obtained shortly after growth, $t \sim 0$) values of ΔE_v lie between ~ 0.45–0.50 eV. The value of ΔE_v then decreases over a period of tens of hours to a room temperature equilibrium value, which is sample dependent, of $\Delta E_v = \sim 0.20$–0.35 eV (this range includes the results in Ref. 7). This apparently general time dependent behavior of ΔE_v (GaAs–Ge) in the period following growth, independent of specific crystallographic orientation, is in sharp contrast to the stable in time behavior of ΔE_v for the reverse grown interface.

The present results show that vacuum annealing the GaAs–Ge interface at the growth temperature for 10–30 min increases ΔE_v to ~ 0.56 eV, the value for the (110) and (100) Ge–GaAs interfaces (for too brief an anneal, how-

ever, the increase is only partial, as the data point in Fig. 4 between intervals I and II illustrates). The time behavior of ΔE_v subsequent to a vacuum anneal depends on anneal time. For an anneal time within a certain range, ΔE_v afterwards decreases to approximately the preanneal equilibrium value on a time scale of tens of hours, as, for example, over interval II in Fig. 3. If the anneal is longer than a certain time (which seems to be sample dependent) ΔE_v exhibits only a small $\sim$0.05–0.1 eV decrease with time, as over intervals II and IV in Fig. 4 and interval II in Fig. 5; in these cases ΔE_v does not recycle to the preanneal equilibrium value. This noncyclical nature of ΔE_v after an extended anneal suggests that a mobile, and perhaps volatile, species such as As may be involved.

Exposure of a sample to an As flux during an anneal causes a large difference in the subsequent initial value and time behavior of ΔE_v in comparison to the vacuum anneal result. The effect of As is clearly demonstrated in Fig. 4 [(110) interface] with intervals III and V, where each begins after an As anneal. The initial ΔE_v values of these intervals are about the same as for $t \sim 0$ and each end point equilibrium value is close to the equilibrium value at the end point of interval I. In addition, the $\sim$0.1 eV drop in ΔE_v at the II–III and IV–V interval boundaries also results from an As anneal. The same type of result was obtained with the (100) interface, as demonstrated in Fig. 5 at the II–III boundary and over interval III. In other words, a combination of vacuum and As anneals results in a ΔE_v cycle of > 0.2 eV for both (110) and (100) interfaces. Reproducing the temperature and the As overpressure conditions present at the GaAs growth restores ΔE_v to about the $t \sim 0$ value.

The observed ΔE_v (GaAs–Ge) changes are caused by corresponding changes in an electrostatic dipole layer that is oriented across the heterojunction interface such that the positive charge is toward the Ge. The absence of linewidth broadening of the XPS core level peaks for large ΔE_v changes indicates that this dipole is localized over very few atomic planes at the interface (the linewidth constancy also means that the interfaces have remained compositionally abrupt after annealing). Since ΔE_v was shown to be influenced by > 0.2 eV as a result of As exposure during annealing, it reasonably follows that As has a role in the variation of this interface electrostatic dipole. The localized nature of the dipole implies that such electrically active As is also localized at the heterojunction interface. The cyclic nature of ΔE_v may thus be due to mobile As that moves to and from the interface as a function of time and temperature. The long time constant associated with the room temperature variation in ΔE_v is suggestive of such atomic motion.

A tendency for creation of antiphase disorder is a distinctive feature of GaAs–Ge interface structure[12,13] that is absent in Ge–GaAs interface structure [antiphase domains have been directly observed for the (100) interface[14,15]]. The ΔE_v (GaAs–Ge) variations that occur as a function of time, temperature, and As exposure thus appear to derive from a mechanism that requires the presence of interface antiphase domain boundaries. Switching of Ge and As atoms at interface antiphase boundaries may be energetically favored[7]; it is therefore possible that such exchanges provide sites related to interface dipole formation in association with mobile As in the GaAs. The sample-to-sample range in ΔE_v (and interface dipole) change may thus be related to a variation in the amount of antiphase disorder that could result from small departures in the exact interface preparation conditions.

V. SUMMARY

The ΔE_v of (110) and (100) oriented heterojunctions made by MBE growth of GaAs onto Ge decreases substantially with time after interface formation (on a scale of tens of hours). The final room temperature value of ΔE_v (GaAs–Ge) is > 0.2 eV lower than the $\sim$0.56 eV value for the stable (reverse grown) Ge–GaAs interface. Annealing in vacuum at the GaAs growth temperature increases ΔE_v (GaAs–Ge) to approximately the Ge–GaAs value. By controlling anneal duration and accompanying As overpressure, ΔE_v (GaAs–Ge) is found to cycle > 0.2 eV with time. This variation in an interface electrostatic dipole is apparently related to a variable amount of electrically active As (i.e., As that participates in dipole formation) that is located at the heterojunction interface. The detailed mechanism involved in creation of this variable interface dipole most likely requires the presence of the antiphase disorder that is expected for heterojunctions formed by growth of GaAs on Ge.

ACKNOWLEDGMENTS

Helpful discussions with Professor W. A. Harrison are gratefully acknowledged. This work was supported by ONR Contract No. N00014-85-0135.

[1] R. L. Anderson, Solid State Electron. **5**, 341 (1962).
[2] W. A. Harrison, J. Vac. Sci. Technol. **14**, 1016 (1977); J. Vac. Sci. Technol. B **3**, 1231 (1985).
[3] W. R. Frensley and H. Kroemer, Phys. Rev. B **16**, 2642 (1977).
[4] J. Tersoff, Phys. Rev. B **30**, 4874 (1984).
[5] P. Zurcher and R. S. Bauer, J. Vac. Sci. Technol. A **1**, 695 (1983).
[6] R. S. Bauer, P. Zurcher, and H. W. Sang, Jr., Appl. Phys. Lett. **43**, 663 (1983).
[7] R. W. Grant, J. R. Waldrop, S. P. Kowalczyk, and E. A. Kraut, J. Vac. Sci. Technol. B **3**, 1295 (1985); Surf. Sci. **168**, 498 (1986).
[8] J. R. Waldrop, R. W. Grant, S. P. Kowalczyk, and E. A. Kraut, J. Vac. Sci. Technol. A **3**, 835 (1985).
[9] B. Z. Olshanetsky, S. M. Repinsky, and A. A. Shklyaev, Surf. Sci. **64**, 224 (1977).
[10] E. A. Kraut, R. W. Grant, J. R. Waldrop, and S. P. Kowalczyk, Phys. Rev. B **28**, 1965 (1983).
[11] P. M. Petroff, J. Vac. Sci. Technol. B **4**, 874 (1986).
[12] L. C. Bobb, H. Holloway, K. H. Maxwell, and E. Zimmerman, J. Appl. Phys. **37**, 4687 (1966).
[13] J. C. Phillips, J. Vac. Sci. Technol. **19**, 545 (1981).
[14] J. H. Neave, P. K. Larsen, B. A. Joyce, J. P. Gowers, and J. F. van der Veen, J. Vac. Sci. Technol. B **1**, 668 (1983).
[15] T. S. Kuan and C.-A. Chang, J. Appl. Phys. **54**, 4413 (1983).

Effect of growth sequence on the band discontinuities at AlAs/GaAs (100) and (110) heterojunction interfaces

J. R. Waldrop, R. W. Grant, and E. A. Kraut
Rockwell International Science Center, Thousand Oaks, California 91360

(Received 29 January 1987; accepted 27 March 1987)

The valence band discontinuity ΔE_v for the AlAs grown on GaAs (AlAs–GaAs) heterojunction interface is compared to the corresponding ΔE_v for the GaAs grown on AlAs interface (GaAs–AlAs) for both (100) and (110) crystallographic orientations by using x-ray photoemission spectroscopy (XPS). Molecular-beam epitaxy within the XPS system was used to prepare the samples. The XPS method has the feature that ΔE_v differences are measured more accurately than the corresponding absolute magnitudes. For the (100) interface, the value of ΔE_v (AlAs–GaAs) is 0.10 ± 0.02 eV larger than ΔE_v (GaAs–AlAs). For the (110) interface, ΔE_v (AlAs–GaAs) is 0.13 ± 0.04 eV larger than ΔE_v (GaAs–AlAs). The average discontinuity magnitudes are: $\Delta E_v(\text{AlAs–GaAs})_{(100)} = 0.46$ eV; $\Delta E_v(\text{GaAs–AlAs})_{(100)} = 0.36$ eV; $\Delta E_v(\text{AlAs–GaAs})_{(110)} = 0.55$ eV; and $\Delta E_v(\text{GaAs–AlAs})_{(110)} = 0.42$ eV. Thus, both a growth sequence effect and an orientation dependence have been found to be intrinsic characteristics of the (100) and (110) AlAs/GaAs heterojunction interfaces. As a consequence, there is an inherent asymmetry in the potential wells associated with AlAs/GaAs quantum well and superlattice structures.

I. INTRODUCTION

The many interesting electrical and optical properties of semiconductor structures based on the AlGaAs/GaAs heterojunction system derive principally from the interface valence band discontinuity ΔE_v and conduction band discontinuity ΔE_c that arise from the band-gap difference ΔE_g of the two materials. For this reason there have been a large number of measurements of these band discontinuities by a diverse set of experimental techniques on samples prepared under different conditions.[1] The results of these measurements, which span the $Al_xGa_{1-x}As$ solid solution range, are often not in full agreement. The extent to which ΔE_v (or, equivalently, ΔE_c) is an intrinsic quantity that is independent of the circumstances of interface formation is thus an important consideration. Growth sequence is a basic feature of interface formation. An early observation[2] of a sizable growth sequence dependence for the band discontinuities of AlAs/GaAs (110) oriented interfaces that was measured by XPS (x-ray photoemission spectroscopy) has been questioned because of a later report[3] of growth problems that can be encountered with molecular-beam epitaxy (MBE) on the (110) surface. Subsequent investigations of the AlGaAs/GaAs (100) interface have reported the absence of a growth sequence effect.[4,5]

In this paper we use XPS to compare the ΔE_v at the AlAs–GaAs interface to the ΔE_v at the GaAs–AlAs interface for a large number of (100) and (110) samples (we use AlAs/GaAs to refer to the heterojunction pair without regard to growth order while AlAs–GaAs designates AlAs grown on GaAs and GaAs–AlAs designates GaAs grown on AlAs). The interfaces were formed by MBE within the ultrahigh vacuum preparation chamber of the XPS system. The results show that ΔE_v has a consistent and significant growth sequence dependence for both the (100) and (110) interfaces.

II. EXPERIMENT

A. Sample preparation

Figure 1 (a) shows the structure of the GaAs–AlAs samples (left-hand side) and the AlAs–GaAs samples (right-

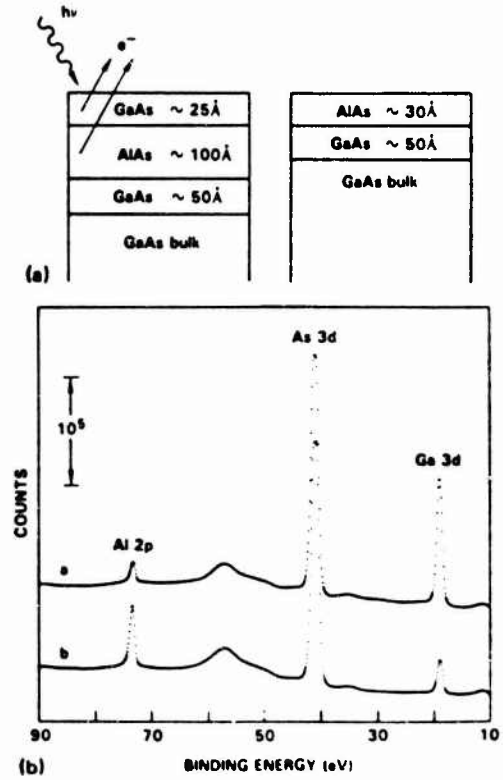

FIG. 1. (a) Structure of the GaAs–AlAs (left-hand side) and AlAs–GaAs (right-hand side) heterojunction samples. (b) Representative XPS binding energy spectra of a GaAs–AlAs (100) sample (spectrum a) and a AlAs–GaAs (100) sample (spectrum b) in the region of the Al2*p*, Ga3*d*, and As3*d* core levels.

 0734-211X/87/041209-06$01.00 © 1987 American Vacuum Society

hand side). The substrate is a $\sim 10 \times 10$ mm piece of bulk GaAs wafer, either (100) or (110) orientation, that is etched for ~ 30 s in 4:1:1 H_2SO_4:H_2O_2:H_2O to remove polishing damage, quenched, dried with N_2, mounted on a Mo plate with In, and immediately put into the x-ray photoemission spectroscopy (XPS) system preparation chamber (base pressure $\sim 2 \times 10^{-10}$ Torr). The ~ 10 Å native oxide is removed by momentary heating to the minimum necessary temperature, nominally ~ 550 °C. The resultant clean surface has no O or C detectable by XPS and exhibits a characteristic low-energy electron diffraction (LEED) pattern.

All the GaAs and AlAs epitaxial layers were grown within a few degrees of the GaAs native oxide removal temperature at a ~ 0.3–0.6 Å/s rate. The As_4 source, which was located ~ 2 cm from the sample, was a miniature quartz oven filled with elemental As; the Ga and Al were evaporated from W baskets. The As_4 overpressure during growth was ~ 3–5×10^{-6} Torr, for an As_4 to cation ratio of > 12. A ~ 50-Å GaAs buffer layer was first grown, followed either by a ~ 30-Å-AlAs top layer (AlAs–GaAs samples) or by a ~ 100-Å-AlAs intermediate layer and a ~ 25-Å-GaAs top layer (GaAs–AlAs samples). Layer epitaxy was confirmed by observation of a characteristic LEED pattern. Interface abruptness was assured by alternate activation of the Ga and Al sources. Fifteen heterojunction samples were prepared by individual MBE growths, four each for the AlAs–GaAs (100), GaAs–AlAs (100), and GaAs–AlAs (110) interfaces and three for the AlAs–GaAs (110) interface.

B. XPS measurement of ΔE_v

The HP5950A angle-resolved electron spectrometer system used has a $h\nu = 1486.6$-eV-monochromatic Al $K\alpha$ x-ray source. The effective photoelectron escape depth, λ, for the photoelectron kinetic energies analyzed and the emission angle employed is ~ 16 Å. Thus, for these heterojunction samples in which the interface of interest is at a distance comparable to λ from the surface, photoelectrons that originate from each side of this interface [Fig. 1(a)] will be observed in the same XPS spectrum. For example, Fig. 1(b) shows representative XPS spectra for a GaAs–AlAs (100) sample (spectrum a) and a AlAs–GaAs (100) sample (spectrum b) over a binding energy range that contains the GaAs Ga3*d* and As3*d* core level peaks and the AlAs Al2*p* and As3*d* peaks.

Figure 2(a) is a schematic energy band diagram at the interface region of the AlAs/GaAs heterojunction, where E_c and E_v are the conduction band minimum and valence band maximum, respectively, and $\Delta E_{CL} = (E^{AlAs}_{Al2p} - E^{GaAs}_{Ga3d})$ is the binding energy difference across the interface between the Al2*p* core level in the AlAs and the Ga3*d* core level in the GaAs. The $(E^{AlAs}_{Al2p} - E^{AlAs}_{v})$ and $(E^{GaAs}_{Ga3d} - E^{GaAs}_{v})$ terms, which are core level to valence band maximum binding energy differences, are bulk constants characteristic of the pure materials. By inspection of Fig. 2(a):

$$\Delta E_v = \Delta E_{CL} + (E^{GaAs}_{Ga3d} - E^{GaAs}_{v}) - (E^{AlAs}_{Al2p} - E^{AlAs}_{v}) . \quad (1)$$

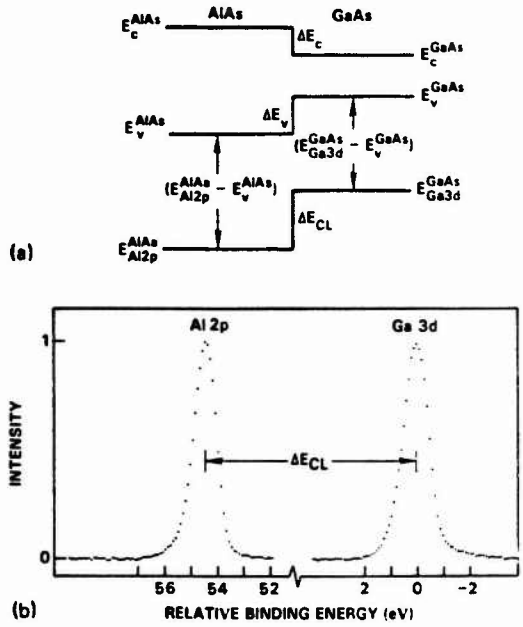

FIG. 2. (a) Schematic energy band diagram of the AlAs/GaAs interface. (b) Measurement of $\Delta E_{CL} = (E^{AlAs}_{Al2p} - E^{GaAs}_{Ga3d})$ [data from spectrum b in Fig. 1(b)].

Hence, of the three quantities needed to determine ΔE_v only ΔE_{CL} is characteristic of the heterojunction. Additional details about the XPS measurement method can be found elsewhere.[6] As discussed in the Appendix, $(E^{GaAs}_{Ga3d} - E^{GaAs}_{v}) = 18.75 \pm 0.03$ eV has been previously measured for GaAs while the measurement of $(E^{AlAs}_{Al2p} - E^{AlAs}_{v}) = 72.70 \pm 0.04$ eV for AlAs is described below. Thus, from Eq. (1),

$$\Delta E_v = \Delta E_{CL} - 53.95 \text{ eV} . \quad (2)$$

This relation between ΔE_v and ΔE_{CL} means that differences measured in ΔE_{CL} among samples give directly the relative differences in ΔE_v [i.e., $\delta(\Delta E_v) = \delta(\Delta E_{CL})$].

The precision measurement of $\Delta E_{CL} = (E^{AlAs}_{Al2p} - E^{GaAs}_{Ga3d})$ is illustrated in Fig. 2(b), which in this example is the AlAs–GaAs spectrum b data in Fig. 1(b). A background function that is proportional to the integrated peak intensity is subtracted from each core level peak (the Al peak also has a small plasmon loss contribution removed before the background subtraction). The peak energy is measured at the half-width point at half-height. The peak width and height are determined consistently by a computerized algorithm in which a third order least squares fit is made to segments at the sides and top of the discrete peak data. With this procedure the ΔE_{CL} measurement uncertainty for these AlAs/GaAs interfaces is estimated to be ± 0.02 eV. Thus, although the uncertainty in the absolute ΔE_v measurements is ± 0.05 eV because the uncertainties in the $(E_{CL} - E_v)$ values dominate, the relative sample-to-sample changes in ΔE_v are measured to ± 0.02 eV.

For each AlAs/GaAs sample a spectrum such as in Fig. 1(b) was obtained by repeatedly scanning a 0–100 eV binding energy window for ~ 24–48 h. Possible surface oxygen buildup was monitored by XPS and was found to range from ~ 0–0.5 monolayers (ML), being typically greater on the AlAs surfaces.

C. Measurement of $(E^{AlAs}_{Al2p} - E^{AlAs}_{v})$

The inset in Fig. 3 is a representative -10 to 90 eV binding energy spectrum from a ~ 100 Å AlAs (100) epitaxial layer grown within the XPS system onto a GaAs substrate under MBE conditions similar to those of the heterojunction samples. Four separate such (100) samples and one (110) sample were prepared. The position of E_v was found by a procedure previously described.[7] In brief, a theoretical valence band density of states (VBDOS) for the semiconductor, on an energy scale where $E_v = 0$ eV, is broadened by convolution with the experimentally determined XPS resolution function. The broadened theoretical VBDOS function, with E_v remaining at zero energy, is least squares fitted to the experimental points in the XPS VBDOS spectrum near E_v to thus transfer the position of E_v from the theoretical function to the XPS data. Because an appropriate theoretical AlAs VBDOS was unavailable, a nonlocal pseudopotential GaAs VBDOS[8] was used instead. This substitution is reasonable because the XPS valence band data near E_v for AlAs and GaAs, shown in Fig. 4 with normalized intensity and superimposed on the same energy scale, were found to have closely matched shapes. This match thus indicates that near E_v the theoretical VBDOS for GaAs is similar enough to that of AlAs for the present purpose. Figure 3 shows the good fit between the broadened theoretical VBDOS function (line) and the XPS valence band data from the inset (points), plotted on an energy scale were $E_v = 0$ eV. The fit is over an interval that terminates at an energy E_{max} below E_v (in this instance $E_{max} = \sim 1$ eV).

Figure 5 gives the results of the valence band fitting procedure for the four (100) samples (upper panel) and the (110) sample (lower panel) in terms of the As3*d* core level to valence band maximum binding energy $(E^{AlAs}_{As3d} - E^{AlAs}_{v})$ vs E_{max}. The error bar at each data point indicates the 95% confidence interval of the fit. The (100) fits are relatively independent of E_{max} and the average value for $(E^{AlAs}_{As3d} - E^{AlAs}_{v})$ is 40.16 eV with an estimated uncertainty of ± 0.04 eV. The (110) result, however, shows a dispersion in the $(E^{AlAs}_{As3d} - E^{AlAs}_{v})$ vs E_{max} plot which indicates a complication that can be encountered when using this method,

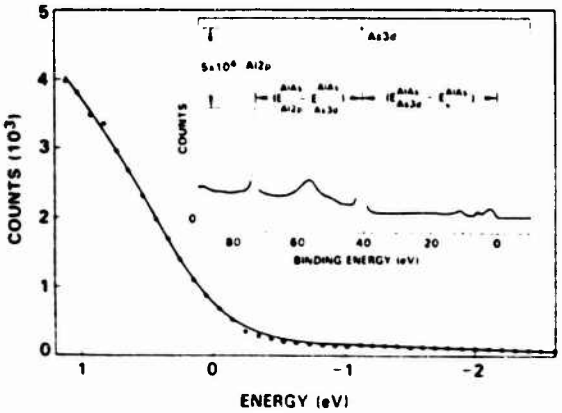

FIG. 3. Fit of the broadened theoretical valence band density of states (solid line) to the XPS valence band data shown in the inset. Energy scale is referenced to $E_v = 0$ eV. Inset: Representative -10 to 90 eV binding energy spectrum for AlAs (100).

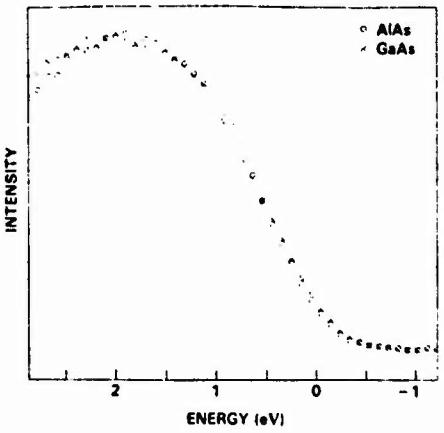

FIG. 4. Comparison of XPS valence band data for AlAs (100) and GaAs (110) near E_v.

most likely from surface state effects that influence the shape of the XPS data. No unique $(E^{AlAs}_{As3d} - E^{AlAs}_{v})$ value can be obtained from the analysis in this instance.

The Al2*p* core level to As3*d* core level binding energy difference $(E^{AlAs}_{Al2p} - E^{AlAs}_{As3d})$ in each AlAs spectrum was measured by using the same procedure described for ΔE_{CL}. The average $(E^{AlAs}_{Al2p} - E^{AlAs}_{As3d})$ for the four (100) samples is 32.54 ± 0.01 eV. Thus, $(E^{AlAs}_{Al2p} - E^{AlAs}_{v}) = 40.16 + 32.54$ eV $= 72.70 \pm 0.04$ eV.

III. RESULTS

A. Growth sequence dependence of ΔE_v

The ΔE_{CL} values for the 15 AlAs/GaAs interfaces investigated are given in Table I. The average ΔE_{CL} value for each growth direction and orientation is also listed. Based on these averages, the $\delta(\Delta E_v)$ column shows the relative

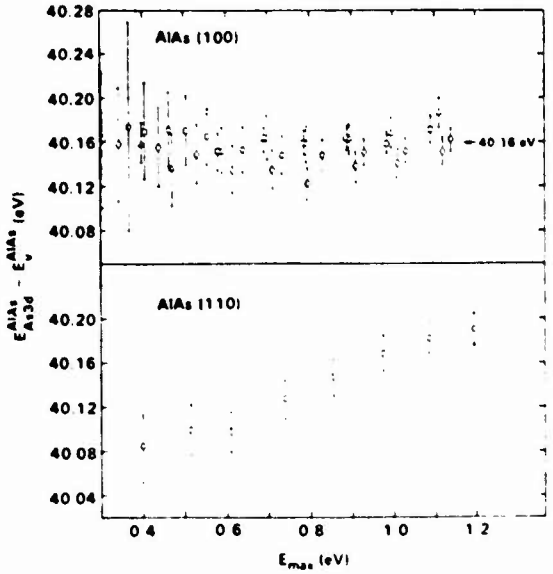

FIG. 5. As3*d* core level to valence band maximum binding energy for four AlAs (100) samples and an AlAs (110) sample as a function of the end point E_{max} of the fitting interval.

TABLE I. $\Delta E_{CL} = (E^{AlAs}_{Al2p} - E^{GaAs}_{Ga3d})$ values for (100) and (110) oriented AlAs–GaAs and GaAs–AlAs heterojunction interfaces.

Interface	Sample	ΔE_{CL} (eV)[a]	$\delta(\Delta E_v)$ (eV)
AlAs–GaAs (100)	a	54.39	
	b	54.41	
	c	54.41	
	d	54.42	
	avg =	54.41	0.00
GaAs–AlAs (100)	e	54.30	
	f	54.30	
	g	54.33	
	h	54.29	
	avg =	54.31	−0.10
AlAs–GaAs (110)	i	54.50	
	j	54.51	
	k	54.50	
	avg =	54.50	+0.09
GaAs–AlAs (110)	l	54.31	
	m	54.41	
	n	54.39	
	o	54.38	
	avg =	54.37	−0.04

[a] ± 0.02 measurement uncertainty.

change in ΔE_v, referenced to the AlAs–GaAs (100) interface, for each type of AlAs/GaAs interface.

For the (100) interface ΔE_v (GaAs–AlAs) is 0.10 ± 0.02 eV < ΔE_v (AlAs–GaAs). In each growth direction, samples a–d and e–h, respectively, the individual ΔE_{CL} values agree to within the measurement uncertainty.

For the (110) interface ΔE_v (GaAs–AlAs) is 0.13 ± 0.04 eV < ΔE_v (AlAs–GaAs). The standard deviation for this difference is large owing to the spread in ΔE_{CL} values for the GaAs–AlAs interface (samples l–o), due principally to sample l being 0.06 eV below the average (samples m–o are in good agreement). The ΔE_{CL} values for the AlAs–GaAs interface agree to within the measurement uncertainty.

Comparison of the (100) and (110) average ΔE_{CL} values indicates an orientation dependence of ΔE_v in addition to the growth sequence effect. For the AlAs–GaAs interfaces ΔE_v (110) is 0.09 eV > ΔE_v (100). For the GaAs–AlAs interfaces ΔE_v (110) is 0.06 eV > ΔE_v (100).

The linewidths of the Al2*p* and the Ga3*d* core level peak data were intercompared to assess if chemically shifted peak components could be affecting the ΔE_{CL} measurements. The average Al2*p* linewidth and average Ga3*d* linewidth values associated with the average ΔE_{CL} measured for each growth direction at the (100) interfaces were in agreement to ± 0.01 eV, respectively. Similarly, for the (110) oriented interfaces the average Ga3*d* linewidth was in ± 0.01 eV agreement for each growth direction. The Al2*p* linewidth values for the AlAs–GaAs (110) interfaces were, however, 0.06–0.13 eV larger than the average value for the reverse growth direction. The origin of this linewidth difference at the (110) interfaces is uncertain but there was no correlation between the Al2*p* linewidth variation and the AlAs–GaAs (110) ΔE_{CL} values.[9]

B. AlAs/GaAs ΔE_v values

The absolute values for ΔE_v that result from substitution of the average ΔE_{CL} value (Table I) for each type of AlAs/GaAs interface into Eq. (2) are listed in Table II. As discussed in Sec. II B, the estimated uncertainty in the magnitude of these values is ± 0.05 eV while the uncertainty of their differences is ± 0.02 eV.

IV. DISCUSSION

The present results are different from the previous AlAs/GaAs (110) XPS data,[2] where ΔE_v (GaAs–AlAs) was 0.25 eV > ΔE_v (AlAs–GaAs). Although the growth sequence effect is observed, as Table I indicates, the (110) ΔE_v difference in the new data is one-half the magnitude and of opposite sign. Between the two experiments there is, however, a significant departure in sample structure and growth conditions. The previous (110) samples had a ~5000 Å GaAs buffer layer grown at a ~3 Å/s rate compared to a ~50-Å-GaAs buffer layer grown at 0.3–0.6 Å/s. The AlAs intermediate layers in the previous GaAs–AlAs samples were ~1000 Å thick compared to ~100 Å presently. The growth temperature and AlAs growth rate were comparable. It has been reported[3] that GaAs growth on the (110) surface at ~3 Å/s with an As_4/Ga flux ratio of ~1.5 results in morphological irregularities for layer thickness > 700 Å (similar problems were also seen for AlGaAs growth). Our present samples were thus grown 10 times more slowly, with substantially thinner layers, and at 10 times the As_4/cation ratio, compared to the conditions for the reported (110) growth instabilities. The present samples were therefore grown under circumstances that should favor formation of more ideal interfaces. We thus ascribe the disparate ΔE_v (110) results to an interface difference, the exact nature and extent of which is undetermined, caused by dissimilar growth conditions.

The absolute (110) ΔE_v values for the two experiments can be compared by substitution of the previous (Ref. 2) average ΔE_{CL} values of 54.25 and 54.50 eV for AlAs–GaAs

TABLE II. ΔE_v for (100) and (110) oriented AlAs–GaAs and GaAs–AlAs heterojunctions.

Interface	ΔE_v (eV)
AlAs–GaAs (100)	0.46
GaAs–AlAs (100)	0.36
AlAs–GaAs (110)	0.55
GaAs–AlAs (110)	0.42

and GaAs–AlAs, respectively, into Eq. (2) [this makes use of refined $(E_{CL} - E_v)$ values]. The result is ΔE_v(AlAs–GaAs) = 0.30 eV and ΔE_v(GaAs–AlAs) = 0.55 eV, compared to the corresponding present values of 0.55 and 0.42 eV, respectively. Hence, growth parameters appear to strongly influence ΔE_v for (110) oriented AlAs/GaAs interfaces and can cause up to a $\sim$0.2 eV ΔE_v variation. The 0.10 eV range for $\Delta E_v(\text{GaAs–AlAs})_{(110)}$ shown in Table I suggests that this interface is unusually sensitive to preparation conditions.

The ΔE_v at the AlAs–GaAs (100) and (110) interfaces differ by 0.09 eV. On the other hand, from a charge transfer analysis Wang *et al.*[10] deduced that ΔE_v was the same at $Al_{0.26}Ga_{0.74}As$–GaAs (100) and (311) interfaces. These contrary results indicate that a comparison of two interface orientations may not always show a ΔE_v difference. The case in which no difference is found can indicate either the absence of an effect or that the effect is the same for each orientation.

A prior XPS experiment that measured the Al2*p* to Ga3*d* binding energy difference for AlAs–GaAs and GaAs–AlAs (100) interfaces has been reported.[5] To within the quoted experimental error ($\pm$0.05 eV) no growth sequence effect was observed. The origin of the disagreement between these and the present XPS data is unknown.

Of the other techniques to determine ΔE_v, some recent electrical measurements that involve single $Al_xGa_{1-x}As$/GaAs (100) interfaces provide an appropriate comparison to the XPS (100) results. By use of the charge transfer technique Wang and Stern[11] measured ΔE_v(AlAs–GaAs) = 0.45 $\pm$ 0.05 eV, which is in agreement with our measurement. The available electrical data perhaps most relevant to the growth sequence effect involves *C–V* profiling through interfaces in the $x < 0.45$ $Al_xGa_{1-x}As$ direct band gap regime. To simply relate the *C–V* derived data to the XPS data it will be assumed that the growth sequence difference between the AlAs–GaAs and GaAs–AlAs interfaces is linear in x, which for the (100) orientation gives $\delta(\Delta E_v)(x) = -100x$ meV [sign convention as in Table I, ΔE_v(AlGaAs–GaAs) > ΔE_v(GaAs–AlGaAs)]. This is reasonable in view of the evidence that ΔE_v appears to be linear in x over the entire alloy composition range.[12]

The *C–V* data of Watanabe *et al.*,[4] from which a $\Delta E_c/\Delta E_v = 62/38$ ratio was found based on $Al_xGa_{1-x}As$–GaAs interfaces, includes three samples with $x = 0.3$ where ΔE_c was measured ($\sim \pm$ 10 meV uncertainty). Two of these samples were the $Al_xGa_{1-x}As$–GaAs interface and one was the GaAs–$Al_xGa_{1-x}As$ interface. The present XPS data predicts a ΔE_v difference of $-$ 30 meV at $x = 0.3$, or, thus, a ΔE_c difference of + 30 meV [ΔE_c(GaAs–AlGaAs) > ΔE_c(AlGaAs–GaAs)] between these two types of interface. It is noteworthy that the *C–V* result for ΔE_c(GaAs–AlGaAs) was 250 meV, which is larger than the value found in both the other two samples, whose average for ΔE_c(AlGaAs–GaAs) was 230 meV. The sign and approximate magnitude of the difference are thus consistent with the XPS prediction, although the *C–V* measurement uncertainty does not permit a decisive comparison.

In another *C–V* profiling experiment, Okumura *et al.*[13] measured ΔE_c ($\pm$ 10 meV uncertainty) for a series of GaAs–$Al_xGa_{1-x}As$ interfaces for x up to 0.42 and found a $\Delta E_c/\Delta E_v = 67/33$ ratio. The XPS results thus indicate that when such small but persistent differences in $\Delta E_c/\Delta E_v$ ratios exist between experiments that feature interfaces with opposite growth directions the influence of a growth sequence effect should be considered.

The ratio of the growth sequence effect magnitude to ΔE_v is $\sim$20%; the corresponding ratio for ΔE_c is thus $\sim$10%. There is, consequently, an intrinsic asymmetry in the potential well structure of AlAs/GaAs quantum well and superlattice structures. This asymmetry, which is a factor of $\sim$2 larger in the valence bands than the conduction bands, may have to be incorporated into refined models of the optical properties and the perpendicular electrical transport related to these structures. The interface electrostatic dipole variation that gives rise to the growth sequence effect will probably be difficult to accommodate in the models that predict heterojunction band discontinuities until more is known about the microscopic detail that distinguishes the AlAs–GaAs and GaAs–AlAs (100) and (110) interfaces.

ACKNOWLEDGMENT

This work was supported by ONR Contract No. N00014-85-C-135.

APPENDIX: XPS MEASURED $(E_{CL} - E_v)$ VALUES FOR SEVERAL SEMICONDUCTORS

As referenced in Table III below, certain core level to valence band binding energies in several semiconductors, including GaAs, have been measured by using the method described in Ref. 7 to analyze XPS valence band data near E_v. An error in a computer program that was involved in these data analyses has been discovered which requires that a small, either $-$ 0.04 or $-$ 0.05 eV, systematic correction be made to the previously reported $(E_{CL} - E_v)$ values. The corrected values are given in Table III, where the entries labeled XPS are measured directly while the entries labeled bulk have been adjusted to remove the effect of surface chemical shifts.

TABLE III. Corrected $(E_{CL} - E_v)$ values for several semiconductors

Semiconductor	Core level	$(E_{CL} - E_v)_{XPS}$[a] (eV)	$(E_{CL} - E_v)_{bulk}$[a] (eV)	Reference
GaAs (110)	Ga3*d*	18.78	18.75	7
	As3*d*	40.70	40.74	
Ge (110)	Ge3*d*	29.52	29.52	7
ZnSe (110)	Zn3*d*	8.86		14
InAs (100)	In4*d*	17.38		15
	As3*d*	40.72		
CdTe ($\bar{1}\bar{1}\bar{1}$)	Cd4*d*	10.24		16
HgTe ($\bar{1}\bar{1}\bar{1}$)	Hg5$d_{5/2}$	7.66[b]		16

[a] $\pm$ 0.03 eV uncertainty
[b] $\pm$ 0.04 eV uncertainty

[1]For references to such work see, for example, the bibliographies in: Ref. 12 below; G. Duggan, J. Vac. Sci. Technol. B 3, 1224 (1985); H. Kroemer, Surf. Sci. 174, 299 (1986).
[2]J. R. Waldrop, S. P. Kowalczyk, R. W. Grant, E. A. Kraut, and D. L. Miller, J. Vac. Sci. Technol. 19, 573 (1981).
[3]W. I. Wang, J. Vac. Sci. Technol. B 1, 630 (1983).
[4]M. O. Watanabe, J. Yoshida, M. Mashita, T. Nakanisi, and A. Hojo, J. Appl. Phys. 57, 5340 (1985).
[5]A. D. Katnani and R. S. Bauer, Phys. Rev. B 33, 1106 (1986).
[6]J. R. Waldrop, R. W. Grant, S. P. Kowalczyk, and E. A. Kraut, J. Vac. Sci. Technol. A 3, 835 (1985).
[7]E. A. Kraut, R. W. Grant, J. R. Waldrop, and S. P. Kowalczyk, Phys. Rev. B 28, 1965 (1983).
[8]J. R. Chelikowsky and M. L. Cohen, Phys. Rev. B 14, 556 (1976).
[9]To estimate a worst case effect that this linewidth difference could have on the magnitude of the (110) growth sequence result, the Al2*p* line shape was modeled by assuming that the Al in the surface monolayer of the AlAs–GaAs (110) samples was contributing a chemically shifted peak component on the high binding energy side of the Al2*p* (in AlAs) peak. The maximum influence on the (110) AlAs–GaAs ΔE_{CL} measurements that could be obtained was ~0.05 eV, which is less than one-half the growth sequence change observed at the (110) interface.
[10]W. I. Wang, T. S. Kuan, E. E. Mendez, and L. Esaki, Phys. Rev. B 31, 6890 (1985).
[11]W. I. Wang and F. Stern, J. Vac. Sci. Technol. B 3, 1280 (1985).
[12]J. Batey and S. L. Wright, J. Appl. Phys. 59, 200 (1986).
[13]H. Okumura, S. Misawa, S. Yoshida, and S. Gonda, Appl. Phys. Lett. 46, 377 (1985).
[14]S. P. Kowalczyk, E. A. Kraut, J. R. Waldrop, and R. W. Grant, J. Vac. Sci. Technol. 21, 482 (1982).
[15]S. P. Kowalczyk, W. J. Schaffer, E. A. Kraut, and R. W. Grant, J. Vac. Sci. Technol. 20, 705 (1982).
[16]S. P. Kowalczyk, J. T. Cheung, E. A. Kraut, and R. W. Grant, Phys. Rev. Lett. 56, 1605 (1986).

Heterojunction band offsets and scaling[a)]

E. A. Kraut
Rockwell International Science Center, Thousand Oaks, California 91360

(Received 27 January 1987; accepted 2 April 1987)

It is shown that accurate x-ray photoemission spectroscopy values of the valence band offsets ΔE_v for Ge/GaAs(110), GaAs/ZnSe(110), and Ge/ZnSe(110) vary linearly with the minimum band-gap difference and obey the simple scaling relation, $\Delta E_v/\Delta E_g(\min) = 3/4$. This empirical observation is compared with the predictions of current theories of heterojunction band lineups and the results are discussed. A theory relating average bulk crystal Hamiltonians to band offsets is developed and this theory is used to calculate band lineups in the tight-binding limit. It is shown that if only interactions between s and p orbitals on adjacent nearest-neighbor atoms are considered, the band lineups coincide with those predicted by Harrison and Tersoff [J. Vac. Sci. Technol. B **4**, 1068 (1986)]. Since the latter do not satisfy the experimentally observed scaling relation, it is concluded that second nearest-neighbor contributions to ΔE_v are important in the tight-binding limit.

I. INTRODUCTION

Semiconductor heterojunctions are formed from elements of the Periodic Table contained in a region (Table I) composed of 4 rows and 5 columns. Compounds consisting of elements belonging to the same row form lattice-matched heterojunctions.

High precision experimental band offset measurements[1] for Ge row heterojunctions Ge/GaAs(110), GaAs/ZnSe(110), and Ge/ZnSe(110) show a remarkably constant ratio of valence band offset to minimum energy band-gap difference (Table II).

It would be interesting to know if a linear trend between valence band offset and minimum energy band-gap difference is theoretically predicted and if similar linear trends also hold for silicon and tin row heterojunctions. Unfortunately, the experimental band offset data needed to test this relationship for the silicon and tin rows are not yet available. The linear dependence equation (1) of valence band offset on band-gap difference observed for lattice-matched Ge row heterojunctions:

$$\Delta E_v/\Delta E_g = \text{constant} \qquad (1)$$

provides a stringent test of current heterojunction band offset theories.

II. COMPARISON OF EXPERIMENT WITH HETEROJUNCTION BAND OFFSET THEORIES

The comparison of experimentally measured and theoretically predicted heterojunction band offsets is complicated by 0.1–0.2 eV uncertainties in the theoretical band offsets. Within an uncertainty of ± 0.2 eV most current band offset theories are in reasonable accord with experiment. Since an order of magnitude improvement in the precision of predicted band offsets is unlikely, regularities, such as those in Table II, can provide additional useful comparisons of theory and experiment. Table III compares room temperature experimental values[1,2] of the ratio in Eq. (1) with theoretically predicted valence band offsets divided by (room temperature) minimum experimental band-gap differences.

The self-consistent local pseudopotential calculations of Frensley[3] and Kroemer [FK(76)][4] using pure Slater exchange are almost in exact agreement with experiment. While this may be fortuitous, their later calculations [FK(77)],[5] using generalized Slater $X\alpha$ exchange with $\alpha = 0.8$ (to improve the accuracy in fitting band gaps) definitely do not agree as well. In the column of Table III labeled SCPP the self-consistent pseudopotential calculations of Pickett and Cohen for Ge–ZnSe(110)[6] and similar calculations by Pickett, Louie, and Cohen for Ge/GaAs(110)[7] are compared with experiment. Unlike the work of Frensley and Kroemer, these calculations do not require the average interstitial potential to remain continuous across the interface. They predict that the potential [averaged parallel to the (110) interface] increases by 0.25 eV going from Ge to

TABLE I. Compounds formed from elements belonging to the same row of the Periodic Table form nearly lattice-matched heterojunctions. Lattice-matched heterojunctions can also be formed from elements belonging to different rows, as for example, AlAs/GaAs.

Mg	Al	Si	P	S
Zn	Ga	Ge	As	Se
Cd	In	Sn	Sb	Te
Hg	Tl	Pb	Bi	Po

TABLE II. Experimental Ge row band offsets (Ref. 1) at 300 K vs differences in minimum (300 K) band gaps. [The band offsets for these heterojunctions are transitive within experimental uncertainty (Ref. 2.)] The minimum bandgaps of Ge, GaAs, and ZnSe at 300 K are 0.66, 1.43, and 2.67 eV, respectively. At 20 K these increase to 0.77, 1.52, and 2.81 eV, respectively.

Heterojunction	ΔE_v (eV)	ΔE_g (min)	$\Delta E_v/\Delta E_g$
Ge–GaAs(110)	0.56 ± 0.04	0.77	0.73 ± 0.05
ZnSe–GaAs(110)	0.94 ± 0.04	1.24	0.76 ± 0.03
Ge–ZnSe(110)	1.53 ± 0.04	2.01	0.76 ± 0.02

 0734-211X/87/041246-04$01.00 © 1987 American Vacuum Society

TABLE III. Experimental values (Refs. 1 and 2) of $\Delta E_v/\Delta E_g$ (min) at 300 K compared to the predictions of several theories discussed in the text.

Heterojunction	Experiment	FK(76)	FK(77)	SCPP	LCAO(77)	LCAO(81)	LCAO(86)	Tersoff(86)	RC(86)	EAR
Ge–GaAs(110)	0.73	0.78	0.92	0.45	0.53	0.87	0.86	0.42	0.66	0.92
GaAs–ZnSe(110)	0.76	0.75	0.89	1.61	0.85	1.14	1.09	0.97	0.77	0.98
Ge–ZnSe(110)	0.76	0.76	0.90	1.61	0.73	1.04	1.00	0.76	0.78	0.98

ZnSe[6] and by the same amount, 0.25 eV, going from GaAs to Ge.[7]

The next two columns of Table III use the Ge row band offsets predicted by Harrison's tight binding theory linear combination of atomic orbitals [LCAO(77)][8] and LCAO(81)[9] based on Herman–Skillman and Hartree–Fock atomic term values, respectively.[10] More recently, Harrison and Tersoff have concluded that interface dipoles play a crucial role in determining band lineups[11] and have shown that self-consistent lineups can be obtained, approximately, by aligning the average sp^3 hybrid energy in the respective semiconductors. Their Ge row predictions[11] divided by the corresponding differences in minimum energy gap are contained in the LCAO(86) column. These predictions correspond to the limit of strong screening of the hybrid energy difference as opposed to the natural band lineups, LCAO(77) and LCAO(81) obtained by omitting screening of the hybrid energy difference.

Tersoff obtains heterojunction band offsets by aligning an energy E_B in the forbidden gap of each semiconductor.[12–14] E_B is chosen so that states higher in the gap are of primarily conduction-band character, while states lower in energy are of primarily valence-band character. The Ge row band offsets predicted this way and divided by the corresponding minimum energy gap differences appear under Tersoff(86)[14] in Table III. It should be pointed out that to improve agreement with Schottky barrier height data on GaAs,[14] Tersoff decreased his original value of E_B for GaAs from 0.70 eV[12] to 0.50 eV[13,14] by fitting the L and X minima correctly rather than the Γ minimum and by including the effect of spin-orbit splitting. Although this improved the agreement with GaAs Schottky barrier data,[14] the band offset predictions for the Ge row are unfavorably affected as Table III shows. The original value of E_B (GaAs) = 0.70 eV[12] predicts an 0.52 eV valence band offset for Ge/GaAs and a valence band offset of 1.00 eV for GaAs/ZnSe. These accord better with the experimental values in Table II than the predictions of 0.32 and 1.20 eV, respectively, based on E_B (GaAs) = 0.50 eV.[13,14]

Most recently Ruan and Ching have modeled corrections to heterojunction band offsets due to the formation of an effective dipole induced by the penetration of bulk-band states into the quantum barrier in the neighboring semiconductor.[15] They use this effective dipole model to calculate corrections to band offsets derived from electron affinities.[16,17] For example, their dipole corrections[15] reduce the valence band offsets of Ge/GaAs, GaAs/ZnSe, and Ge/ZnSe from 0.70, 1.31, and 2.0 eV to 0.52, 0.96, and 1.56 eV, respectively, thus improving agreement with experiment as Tables II and III show. The last column of Table III lists the electron affinity rule predictions (EAR)[16,17] for the ratio of Eq. (1) for comparison. It is interesting to note that of the various theories compared in Table III, the self-consistent pseudopotential calculations of Frensley and Kroemer,[4,5] the dipole model of Ruan and Ching,[15] and the electron affinity rule[16,17] come closest to capturing the linear scaling of valence band offset with minimum band gap difference for Ge row heterojunctions.

III. NATURAL BAND LINEUP

For the lattice-matched Ge/GaAs(110), GaAs/ZnSe(110) heterojunctions of the Ge row, the interface dipole contribution to ΔE_v should be small since all the planes parallel to the interface are charge neutral. The calculations of Pickett, Louie, and Cohen for Ge/GaAs(110)[7] predict that the difference in bonding across an abrupt (110) interface separating bulk Ge from bulk GaAs produces an interface dipole of 0.05 eV. Thus, an accurate calculation of the natural band offset ΔE_v should be expected to give a value close to three-quarters of the minimum band-gap difference ΔE_g (min). The same conclusion applies to the remaining Ge row heterojunctions.

Figure 1 shows a scheme for determining the natural band lineup ΔE_v between a pair of bulk semiconductors, with valence band edges E_v and E_v' and average Hamiltonians $-H_{av}$ and H_{av}', determined relative to a common vacuum reference level. The average Hamiltonian is defined by

$$H_{av} = (1/n)\mathrm{Tr}[H(k_B)]\,, \tag{2}$$

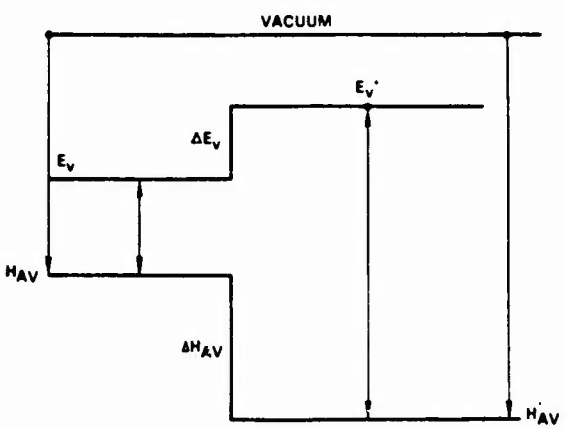

FIG. 1. Energy band diagram for determining ΔE_v; H_{av} and H_{av}' are the average bulk crystal Hamiltonians.

where n is the number of eigenvalues of the Hamiltonian H at the mean-value point, i.e., at the Baldereschi point $k = k_B$ of the Brillouin zone. For diamond and zinc-blende semiconductors, $k_B = (2\pi/a)\,(0.6223, 0.2953, 0)$, where a is the lattice constant of the semiconductor.[18] Since the Ge-row heterojunctions are lattice matched with a lattice constant of 5.65 Å, they all have the same mean-value point. It follows from Fig. 1, that the band offset ΔE_v is given by

$$\Delta E_v = (H'_{av} - E'_v) - (H_{av} - E_v) - \Delta H_{av} . \tag{3}$$

In the absence of an interface dipole, the natural band lineup given by Eq. (3) shows that the valence band offset ΔE_v is completely determined from a knowledge of the positions of the valence band edges relative to the average crystal Hamiltonians in each bulk semiconductor combined with the known difference ΔH_{av} between the average Hamiltonians. This difference is calculated explicity in terms of the definition in Eq. (2) of H_{av}. For tight-binding band theory using only s- and p-type orbitals with two atoms per unit cell and four orbitals per atom, the resulting Hamiltonian has eight rows and eight columns and the evaluation of Eq. (2) becomes particularly simple. The eight diagonal matrix elements are given by

$$H_{11} = \epsilon_s^c + (ss\sigma)_2^{cc} \sum_{2NN} \exp[i(\alpha u + \beta v + \gamma w)] , \tag{4}$$

$$H_{22} = \epsilon_f^c + \sum_{2NN} [(u^2/8)(pp\sigma)_2^{cc} + (1 - u^2/8)(pp\pi)_2^{cc}] \times \exp[i(\alpha u + \beta v + \gamma w)] , \tag{5}$$

$$H_{33} = \epsilon_p^c + \sum_{2NN} [(v^2/8)(pp\sigma)_2^{cc} + (1 - v^2/8)(pp\pi)_2^{cc}] \times \exp[i(\alpha u + \beta v + \gamma w)] , \tag{6}$$

$$H_{44} = \epsilon_p^c \sum_{2NN} [(w^2/8)(pp\sigma)_2^{cc} + (1 - w^2/8)(pp\pi)_2^{cc}] \times \exp[i(\alpha u + \beta v + \gamma w)] , \tag{7}$$

$$H_{55} = \epsilon_s^a + (ss\sigma)_2^{aa} \sum_{2NN} \exp[i(\alpha u + \beta v + \gamma w)] , \tag{8}$$

$$H_{66} = \epsilon_p^a + \sum_{2NN} [(u^2/8)(pp\sigma)_2^{aa} + (1 - u^2/8)(pp\pi)_2^{aa}] \times \exp[i(\alpha u + \beta v + \gamma w)] , \tag{9}$$

$$H_{77} = \epsilon_p^a + \sum_{2NN} [(v^2/8)(pp\sigma)_2^{aa} + (1 - v^2/8)(pp\pi)_2^{aa}] \times \exp[i(\alpha u + \beta v + \gamma w)] , \tag{10}$$

$$H_{88} = \epsilon_p^a + \sum_{2NN} [(w^2/8)(pp\sigma)_2^{aa} + (1 - w^2/8)(pp\pi)_2^{aa}] \times \exp[i(\alpha u + \beta v + \gamma w)] . \tag{11}$$

In these equations, ϵ_s^c and ϵ_p^c are s- and p-state cation energies, and ϵ_s^a and ϵ_p^a are the anion s- and p-state energies, respectively. The $(ss\sigma)$, $(pp\pi)$ $(pp\sigma)$ symbols are second nearest-neighbor Slater-Koster LCAO parameters.[19] The superscript cc refers to matrix elements between second nearest cation neighbors and the superscript aa refers to second nearest-neighbor anion interactions. The subscript 2 indicates a second nearest neighbor Slater–Koster matrix element.

The parameters $(\alpha, \beta, \gamma) = (k_x, k_y, k_z)\, a/4 = ka/4$ represent the k vector in the Brillouin zone where, a, is the lattice constant. The summations are taken over the 12-s nearest neighbors of the diamond and zinc-blende structures using as summation indices, u, v, w.

At the Baldereschi point $(\alpha, \beta, \gamma) = k_B a/4$ and Eq. (3) can be evaluated using Eqs. (4)–(11) and $n = 8$. If only first nearest-neighbor interactions are considered, then

$$H_{av} = 1/2[(\epsilon_s^c + 3\epsilon_p^c)/4 + (\epsilon_s^a + 3\epsilon_p^a)/4] \tag{12}$$

which is just the average hybrid energy of the bulk material. If the average hybrid energy is the same in two bulk crystals forming a lattice-matched heterojunction, then ΔH_{av} vanishes, and Eq. (3) above is identical to Eq. (3) in the theory of Harrison and Tersoff[11] and would predict the same band offsets. As we have seen, these band offsets do not obey the observed scaling relation for lattice-matched Ge row heterojunctions. Therefore, one may conclude that second neighbor contributions to H_{av} (and possibly d-orbital contributions as well) should be included in calculating ΔE_v from Eq. (3).

IV. SUMMARY

The simple experimentally observed scaling relation $\Delta E_v / \Delta E_g(\min) = 3/4$ satisfied by Ge/GaAs(110), GaAs/ZnSe(110), and Ge/ZnSe(110) heterojunctions has been compared with several recent theoretical predictions. Of these, the most successful at reproducing the experimentally observed trend is the original pseudopotential work of Frensley and Kroemer.[4] A relationship between average crystal Hamiltonians and band offsets has been developed and a solution of the band lineup problem in terms of these averages has been obtained.

It has been shown that for s–p bonded tetrahedral semiconductors in the nearest-neighbor approximation, the theory is equivalent to that presented by Harrison and Tersoff[11] and predicts the same band lineups. Since these lineups do not obey the experimentally observed scaling relation for Ge row heterojunctions it is concluded that the contributions of higher-order neighbor interactions to ΔE_v need to be retained in the theory. It is interesting to note that only second nearest neighbor matrix elements contribute to ΔH_{av}. A universal theory exists for first nearest neighbor LCAO matrix elements[19] and its extension to second nearest-neighbor matrix elements would facilitate a test of the predictive accuracy of the present theory.

a) Supported by ONR Contract No. N00014-85-C-0135.

[1] J. R. Waldrop, R. W. Grant, S. P. Kowalczyk, and E. A. Kraut, J. Vac. Sci. Technol. A 3, 835 (1986).
[2] S. P. Kowalczyk, E. A. Kraut, J. R. Waldrop, and R. W. Grant, J. Vac. Sci. Technol. 21, 482 (1982).
[3] W. R. Frensley, Ph. D. thesis, University of Colorado, Boulder, Colorado, 1976.
[4] W. R. Frensley and H. Kroemer, J. Vac. Sci. Technol. 13, 810 (1976).
[5] W. R. Frensley and H. Kroemer, Phys. Rev. B 16, 2642 (1977).
[6] W. E. Pickett and M. L. Cohen, Phys. Rev. B 18, 939 (1978).

[7]W. E. Pickett, S. G. Louie, and M. L. Cohen, Phys. Rev. B 17, 815 (1978).
[8]W. A. Harrison, J. Vac. Sci. Technol. 14, 1016 (1977).
[9]W. A. Harrison, Phys. Rev. B 24, 5835 (1981).
[10]E. A. Kraut, J. Vac. Sci. Technol. B 2, 486 (1984).
[11]W. A. Harrison and J. Tersoff, J. Vac. Sci. Technol. B 4, 1068 (1986).
[12]J. Tersoff, Phys. Rev. B 30, 4874 (1984).
[13]J. Tersoff, J. Vac. Sci. Technol. B 4, 1066 (1986).
[14]J. Tersoff, Surf. Sci. 168, 275 (1986).
[15]Y. C. Ruan and W. Y. Ching, J. Appl. Phys. 60, 4035 (1986).
[16]R. L. Anderson, Solid-State Electron. 5, 341 (1962).
[17]A. G. Milnes and D. L. Feucht, *Heterojunctions and Metal-Semiconductor Junctions* (Academic, New York, 1972), p. 9.
[18]A. Baldereschi, Phys. Rev. B 7, 5212 (1973).
[19]S. Froyen and W. A. Harrison, Phys. Rev. B 20, 2420 (1979).

CHAPTER 4

INTERFACE CONTRIBUTIONS TO HETEROJUNCTION BAND DISCONTINUITIES: X-RAY PHOTOEMISSION SPECTROSCOPY INVESTIGATIONS

R.W. GRANT, E.A. KRAUT, J.R. WALDROP and S.P. KOWALCZYK *

Rockwell International Corporation
Science Center
Thousand Oaks, CA 91360, USA

* Permanent address: IBM Thomas J. Watson Research Center, Yorktown Heights, NY, USA.

Heterojunction Band Discontinuities: Physics and Device Applications
Edited by F. Capasso and G. Margaritondo
© Elsevier Science Publishers B.V., 1987

Contents

1. Introduction 169
2. The XPS technique for observing interface dipoles and determining ΔE_v 170
   2.1. Measurement of interface contributions to ΔE_v by XPS 170
   2.2. Determination of ΔE_v 176
3. Experimental observations of interface contributions to ΔE_v 181
   3.1. Dependence of ΔE_v on crystallographic orientation 181
      3.1.1. Orientation dependence of Ge/GaAs interface dipoles 181
      3.1.2. Polar versus nonpolar heterojunction interfaces 185
   3.2. Growth-sequence dependence of ΔE_v 190
      3.2.1. Interface chemistry 191
      3.2.2. Compound–elemental (110) semiconductor heterojunctions 192
         3.2.2.1. Compound semiconductor–Ge(110) ΔE_v systematics 193
         3.2.2.2. Instability of the GaAs/Ge(110) interface 194
         3.2.2.3. Possible role of antiphase disorder 198
      3.2.3. Isocolumnar (110) heterojunctions 200
   3.3. Transitivity of ΔE_v 201
4. Summary 204
References 205

1. Introduction

Semiconductor heterojunctions are used in electronic devices to provide selective control over carrier transport by means of energy band discontinuities. The band gap discontinuity, ΔE_g, at the interface between two dissimilar semiconductors is the sum of the valence-band discontinuity, ΔE_v, and the conduction-band discontinuity, ΔE_c. The distribution of ΔE_g between the valence and conduction bands is thus of fundamental interest and importance, both to semiconductor device design and to the interpretation of device characteristics. Reproducible heterojunction fabrication techniques and an understanding of factors that affect heterojunction band discontinuities will be necessary before semiconductor heterojunctions are optimally utilized in device applications.

To be most useful in semiconductor device design and fabrication, heterojunction band discontinuities must be known and controlled to approximately the thermal energy, ~ 0.025 eV at room temperature. Recent progress in fabricating abrupt heterojunction interfaces by molecular beam epitaxy (MBE) and chemical vapor deposition has renewed interest in measuring and predicting heterojunction band discontinuities. Band discontinuities measured on such abrupt heterojunction interfaces are considered to be more reproducible and appropriate for comparison with theoretical models of ideal interfaces. There are several theories to predict heterojunction band discontinuities [1–4]. These theories are based on linear models which estimate band discontinuities from differences in absolute energies associated with the two semiconductors that form the heterojunction. Comparison of Harrison's LCAO model [1] with selected experimental data has suggested [5–8] that the accuracy of prediction is at present ~ ±0.2 eV; similar predictive accuracy has been indicated [9] for Tersoff's heterojunction model [4]. Linear heterojunction models do not account for band discontinuity contributions that are due to the presence of interface dipoles caused by interface microscopic structure. Although the contribution of these interface dipoles may in most cases be only a few tenths of an eV, they are significant and may account in part for the differences observed between theory and experiment.

Because interface dipoles can alter heterojunction band discontinuities by substantially more than the thermal energy, it is important to understand the origin of these dipoles and to provide results for critical tests and refinements of theoretical models. For the investigation of interface contributions to heterojunction band discontinuities, it is essential to utilize a measurement technique that will detect changes in band discontinuities with an experimental uncertainty considerably smaller than the observed effect. Various techniques for measuring heterojunction band discontinuities have recently been critically reviewed [6]; in most cases measurement accuracy better than ± 0.1 eV is difficult to achieve in other than specialized cases. Although important results have been obtained at this level of accuracy, an improvement would clearly be beneficial. A technique based on the use of X-ray photoemission spectroscopy (XPS) has been developed [10,11] that is capable of measuring changes in ΔE_v with an uncertainty of ± 0.01 eV. This XPS technique is thus particularly well suited to study interface dipole contributions to ΔE_v for a given heterojunction formed between two semiconductors as a function of interface preparation variables. The XPS technique is also capable of measuring the absolute value of ΔE_v with sufficient accuracy for comparison with theory [11–13]. As will be discussed, this measurement requires the determination of core-level to valence-band maximum binding energy differences and the consequent introduction of additional uncertainty into the measurement. However, in favorable cases absolute ΔE_v values have been determined to ± 0.04 eV, which compares well with most other measurement techniques.

This chapter will provide a description of the XPS technique for measuring interface contributions to heterojunction band discontinuities and the extension of this method used to obtain absolute values of ΔE_v. Several studies that directly observe interface dipoles at specific heterojunction interfaces (by using the XPS method) will be discussed. Possible origins of these interface contributions to ΔE_v will be noted.

2. The XPS technique for observing interface dipoles and determining ΔE_v

This section discusses the XPS method for measuring interface contributions to heterojunction band discontinuities and the extension of the method which enables the measurement of absolute ΔE_v values.

2.1. Measurement of interface contributions to ΔE_v by XPS

A key point made in this section is that it is not necessary to measure the

absolute magnitude of ΔE_v with precision in order to measure changes (interface contributions) in ΔE_v with precision.

The most common application of XPS is the analysis of interface elemental and chemical composition [14]. However, it is also well established [15,16] that the kinetic energy, E_k, of electrons emitted from a semiconductor depends on the position of the Fermi level, E_F, within the semiconductor band gap. This latter aspect of XPS makes it possible to determine E_F relative to the valence-band maximum, E_v, in the region of the semiconductor from which the photoelectrons originate. XPS can therefore be used as a contactless nondestructive technique to measure interface-potential related quantities such as heterojunction band discontinuities.

The escape depth, λ, for photoelectrons produced within a solid by incident radiation increases monotonically from ~ 5 to ~ 25 Å as the electron E_k increases from about 100 to 1500 eV [17]. A monochromatic AlKα ($h\nu = 1486.6$ eV) X-ray source is convenient for XPS measurements. Most semiconductors will contain an element that has an outer core level with binding energy, E_B, less than 100 eV. The escape depth for photoelectrons excited from an outer core level will therefore be ~ 25 Å and thus the photoelectron signal is averaged over many atomic layers. It is desirable to use outer core levels in XPS heterojunction band discontinuity studies because photoelectrons originating from these levels will in general have the narrowest linewidths (as determined by final-state lifetimes); in addition, when measuring absolute values of ΔE_v (see sect. 2.2), there is an advantage to keeping the core level to E_v binding energy difference relatively small.

A schematic diagram of a typical heterojunction sample that is suitable for XPS band discontinuity measurements is illustrated in fig. 1. The overlayer thickness of semiconductor B must be comparable to λ and the interface width must be a small fraction of λ.

The measurement of interface contributions to ΔE_v is shown in fig. 2 by a schematic energy band diagram appropriate for the sample shown in fig. 1 (with an abrupt interface). The quantities E_{CL}^A, E_v^A, and E_c^A are, respectively, a core-level binding energy, the valence-band maximum, and the conduction-band minimum associated with semiconductor A; similar energies are defined for semiconductor B. The core-level binding energy difference across the interface is $\Delta E_{CL} = E_{CL}^A - E_{CL}^B$. If a change in an interface dipole occurs, all energy levels in semiconductor A will be shifted by an equal amount relative to the energy levels in semiconductor B (as indicated by dotted lines in fig. 2). Thus a change in the heterojunction

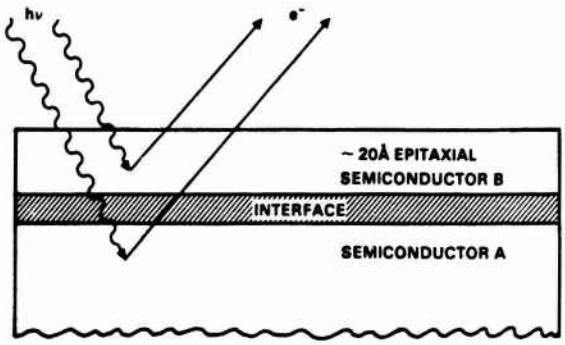

Fig. 1. Schematic illustration of a heterojunction sample that is suitable for XPS band discontinuity measurements.

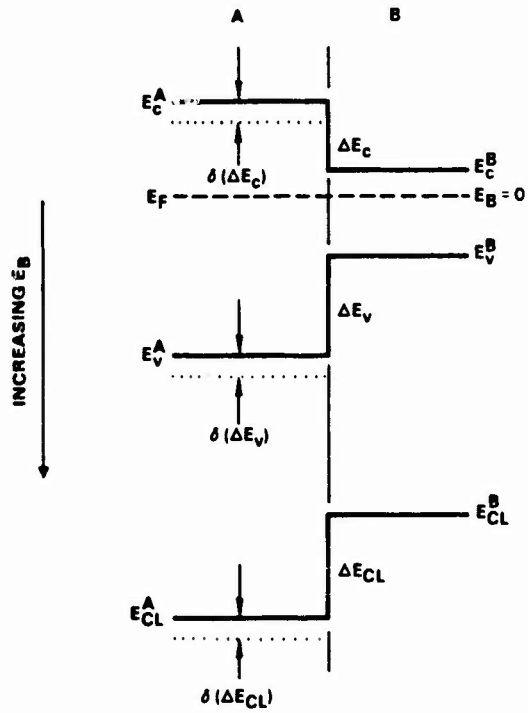

Fig. 2. Schematic energy-band diagram that illustrates the XPS measurement of interface contributions to ΔE_v.

valence-band discontinuity, $\delta(\Delta E_v)$, caused by an interface dipole, will be accompanied by a change in the heterojunction conduction-band discontinuity, $\delta(\Delta E_c)$, and a corresponding change in the core-level binding energy difference, $\delta(\Delta E_{CL})$. A change in an interface contribution to a heterojunction band discontinuity will therefore be observed as $|\delta(\Delta E_v)| = |\delta(\Delta E_c)| = |\delta(\Delta E_{CL})|$, with the signs of these energy differences determined by the relative positions of the corresponding energy levels in semiconductors A and B. Interface contributions to heterojunction band discontinuities are measured by using XPS to determine $\delta(\Delta E_{CL})$. As shown in fig. 1, photoelectrons which originate in semiconductor A pass through any dipole layer at the interface in order to be emitted from the surface and detected while photoelectrons that originate in semiconductor B do not pass through this layer. For example, a photoelectron from semiconductor A passing through the dipole layer from lower-to-higher electron density will experience a deceleration. The resulting decrease in relative E_k is proportional to the dipole moment per unit area at the interface. This E_k decrease will directly be measured as a relative increase in E_{CL}^{A}. For the energy band diagram shown in fig. 2, the resulting increase in the core-level binding energy difference, $\delta(\Delta E_{CL})$, is a direct measure of the equivalent increase in the heterojunction valence-band discontinuity, $\delta(\Delta E_v)$. For well-resolved outer core levels, it is possible to measure ΔE_{CL} to ± 0.01 eV [10,11]. As an example, table 1 provides ΔE_{CL} measurements on two different heterojunction samples of Ge grown on GaAs(110). Five independent measurements of $\Delta E_{CL} = E_{Ga3d}^{GaAs} - E_{Ge3d}^{Ge}$ were obtained for sample A

Table 1
Measurement of Ga3d–Ge3d core-level binding energy differences for two different Ge/GaAs(110) heterojunctions.

Sample	Ge layer thickness (Å)	$E_{Ga3d}^{GaAs} - E_{Ge3d}^{Ge}$ * (eV)
A	14	−10.194
		−10.200
		−10.195
		−10.202
		−10.201
B	17	−10.210
		−10.208

* Uncertainty is ±0.01 eV.

and two independent ΔE_{CL} measurements were obtained for sample B. The scatter in values for a single sample is < 0.01 eV (however, consideration of spectrometer energy-scale calibration accuracy increases the measurement uncertainty to ± 0.01 eV). Thus, as noted at the beginning of this section, it is possible to measure interface contributions to heterojunction band discontinuities with an uncertainty of ± 0.01 eV without measuring the absolute value of ΔE_v.

The measurement of interface contributions to ΔE_v as described has been simplified in some important ways. One assumption is that the interface is atomically abrupt. It is well-known [18] that chemical reactions and interdiffusion can occur on a monolayer scale to broaden semiconductor interfaces even when they are formed at room temperature. These effects may alter the potential distribution due to the formation of an interfacial dipole layer of finite width in the immediate vicinity of the interface. In addition, interface chemical bonding [19] and the vacuum interface may contribute chemically shifted components to the core-level peaks; if not experimentally resolved, these chemical shifts could alter the apparent value of ΔE_{CL}. Even for an ideally abrupt interface, calculations have shown that potential variations occur within one or two atomic layers normal to the interface (see, e.g., refs. [20,21]). These considerations suggest that there is an advantage to collecting the photoelectron signal primarily from a region near, but not precisely at, an abrupt interface. An ideal situation would be to have sufficient energy resolution to resolve photoelectron signals which originate in the interface region from those that originate in the bulk semiconductor very near the interface. As a rough generality, the energy resolution associated with the various forms of photoelectron spectroscopy improves for decreasing E_k analysis. However, for low E_k electrons that originate from outer core levels, the fraction of the total electron signal that originates in the bulk semiconductor very near the interface may be small due to the small λ. Thus, in some cases it may be advantageous to sacrifice energy resolution in order to obtain a fairly large λ and thus minimize the fraction of photoelectron signal which originates from the monolayer or two interfacial region. In practice, the linewidths for the XPS photoelectron peaks and a dependence of results on overlayer thickness are monitored to assess the influence of interface potential variations or chemical shifts on the measured ΔE_{CL}.

Even without the possible complications in measuring ΔE_{CL} that are of microscopic origin (as discussed in the previous paragraph), the measurement of interface contributions to ΔE_v (as illustrated in fig. 2) has been simplified by assuming a flat-band condition on both sides of the hetero-

junction interface. The potential variation away from the interface region follows a solution of the Poisson equation. For a fixed interface E_F position, the depletion width for a given semiconductor will increase for decreased doping density. Thus, when using large λ to minimize the fraction of the photoelectron signal which originates from the monolayer or two interfacial region, it is beneficial to have moderately or lightly doped semiconductors to minimize the potential variation within the sampling depth. In general, a measurement error of < 0.01 eV is expected for a doping density $\lesssim 10^{17}$ cm^{-3} and $\lambda \sim 25$ Å. The practical lower limit on doping is that the sample does not become insulating and thus charges under the influence of the X-ray beam.

Sample preparation is, of course, an important aspect of applying the XPS method of measuring interface contributions to heterojunction band discontinuities. In most cases, it is necessary to fabricate samples of the type shown in fig. 1 within the ultrahigh vacuum system of the XPS spectrometer to avoid contamination and/or oxidation of the sample surface. A fairly general-purpose experimental apparatus for XPS interface studies is shown schematically in fig. 3. With this apparatus a clean substrate is prepared by ion sputtering and/or thermal annealing. The surface cleanliness is determined by XPS and surface order is assessed by low-energy electron diffraction (LEED). MBE is used to fabricate the ~ 20 Å thick epitaxial overlayer and again XPS and LEED are used to assess surface cleanliness and order.

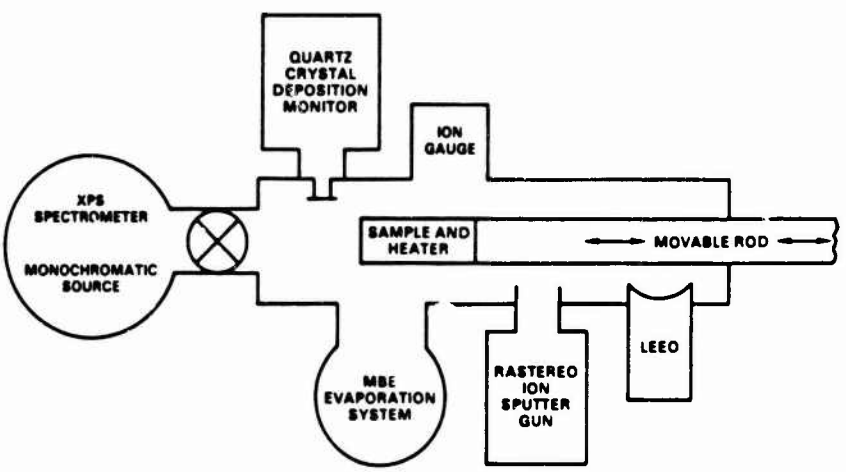

Fig. 3. Schematic diagram of an XPS system for ΔE_v measurements.

2.2. Determination of ΔE_v

The XPS method for measuring interface contributions to heterojunction band discontinuities can be extended to determine absolute values of ΔE_v. The approach is illustrated by the schematic band diagram shown in fig. 4. The assumptions made in drawing this idealized flat-band diagram were discussed in sect. 2.1. While the investigation of interface contributions to ΔE_v requires only the measurement of ΔE_{CL}, the determination of the absolute magnitude of ΔE_v requires measurement of two additional parameters, namely the core level to E_v binding energy difference in bulk semiconductors A and B, $(E_{CL}^A - E_v^A)$ and $(E_{CL}^B - E_v^B)$ respectively. By inspection of fig. 4 it is seen that

$$\Delta E_v(\mathrm{A}-\mathrm{B}) = \left(E_{CL}^B - E_v^B\right) - \left(E_{CL}^A - E_v^A\right) + \Delta E_{CL}(\mathrm{A}-\mathrm{B}). \qquad (1)$$

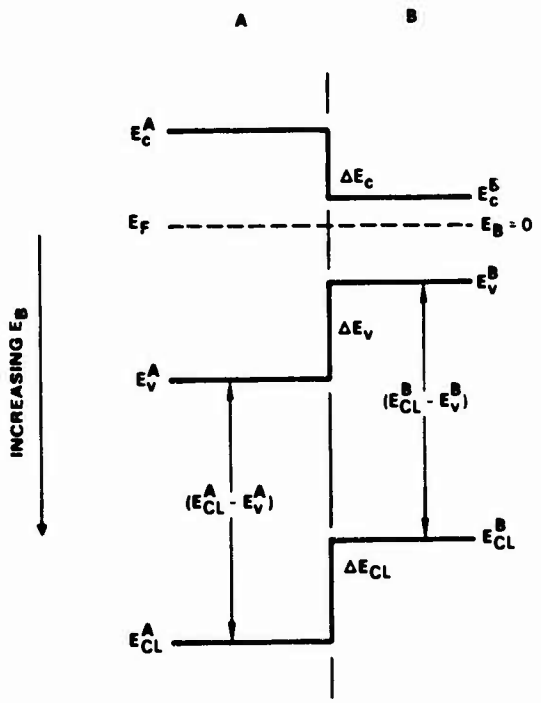

Fig. 4. Schematic energy-band diagram that illustrates the measurement of the absolute value of ΔE_v by XPS.

Thus, to apply XPS for ΔE_v measurements it is essential to determine the bulk semiconductor material parameters $(E_{CL} - E_v)$ for those semiconductors which are to form the heterojunctions of interest. A method for determining these parameters with precision is outlined in this section.

Many $(E_{CL} - E_v)$ measurements for semiconductors have been reported in the literature (see ref. [22] for a recent tabulation). In general, the precision of most measurements has been limited to about ± 0.1 eV. A primary difficulty with the measurement of $(E_{CL} - E_v)$ is the accurate determination of the E_v position in photoemission spectra. The most frequently employed method involves extrapolation of a tangent line to the leading edge of the valence-band spectrum to the energy axis; this intercept is defined as E_v. It has been noted that this procedure can lead to substantial uncertainties [23]. In addition to the XPS method for measuring ΔE_v (described in this section), there are other photoemission methods for measuring ΔE_v that employ the linear extrapolation procedure of determining E_v in the photoemission spectrum (see, e.g., ref. [24]). Use of this extrapolation procedure accounts in large part for the typical ± 0.1 eV uncertainty in ΔE_v associated with these other photoemission measurements.

A method that largely overcomes the difficulty in determining the E_v position in XPS data has been reported [12,13]. In essence the approach involves a least-squares fitting of the XPS data in a limited region around the estimated position of E_v with an instrumentally broadened valence-band density of states (VBDOS) defined as

$$N_v(E) = \int_0^\infty n_v(E')\, g(E - E')\, \mathrm{d}E', \tag{2}$$

where $n_v(E')$ is the theoretical VBDOS and $g(E)$ is the instrumental response function. The XPS spectral intensity $I(E)$ is assumed to have the form

$$I(E) = SN_v(E - E_v) + B, \tag{3}$$

where S is a scale factor, and B is a constant random noise background. As an example of determining the position of E_v, angle-resolved XPS data collected from a Ge(110) surface are shown in fig. 5. The solid curve is a least-squares fit of $N_v(E)$ to the experimental data where a nonlocal pseudopotential VBDOS [25] was used for $n_v(E')$. The position of E_v^{Ge} corresponds to $N_v(0)$.

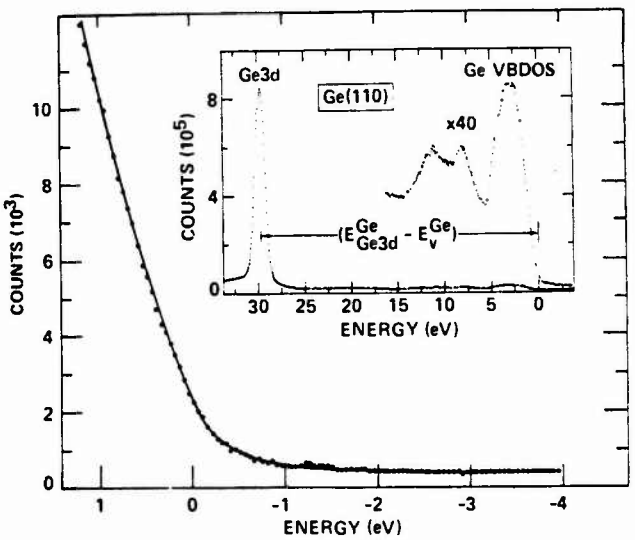

Fig. 5. Least-squares fit of the instrumentally broadened VBDOS (solid curve) to XPS data in the region of E_v. Inset shows the XPS spectrum which contains the VBDOS and the Ge3d core level. The energy scale is zero at E_v. Data were taken from ref. [13].

A primary difficulty with the determination of E_v in XPS spectra is the possibility of VBDOS distortion due to occupied surface states in the vicinity of E_v. To detect possible VBDOS distortion, sets of angle-resolved measurements are analyzed and compared. Because the XPS photoelectron cross section is expected to depend on the orbital character of filled surface states [26,27], it should be possible to detect the presence or absence of these states by studying the angular variation of the XPS valence-band spectrum in the vicinity of E_v. In fig. 6a, a convenient polar-coordinate system is defined to relate the photoemission direction e to the crystallographic axes of the Ge(110) surface. The polar angle for the measurements described here was 51.5° and only the azimuthal angle α was varied. Although the Ge(110) surface has been studied by LEED [28] little is known about the corresponding electronic structure. Figure 6b shows the results of analyzing two sets of Ge(110) data for $\alpha = 0°$ and 90°. The error bars represent a 95% confidence interval for the least-squares procedure [13]. The quantity E_{max} is the end point of the fitting interval. The relatively constant value of $(E^{Ge}_{Ge3d} - E^{Ge}_{v}) = 29.52$ eV independent of E_{max} and α suggests that any filled Ge(110) surface states below E^{Ge}_{v} are either very weakly localized near the surface or lie well outside the energy interval

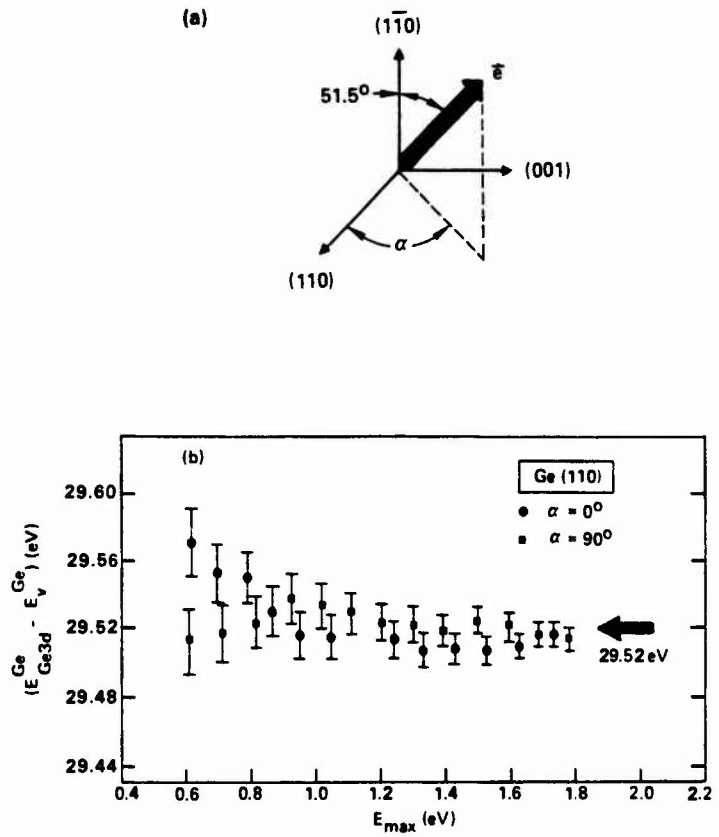

Fig. 6. (a) Polar-coordinate system relating photoelectron emission direction e to crystallographic axes for a (110) crystal surface. The azimuthal angle α is in the plane of the crystal surface. (b) Position of E_v^{Ge} measured relative to E_{Ge3d}^{Ge} as a function of the end point, E_{max}, of the fitting interval. Results are shown for data obtained at two different photoelectron emission directions. Data were taken from ref. [13].

analyzed. In either case, surface states do not appear to complicate the determination of $(E_{Ge3d}^{Ge} - E_v^{Ge})$ from Ge(110) XPS data; the situation is quite different for Ge(111) XPS data where the apparent value of $(E_{Ge3d}^{Ge} - E_v^{Ge})$ is found to depend on the fitting interval [13].

As can be seen from eq. (1), the uncertainty in the bulk semiconductor $(E_{CL} - E_v)$ binding energy difference directly influences the uncertainty in the measurement of ΔE_v by the XPS method. Factors that contribute to the uncertainty in determining $(E_{CL} - E_v)$ bulk binding-energy differences

Table 2
$E_{CL} - E_v$ binding energy differences in eV as measured by XPS.

Semiconductor surface	core level	$(E_{CL} - E_v)_{XPS}$	$(E_{CL} - E_v)_b$
Ge(110)	Ge3d	29.52 ± 0.03	29.52 ± 0.03
GaAs(110)	Ga3d	18.78 ± 0.03	18.75 ± 0.03
	As3d	40.70 ± 0.03	40.74 ± 0.03
ZnSe(110)	Zn3d	8.86 ± 0.03 *	-
InAs(100)	In4d	17.38 ± 0.03 *	-
	As3d	40.72 ± 0.03 *	-
CdTe($\bar{1}\bar{1}\bar{1}$)	Cd4d	10.24 ± 0.03	-
HgTe($\bar{1}\bar{1}\bar{1}$)	$Hg5d_{5/2}$	7.66 ± 0.04	-
AlAs(100)	As3d	40.16 ± 0.04	-
	Al2p	72.70 ± 0.04	-

* Error limits refined subsequent to initial publication.

have been considered in detail [13]. These factors include band bending, surface chemical shifts, background effects associated with inelastic scattering processes, instrumental line shape, and spectrometer calibration accuracy. It is concluded that $(E_{CL} - E_v)$ can be determined for the 3d levels of Ge and GaAs with an uncertainty of $\leqslant 0.026$ eV. As discussed in sect. 2.1, ΔE_{CL} can be measured with an uncertainty of ± 0.01 eV. If $(E_{CL} - E_v)$ parameters for bulk semiconductors are known with an uncertainty of 0.026 eV, eq. (1) indicates that XPS measurements of ΔE_v are possible with an uncertainty of $\sim \pm 0.04$ eV; this is a considerable improvement over the ± 0.1 eV measurement accuracy reported for many ΔE_v measurement techniques.

One final point is that surface chemical shifts can alter XPS measured $(E_{CL} - E_v)$ parameters by a few hundredths of an eV. If these surface chemical shifts are well known, as for the GaAs (110) surface [29], an accurate correction can be made to obtain the bulk semiconductor $(E_{CL} - E_v)$ value. The XPS measured and the surface chemical shift corrected bulk semiconductor values of $(E_{CL} - E_v)$ will be denoted as $(E_{CL} - E_v)_{XPS}$ and $(E_{CL} - E_v)_b$, respectively. Values of these parameters for Ge [13], GaAs [13], ZnSe [30], InAs [31], CdTe [32], HgTe [32] and AlAs [33], are collected in table 2 [34]. To increase the generality of the XPS method for measuring ΔE_v, additional $(E_{CL} - E_v)_b$ values will need to be determined for semiconductors of interest.

3. Experimental observations of interfac.. contributions to ΔE_v

This section primarily discusses studies that use the XPS method (sect. 2.1) to determine interface contributions to ΔE_v. As previously noted, there is considerable evidence that interface dipoles can alter ΔE_v for some heterojunctions by at least a few tenths of an eV. A few tenths of an eV variation in ΔE_v is large compared to kT and thus can influence the characteristics of semiconductor heterostructure devices. Observations of a ΔE_v dependence on crystallographic orientation and on growth sequence will be discussed. Also, a test of ΔE_v transitivity for a series of three heterojunctions will be described; such tests may be useful to select values of ΔE_v least influenced by interface dipoles and therefore most suitable for comparison with linear predictive models.

3.1. Dependence of ΔE_v on crystallographic orientation

A study of Ge/GaAs heterojunctions has provided clear evidence that ΔE_v depends on crystallographic orientation for these heterojunctions. A fundamental difference between heterojunctions formed on polar and nonpolar crystallographic faces that offers an explanation of the ΔE_v crystallographic orientation dependence is discussed.

3.1.1. Orientation dependence of Ge / GaAs interface dipoles

Observation of a ΔE_v crystallographic orientation dependence for abrupt vapor-grown Ge/GaAs heterojunctions based on transport measurements has been reported [35]. Unfortunately, the experimental uncertainty in these measurements is about as large as the measured effects (a few tenths of an eV). A study of the ΔE_v crystallographic orientation dependence for abrupt MBE-grown Ge on GaAs heterojunctions that utilized the XPS method has also been reported [10,11,36]. The results of this latter study are discussed here.

Heterojunctions of Ge/GaAs were prepared on GaAs substrates with (110), (100) and (111) orientations that had been cut from the same boule of GaAs material. The substrates were cleaned by sputtering with 750 eV Ar^+ ions and annealed at $\simeq 460\,^\circ$C to remove sputter damage. Prior to growth of the epitaxial layers, the room temperature GaAs substrate LEED patterns were: (110) (1×1), (111)Ga (2×2), $(\bar{1}\bar{1}\bar{1})$As (1×1) and (100)Ga $c(8 \times 2)$; the (100)As LEED pattern was either $c(2 \times 8)$ or (2×4). Very thin (~ 20 Å) epitaxial layers of Ge were grown at ~ 1 Å/s deposition rates under ultra-high vacuum (UHV) conditions on these substrates. A low-

growth temperature (~ 340 °C) was used to maximize interface abruptness. Following growth the samples were cooled to room temperature and LEED was used to confirm the epitaxy of the Ge overlayers.

The Ge3d and Ga3d core levels were studied to determine the crystallographic orientation dependence of ΔE_v; these core levels are well-resolved and are in a region of the XPS spectrum where the inelastically scattered electron background is smooth and featureless. A typical XPS spectrum obtained from a heterojunction that consisted of a thin epitaxial layer of Ge grown on a GaAs(110) (1 × 1) substrate is shown in fig. 7. To determine

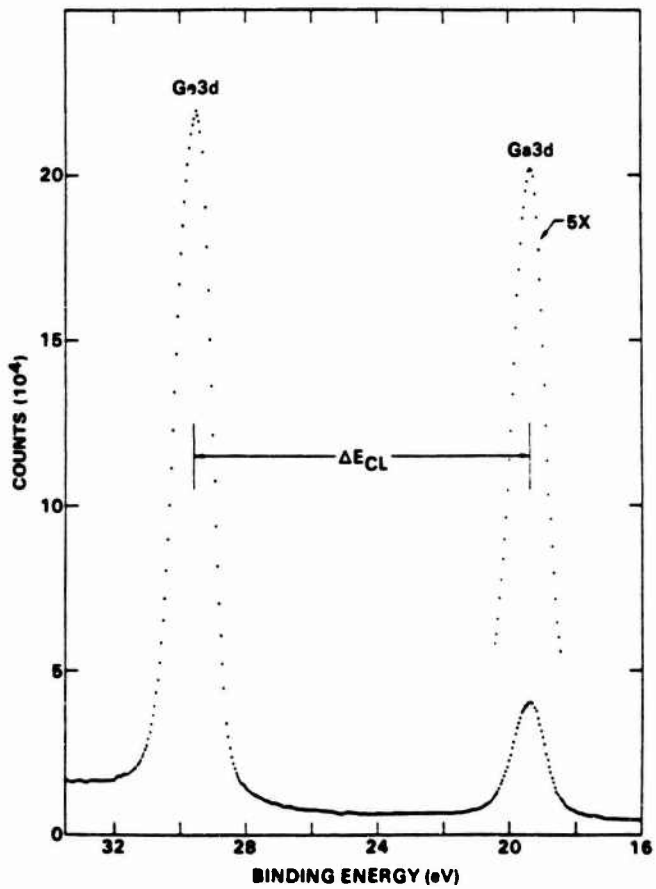

Fig. 7. XPS spectrum in the binding energy region of the Ga3d and Ge3d core levels obtained from a Ge/GaAs(110) heterojunction. Data were taken from ref. [10].

$\Delta E_{CL} = E^{GaAs}_{Ga3d} - E^{Ge}_{Ge3d}$, a background function that is proportional to the integrated photoelectron peak area was subtracted from the XPS data to correct for the effect of inelastic photoelectron scattering. The quantity ΔE_{CL} was measured between the centers of the peak widths at half of the peak heights. This procedure makes it unnecessary to resolve the spin–orbit splitting of the Ge3d and Ga3d levels (~ 0.5 eV) to obtain high precision peak positions.

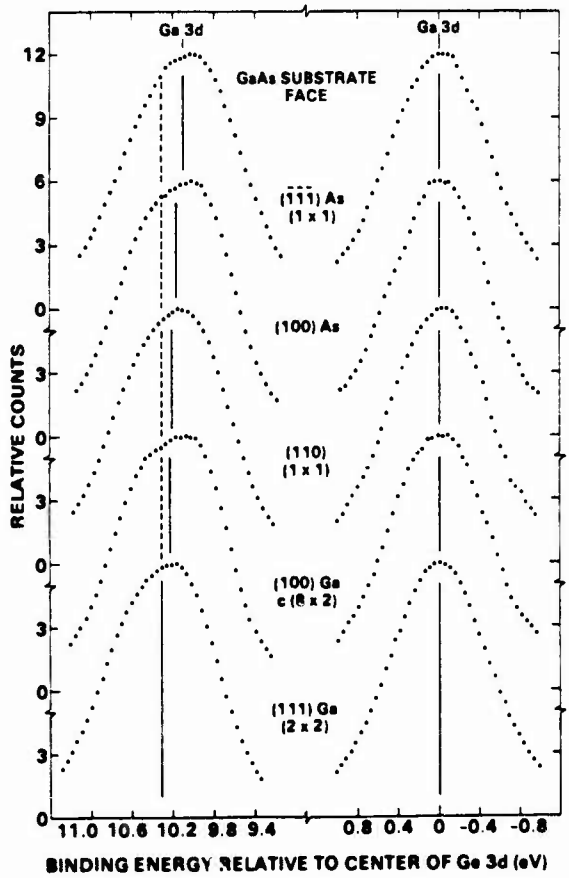

Fig. 8. XPS spectra in the binding energy region of the Ga3d and Ge3d core levels obtained for five different crystallographically oriented heterojunctions. The GaAs substrate crystal faces on which the thin epitaxial Ge overlayers were grown are indicated in the figure. The vertical lines indicate the centers of the various peaks as discussed in the text. Data were taken from ref. [11].

Thirty-three independent measurements were made on eight different Ge/GaAs heterojunctions. Figure 8 shows representative background subtracted XPS spectra from samples having each of the crystallographic faces studied. For easy comparison, each peak shown in this figure has been normalized to an equal height and the center (half-width at half-height) of each peak is indicated by a vertical solid line in the figure. The centers of the five Ga3d peaks have been aligned. The dashed vertical reference line that runs through the Ge3d peaks is the center of the Ge3d peak observed for the heterojunction that was grown on the GaAs(111)Ga(2 × 2) substrate. Inspection of fig. 8 directly indicates that ΔE_{CL} is dependent on the crystallographic orientation of the interface. As noted in sect. 2.1., the change in ΔE_{CL} is a direct measure of the change in ΔE_v and it is not necessary to know the actual magnitude of ΔE_v in order to detect the crystallographic orientation dependent interface contributions to ΔE_v.

Measurement results on eight different Ge/GaAs interfaces are given in table 3. In general, three to five independent measurements were made on each interface and the average ΔE_{CL} values are given in the table. In every case the measurement reproducibility for ΔE_{CL} was $< \pm 0.01$ eV and in most cases it was $< \pm 0.005$ eV. Spectrometer energy-scale calibration uncertainty increases the total error limit for ΔE_{CL} to ± 0.01 eV. The average linewidths, Γ, of the Ge3d and Ga3d photoelectron peaks that were measured at half of the peak height and the Ge epitaxial layer thickness for the eight Ge/GaAs interfaces are also given in table 3. If a

Table 3
The Ge epitaxial layer thickness, Ge3d and Ga3d photoelectron linewidths, Ge3d–Ga3d core-level binding energy differences, the average variation in ΔE_v relative to the (110) interface, and the ΔE_v value for eight different Ge–GaAs interfaces.

Substrate surface	Ge layer thickness (Å)	Γ(Ga3d) (eV)	Γ(Ge3d) (eV)	$E^{GaAs}_{Ga3d} - E^{Ge}_{Ge3d}$ [a] (eV)	$\delta(\Delta E_v)_{AVE}$ (eV)	(ΔE_v) [b] (eV)
(111)Ga (2×2)	13	1.17 ± 0.02	1.25 ± 0.01	−10.27	−0.085	0.50
	20	1.22 ± 0.02	1.26 ± 0.01	−10.31		0.46
(100)Ga c(8×2)	22	1.19 ± 0.02	1.25 ± 0.01	−10.22	−0.015	0.55
(110) (1×1)	14	1.13 ± 0.01	1.29 ± 0.01	−10.20	0	0.57
	17	1.16 ± 0.01	1.27 ± 0.01	−10.21		0.56
(100)As	14	1.15 ± 0.02	1.25 ± 0.01	−10.17	+0.035	0.60
($\bar{1}\bar{1}\bar{1}$)As (1×1)	13	1.21 ± 0.01	1.32 ± 0.01	−10.11	+0.10	0.66
	18	1.22 ± 0.01	1.28 ± 0.01	−10.10		0.67

[a] Uncertainty is ±0.01 eV.
[b] Uncertainty is ±0.04 eV.

sizeable potential variation occurred, either within the heterojunction area sampled or within the photoelectron escape depth, Γ would be broadened. A similar Γ broadening would occur if interface or surface chemical shifts were substantially affecting the measurements. Although the Γ values scatter somewhat, there is little significant systematic variation with crystallographic orientation or with Ge overlayer thickness. The ΔE_{CL} measurements for the two heterojunctions grown on each of the (110) (1×1) and $(\bar{1}\bar{1}\bar{1})$As(1×1) substrates reproduce within 0.01 eV. This agreement indicates that while ΔE_v for the heterojunction formed on the $(\bar{1}\bar{1}\bar{1})$As(1×1) substrate is ~ 0.10 eV larger than ΔE_v for the heterojunction formed on the (110) (1×1) substrate, the sample-to-sample reproducibility of ΔE_v for heterojunctions formed on these two substrates is 0.01 eV. The 0.04 eV variation in ΔE_{CL} for the two heterojunction samples formed on the (111)Ga(2×2) substrates appears to be outside of experimental error and most likely represents a real sample preparation-dependent ΔE_v difference between these two samples. In table 3, the column labeled $\delta(\Delta E_v)_{AVE}$ is the difference in the average ΔE_v values for the different crystallographic orientations referred to the results for the (110) interface; as discussed in sect. 2.1, this was evaluated from $\delta(\Delta E_v) = -\delta(\Delta E_{CL})$. The $(E_{CL} - E_v)$ values listed in table 2 for Ge3d and Ga3d have been used to evaluate the values of ΔE_v shown in the last column of table 3.

An explanation for the ΔE_v crystallographic orientation dependence of Ge/GaAs heterojunctions is offered in the next section.

3.1.2. Polar versus nonpolar heterojunction interfaces

A consideration of electrostatics leads to the conclusion that there is a fundamental difference between polar and nonpolar heterojunction interfaces [37] that offers a mechanism for obtaining a crystallographic orientation dependent interface dipole. To illustrate the concept, the electrostatics associated with a nonpolar (110) and a polar (100) Ge/GaAs interface will be compared.

Figure 9 shows a nonpolar Ge/GaAs (110) interface viewed along a $[\bar{1}10]$ direction. To simplify the discussion an ideal tetrahedral bonding arrangement is assumed and bond polarization effects are ignored. In an ideal tetrahedral bonding arrangement all bonds contain two electrons. This is independent of whether the bonds are Ge–Ge, Ge–Ga, Ge–As, or Ga–As. The net charge on an interface plane is, therefore, determined by the relative nuclear charge on the plane. A Ga atom has one proton less than a Ge atom while an As atom has one more proton. For the (110)

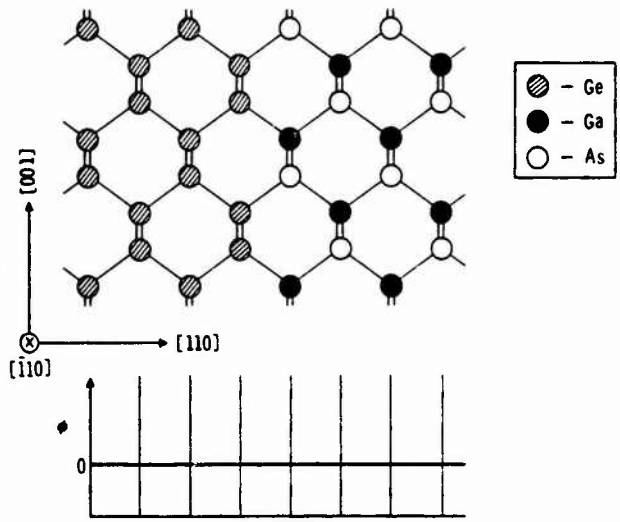

Fig. 9. A (110) heterojunction between Ge and GaAs. Every plane of atoms parallel to this nonpolar heterojunction is on average charge neutral. The symbols used to identify specific atoms are defined in this figure, and are the same for figs. 10–12. All atoms are tetrahedrally bonded; the "double" bonds schematically illustrated are two tetrahedral bonds projected onto the plane of the figure. If the potential, ϕ, is zero in the Ge, it will also be zero in the GaAs as shown at the bottom of the figure. This figure and figs. 10–12 were reproduced from ref. [37].

Ge/GaAs interface, the net charge on atom planes parallel to the interface is the same in Ge and GaAs as equal numbers of Ga and As atoms occupy the planes in GaAs. If the potential, ϕ, is zero in the Ge part of the heterojunction, integration of the Poisson equation from the Ge on the left through the interface into the GaAs on the right will cause no potential variation, as shown at the bottom of fig. 9. This corresponds to the absence of both a dipole layer and a charge accumulation at the interface.

The situation is quite different for a polar interface. Figure 10 illustrates a (001) Ge/GaAs heterojunction viewed along a [$\bar{1}$10] direction where the GaAs terminates with a Ga plane. The net charge on atom planes parallel to the interface is now different in GaAs and Ge. If it is again assumed that ϕ is zero in the Ge part of the heterojunction, integration of the Poisson equation from left to right yields the potential variation shown at the bottom of fig. 10. Upon crossing the first plane of negatively charged Ga atoms the potential gradient becomes positive and constant; the potential gradient returns to zero upon crossing the next plane of positively charged

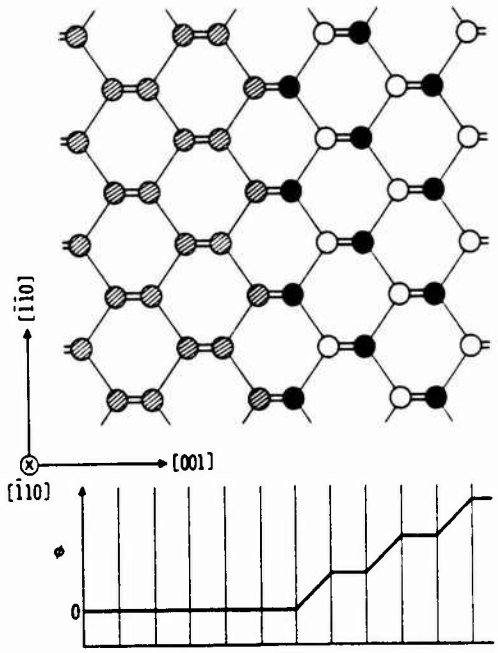

Fig. 10. A (001) heterojunction between Ge and GaAs. Note that the first atomic plane to the right of the junction consists entirely of Ga atoms that (without bond polarization) are negatively charged. The potential (assumed to be zero in Ge) averaged over planes parallel to the junction, is obtained by integrating the Poisson equation from left to right, as shown at the bottom of the figure.

As atoms. The result is a potential staircase function that has an average gradient and a fluctuating component. This average potential gradient is associated with interface charge accumulation [37] and produces a potential that cannot be sustained in a real heterojunction because the potential variation over a few atom distances would exceed the bandgap and result in spontaneous carrier generation.

The interface charge accumulation can be eliminated by adjusting the atomic composition of the interface region. One possibility is shown in fig. 11 where a transition plane with an equal number of Ga and Ge atoms is inserted between the bulk Ge and GaAs. Again the potential variation can be obtained (as shown at the bottom of fig. 11) by assuming $\phi = 0$ in the Ge and integrating the Poisson equation through the heterojunction. The single transition plane has eliminated the average potential gradient in the GaAs and produced an interface dipole shift, δ, which is estimated to be

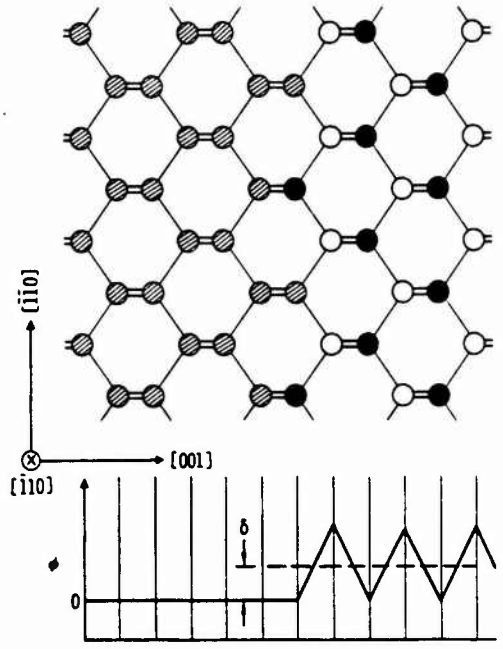

Fig. 11. A (001) heterojunction as in fig. 10, but with half of the Ga atoms in the junction plane replaced by Ge atoms. The potential obtained as previously described, is shown at the bottom of the figure. Although the average electric field in the GaAs has been eliminated, there remaines a dipole shift, δ, which is much larger than is experimentally observed.

~ 0.37 eV [37]. The observed dipole shifts of polar Ge–GaAs interfaces relative to the nonpolar Ge–GaAs(110) interface (sect. 3.1.1.) are much smaller than 0.37 eV, which suggests that the simplest ideal single transition plane interface geometry needed to eliminate charge accumulation at a polar interface does not occur.

By adjusting the atomic composition of the interface region on two transition planes as shown in fig. 12, it is possible to eliminate both charge accumulation and the dipole shift. The potential variation for this interface is shown at the bottom of fig. 12. Thus, a polar interface modification that eliminates both charge accumulation and dipole shifts requires an interface region with at least two transition planes. It seems likely that the growth process produces a nonplanar polar heterojunction as an interface of lowest energy. To explain the observed ~ 0.1 eV dipole shifts between polar and nonpolar Ge–GaAs interfaces (sect. 3.1.1), a deviation from the idealized interface structure shown in fig. 12 must occur. The simplest kind of

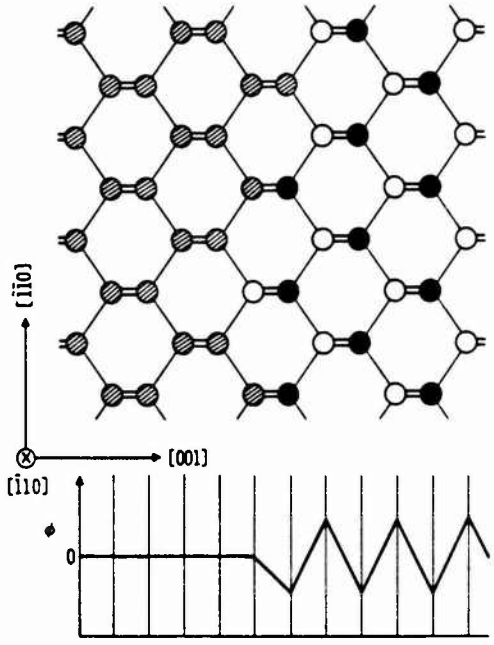

Fig. 12. A (001) heterojunction as in figs. 10 and 11 but with two compositionally adjusted junction transition planes. This is the simplest interface geometry that eliminates both charge accumulation and a dipole shift.

deviation would involve interchange of atom pairs with differing nuclear charge. An interchange of about one in fifteen interface atom pairs (which resulted in the transfer of one unit of nuclear charge between adjacent planes) would produce a dipole shift of ~ 0.1 eV [37].

Kroemer [6] has pointed out that it is unlikely for the polar interface atomic rearrangement to proceed far enough toward completion so as to completely eliminate interface charge accumulation and dipole shifts. He, therefore, argues that ΔE_v and interface charge for polar heterojunctions should be expected to be sample preparation-dependent and hence poorly reproducible.

As a final point, it has been shown that polar interfaces differ fundamentally from nonpolar interfaces by requiring at least two transition planes to eliminate charge accumulation and interface dipole contributions to ΔE_v that are substantially larger than experimental observations. It may appear that considerably nonabrupt interfaces are favored for polar heterojunc-

tions. Recent tight-binding calculations of atomic substitution energies have shown that atomic exchange at many ideal abrupt interfaces (including the Ge–GaAs interface) is not favored [38]. Competing factors may thus favor an optimum width for abrupt polar heterojunction interfaces of about two transition planes.

3.2. Growth-sequence dependence of ΔE_v

The order in which a heterojunction is fabricated (i.e., the growth sequence) can result in a ΔE_v variation [30,39,40]. This observation of an interface contribution to ΔE_v due to growth sequence indicates that the atomic arrangement near an interface must depend on details of the growth process which at least in some cases are likely determined by chemical considerations. It has been noted [41] that in some cases thermodynamics may favor the formation of compounds more stable than either of the semiconductors that form the heterojunction.

As discussed in sect. 3.1, interface dipoles are observed and should be expected for polar heterojunction interfaces formed between semiconductors that contain elements from different columns of the periodic table. Any mechanism which causes atoms from different columns of the periodic table to transfer across a heterojunction interface may produce interface dipoles. To separate interface contributions to ΔE_v that are growth-sequence related in origin from those that depend on crystallographic orientation, heterojunctions formed on the nonpolar (110) interface can be studied. For this reason all experimental observations described in this section involve (110) interfaces.

The formation of a heterojunction interface by MBE involves a nonequilibrium growth process. Thus, it may not be surprising if in some cases interface chemistry is found to depend on growth sequence. An extreme example of this type is noted in sect. 3.2.1. The growth of a compound semiconductor on an elemental semiconductor involves an ambiguity in nucleation site which may cause antiphase domain disorder; the reverse growth sequence has no nucleation site ambiguity. Experimental observations of a growth sequence dependence for interfaces formed between compound semiconductors and Ge(110) are discussed in sect. 3.2.2 and a possible means by which antiphase domain disorder may contribute to interface dipoles is given. The fabrication of a nonpolar (110) heterojunction from semiconductors that contain elements from the same columns (isocolumnar) of the periodic table is perhaps a case where one would least expect to observe growth-sequence variations in ΔE_v. However, even in this

case, as noted in sect. 3.2.3, interface contributions to ΔE_v of growth-sequence origin have been found.

3.2.1. Interface chemistry

If atoms from different columns of the periodic table are exchanged across a heterojunction, interface dipoles may be formed. A driving force for atom exchange at an interface may be chemical in origin. If interface chemical reactions depend on the order in which a heterojunction is formed, these reactions may contribute to a growth-sequence dependence of ΔE_v. An extreme example of interface chemistry growth-sequence dependence is given in this section.

The semiconductors Ge, GaAs, ZnSe and CuBr, which contain elements from row four of the periodic table, can be used to form many well-lattice-matched heterojunctions. It has been observed [42] that CuBr can be formed epitaxially on Ge(110) at $\sim 150\,^{\circ}$C with no evidence of interface chemical reaction. However, the situation is markedly different for the reverse growth sequence [43].

The growth-sequence dependence of interface chemical reactivity for the Ge–CuBr interface was investigated by XPS [43]. This phenomenon was studied by comparing core-level spectra from Ge on CuBr(110) [Ge/CuBr(110)] and CuBr on Ge(110) [CuBr/Ge(110)] interfaces that were formed at room temperature and then annealed for 1 min at 25 °C temperature steps between 25 and 150 °C. Core-level spectra of Ge3d, Br3d, and Cu3p were obtained at room temperature after each anneal. The CuBr/Ge sample consisted of ~ 15 Å of CuBr deposited at room temperature on a Ge(110) substrate; the Ge/CuBr sample consisted of ~ 20 Å of Ge deposited onto a ~ 1000 Å thick film of CuBr that was grown epitaxially on a GaAs(110) substrate. Relative changes in the Br3d/Cu3p, Ge3d/Cu3p, and Ge3d/Br3d peak area ratios were used to monitor the interface chemistry for each heterojunction. Data for the Br3d/Cu3p peak area ratio are shown in fig. 13. For the CuBr/Ge(110) interface the Br3d/Cu3p peak area ratio is ~ 1.4. This ratio remains constant up to $\sim 125\,^{\circ}$C and is the same value as is observed for a thick stoichiometric CuBr film. Above $\sim 150\,^{\circ}$C, the XPS peak area ratio data indicate that CuBr evaporates from the Ge(110) surface. For temperatures between 25 and 125 °C the constant Br3d/Cu3p peak area ratio is consistent with the CuBr/Ge interface being essentially abrupt and chemically inert. The Br3d/Cu3p peak area ratio data for the Ge/CuBr(110) interface are also shown in fig. 13. These data suggest that a chemical reaction occurs

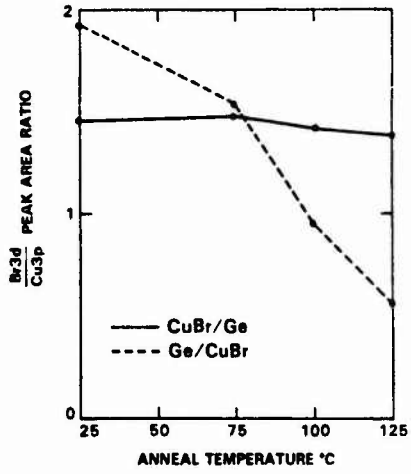

Fig. 13. Variation of the Br3d/Cu3p core-level peak area ratio for CuBr/Ge(110) and Ge/CuBr(110) interfaces as a function of anneal temperature. Data were taken from ref. [43].

immediately upon Ge deposition and continues at each anneal step. The peak area ratio changes are consistent with the reaction

$$Ge + 2\ CuBr \rightarrow 2\ Cu + GeBr_2 \uparrow,$$

in which there is a loss of Br and Ge from the sample surface and an accumulation of metallic Cu.

The interface between CuBr and Ge is therefore an extreme example of an interface chemistry growth-sequence dependence with the CuBr/Ge(110) interface being essentially inert and the Ge/CuBr(110) interface reacting to form many monolayers of chemically distinct products. The chemical reactivity for the Ge/CuBr(110) interface is so severe that it is not possible to prepare an epitaxial Ge/CuBr(110) heterojunction. This asymmetry in chemical reactivity is not explained by bulk thermodynamic considerations and may result from the nonequilibrium conditions under which these interfaces were formed. As chemical reactivity may be a driving force to cause atom exchange across an interface, a growth sequence dependent chemical reactivity may be a contributing factor to observed growth sequence variations in ΔE_v.

3.2.2. Compound–elemental (110) semiconductor heterojunctions

The growth of a compound semiconductor on an elemental semiconductor involves a site allocation ambiguity which is not present for the reverse

growth sequence. The importance of solving this site allocation problem for producing device quality heterojunctions from compound on elemental semiconductor growth has been discussed [6,8]. It has been suggested that antiphase domain disorder may cause the formation of an interface dipole at a heterojunction formed by growing a compound on elemental semiconductor [44]. In this section some systematics of ΔE_v growth sequence variations for compound semiconductor–Ge(110) interfaces are reviewed, observations of a time dependent ΔE_v variation for the GaAs/Ge(110) heterojunction interface are discussed, and a mechanism by which antiphase domain disorder may produce an interface contribution to ΔE_v is considered.

3.2.2.1. Compound semiconductor–Ge(110) ΔE_v systematics

The observation of a growth sequence variation for a compound semiconductor–Ge(110) interface has been reported for the ZnSe–Ge semiconductor pair [30]. The valence-band discontinuity for Ge formed epitaxially on ZnSe (Ge/ZnSe) was 1.53 ± 0.04 eV, while ΔE_v for ZnSe formed epitaxially on Ge (ZnSe/Ge) was 1.30 ± 0.04 eV [45]. A growth-sequence variation has also been reported [39] for the GaAs–Ge(110) interface, where it is found that $\Delta E_v(\text{Ge/GaAs}) > \Delta E_v(\text{GaAs/Ge})$ by about 0.2 eV; independent measurements have confirmed this result [40].

A third compound semiconductor–Ge(110) interface for which a growth sequence can be inferred involves CuBr and Ge. It is observed [42,43] that the difference between $\Delta E_v[\text{Ge/GaAs(110)}] + \Delta E_v[\text{CuBr/GaAs(110)}]$ and $\Delta E_v[\text{CuBr/Ge(110)}]$ is $+0.70 \pm 0.05$ eV. Antiphase disorder at the CuBr/Ge(110) interface has been suggested [44] as a possible cause of this large nonzero result (a further discussion of the ΔE_v relationship between these semiconductors is given in sect. 3.3). Unfortunately, as discussed in sect. 3.2.1., the preparation of a heterojunction with the reverse growth sequence [i.e., Ge/CuBr(110)] is not possible due to interface chemical reactions that occur when Ge is deposited on CuBr(110). However, if the large positive deviation from zero for the difference $\{\Delta E_v[\text{Ge/GaAs(110)}] + \Delta E_v[\text{CuBr/GaAs(110)}]\} - \Delta E_v[\text{CuBr/Ge(110)}]$ is assumed to be associated primarily with the CuBr/Ge(110) interface, it follows that $\Delta E_v[\text{CuBr/Ge(110)}]$ would be less than $\Delta E_v[\text{Ge/CuBr(110)}]$.

The ΔE_v for three compound semiconductors (i.e., GaAs, ZnSe and CuBr) grown on Ge(110) is systematically found to be smaller than ΔE_v for heterojunctions formed by the reverse growth sequence. These heterojunctions involve band alignments in which the smaller Ge band gap is completely contained within the larger band gap of the compound semicon-

ductor. Thus the systematically smaller ΔE_v for compound semiconductor/Ge(110) interfaces as compared to the reverse growth sequence is consistent with the formation of an interface dipole at the compound semiconductor/Ge(110) interface that has positive charge on the Ge side of the interface and negative charge in the compound semiconductor overlayer. The systematic variation of the compound semiconductor/Ge(110) growth-sequence effect suggests that a similar mechanism may be involved in each case.

3.2.2.2. Instability of the GaAs/Ge(110) interface

The interface dipole present at the GaAs/Ge(110) interface is found to vary with both time after interface formation and subsequent annealing conditions [40,46,47]. Thus, although as noted in sect. 3.2.2.1. the size of the interface dipole at the GaAs/Ge(110) interface causes ΔE_v[Ge/GaAs(110)] to be larger than ΔE_v[GaAs/Ge(110)], the magnitude of the difference depends on several factors (which will be discussed in this section) and indicates that the GaAs/Ge(110) interface is unstable.

A typical XPS spectrum for a GaAs/Ge(110) heterojunction is shown in fig. 14 where the binding energy region contains the Ga3d, Ge3d and As3d core levels. This heterojunction sample (C) and two others (D and E) were

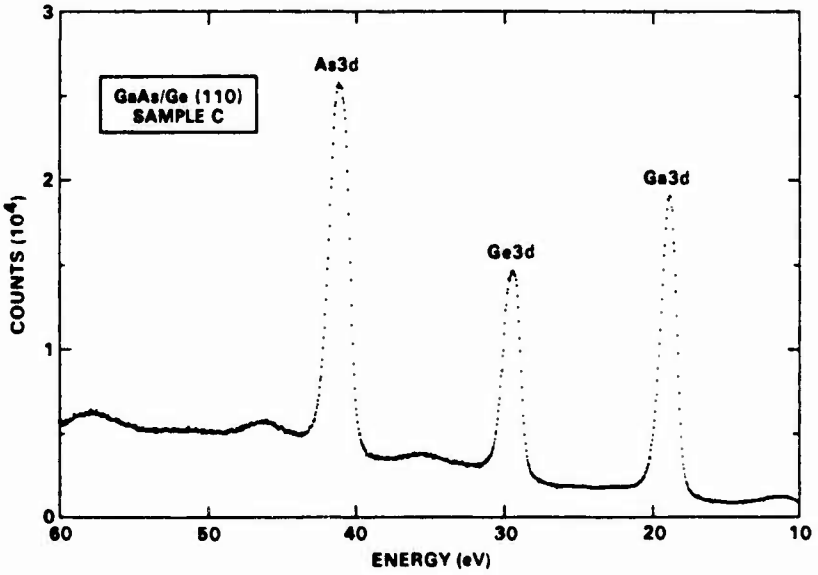

Fig. 14. Typical XPS spectrum of a GaAs/Ge(110) sample in the Ga3d, Ge3d, and As3d binding energy region. Data were taken from ref. [46].

prepared by sputtering and annealing a Ge(110) substrate, growing a few hundred Å thick epitaxial Ge layer (at ~ 450 °C), and growing a thin (~ 22 Å) epitaxial GaAs layer by MBE at ~ 350 °C. An additional sample (F) was prepared by growing the GaAs epitaxial layer directly on the sputtered and annealed Ge(110) substrate. Variations in the interface dipole present at the GaAs/Ge(110) interface were monitored by measuring $E^{Ge}_{Ge3d} - E^{GaAs}_{Ga3d}$.

Room-temperature spectra similar to that shown in fig. 14 were recorded at several times t following interface formation. Because data collection required several hours, t was taken as the midpoint of the data accumula-

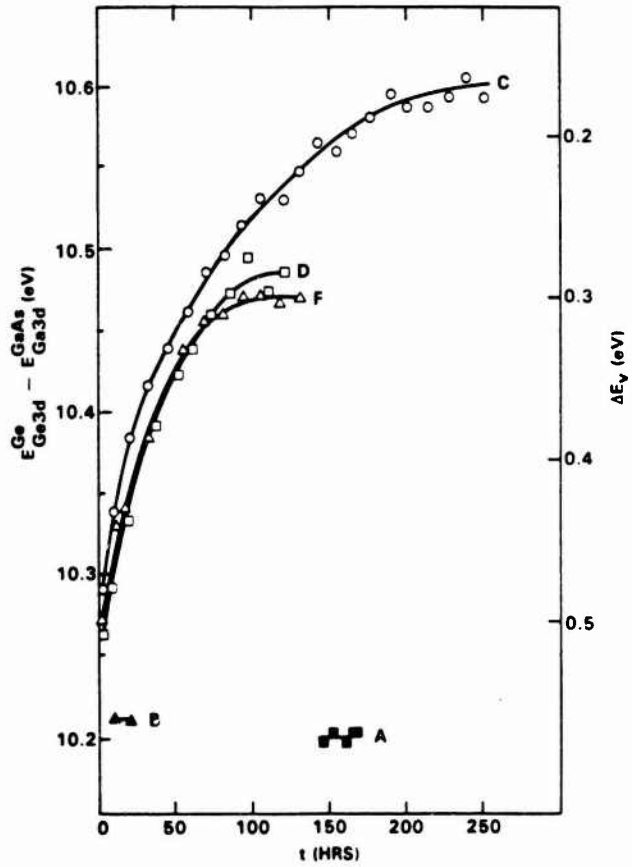

fig. 15. Variation of $E^{Ge}_{Ge3d} - E^{GaAs}_{Ga3d}$ (and of ΔE_v) with time after interface formation for three GaAs/Ge(110) heterojunctions (labelled C, D and F) and for two Ge/GaAs(110) heterojunctions (labeled A and B). Data were taken from refs. [40,46].

tion period. The core-level binding energy difference, $E^{Ge}_{Ge3d} - E^{GaAs}_{Ga3d}$ (and the corresponding value of ΔE_v) measured as a function of t for samples C, D and F is plotted in fig. 15. For comparison, data from table 1 for two Ge/GaAs(110) heterojunctions (labeled A and B) prepared as discussed in sect. 3.1.1 are also shown. As can be seen from this figure, there is a substantial variation of ΔE_v with time for GaAs/Ge(110) heterojunctions. This variation indicates interface dipole formation caused by GaAs/Ge(110) interface structural instability. No similar instability for heterojunctions formed by the reverse growth sequence [i.e., Ge/GaAs(110)] is observed.

The Ga3d, Ge3d and As3d linewidths, the Ga3d/As3d and Ge3d/Ga3d

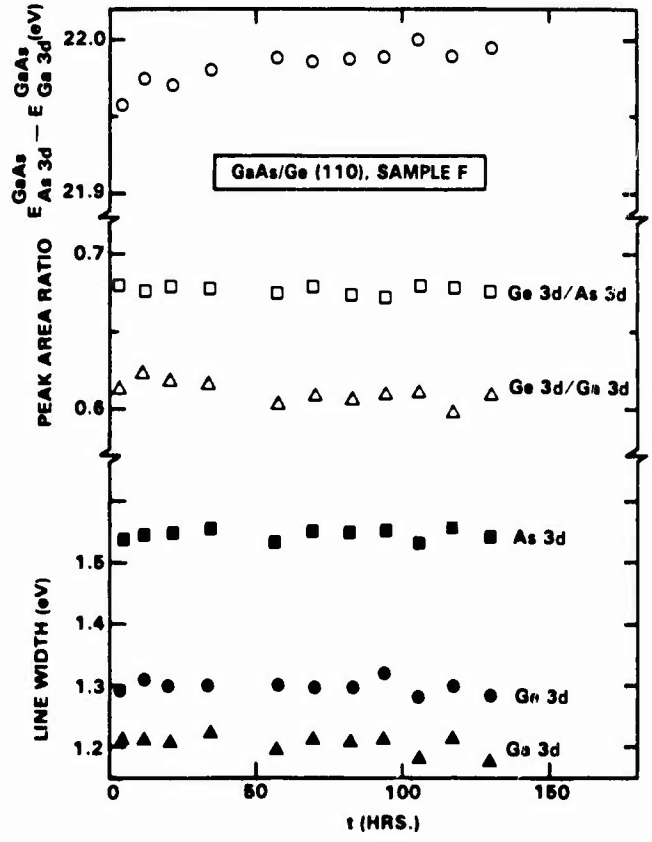

Fig. 16. XPS data for sample F obtained as a function of time after GaAs/Ge(110) interface formation. Top: $E^{GaAs}_{As3d} - E^{GaAs}_{Ga3d}$; middle: Ga3d/As3d and Ge3d/Ga3d peak area ratios; bottom: As3d, Ge3d, and Ga3d linewidths. Data were taken from ref. [40].

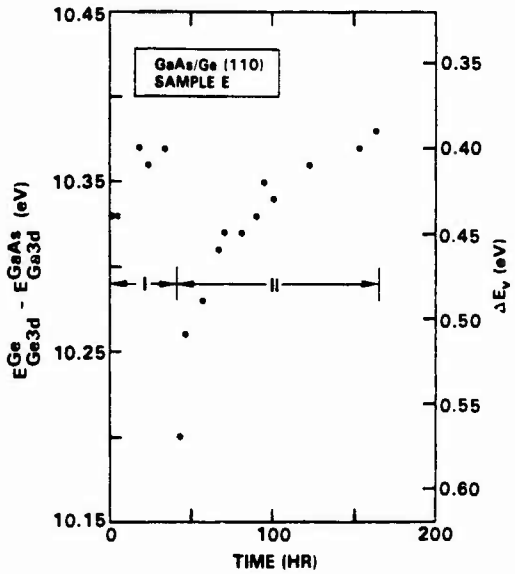

Fig. 17. Variation of $E^{Ge}_{Ge3d} - E^{GaAs}_{Ga3d}$ (and of ΔE_v) with time for a GaAs/Ge(110) heterojunction (sample E). Interval I follows the normal heterojunction growth procedure. Interval II follows a 10 min vacuum anneal at ~ 325° C. Data were taken from ref. [47].

peak area ratios and the As3d to Ga3d core-level binding energy difference, $E^{GaAs}_{As3d} - E^{GaAs}_{Ga3d}$, were also monitored as a function of t. As an example, these parameters derived from XPS data on sample F are shown in fig. 16. Except for a very small increase (~ 0.03 eV) in $E^{GaAs}_{As3d} - E^{GaAs}_{Ga3d}$ (which may be associated with a change in GaAs surface chemical shifts) there is no systematic variation in any of the parameters. The data in fig. 16 rule out the possibility that substantial interface chemical reactions are occurring to cause the large (> 0.2 eV) variations in $E^{Ge}_{Ge3d} - E^{GaAs}_{Ga3d}$ shown in fig. 15.

An additional observation of GaAs/Ge(110) interface instability is derived from XPS data [47] on sample E, as shown fig. 17. At ~ 42 h after interface formation, this sample was annealed at ~ 325° C in vacuum for 10 min. The value of $E^{Ge}_{Ge3d} - E^{GaAs}_{Ga3d}$ decreased to 10.20 eV, which is the same value as observed for the stable Ge/GaAs(110) interface (see table 1 and the data for samples A and B shown in fig. 15). This decrease indicates that the GaAs/Ge(110) interface dipole has been removed by the annealing treatment. Following this anneal the value of $E^{Ge}_{Ge3d} - E^{GaAs}_{Ga3d}$ again slowly increased as the interface dipole was reformed. Several annealing studies (both in vacuum and with an As overpressure) have been performed on

GaAs/Ge(110) and GaAs/Ge(100) samples [47]. Although there are some sample-to-sample variations (as also indicated by the data in fig. 15), results similar to those shown in fig. 17 are always obtained. A possible mechanism by which antiphase domain disorder may be related to the observed GaAs/Ge(110) interface instability is considered in the next section.

3.2.2.3. Possible role of antiphase disorder

The valence-band discontinuity for a heterojunction formed by growth of a lattice-matched compound semiconductor on Ge(110) is systematically smaller than for the reverse growth sequence. There is evidence (see sect. 3.3.) that interface contributions to ΔE_v may be small for Ge grown on compound semiconductor (110) heterojunctions. The relative magnitude of the compound semiconductor–Ge(110) growth-sequence effect can therefore be used to infer that at a compound semiconductor/Ge(110) interface, positive charge is transferred into the Ge and negative charge into the compound semiconductor overlayer.

The possible presence of antiphase disorder is a distinct growth-sequence difference for compound–elemental semiconductor (110) heterojunctions. The presence of this disorder would not necessarily affect ΔE_v unless it caused charge to be transferred across the interface to create an interface dipole. As discussed previously, atom transfer across a heterojunction interface that involves atoms from different columns of the periodic table can produce interface dipoles. If the compound semiconductor–Ge(110) ΔE_v growth-sequence effect is caused by atom transfer, as suggested by the long time constants associated with GaAs/Ge(110) interface instability, the electrostatic model of heterojunction interfaces (sect. 3.1.2) can be used to infer that anions (i.e., As, Se and Br) rather than cations preferentially exchange with Ge at a compound semiconductor/Ge(110) interface.

A large variety of antiphase domain walls can be imagined. However, the crystallographic planes associated with these walls may be characterized by whether one, two or three bonds between like atoms exist at the domain boundary. If attention is restricted to only those cases where the common atom bonds involve atoms in the compound semiconductor plane that is adjacent to the last Ge(110) plane, only three nearest-neighbor bonding arrangements are possible for the abrupt (110) interface as shown in fig. 18.

The energetics of atomic exchange across an interface are primarily associated with bonds formed or broken during the exchange. Energies of atomic substitution calculated by tight-binding theory [38] have shown that atomic exchange at an ideal abrupt compound semiconductor–Ge interface is not favored. However, at an antiphase domain boundary like those

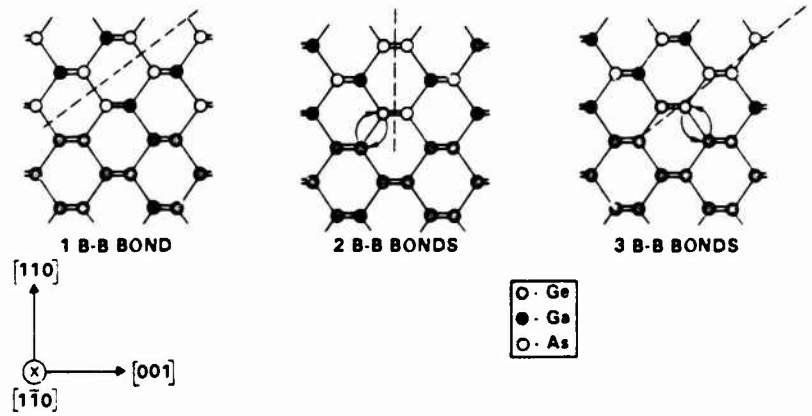

Fig. 18. Examples of arsenic antiphase domain boundaries (- - - - -) with one, two or three As–As bonds. The arrows suggest an atomic exchange across the GaAs/Ge(110) interface that may be related to the observed interface instability. Figure was taken from ref. [40].

shown in fig. 18, there are bonds between like atoms that are not present at the ideal interface. The atoms involved in these bonds may favor exchange. This possibility was investigated [40] by considering the sum of bond formation energies associated with a single atomic exchange as, for example, is shown by arrows in the center and at the right of fig. 18. The result was that a bonding arrangement that involved only one bond between like atoms (shown at the left of fig. 18) is stable while interfaces that involve two (middle of fig. 18) or three (right-hand side of fig. 18) bonds between like atoms favor the exchange indicated by the arrows. The present accuracy of the theory does not specify a preference for anion or cation exchange.

Some insight into the cause of the observed ΔE_v growth-sequence effect at compound–elemental semiconductor heterojunctions can be obtained although a detailed mechanism is not yet known. The slow time constant at room temperature for formation of the GaAs/Ge(110) interface dipole suggests that atomic motion is involved. The sign of the growth-sequence effect infers that anions are preferentially interchanged with Ge at a compound semiconductor/Ge(110) interface. Bond formation energy considerations favor atom exchange where certain antiphase domain boundaries intersect the Ge(110) interface. If the atom exchange mechanism has a constant probability per unit time and there are a fixed number of available sites at which the exchange can occur, an exponential variation of ΔE_v with

time would be expected, as can be seen in fig. 15. For the GaAs/Ge(110) interface, the XPS linewidth data indicate that the dipole is localized over a very few atomic planes at the interface. The reversible variation of the GaAs/Ge(110) interface dipole with suitable sample annealing conditions (fig. 17) suggests that a mobile atom species (perhaps interstitial As) is involved in the dipole formation mechanism. Finally, variations in anti-phase domain structure between samples could account for the observed sample-to-sample differences in the growth sequence effect.

3.2.3. Isocolumnar (110) heterojunctions

As noted previously an interchange of atoms from different columns of the periodic table can produce interface dipole contributions to ΔE_v. As atom interchange may be impossible to prevent, it might be expected that heterojunctions formed on nonpolar surfaces between semiconductors that contain elements from the same columns of the periodic table (isocolumnar) would be least likely to exhibit a growth-sequence effect. However, as noted in this section, a growth-sequence ΔE_v variation has been observed [33] even for isocolumnar (110) heterojunctions formed between AlAs and GaAs.

Heterojunction samples of AlAs–GaAs with a structure similar to that shown in fig. 1 were prepared by MBE. The substrates were (110) GaAs with a ~ 50 Å GaAs epitaxial buffer layer. The AlAs/GaAs heterojunctions were formed by growing ~ 30 Å of epitaxial AlAs onto the GaAs buffer layer. The GaAs/AlAs heterojunctions were formed by growing ~ 100 Å of AlAs followed by ~ 25 Å of GaAs onto the GaAs buffer layer. All of the epitaxial layers were grown at ~ 550 °C.

The Al2p to Ga3d core-level binding energy difference was measured for four GaAs/AlAs(110) and three AlAs/GaAs(110) samples. The results are shown in table 4. As discussed in sect. 2.1, a change in the core-level binding energy difference, $\delta(\Delta E_{CL})$, is a direct measure of a change in the valence-band discontinuity, $\delta(\Delta E_v)$; in this case $\delta(\Delta E_{CL}) = \delta(\Delta E_v)$. It is therefore observed that ΔE_v[GaAs/AlAs(110)] is smaller than ΔE_v[AlAs/GaAs(110)] by ~ 0.13 eV; a 0.1 eV range of ΔE_v values is noted in the GaAs/AlAs(110) ΔE_v results. A similar ΔE_v growth-sequence effect with the same sign and approximately the same magnitude has been observed [33] for AlAs–GaAs(100) heterojunctions prepared by the same procedure described above. Corresponding values of ΔE_v are ~ 0.1 eV smaller for the (100) than for the (110) heterojunction interfaces.

The ΔE_v growth-sequence results for the AlAs–GaAs heterojunction

Table 4
Al2p to Ga3d core-level binding energy differences for several GaAs/AlAs(110) and AlAs/GaAs(110) heterojunctions.

Interface	Sample	ΔE_{CL} [a] (eV)	$(\Delta E_{CL})_{AVG}$ (eV)
GaAs/AlAs	1	54.31	
	2	54.41	54.37
	3	54.39	
	4	54.38	
AlAs/GaAs	5	54.50	
	6	54.51	54.50
	7	54.50	

[a] Uncertainty is ± 0.02 eV.

system indicate that the atomic arrangement in the interface region depends on growth sequence at least for the conditions used to prepare these samples. The growth of $Ga_{1-x}Al_xAs$ on GaAs(100) exhibits a smooth surface morphology, while growth on GaAs(110) can be complicated by relatively rough surface morphology and alloy clustering [48]. The exchange reaction between Al and Ga at the GaAs(110) surface [49] may be a cause of the alloy clustering phenomenon. For a given crystallographic orientation, an exchange reaction between Ga and Al might be expected to depend on growth sequence. As these elements are from the same column of the periodic table and have very similar electronegativities, an interface dipole formed directly by this exchange reaction would be expected to be extremely small. However, if antisite and/or antistructure defects were formed as a result of the exchange reaction, it is possible that a sizeable growth-sequence dependent interface dipole could result. Although further study of microscopic interface structure will be needed to understand the origin of interface contributions to ΔE_v for AlAs–GaAs heterojunctions, it is plausible that the effects mentioned here will be contributing factors.

3.3. Transitivity of ΔE_v

As mentioned previously, the several theories [1–4] which are currently in use to predict ΔE_v at abrupt interfaces are all based on linear models that estimate band discontinuities from the difference in an absolute energy associated with each of the semiconductors that form the heterojunction. These theories, therefore, specifically ignore the interface contributions to

ΔE_v that have been discussed in this chapter. If one considers ΔE_v for heterojunctions formed between three semiconductors (A, B and C), a fundamental property of all linear heterojunction models is that if ΔE_v(A–B) and ΔE_v(B–C) are known, ΔE_v(A–C) is also specified; this transitive property of ΔE_v for linear models has been previously noted [2]. It is, therefore, possible to test experimentally an underlying assumption of all linear models by measuring ΔE_v for three appropriate heterojunctions. Conversely, although not on a rigorous logical basis, it may be possible to use ΔE_v transitivity tests to select experimental ΔE_v values least affected by interface dipole contributions and, therefore, most suitable for comparison with the prediction of linear models.

If ΔE_v for a set of three heterojunctions is transitive, the following relation is, by definition, satisfied

$$\Delta E_v(\text{A–B}) + \Delta E_v(\text{B–C}) - \Delta E_v(\text{A–C}) = 0, \tag{4}$$

where in order to specify a unique sign convention, the semiconductor band gaps have been chosen such that $E_g^A > E_g^B > E_g^C$. Equation (1) expressed ΔE_v(A–B) as $(E_{CL}^B - E_v^B) - (E_{CL}^A - E_v^A) + \Delta E_{CL}$(A–B). Substitution of this expression and similar expressions for ΔE_v(B–C) and ΔE_v(A–C) into eq. (4) results in a cancellation of all the $E_{CL} - E_v$ terms; in order for ΔE_v to be transitive, the quantity $T(\Delta E_{CL})$ must be zero where

$$T(\Delta E_{CL}) = \Delta E_{CL}(\text{A–B}) + \Delta E_{CL}(\text{B–C}) - \Delta E_{CL}(\text{A–C}). \tag{5}$$

Thus, the relation in eq. (5) can be used to provide a sensitive test of transitivity.

Values of ΔE_{CL} measured by XPS for abrupt (110) heterojunction interfaces are given in table 5. The core levels are identified and to specify a unique sign convention, the binding energy associated with the core level in the semiconductor with the largest band gap was subtracted from the binding energy of the core level in the semiconductor with the smallest bandgap. Also listed in table 5 are corresponding values of ΔE_v for each interface. These ΔE_v values were evaluated from eq. (1) by using the appropriate $E_{CL} - E_v$ values given in table 2. Error limits are not specified for ΔE_v associated with heterojunctions that involve CuBr because the value of $E_{Br3d}^{CuBr} - E_v^{CuBr}$ has only been approximately determined.

To test for ΔE_v transitivity, experimental ΔE_{CL} data for appropriate heterojunction sets formed between at least three semiconductors are needed. By using the data in table 5, five tests of ΔE_v transitivity can be obtained.

Table 5
Core-level binding energy differences and associated ΔE_v values at (110) heterojunction interfaces as measured by XPS.

Interface	Core levels	ΔE_{CL} (eV)	ΔE_v (eV)	Ref.
Ge/GaAs	Ga3d–Ge3d	-10.21 ± 0.01	0.56 ± 0.04	[10,42]
	As3d–Ge3d	11.78 ± 0.02		
ZnSe/GaAs	Zn3d–Ga3d	-8.95 ± 0.02	0.94 ± 0.04	[30]
CuBr/GaAs	Br3d–As3d	28.77 ± 0.03	0.8	[42,43]
InAs/GaAs	Ga3d–In4d	1.55 ± 0.06	0.18 ± 0.07	[31]
AlAs/GaAs	Al2p–Ga3d	54.50 ± 0.02	0.55 ± 0.05	[33]
GaAs/AlAs	Al2p–Ga3d	54.37 ± 0.06 [a]	0.42 ± 0.08 [a]	[33]
Ge/AlAs	Al2p–Ge3d	44.22 ± 0.02	1.04 ± 0.05	[43]
Ge/ZnSe	Zn3d–Ge3d	-19.13 ± 0.02	1.53 ± 0.04	[30]
ZnSe/Ge	Zn3d–Ge3d	-19.36 ± 0.02	1.30 ± 0.04	[30]
CuBr/Ge	Br3d–Ge3d	39.85 ± 0.03	0.65	[42,43]

[a] Because of the range of values given in table 4, a maximum variation is quoted rather than a measurement uncertainty.

The five possible combinations of three heterojunction interfaces are listed in table 6 along with the experimental value of $T(\Delta E_{CL})$. As can be seen from table 6, the first two heterojunction sets provide a positive test of transitivity; sets 3 and 4 are markedly nontransitive while set 5 is less so.

Some systematic trends are apparent from the data in table 6. The first two heterojunction sets where ΔE_v transitivity is satisfied involve only growth of interfaces where site allocation is not an issue. In contrast, the nontransitive ΔE_v observation for sets 3 and 4 involve interfaces formed by growing a compound on an elemental semiconductor where site allocation ambiguity may be present. These observations are consistent with the suggested role of antiphase disorder in contributing to interface dipole formation.

Table 6
Transitivity tests for five (110) heterojunction sets.

Set	Interfaces			$T(\Delta E_{CL})$ (eV)
	A	B	C	
1	ZnSe/GaAs	Ge/GaAs	Ge/ZnSe	-0.03 ± 0.03
2	GaAs/AlAs	Ge/GaAs	Ge/AlAs	-0.06 ± 0.06
3	CuBr/GaAs	Ge/GaAs	CuBr/Ge	$+0.70 \pm 0.05$
4	ZnSe/GaAs	Ge/GaAs	ZnSe/Ge	$+0.20 \pm 0.05$
5	AlAs/GaAs	Ge/GaAs	Ge/AlAs	$+0.07 \pm 0.03$

The only difference between heterojunction sets 2 and 5 involves the AlAs–GaAs heterojunction growth sequence. As it was noted in sect. 3.2.3 that this growth sequence leads to an ~ 0.13 eV difference in ΔE_v, it is not surprising that if set 2 is transitive, set 5 exhibits a small deviation from transitivity. Some possible causes for the growth-sequence effect on ΔE_v(AlAs–GaAs) were previously given.

The last point considered here is the possible use of transitivity tests to select data least affected by interface dipole contributions to ΔE_v for comparison with theories that ignore interface effects. The obvious flaw in this logic is that interface contributions to ΔE_v for different members of a given heterojunction set could have opposite signs thus producing a cancellation and a $T(\Delta E_{CL})$ of ~ 0. However, in lieu of a better selection criterion, experimental ΔE_v values for the five interfaces involved in the first two heterojunction sets of table 6 would appear to be good candidates for comparison with predictions of linear models.

4. Summary

Interface contributions to heterojunction band discontinuities can be substantially larger than the thermal energy and can therefore influence semiconductor devices that incorporate heterojunction interfaces. To investigate these interface contributions to ΔE_v it is essential to utilize a measurement technique that has an experimental uncertainty considerably smaller than the observed effects. A technique based on X-ray photoemission spectroscopy has been described that is capable of measuring changes in interface contributions to ΔE_v with an uncertainty of ± 0.01 eV. In favorable cases, the technique can be extended to yield absolute ΔE_v values with an uncertainty of ± 0.04 eV.

Several experimental observations of interface contributions to ΔE_v have been described that include crystallographic orientation and growth-sequence effects. A consideration of electrostatics leads to the conclusion that when interfaces are formed on polar crystallographic planes between semiconductors that contain elements from different columns of the periodic table, interface dipole contributions to ΔE_v may be expected. Several observations of heterojunction growth-sequence effects were described and possible mechanisms that can contribute to charge transfer and interface dipole formation were reviewed. It is possible to test ΔE_v transitivity from data derived solely by the XPS technique. These tests suggest a means to select ΔE_v data least likely affected by interface dipoles for comparison

with existing ΔE_v theories based on linear models and to identify interfaces with large interface dipole contributions to ΔE_v for systematic study. A better understanding of interface contributions to heterojunction band discontinuities is clearly needed if semiconductor heterojunctions are to be used most advantageously in device applications.

Acknowledgments

The authors acknowledge the collaboration of Prof. W.A. Harrison (Stanford University) on many of the subjects reviewed in this chapter and several useful discussions with Prof. H. Kroemer (University of California, Santa Barbara). Much of the original work which this chapter reviewed was supported by the Office of Naval Research.

References

[1] W.A. Harrison, Electronic Structure and the Properties of Solids (Freeman, San Francisco, 1980) p. 252.
[2] W.R. Frensley and H. Kroemer, Phys. Rev. B 16 (1977) 2642.
[3] R.L. Anderson, Solid State Electron. 5 (1962) 341.
[4] J. Tersoff, Phys. Rev. B 30 (1984) 4874.
[5] G. Margaritondo, Surf. Sci. 132 (1983) 469.
[6] H. Kroemer, Surf. Sci. 132 (1983) 543.
[7] H. Kroemer, J. Vac. Sci. & Technol. B 2 (1984) 433.
[8] H. Kroemer, in: Proc. NATO Advanced Study Institute on Molecular Beam Epitaxy and Heterostructures, Erice, Sicily, 1983, eds L.L. Chang and K. Ploog (Martinus Nijhoff, The Hague, 1984) p. 331.
[9] G. Margaritondo, Surf. Sci. 168 (1986) 439.
[10] R.W. Grant, J.R. Waldrop and E.A. Kraut, Phys. Rev. Lett. 40 (1978) 656.
[11] R.W. Grant, J.R. Waldrop and E.A. Kraut, J. Vac. Sci. & Technol. 15 (1978) 1451.
[12] E.A. Kraut, R.W. Grant, J.R. Waldrop and S.P. Kowalczyk, Phys. Rev. Lett. 44 (1980) 1620.
[13] E.A. Kraut, R.W. Grant, J.R. Waldrop and S.P. Kowalczyk, Phys. Rev. B 28 (1983) 1965.
[14] K. Siegbahn, C. Nordling, A. Fahlman, R. Nordberg, K. Hamrin, J. Hedman, G. Johansson, T. Bergmark, S.-E. Karlsson, I. Lindgren and B. Lindberg, Nova Acta Regiae Soc. Sci. Ups. 20 (1967).
[15] J. Auleytner and O. Hörnfeldt, Ark. Fys. 23 (1963) 165.
[16] J. Hedman, Y. Baer, A. Berndtsson, M. Klasson, G. Leonhardt, R. Nilsson and C. Nordling, J. Electron Spectrosc. & Relat. Phenom. 1 (1972/3) 101.
[17] M.P. Seah and W.P. Dench, Surf. & Interface Anal. 1 (1979) 2.
[18] L.J. Brillson, Surf. Sci. Rep. 2 (1982) 123.
[19] G. Margaritondo, A.D. Katnani, N.G. Stoffel, R.R. Daniels and Te-Xiu Zhao, Solid State Commun. 43 (1982) 163.

[20] G.A. Baraff, J.A. Applebaum and D.R. Hamann, J. Vac. Sci. & Technol. 14 (1977) 999.
[21] W.E. Pickett and M.L. Cohen, Phys. Rev. B 18 (1978) 939.
[22] R.W. Grant, E.A. Kraut, S.P. Kowalczyk and J.R. Waldrop, J. Vac. Sci. & Technol. B 1 (1983) 320.
[23] J. Olivier and R. Poirier, Surf. Sci. 105 (1981) 347.
[24] A.D. Katnani and G. Margaritondo, Phys. Rev. B 28 (1983) 1944.
[25] J.R. Chelikowsky and M.L. Cohen, Phys. Rev. B 14 (1976) 556.
[26] See, e.g., V.G. Aleshin and Yu.N. Kucherenko, J. Electron Spectrosc. 9 (1976) 1.
[27] U. Gelius, in: Electron Spectroscopy, ed. D.A. Shirley (North-Holland, Amsterdam, 1972) p. 311.
[28] B.Z. Olshanetsky, S.M. Repinsky and A.A. Shklyaev, Surf. Sci. 64 (1977) 224.
[29] D.E. Eastman, T.-C. Chiang, P. Heimann and F.J. Himpsel, Phys. Rev. Lett. 45 (1980) 656.
[30] S.P. Kowalczyk, E.A. Kraut, J.R. Waldrop and R.W. Grant, J. Vac. Sci. & Technol. 21 (1982) 482.
[31] S.P. Kowalczyk, W.J. Schaffer, E.A. Kraut and R.W. Grant, J. Vac. Sci. & Technol. 20 (1982) 705.
[32] S.P. Kowalczyk, J.T. Cheung, E.A. Kraut and R.W. Grant, Phys. Rev. Lett. 56 (1986) 1605.
[33] J.R. Waldrop, R.W. Grant and E.A. Kraut, J. Vac. Sci. & Technol., (1987) in press.
[34] Some of these $E_{CL} - E_v$ values have been adjusted by either -0.04 eV or -0.05 eV to correct for a computer program error that was present in the original analyses. In this chapter those ΔE_v values affected by this adjustment have been corrected.
[35] F.F. Fang and W.E. Howard, J. Appl. Phys. 35 (1964) 612.
[36] J.R. Waldrop, E.A. Kraut, S.P. Kowalczyk and R.W. Grant, Surf. Sci. 132 (1983) 513.
[37] W.A. Harrison, E.A. Kraut, J.R. Waldrop and R.W. Grant, Phys. Rev. B 18 (1978) 4402.
[38] E.A. Kraut and W.A. Harrison, J. Vac. Sci. & Technol. B 3 (1985) 1267.
[39] P. Zurcher and R.S. Bauer, J. Vac. Sci. & Technol. A 1 (1983) 695.
[40] R.W. Grant, J.R. Waldrop, S.P. Kowalczyk and E.A. Kraut, J. Vac. Sci. & Technol. B 3 (1985) 1295.
[41] D.-W. Tu and A. Kahn, J. Vac. Sci. & Technol. A 3 (1985) 922.
[42] J.R. Waldrop and R.W. Grant, Phys. Rev. Lett. 43 (1979) 1686.
[43] J.R. Waldrop, R.W. Grant, S.P. Kowalczyk and E.A. Kraut, J. Vac. Sci. & Technol. A 3 (1985) 835.
[44] J.C. Phillips, J. Vac. Sci. & Technol. 19 (1981) 545.
[45] The uncertainty analysis of these results was refined after initial publication, see ref. [43].
[46] R.W. Grant, J.R. Waldrop, S.P. Kowalczyk and E.A. Kraut, Surf. Sci. 168 (1986) 498.
[47] J.R. Waldrop, R.W. Grant and E.A. Kraut, J. Vac. Sci. & Technol. B 4 (1986) 1060.
[48] P.M. Petroff, A.Y. Cho, F.K. Reinhart, A.C. Gossard and W. Wiegmann, Phys. Rev. Lett. 48 (1982) 170.
[49] C.B. Duke, A. Paton, R.J. Meyer, L.J. Brillson, A. Kahn, D. Kanani, J. Carelli, J.L. Yeh, G. Margaritondo and A.D. Katnani, Phys. Rev. Lett. 46 (1981) 440.

Energies of substitution and solution in semiconductors

Walter A. Harrison* and Edgar A. Kraut
Rockwell International Science Center, P.O. Box 1085, Thousand Oaks, California 91360
(Received 27 April 1987)

The tight-binding theory of cohesion in pure semiconductors, based upon universal parameters, is presented and applied to systems with an impurity. Results are given in terms of an energy of substitution, defined as the energy required to remove a single atom from a semiconductor, leaving it as a free atom in the ground state, and replacing it by a free atom of another element; any excess or deficit of electrons is placed at the valence-band maximum. Calculated values are in reasonable accord with the recent measurements by Su and Brebrick [J. Phys. Chem. Solids 46, 963 (1985)] for Zn, In, and Sn in Ge. Lattice distortions and relaxation energies are also calculated. Agreement with the limited amount of data is mixed but predictions are tabulated for a large array of systems. Relaxation is seen to reduce the misfit energy by a factor of order 4. Comparison of predicted force constants with experiment suggests that the theory underestimates the misfit energy by a similar factor so theoretical energies of unrelaxed substitution provide estimates of the experimental energies of relaxed substitution. Such predictions are in reasonable accord with experiment for homovalent substitutions, which are dominated by misfit energy. For heterovalent substitutions, the enthalpy is dominated by a redistribution of bond polarities in the substitution. Extensive tables of energies of substitution for elements and compounds from the third (silicon), fourth (germanium), and fifth (tin) rows of the Periodic Table are given, permitting direct estimates of the energy change for a wide variety of atomic rearrangements.

I. INTRODUCTION

Enthalpies of solution of one semiconductor in another are only poorly known experimentally, partly because semiconductors are generally quite insoluble in each other so that the heat of solution is difficult to measure. In addition, their determination from experiment frequently involves paths through the liquid phase, and data are most frequently for the solid and the liquid at the melting temperature.[1] Heats of solution do exist for a number of isovalent solutions,[2] e.g., III-V compounds dissolved in each other, and a few recent direct measurements on heterovalent solutions have been made by Su and Brebrick.[3]

The theory is also difficult. An earlier phenomenological approach was made by Weiser[4] and a dielectric theory was given by Van Vechten,[5] both again directed principally at the segregation coefficients. More recently, there have been estimates of the heats of solution by Stringfellow[2] and Martins and Zunger[6] under the assumption that it was dominated by elastic misfit, which we shall see appears to be appropriate for isovalent solutions. There have also been microscopic quantum-mechanical theories of isolated cases of individual impurities,[7–9] based in most cases on using a Green's function to represent the crystalline environment. Baraff and Schlüter,[10] in particular, obtained reaction energies for transformation between various defects in gallium arsenide. Here, we seek a wider sampling of systems, again from microscopic theory, but in a simple enough way to allow very general application.

Recently, tight-binding theory, based on universal parameters,[11] and on individual bond energies with corrections (called metallization) due to coupling with neighbors, proved successful in predicting equilibrium bond lengths and cohesive energies of elemental and compound semiconductors. This approach did not depend on lattice periodicity and is therefore directly applicable to the total energy of systems containing impurities. Preliminary accounts[12,13] of such calculations have been given; here we give a full account of the method and results.

We shall begin in Sec. II with a restatement of the total-energy change in forming a crystal from the free atoms—the cohesive energy—since that gives the basic approach for all of the calculations and since we shall need those numbers also. In Sec. III, we calculate the energy of substitution, defined to be the energy change if an atom is removed from the crystal, left as a free atom in the ground state, and a second atom of a different element replaces the first. This is done first without allowing the positions of the other atoms in the crystal to change. The results are compared with the few available experimental values. From such energies of substitution and the cohesive energies it is possible to predict heats of solution and a number of other interesting properties.

In Sec. IV, we allow for the relaxation of the neighbors to the impurity. We first discuss the determination of equilibrium spacings in pure semiconductors by minimization of the energy, writing down the terms in the energy which depend upon spacing. Then, when an impurity is substituted, we make the appropriate changes in the terms in the total energy and calculate the relaxed bond lengths.

In Sec. V, we obtain in the heats of solution which are compared with experiment for isovalent solutions, such as InSb in GaAs, which are the systems for which the

 © 1988 The American Physical Society

most data were available and at which most earlier theory is directed. These are seen to be dominated by the misfit energy, or elastic energy, as assumed in earlier theories. The heat of solution for heterovalent systems, such as germanium in gallium arsenide is seen to be dominated by electronic-structure effects with the misfit energies playing a smaller role. We also calculate interchange energies, such as a germanium atom from germanium with an arsenic atom from gallium arsenide. In the heterovalent case this dopes both semiconductors and the dependence of the interchange energy on the doping of the two systems is described.

II. THE TIGHT-BINDING THEORY OF COHESION

We begin with free atoms, one metallic atom from column Z^+ (≤ 4) and one nonmetallic atom from column $Z^- = 8 - Z^+$. We will use these $\pm$ superscripts to denote each of the parameters which enters, as we proceed step by step to construct the solid from the isolated free atoms. Values are given at each step for gallium arsenide using Hartree-Fock term values tabulated by Mann[14] and listed in Table I for the elements which will be needed here.

A. Promotion energy

To form individual two-center bonds we must prepare each atom in an sp^3 configuration. For all cases we consider ($Z^+ \geq 2$), we must first raise one electron on each atom from an s state to a p state, with an energy change (or costing an energy) $\varepsilon_p^+ - \varepsilon_s^+ + \varepsilon_p^- - \varepsilon_s^-$ per atom pair. Then, unless $Z^+ = 4$, we must transfer electrons from the nonmetallic p states to the metallic p states, costing $(Z^- - 4)(\varepsilon_p^+ - \varepsilon_p^-)$, for a total promotion energy of

$$E_{\text{pro}} = \varepsilon_p^+ - \varepsilon_s^+ + \varepsilon_p^- - \varepsilon_s^- + (Z^- - 4)(\varepsilon_p^+ - \varepsilon_p^-) \quad (1)$$

per atom pair. This is 19.12 eV for GaAs.

B. Bond-formation energy

The eight electrons per atom pair may now be put, with no cost in energy, into hybrid states of energy

$$\varepsilon_h^\pm = (\varepsilon_s^\pm + 3\varepsilon_p^\pm)/4 \quad (2)$$

corresponding in gallium arsenide to $\varepsilon_h^+ = -7.14$ eV and $\varepsilon_h^- = -11.46$ eV with an average hybrid energy of $\bar{\varepsilon}_h$ (-9.30 eV). The energy difference is written as twice the polar energy V_3 defined by

$$V_3 = (\varepsilon_h^+ - \varepsilon_h^-)/2 \quad (3)$$

and equal to 2.16 eV in GaAs. When they are placed in a solid, each of these hybrids is coupled to the other hybrid forming a two-center bond by the covalent energy[15]

$$V_2 = -3.22\frac{\hbar^2}{md^2} \quad (4)$$

(-4.09 eV). The equilibrium bond length will be listed in Table III. In the solid, the hybrids form bonds of energy $\bar{\varepsilon}_h - (V_2^2 + V_3^2)^{1/2}$, thus gaining a bond-formation (BF) energy of

$$E_{\text{BF}} = -8(V_2^2 + V_3^2)^{1/2} \quad (5)$$

(-36.99 eV) per atom pair. With $V_3 \neq 0$ these are polar bonds and the polarity

$$\alpha_p = V_3/(V_2^2 + V_3^2)^{1/2} \quad (6)$$

enters many of the formulae for their properties.

C. Overlap energy

This attractive bond-formation energy, predominantly potential, is opposed by an overlap interaction $V_0(d)$ arising principally from the excess kinetic energy of the electrons of the two overlapping hybrids. We derive a form for this interaction in Ref. 11,

$$V_0(d) = \eta_0 V_2^2(d)/|\langle \varepsilon_h \rangle| , \quad (7)$$

TABLE I. Hartee-Fock term values in units of eV from Mann (Ref. 14). The upper number is $-\varepsilon_s$ and the lower number is $-\varepsilon_p$. An asterisk denotes values extrapolated from surrounding values.

I	II	III	IV	V	IV
	Mg	Al	Si	P	S
	6.88	10.70	14.79	19.22	24.01
	3.84*	5.71	7.59	9.54	11.60
	Zn	Ga	Ge	As	Se
	7.96	11.55	15.15	18.91	22.86
	4.02*	5.67	7.33	8.98	10.68
	Cd	In	Sn	Sb	Te
	7.21	10.14	13.04	16.02	19.12
	3.99*	5.37	6.76	8.14	9.54
	Hg	Tl	Pb	Bi	Po
	7.10	9.82	12.38	15.19	17.96
	3.95*	5.23	6.53	7.79	9.05

with $\langle \varepsilon_h \rangle$ the average of the hybrid energies of the two constituents, and we shall use that form here. The basis of the derivation was that the nonorthogonality S shifts both the bonding and antibonding levels upward by $-SV_2$ and extended Hückel theory relates the coupling V_2 to the nonorthogonality by $V_2 = K \mid \langle \varepsilon_h \rangle \mid S$, with K an empirical constant. We adjusted the constant η_0 such that the total energy was minimum at the observed spacing for diamond, silicon, germanium, and tin, and took these values ($\eta_0 = 1.23$, 1.95, 1.87, and 2.16, respectively) to apply for compounds constructed from the same row (e.g., 1.87 for GaAs), using geometric means for "skew compounds." Here we use a fit that should be slightly more accurate. We fit η_0 to give the correct spacing for each compound. For bonds which do not exist in the pure tetrahedral compounds (e.g., Zn-Sb) we take the geometric mean of the values for the two compounds which contain elements from the same rows and also contain one constituent (values for ZnTe and GaSb in the case of the Zn-Sb repulsion). This is a generalization of the use of a value fit to the observed spacing for the case of existing compounds.

This overlap interaction is perhaps the weakest part of the tight-binding theory of cohesion. It is necessary to adjust η_0, as suggested above, and use the same values to predict bond lengths. Using η_0 values for elemental semiconductors did not give very accurate predictions of bond lengths for compounds isoelectronic with them and the limited tests we shall make of distortions here are not too encouraging. Cohesions predicted using this approach are quite good, but radial force constants, $k = \partial^2 E_{\text{coh}} / \partial d^2$, are not well given, typically being too small by a factor of as much as 3. Thus we can have much more confidence in our heats of solution then in our distortions and relaxation energies. The results will nevertheless be informative.

There are four bonds per atom pair so we may write the overlap energy per atom pair as

$$E_{\text{over}} = 4\eta_0 V_2^2 / \mid \langle \varepsilon_h \rangle \mid \ . \tag{8}$$

This is 13.72 eV for GaAs.

D. Metallization

The calculation to this point has neglected any coupling except between the two hybrids making up the two-center bond. Corrections to this approximation are called metallization, the leading term being from coupling between two different hybrids on the same atom. This coupling matrix element $\langle h' \mid H \mid h \rangle$ is called the "metallic energy"

$$V_1^{\pm} = (\varepsilon_s^{\pm} - \varepsilon_p^{\pm})/4 \tag{9}$$

(-1.47 eV, -2.48 eV). This couples bonds to neighboring bonds, but since both are fully occupied that does not affect the total energy. It also couples each bond to the neighboring antibonds and the corresponding lowering of the energy is called metallization. We compute it in second-order perturbation theory.

We note first (see, for example, Ref. 11) that the bond orbital is a linear combination of the two hybrids with a coefficient on the nonmetallic atom of $[(1+\alpha_p)/2)]^{1/2}$ and on the metallic atom of $[(1-\alpha_p)/2]^{1/2}$, where α_p is the polarity, given in Eq. (8). For the antibonding orbitals the magnitudes are interchanged and one is changed in sign. Thus, the coupling between the bond orbital and a neighboring antibonding orbital sharing a nonmetallic atom has the magnitude $(1-\alpha_p^2)^{1/2} V_1^- /2$. This is to be squared, divided by the energy difference, $2(V_2^2 + V_3^2)^{1/2}$, and multiplied by 3 for the three neighboring antibonds. The corresponding term for the coupling through the metallic atom is added, the result multiplied by 2 for spin and 4 for the number of bonds per atom pair to obtain the metallization energy of

$$E_{\text{met}} = -3(1-\alpha_p^2)(V_1^{+2} + V_1^{-2})/(V_2^2 + V_3^2)^{1/2} \tag{10}$$

per atom pair (for GaAs it is -4.22 eV).

E. Cohesion

The total change in energy is the negative of the cohesive energy per atom pair, E_{coh},

$$-E_{\text{coh}} = E_{\text{pro}} + E_{\text{BF}} + E_{\text{over}} + E_{\text{met}} \ . \tag{11}$$

This is 8.37 eV for GaAs. In Table II we give the corresponding valucs for a wide range of compounds, along with experimental values. These values differ from those given in Ref. 11 due to an error in the analysis of the V_0 in Ref. 11, noted in Ref. 12.

We see that we predict a decrease in cohesion with polarity, as observed. Both that trend and the decrease with increasing average atomic number are rather well given.

F. The valence-band maximum

We need an additional parameter for the pure compound in our calculation of substitution energies; that is the energy of the valence-band maximum, on the same scale as the atomic term values we have used. This is needed since if we substitute an atom of column $Z+1$ for an atom of column Z, the extra electron is to be placed at the Fermi energy of the semiconductor, which we take by

TABLE II Calculated and experimental cohesive energy (in units of eV per atom-pair). The observed bond length is d (in units of Å).

Compound	d (Å)	Cohesion (eV/atom-pair) Theory	Experiment[a]
Si	2.35	9.93	9.28
Ge	2.44	9.19	7.76
Sn	2.80	7.05	6.24
AlP	2.36	10.47	8.52
GaAs	2.45	8.37	6.52
InSb	2.81	6.20	5.60
ZnSe	2.45	8.87	5.16
CdTe	2.81	6.93	4.12

[a]Reference 16.

convention to be at the valence-band maximum. Thus, an additional promotion energy arises.

The energy of the valence-band maximum is obtained in tight-binding theory[15,16] as

$$E_v^{TB}=(\varepsilon_p^+ +\varepsilon_p^-)/2-\{[(\varepsilon_p^+ -\varepsilon_p^-)/2]^2 +(1.28\hbar^2/md^2)^2\}^{1/2}, \quad (12)$$

based upon the matrix elements we are using here. However, that energy is shifted by the same nonorthogonality which gives the overlap interaction, as noted by Enderlein.[17] Enderlein and Harrison[17] estimated this shift as the average shift for all electrons, $V_0/2$, but it may be preferable to estimate it specifically in terms of orbitals which enter the state, as in the calculations in the Appendix of Ref. 11. This reduces the shift by a factor of $(1.28/3.22)^2$. Then the valence-band maximum becomes

$$E_v=E_v^{TB}+(1.28/3.22)^2V_0/2 . \quad (13)$$

For GaAs it is $-9.64+0.27=-9.37$ eV. Corresponding values for the other semiconductors are listed in Table III. This correction to E_v^{TB} is considerably smaller than the average value used by Enderlein and Harrison. Values for the valence-band maximum, Eq. (12), have been widely used to estimate heterojunction band discontinuities; it would appear that this correction would have negligible effect on those predictions.

G. The force constant

It will be useful in our discussion to obtain one more parameter, though it is not used in our numerical calculations. That is the force constant, equal to the second derivative of the energy per bond with respect to bond length (varying all bonds in the crystal together). We have adjusted η_0 for each compound such that the minimum energy comes at the observed internuclear distance d. We may now evaluate the energy at a slightly larger and a slightly smaller d and extract the second derivative numerically. Such values are listed in Table III. They are considerably smaller than the corresponding values we obtained in Ref. 13. These values did not contain the effects of metallization and were considerably larger. An experimental value is directly obtainable from the bulk modulus; values are included in Table III for comparison.

We see that our procedure has considerably underestimated this constant, though the cohesive energies themselves are well given. This must ultimately be a failure of the form, Eq. (7), for the overlap interaction. If we were to adjust also the exponent of d in that expression to obtain the observed bulk modulus we would spoil the predictions of the cohesion. Changes in the form of the overlap interaction should not be made without a better understanding of their origin, so we shall simply note the discrepancy for later use, and proceed as we have described.

TABLE III. Calculated valence-band maximum, on the scale of Table I, obtained in tight-binding theory, E_v^{TB}, and corrected for nonorthogonality, E_v, as in Eq. (13). Also listed are the theoretical and experimental (Ref. 16) force constants k (in units of eV/Å^2).

Compound	E_v^{TB} (eV)	E_v (eV)	Force constant k (eV/Å^2) Theory	Experiment
Si	−9.35	−9.04	4.06	9.96
Ge	−8.97	−8.70	2.74	8.01
Sn	−8.00	7.80	1.39	
AlP	−10.22	−9.93	4.46	
GaAs	−9.64	−9.37	3.90	7.90
InSb	−8.61	−8.41	2.29	5.62
ZnSe	−11.06	−10.82	2.68	6.33
CdTe	−9.80	−9.63	1.43	5.12

III. THE SUBSTITUTION ENERGY

We turn now to the change in energy if an atom in the compound is replaced by an impurity atom. At first we neglect any distortion of the host lattice. We shall give numbers at each step for substituting a germanium atom for a gallium atom in gallium arsenide. This is directly evaluated as the change in the various contributions given above during this substitution, beginning with a gallium arsenide crystal and a free germanium atom and ending with a germanium impurity in GaAs and a free gallium atom.

A. Promotion energy

The first step is to break four gallium-arsenide bonds (we return to that energy in Sec. III B) and carry out the gallium atom (actually a Ga^- ion) with one electron in each of the four hybrids. We then gain an energy $\varepsilon_s^+-\varepsilon_p^+$ by letting one of the p electrons drop into an s state. A second p electron should be inserted in the compound at the valence-band maximum, costing an energy $(4-Z^+)(E_v-\varepsilon_p^+)$, leaving a free gallium atom in its ground state. We must then promote an electron in the germanium, costing $(\varepsilon_p^s-\varepsilon_s^s)$, where the super s refers to the substituting atom. If the column of the substituting atom were not 4, we would need to transfer $4-Z^s$ electrons from the valence-band maximum to the atom costing $(4-Z^s)(\varepsilon_p^s-E_v)$ in order to have one electron in each hybrid. This puts us in the promoted state with a change in the promotion energy given by

$$\delta E_{pro}=\varepsilon_p^s-\varepsilon_s^s+(4-Z^s)(\varepsilon_p^s-E_v) -(\varepsilon_p^+-\varepsilon_s^+)-(4-Z^+)(\varepsilon_p^+-E_v) . \quad (14)$$

This is -1.76 eV for Ga(Ge)As.

B. Bond-formation energy

Breaking the four bonds costs the entire bond-formation energy, $8(V_2^2+V_3^2)^{1/2}$, for the four bonds surrounding the gallium atom, but reinserting the germanium atom between the four arsenic neighbors gains back a similar amount. Since the lattice is not allowed to dis-

tort, the bond length and, therefore V_2, remains the same. However, the polar energy is different. We define it to be

$$V_3^{s-}=(\varepsilon_h^s-\varepsilon_h^-)/2\ . \tag{15}$$

In this case it is positive, 1.09 eV, but if we were to substitute the germanium for an arsenic, ε_h^- would be replaced by ε_h^+ and V_3^s would be negative. The change in bond-formation energy becomes

$$\delta E_{\rm BF}=8(V_2^2+V_3^2)^{1/2}-8[V_2^2+(V_3^s)^2]^{1/2}\ , \tag{16}$$

equal to 3.15 eV in this case.

C. Overlap energy

The overlap energy for the four bonds surrounding the impurity is modified from the substitution. Before substitution it was given by Eq. (8) with $\langle\varepsilon_h\rangle$ the average of the gallium and arsenic hybrids and η_0 determined as indicated in Sec. IC, in this case adjusted to give the correct spacing in gallium arsenide. After substitution $\langle\varepsilon_h\rangle$ becomes the average of the germanium and arsenic hybrids and η_0 is replaced by η_0' determined as indicated in Sec. II C, in this case the geometric mean of values adjusted to give the correct spacings for germanium and gallium arsenide. [If silicon were substituted for gallium in gallium arsenide it would be the geometric mean of the values fit to give the correct spacing for SiGe (the average of the Si and Ge values, by Vegard's law) and for AlAs.] Thus the change is

$$\delta E_{\rm over}=8V_2^2(\eta_0'/|\varepsilon_h^s+\varepsilon_h^-|-\eta_0/|\varepsilon_h^++\varepsilon_h^-|)\ . \tag{17}$$

This is -1.52 eV for Ge substituted in GaAs.

D. Metallization

Replacing a gallium atom by a germanium changes the metallization of the surrounding four bonds and also that of the three bonds which share each of the four neighboring arsenic atoms, illustrated in Fig. 1.

Enderlein and Harrison[17] also calculated this contribution. We see that it is small, but not negligible. We may specify the change by writing a formula for all metallization terms which are influenced by the substituted atom. We then should subtract the energy obtained from that formula with s replaced by $+$.

Each of the eight electrons in a germanium-arsenic bond has a metallization contribution with each of the other three germanium-arsenic antibonds with which it shares a germanium atom. We must be careful with the signs for these atoms. The coefficient of the bond orbital for the hybrid on the arsenic atom is $[(1+\alpha_p^{s-})/2]^{1/2}$, where

$$\alpha_p^{s-}=V_3^{s-}/[V_2^2+(V_3^{s-})^2]^{1/2}\ , \tag{18}$$

which in this case is positive. The coefficient for the antibond of the hybrid on the germanium is $[(1-\alpha_p^{s-})/2]^{1/2}$. Thus, the coupling between a bond and an antibond is $V_1^s[1-(\alpha_p^{s-})^2]^{1/2}/2$, with V_1^s the coupling between the two hybrids on a germanium atom. The energy denominator is minus twice $[V_2^2+(V_3^{-s})^2]^{1/2}$ and the shift in energy of each bond electron due to coupling with one antibond sharing the germanium is thus

$$-(V_1^s)^2[1-(\alpha_p^{s-})^2]/8[V_2^2+(V_3^{s-})^2]^{1/2}\ .$$

Further, there is metallization of each electron in a germanium-arsenic bond with three antibonds which share the arsenic atom. The coefficient for the bond of the hybrid on the arsenic is $[(1+\alpha_p^{s-})/2]^{1/2}$ and that for the antibond hybrid on the arsenic is $[(1-\alpha_p)/2]^{1/2}$.

The energy denominator is the difference between the Ga—As antibond and the Ge—As bond,

$$(\varepsilon_h^{s-})_{\rm av}-[V_2^2+(V_3^{s-})^2]^{1/2}-[(\varepsilon_h)_{\rm av}+(V_2^2+V_3^2)^{1/2}]\ . \tag{19}$$

The parameters in the second two terms, apply to the gallium-arsenic antibond. There is also metallization of the two electrons in each of the twelve Ga—As bonds with a Ge—As antibond. It differs from contributions we have just estimated only in that the product of the squared coefficients is $(1-\alpha_p^{s-})(1+\alpha_p)/4$ and the $(\varepsilon_h)_{\rm av}$ and $(\varepsilon_h^{s-})_{\rm av}$ in the denominator are changed in sign. It is convenient also to note that

$$(\varepsilon_h)_{\rm av}-(\varepsilon_h^{-s})_{\rm av}=V_3^{+s}=(\varepsilon_h^+-\varepsilon_h^s)/2\ .$$

We may combine the three sets of terms to obtain

$$\begin{aligned}E_{\rm met}=&-3(V_1^s)^2[1-(\alpha_p^{s-})^2]/[V_2^2+(V_3^{s-})^2]^{1/2}\\&-6(V_1^-)^2(1+\alpha_p^{s-})(1-\alpha_p)/\{(V_2^2+V_3^2)^{1/2}+[V_2^2+(V_3^{s-})^2]^{1/2}-V_3^{s+}\}\\&-6(V_1^-)^2(1-\alpha_p^{s-})(1+\alpha_p)/\{(V_2^2+V_3^2)^{1/2}+[V_2^2+(V_3^{s-})^2]^{1/2}+V_3^{s+}\}\ .\end{aligned} \tag{20}$$

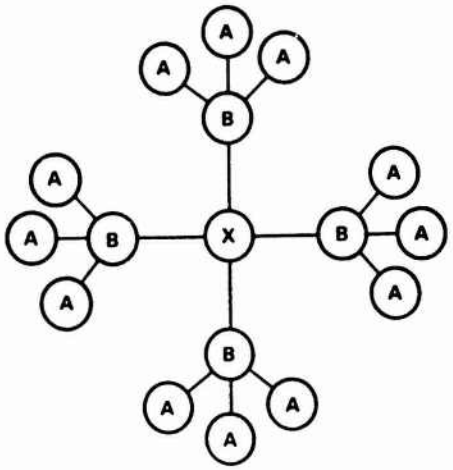

FIG. 1. An atom X is substituted for an atom A in the compound AB. Then, calculations of metallization and of distortion can be made on the cluster containing X, its four neighboring B atoms, and 12 second-neighbor A atoms. For X, a germanium atom, A, a gallium atom, and B, an arsenic atom, this cluster is sufficient for including all metallization terms which depend upon the Ge-As distance.

We are to evaluate this, obtaining -10.19 eV for germanium in a gallium site in gallium arsenide, and subtract the value obtained with V_1^s replaced by V_1^+ and α_p^{s-} replaced by α_p, V_3^{s-} replaced by V_3, and V_3^{s+} replaced by zero. This value is -7.35 eV, giving a change in metallization of -2.86 eV.

If we were instead to substitute a germanium atom for an arsenic atom, metallic and nonmetallic atoms are interchanged everywhere. This has the effect of replacing V_3^{s-} by V_3^{s+}, which is negative, in the corresponding α_p^{s+} from Eq. (18). V_1^- is replaced by V_1^+, V_3^{s+} is replaced by V_3^{s-}, and α_p is replaced by $-\alpha_p$. From this we are to subtract the value obtained with V_1^s replaced by V_1^- and with α_p^{s+} replaced by $-\alpha_p$, V_3^{s+} replaced by $-V_3$, and V_3^{s-} replaced by zero.

E. The total

We may add the four contributions to obtain a substitution energy of germanium in the gallium site of gallium arsenide of $E_{GaAs}(Ge_{Ga})=-3.01$ eV; the energy is lowered by the substitution. Such a value was used directly with the Born-Haber cycle to discuss core shifts in Refs. 12 and 17. Values obtained in exactly this way for a wide range of energies of substitution are given in Table IV.

Interestingly enough exactly these substitution energies have been measured carefully for a few systems by Su and Brebrick.[3] They give values of 3.47, 1.95, and 0.83 eV per atom for neutral Zn, In, and Sn in germanium. In our calculation for zinc we have removed two electrons from the valence band, by convention, whereas in a neutral zinc impurity the corresponding two holes would be bound in a deep acceptor level. Su and Brebrick give the energy to remove those two holes to the valence band as 0.12 eV, so one should really add this to obtain 3.59 eV to be compared with ours; the correction is small, and even smaller for indium. Our predicted values are 6.06, 3.91, and 1.12 eV for Zn, In, and Sn, respectively.

Our values have given the correct general magnitudes for the heterovalent as well as the isovalent substitutions. We would guess the accuracy of the measurements to be much better than that of the theory so the comparison should give some idea of our accuracy. They are the only values we found for the substitution energy, and the only experimental quantities related to heterovalent substitutions. Our other comparisons with experiment will be for homopolar systems only, and will be enthalpies of solution, obtainable in terms of the energies of substitution.

Energies of substitution may not be interesting in themselves, but they may be used directly to obtain other quantities of interest. Their lack of direct interest is reflected in the lack of apparent systematics from one system to another. When we substitute a germanium for a gallium in gallium arsenide, we are left with an isolated gallium atom rather than an isolated germanium, with quite different electronic energy. Further, the smaller germanium atom has an overlap repulsion lower than the gallium it replaces by a large amount, of first order in the size difference. On the other hand, when we interchange a gallium and a germanium across an interface, by combining the two substitution energies, there is no change in external isolated atoms and the first-order change in overlap interaction cancels out, leaving only a second-order effect. There is always a considerable degree of cancellation of terms when we calculate quantities of physical significance and the systematics may be present in the final result.

IV. LATTICE DISTORTIONS

For systems such as an In atom substituted for Ga in GaAs, we may readily estimate lattice distortions with an elastic model, such as that used by Martins and Zunger[6] and Shih *et al.*,[18] assuming that the equilibrium bond lengths for the In—As and Ga—As bonds are the same as those of the pure InAs or GaAs compound. However, in other solutions, such as Zn in Ge, we do not know what equilibrium bond length to use, so we turn first to a discussion of these equilibrium lengths.

A. Natural bond lengths

We have given the total energy for pure materials in Sec. II, and a procedure for obtaining parameters for the overlap interaction. We could in fact have written it in terms of each individual bond length d_i in the system and the partial derivative of the energy with respect to each d_i would have been zero at the equilibrium spacing, just as was the total derivative with respect to all of the $d_i=d$ in the crystal. In Sec. III we gave that total energy for a system containing an impurity without distortion of the lattice; that is, with each d_i equal to the host d. This also could be written in terms of the individual d_i. The bond-formation energy, the overlap interaction, and the metallization are all modified and the partial derivatives of the energy with respect to the d_i near the impurity are no longer zero. *This suggests that we define a natural impurity-host bond length by minimizing the energy with respect to the impurity-host d_i, holding all other d_i constant.* It yields the impurity-host bond length that the system would "like to have" if there were no elastic constraints from the host lattice. (We shall return to the calculation of the equilibrium bond length when the elastic constraints are included.) We could obtain, for example, a natural indium-arsenic bond length for indium substituted for gallium in gallium arsenide. This seems a very useful set of numbers to have, and we have a means of predicting them. Unfortunately, the results do not appear to be very reliable but they may nevertheless be informative.

Note that the natural bond length for a particular pair will depend upon the compound in which the bond is embedded. Thus the In—As natural bond length will be different for In in GaAs than it will be for pure InAs. In tight-binding theory such dependencies arise from the metallization energy. We find the differences to be large in some cases; if true this argues against the use of *any* covalent radii since the bond lengths obtained from such radii do not distinguish different environments.

The calculation may be understood in terms of Fig. 1. We let the bond length between the central atom and the four B neighbors be d', different from the host d; the

TABLE IV. Calculated energies of substitution $E_{AB}(X_A)$ and $E_{AB}(X_B)$ (in units of eV, for atom X substituted, respectively, for atom A or for atom B in compound AB.

$E_{AB}(X_A)$ or $E_{AB}(X_B)$ \ X	Mg	Zn	Cd	Al	Ga	In	Si	Ge	Sn	P	As	Sb	S	Se	Te
$E_{SiSi}(X_{Si})$	6.22	7.20	8.09	3.03	3.74	4.94		0.42	1.85	−2.00	−1.50	0.32	−2.65	−2.08	−0.87
$E_{GeGe}(X_{Ge})$	5.31	6.06	6.62	2.34	3.11	3.91	−0.33		1.12	−2.04	−1.51	0.0	−2.30	−1.91	−0.79
$E_{SnSn}(X_{Sn})$	3.38	4.14	4.13	1.46	1.83	2.32	−1.30	−1.14		−3.08	−2.58	−1.01	−3.05	−2.42	−1.25
$E_{AlP}(X_{Al})$	2.49	3.79	4.20		0.93	1.34	−2.32	−1.90	−1.30	−4.80	−4.30	−2.82	−7.43	−6.53	−4.61
$E_{GaP}(X_{Ga})$		2.83					−3.19	−2.77		−5.59	−5.10	−3.67		−17.81	
$E_{GaAs}(X_{Ga})$	1.49	2.62	2.83	−1.03		0.25	−3.46	−3.01	−2.35	−6.39	−5.62	−3.87	−9.33	−8.25	−5.77
$E_{GaSb}(X_{Ga})$		2.27					−3.38	−3.18		−6.46	−5.89	−3.70		−7.54	
$E_{InP}(X_{In})$		2.40			0.06		−2.96	−2.59		−6.46	−5.79	−3.88		−17.28	
$E_{InSb}(X_{In})$	0.96	1.93	1.74	−0.66	−0.13		−3.89	−3.71	−2.42	−8.44	−7.62	−4.66	−11.71	−10.42	−7.15
$E_{ZnS}(X_{Zn})$					−3.28		−6.59	−6.03		−9.02	−8.57	−8.44		−12.46	
$E_{ZnSe}(X_{Zn})$	−1.22		−0.18	−3.91	−2.85	−3.29	−6.11	−5.75	−6.06	−9.73	−8.98	−7.89	−16.72	−14.45	−10.75
$E_{CdTe}(X_{Cd})$	−0.69	0.53		−2.17	−1.39	−1.98	−4.88	−4.62	−4.22	−18.00	−10.47	−6.89	−27.13	−18.75	−11.82
$E_{AlP}(X_P)$	17.88	18.63	20.45	11.11	11.82	14.32	4.68	5.44	8.24		1.11	4.17	−2.85	−1.53	0.70
$E_{GaP}(X_P)$		18.06			11.55		4.34	5.16			1.24	3.71		−1.39	
$E_{InP}(X_P)$		18.67			12.01		4.73	5.36			1.13	3.57		−1.63	
$E_{GaAs}(X_{As})$	13.53	14.23	15.34	7.76	8.68	10.34	2.49	3.21	5.21	−1.12		2.17	−2.90	−1.86	−0.22
$E_{GaSb}(X_{Sb})$		8.65			4.59		−0.11	0.45		−2.72	−1.78			−2.55	
$E_{InSb}(X_{Sb})$	9.28	9.88	10.33	4.94	5.36	6.53	0.22	0.71	2.34	−2.91	−1.93		−4.12	−3.00	−1.46
$E_{ZnS}(X_S)$		38.21			26.47		14.36	15.54		5.98	7.88	11.43		1.88	
$E_{ZnSe}(X_{Se})$	31.02	31.17	32.78	19.97	20.85	23.42	10.24	11.31	14.32	3.04	4.77	7.93	−1.74		2.57
$E_{CdTe}(X_{Te})$	23.42	23.47	24.25	14.33	14.71	16.53	5.84	6.66	8.98	−0.23	1.25	−3.86	−3.79	−2.18	

A—B bond lengths remain as d. One of the terms in the energy which depends upon d' is the X-B overlap repulsion. In its evaluation we indicated in Sec. II C that for Si—As, for example, for $\langle \varepsilon_h \rangle$ we use the average of the hybrid energies for Si and As. For η_0 we use the geometric mean of the values fit for SiGe and AlAs (since Ge is in the same row as As and Al is in the same row as Si). The other terms depending upon d' are the X—B bond-formation energy, the metallization energy of the X—B bonds with the X—B antibonds and with the A—B antibonds, and the metallization of the A—B bonds with the X—B antibonds. We have written all of these energies, though up to now we have not distinguished the V_2 which are determined by d' from those determined from d.

Making that distinction we wrote a small program which evaluates the energies for the pure compound, adjusting the η_0 for the overlap interaction such that the total energy is minimum at the observed bond length. It then evaluated the cohesive energy, the force constant, and the valence-band maxima which we have tabulated. Then for any specified impurity it obtained the substitution energy without distortion and minimized the energy by varying the impurity-host d' numerically. Finally, it evaluated the relaxation energy for that impurity-host combination.

We consider first the natural bond lengths obtained with the program. Listed in Table V are the natural bond lengths obtained for a wide range of impurities in the compounds in Tables II and III. In discussing the results we use these values, as well as other values obtained with the same program.

There is seen to be significant dependencies upon environment. Note from Table V that we obtain a natural bond length of 2.19 Å for the Si—P bond in AlP, while from Table V it is 2.24 Å for P embedded in silicon, which is nonpolar. Similarly the natural Zn—P bond length was found to be 2.63, 2.64, and 2.59 Å in AlP, GaP, and InP, respectively (with of course Zn substituted for the metallic atom). On the other hand, it was the single value 2.53 Å in ZnS, ZnSe, and ZnTe (with P substituted for the nonmetallic atom). The larger natural bond lengths occur when the polarity is lower and therefore the effects of metallization larger, the differences being largest when one of the environments is homopolar.

We see that for a given environment the natural bond length ordinarily decreases as the impurity is taken from further right in the Periodic Table due to the increasing energy in the denominator of the overlap interaction. For an extreme case, such as Zn substituted for As in GaAs, the energy decreases monotonically with spacing so there is no natural bond length in our model. This is also true in the other extreme with Se substituted for Ga in GaAs, due in this case to the very large metallization energy. The difficulty appears to be the very soft, long-range interatomic repulsion obtained with this formulation; it led also to force constants much smaller than experiment. We may surmise that we have overestimated the effects in other cases also, but expect that the qualitative trends are correct.

An interesting comparison is the In—As natural bond length of 2.65 Å in GaAs, as opposed to 2.61 Å in InAs; the Ga—As natural bond length is 2.43 Å in InAs as opposed to 2.45 Å in GaAs. Note that the two deviations are of opposite sign so the average of the impurity-host bond lengths, 2.54 Å, is almost exactly equal to the average of the bulk bond lengths, 2.53 Å, so we predict Vegard's law to be accurately satisfied.

An important case is the substitution of As for Ga in GaAs; that is, the arsenic antisite defect in GaAs. The natural bond length from Table V is 2.40 Å, which we shall see corresponds to a relaxed bond length in the crystal of 2.41 Å. Bachelet and Scheffler[19] have made a much more complete calculation of the relaxation of the neighbors to arsenic and find the displacements to be very small. In the doubly ionized state, appropriate to our calculation, they also find an inward relaxation, but smaller than the one we find.

The particular combinations Si—P and Zn—P are of interest since there are nontetrahedral compounds SiP_2 and Zn_3P_2 containing these bonds. In the case of SiP_2, the P is tetrahedrally coordinated and there is a P—P bond of 2.13 Å, in good agreement with the 2.15 Å from Table V. In Zn_3P_2 the phosphorus is sixfold coordinated and the Zn fourfold coordinated with a separation of 2.48 Å, smaller than the 2.53 Å (P in ZnSe) and the 2.63 Å (Zn in AlP) obtained from Table V. There must be important effects aside from coordination. This and some further comparisons in Sec. IV B suggest that the predictions are not reliable.

Our natural bond lengths are very nearly equal to the pure-material bond lengths for tetrahedral, IV-IV, III-V, and II-VI bonds. These are the systems where the variations of natural bond length are important to the heats of solution; extrapolations to the other bonds, II-V, etc., are less important to the heats of solution since other terms dominate.

B. Distortion and relaxation energy at impurity atoms

We now wish to use the natural bond lengths discussed in the preceding section to predict the properties of impurities. To do this we use a simple model which will give us the relaxed bond length in terms of the natural impurity-host bond length and the host bond length; it will also give us the relaxation energy in terms of that which we have already calculated for full relaxation without constraints from the lattice. We can then obtain the needed results directly from the numbers obtained above.

1. The relaxation

In the cluster model,[6,18] the outer 12 atoms in Fig. 1, labeled A, are held fixed. It is very easy to solve for a small radial displacement u of the nearest-neighbor atoms labeled B by setting the total force on one of them equal to zero, assuming that the radial forces dominate the problem and a single force constant k is appropriate. There is a force on the B atom given by k times the natu-

ral bond length d_n for the X—B bond minus the host bond length d_0, minus the displacement of the B atom; $F=k(d_n-d_0-u)$. There are also forces from the A atoms due to the displacement. We must take components of the displacement ($u/3$) along the second-neighbor (A—B) bonds, take the radial component of the resulting force ($-ku/9$), and add it for the three bonds to A atoms to obtain $ku/3$. Setting the total equal to zero gives the equilibrium displacement

$$u=\tfrac{3}{4}(d_n-d_0)\ . \tag{21}$$

The impurity-host bond stretches three quarters of the way from the host bulk length d_0 to its natural bond length d_n as follows:

$$d=(d_0+3d_n)/4\ . \tag{22}$$

Note that we have taken all the same force constants and then they cancel from the result. Our underestimate of the force constants seen in Table III does not directly lead to error in the relaxed bond length.

We may then use the natural bond lengths from Table V to directly predict the equilibrium distortions for various impurities. Unfortunately, only a few have been measured or calculated by more accurate methods.

Recently Erbil, Weber, Cargill, and Boehme[20] used extended x-ray-absorption fine structure (EXAFS) to determine that the As-Si distance for As dissolved in silicon is 2.41±0.02 Å, greater than the bulk-silicon bond length by 0.06 Å. From Table V we obtain a natural As—Si bond length of 2.31 Å and thus a relaxed bond length of 2.32 Å. We find a relaxation of the opposite sense to that given by the measurements. Self-consistent Green's-function calculations by Scheffler *et al.*[21] appear to have been in the same direction as the experiment, but smaller by a factor of 2. Note that this is a shallow impurity level so no appreciable effects of the charge state of the impurity are expected.

More recently Sette, Pearton, Poate, Rowe, and Stöhr[22] similarly found the Ga-S distance for S dissolved in GaAs to be 2.43±0.04 Å compared with our estimated 2.19 Å using Table V. In this case we seem to have considerably overestimated the distortion.

Preliminary self-consistent local-density calculations by Froyen and Zunger[23] have given 2.47 Å for the Si-Mg distance for Mg substituted in Si. We considerably overestimate the spacing at 2.97 Å, obtained using the 3.18 Å natural bond length from Table V.

Mikkelsen and Boyce[24] have measured the In-As distance for In dissolved in GaAs and the Ga-As distance for Ga dissolved in InAs but these are fitted well by the use of pure-compound bond lengths as natural bond lengths and that is close to what we predict.

2. *The relaxation energy*

The total elastic energy initially arose from the distortion of the four impurity-host bonds and was $4\times\frac{1}{2}k(d_n-d_0)^2$. After relaxation is included the reduced elastic energy of the four impurity-host bonds plus the elastic energy of the twelve B—A springs; that equals $\frac{1}{2}k(d_n-d_0)^2$. The reduction in energy therefore is three-quarters of the initial elastic energy. In our calculation of the natural bond length in Sec. IV A, we allowed the full unrestricted relaxation, corresponding to a relaxation of all of the elastic energy. Thus, the relaxation energy of the impurity is approximately three-quarters of the full unrestricted relaxation energy.

Because of this large cancellation it is essential to treat the relaxation in the same approximation that gave the initial misfit energy. This would be accomplished if we simply took three-quarters of the relaxation energy obtained in the tight-binding program described in the preceding section, though our underestimate of the spring constant by a factor of order 3 would suggest that we underestimate both misfit and relaxation by a factor of order 3, assuming that our natural bond lengths are well given. A simple way of approximately correcting the total-energy estimate is simply to use the unrelaxed energy of substitution. This underestimates the misfit by a factor of order 3, but neglects the fact that relaxation would reduce that misfit by a factor of order 4. It may not be the most appealing way to correct an intrinsic inaccuracy of the theory, but in the context of the cluster approximation and the inaccuracy of the force-constant prediction it may be as accurate as we can be.

As we have indicated, the substitution energies are not as easy to interpret as the properties we calculate in terms of them. We therefore turn to enthalpies of solution and heats of mixing.

V. ENTHALPY OF SOLUTION AND THE HEAT OF MIXING

In order to use our tables for determining a property we must specify exactly what experimental quantity is being evaluated. We define an energy of substitution of a free atom X for an atom A in the compound AB leaving the atom A as a free atom. This was well defined but ordinarily not the quantity directly measured. The enthalpy of solution of the compound AB in the compound CD may be defined as the energy required to remove an A and a B atom from the compound, to substitute the A atom for a C atom and the B atom for a D atom in CD, and to return the C atom and the D atom to the bulk CD. This energy is

$$H_{CD}(AB)=E_{\rm coh}(AB)+E_{CD}(A_C)+E_{CD}(B_D)-E_{\rm coh}(CD) \tag{23}$$

per atom pair. This would be the energy for an AB pair to leave a step in a heterojunction between AB and CD and dissolve into the CD. The pair was removed from a step so the interface energy does not change; the step simply moves.

For example, the enthalpy of solution for Ge in GaAs from this formula is the cohesive energy of germanium, given in Table II as 9.19 eV per atom pair. Energies of substitution are obtained from Table IV. In particular, $E_{\rm GaAs}({\rm Ge}_{\rm Ga})$ is -3.01 eV, $E_{\rm GaAs}({\rm Ge}_{\rm As})$ is $+3.21$ eV, and $E_{\rm coh}({\rm GaAs})$ is 8.37 eV for a total of 1.02 eV per pair. This is a large positive enthalpy of solution. Germanium

ral bond length d_n for the X—B bond minus the host bond length d_0, minus the displacement of the B atom; $F=k(d_n-d_0-u)$. There are also forces from the A atoms due to the displacement. We must take components of the displacement ($u/3$) along the second-neighbor (A—B) bonds, take the radial component of the resulting force ($-ku/9$), and add it for the three bonds to A atoms to obtain $ku/3$. Setting the total equal to zero gives the equilibrium displacement

$$u=\tfrac{3}{4}(d_n-d_0)\ . \tag{21}$$

The impurity-host bond stretches three quarters of the way from the host bulk length d_0 to its natural bond length d_n as follows:

$$d=(d_0+3d_n)/4\ . \tag{22}$$

Note that we have taken all the same force constants and then they cancel from the result. Our underestimate of the force constants seen in Table III does not directly lead to error in the relaxed bond length.

We may then use the natural bond lengths from Table V to directly predict the equilibrium distortions for various impurities. Unfortunately, only a few have been measured or calculated by more accurate methods.

Recently Erbil, Weber, Cargill, and Boehme[20] used extended x-ray-absorption fine structure (EXAFS) to determine that the As-Si distance for As dissolved in silicon is 2.41±0.02 Å, greater than the bulk-silicon bond length by 0.06 Å. From Table V we obtain a natural As—Si bond length of 2.31 Å and thus a relaxed bond length of 2.32 Å. We find a relaxation of the opposite sense to that given by the measurements. Self-consistent Green's-function calculations by Scheffler *et al.*[21] appear to have been in the same direction as the experiment, but smaller by a factor of 2. Note that this is a shallow impurity level so no appreciable effects of the charge state of the impurity are expected.

More recently Sette, Pearton, Poate, Rowe, and Stöhr[22] similarly found the Ga-S distance for S dissolved in GaAs to be 2.43±0.04 Å compared with our estimated 2.19 Å using Table V. In this case we seem to have considerably overestimated the distortion.

Preliminary self-consistent local-density calculations by Froyen and Zunger[23] have given 2.47 Å for the Si-Mg distance for Mg substituted in Si. We considerably overestimate the spacing at 2.97 Å, obtained using the 3.18 Å natural bond length from Table V.

Mikkelsen and Boyce[24] have measured the In-As distance for In dissolved in GaAs and the Ga-As distance for Ga dissolved in InAs but these are fitted well by the use of pure-compound bond lengths as natural bond lengths and that is close to what we predict.

2. *The relaxation energy*

The total elastic energy initially arose from the distortion of the four impurity-host bonds and was $4\times\frac{1}{2}k(d_n-d_0)^2$. After relaxation it included the reduced elastic energy of the four impurity-host bonds plus the elastic energy of the twelve B—A springs; that equals $\frac{1}{2}k(d_n-d_0)^2$. The reduction in energy therefore is three-quarters of the initial elastic energy. In our calculation of the natural bond length in Sec. IV A, we allowed the full unrestricted relaxation, corresponding to a relaxation of all of the elastic energy. Thus, the relaxation energy of the impurity is approximately three-quarters of the full unrestricted relaxation energy.

Because of this large cancellation it is essential to treat the relaxation in the same approximation that gave the initial misfit energy. This would be accomplished if we simply took three-quarters of the relaxation energy obtained in the tight-binding program described in the preceding section, though our underestimate of the spring constant by a factor of order 3 would suggest that we underestimate both misfit and relaxation by a factor of order 3, assuming that our natural bond lengths are well given. A simple way of approximately correcting the total-energy estimate is simply to use the unrelaxed energy of substitution. This underestimates the misfit by a factor of order 3, but neglects the fact that relaxation would reduce that misfit by a factor of order 4. It may not be the most appealing way to correct an intrinsic inaccuracy of the theory, but in the context of the cluster approximation and the inaccuracy of the force-constant prediction it may be as accurate as we can be.

As we have indicated, the substitution energies are not as easy to interpret as the properties we calculate in terms of them. We therefore turn to enthalpies of solution and heats of mixing.

V. ENTHALPY OF SOLUTION AND THE HEAT OF MIXING

In order to use our tables for determining a property we must specify exactly what experimental quantity is being evaluated. We define an energy of substitution of a free atom X for an atom A in the compound AB leaving the atom A as a free atom. This was well defined but ordinarily not the quantity directly measured. The enthalpy of solution of the compound AB in the compound CD may be defined as the energy required to remove an A and a B atom from the compound, to substitute the A atom for a C atom and the B atom for a D atom in CD, and to return the C atom and the D atom to the bulk CD. This energy is

$$H_{CD}(AB)=E_{\rm coh}(AB)+E_{CD}(A_C)+E_{CD}(B_D)-E_{\rm coh}(CD) \tag{23}$$

per atom pair. This would be the energy for an AB pair to leave a step in a heterojunction between AB and CD and dissolve into the CD. The pair was removed from a step so the interface energy does not change; the step simply moves.

For example, the enthalpy of solution for Ge in GaAs from this formula is the cohesive energy of germanium, given in Table II as 9.19 eV per atom pair. Energies of substitution are obtained from Table IV. In particular, $E_{\rm GaAs}({\rm Ge_{Ga}})$ is -3.01 eV, $E_{\rm GaAs}({\rm Ge_{As}})$ is $+3.21$ eV, and $E_{\rm coh}$(GaAs) is 8.37 eV for a total of 1.02 eV per pair. This is a large positive enthalpy of solution. Germanium

is quite insoluble in gallium arsenide.

We may note here that the misfit and relaxation are rather small on the scale of $H_{CD}(AB)$. We calculate an unrestricted relaxation for the two cases of -0.193 eV and -0.083 eV, for germanium on the gallium and the arsenic sites, respectively. This corresponds to a misfit energy of 0.27 eV included in our calculated value, only a quarter of the total. We also argue that this is an underestimate, but that relaxation of the full value brings the total near to the 1.02 eV we obtain from the program.

These are heterovalent solutions, since Ge is from column IV and GaAs is a III-V compound. However, note that though in substituting Ge for Ga we place an electron at the valence-band maximum, we remove it in the substitution of Ge for As. This will generally be true for molecular solutions of this kind. If we dissolve GaAs in Ge, the p-type doping of the Ga cancels the n-type doping of the As. In contrast, if we were to dissolve Ga from metallic gallium into germanium, electrons would be removed from the germanium at the Fermi energy. If the germanium is p type the Fermi energy lies at the valence-band maximum as we have assumed. If the germanium is n type, the electrons would again be added at the Fermi energy, which now is at the conduction-band minimum. The enthalpy of solution would be reduced by an energy equal to the band gap in germanium. We shall consider such a case in Sec. V C.

It will generally be true for heterovalent solutions that $H_{CD}(AB)$ is large and positive and that the relaxation is quite small in comparison. In contrast, for homovalent solutions, such as InAs in GaP, $H_{CD}(AB)$ is dominated by the misfit energy, some three-quarters of which is cancelled by relaxation. Again we expect an underestimate of a factor of order 3 so our unrelaxed estimate should be approximately correct. Indeed, it was noted earlier[13] in a similar calculation that the unrelaxed estimate was in reasonable accord with experiment, while relaxation reduced it far below the experimental values. We now understand why.

The comparison with the experiment is frequently made for the heat of mixing, which for ideal solutions is given by $\Delta H^m=\Omega X(1-X)$, where X is the concentration of one constituent.[2] This assumes that $H_{AB}(CD)=H_{CD}(AB)$, which is only approximately true experimentally and in our calculation. However, we may compare experimentally determined values of Ω with the average enthalpy of solution

$$\Omega_{\text{theor}}=[H_{AB}(CD)+H_{CD}(AB)]/2$$
$$=[E_{CD}(A_C)+E_{CD}(B_D)+E_{AB}(C_A)+E_{AB}(D_B)]/2, \quad (24)$$

where we have noted that when Eq. (23) is inserted, the cohesive energies cancel out.

Experimental values for Ω are available for a number isolvent solutions[2] so we consider those first. We then treat heterovalent solutions and ones which result in doping.

A. Isovalent solutions

Predicted values for Ω are directly obtained from Eq. (24) using the energies of substitution from Table IV. These are listed in Table VI for a number of isovalent mixtures along with experimental values where available,[2] and predictions of the Martins and Zunger[6] model B discussed above. All are positive (or essentially zero), indicating energy must be supplied to transfer atoms across the interface. Our estimates are in reasonable accord with experiment, as are the Martins and Zunger values.

We may see from our calculations that our estimate is principally misfit energy by calculating that misfit energy using the cluster model and the force constant which

TABLE VI. Heat of mixing Ω (in units of eV per molecule of mixture) for isovalent mixtures.

Compound	Total [Eq. (24)]	Misfit [Eq. (25)]	Martins[a] and Zunger	Experiment[b]
AlAs/GaAs	0.00	0.00	0.00	0.00
AlAs/InAs	0.22	0.11	0.31	0.22
AlSb/GaSb	0.00	0.00	0.00	0.00
AlSb/InSb	0.10	0.06	0.18	0.05
GaP/GaAs	0.06	0.03	0.10	0.03, 0.09
GaP/GaSb	0.50	0.31		
GaP/InP	0.24	0.12	0.39	0.30, 0.28
GaAs/GaSb	0.20	0.13	0.40	0.35, 0.39
GaAs/InAs	0.16	0.09	0.22	0.14, 0.26, 0.17
GaSb/InSb	0.10	0.06	0.22	0.13, 0.16
InP/InAs	0.03	0.02	0.06	0.03
InP/InSb	0.33	0.20		
InAs/InSb	0.16	0.11	0.25	0.20, 0.25
Ge/Si	0.09	0.03	0.14	0.10
Si/Sn	0.55	0.55	2.38	1.69
Ge/Sn	−0.02	0.27	1.33	0.65

[a]Reference 6.
[b]Reference 2.

come from our calculation. We see from Eq. (24) that our estimate of Ω is one-half the energy to interchange an atom pair between the two compounds. Let the bond lengths and force constants for the two materials be d_1, d_2, k_1, and k_2. Let the natural bond length at an interchanged atom be $\frac{1}{2}(d_1+d_2)$ and the spring constant be $\frac{1}{2}(k_1+k_2)$; then without relaxation, as we calculate it, each of the 16 new bonds from the interchanged atom pairs has a bond differing by $\frac{1}{2}(d_2-d_1)$ from its natural bond length, for a misfit energy per bond of $\frac{1}{2}[\frac{1}{2}(k_1+k_2)][\frac{1}{2}(d_2-d_1)]^2$. There are 16 such bonds and we are to divide by 2 to obtain Ω_{misfit},

$$\Omega_{\text{misfit}}=\tfrac{1}{2}(k_1+k_2)(d_2-d_1)^2 . \tag{25}$$

These values are also listed in Table VI. The two theoretical calculations are totally different, but the values are rather similar. This confirms the fact that for homopolar mixing the heat of mixing is dominated by misfit energy. To the extent that the solutions are ideal, it also follows that the individual enthalpies of solution are dominated by misfit.

Under these circumstances it is probably preferable to use the cluster model and experimental lattice constants and force constants as Martins and Zunger[6] did for homopolar substitutions where all of these parameters are known. Their values are essentially $\Omega_{\text{misfit}}/4$, based on empirical k_i and d_i. For heterovalent substitutions we must proceed with a more complete description, as we have done here. Then the fact that we have obtained reasonable results for the simpler homopolar case lends support to the method.

B. Heterovalent solutions

We may immediately evaluate the enthalpies of solution using Eq. (23) and Table IV. Results for a number of heterovalent and isovalent systems are given in Table VII. The values are much larger than for the isovalent case. They are also much larger than the misfit contribution, obtained from Eq. (25). Unfortunately, there appear not to be experimental values with which to compare, although the comparison of experimental and theoretical energies of substitution in Sec. III E would suggest that they are approximately correct.

We may see what the principal contribution is by considering the individual terms. There is again no change in promotion energy in the solution process, but the sum of bond energies, $-2(V_2^2+V_3^2)^{1/2}$ does change and this is the dominant term. This contribution is in fact the same as that treated empirically by Van Vechten[25] in the Phillips–Van Vechten dielectric model. For this reason, our treatment of antistructure defects in polar semiconductors,[12] gave values very close to those obtained earlier by Van Vechten. Indeed, antistructure defects consist of heterovalent substitutions. This is also the reason why the dielectric model did rather poorly in describing the heats of solution of isovalent impurities[2,5] which are dominated by misfit.

We may evaluate this contribution to the enthalpy of solution, by summing $-2(V_2^2+V_3^2)^{1/2}$ over the bonds before and after substitution. Since this is done bond by bond, it also makes it possible to make the evaluation for complex geometries such as transferring interface atoms across a heterojunction; this is the procedure used by Grant *et al.*[26] Applying it to an enthalpy of solution, for example, dissolving two germanium atoms into gallium arsenide, without relaxation, replaces four germanium-germanium bonds ($8V_2$ with $V_2=-4.09$ eV) and four gallium-arsenide bonds [$-8(V_2^2+V_3^2)^{1/2}$ with $V_3=2.16$ eV] by four gallium-germanium bonds and four germanium-arsenic bonds ($-16\,[V_2^2+(V_3/2)^2]^{1/2}$), for an increase in energy of 2.04 eV. This is to be compared with the value of 1.02 eV from Eq. (23) or Table VII. Adding the change in overlap interaction would raise our estimate even higher, but the change in metallization has brought it down to 1.02 eV. These estimates are qualitatively correct, indicating that the insolubility of the heterovalent systems arises because it is unfavorable energetically to replace strongly and weakly polar bonds by bonds of intermediate polarity. To be at all quantitative in the predictions requires the inclusion of the metallization.

C. Solutions of dopants

The solutions described above were specifically chosen such that the atomic interchange involved no net transfer of charge. Of more importance are solutions, such as arsenic in germanium, in which there is a charge transfer and, as a consequence, carriers are added or subtracted—the system is doped.

TABLE VII. Enthalpy of solution $H_{CD}(AB)$ of AB in CD (in units of eV per atom pair).

AB \ CD	SiSi	GeGe	SnSn	AlP	GaAs	InSb	ZnSe	CdTe
SiSi		0.08	0.28	1.82	0.59	0.06	5.19	3.96
GeGe	0.10		−0.14	2.26	1.02	−0.01	5.88	4.30
SnSn	0.82	0.106		3.52	1.54	0.77	6.44	4.88
AlP	1.57	1.58	1.80		−0.05	0.70	0.73	1.14
GaAs	0.68	0.78	0.57	−0.06		0.11	1.42	1.30
InSb	1.53	0.92	0.46	1.24	0.25		1.97	1.15
ZnSe	4.06	3.83	3.53	0.66	1.26	1.60		0.29
CdTe	4.22	3.57	−0.03	1.36	1.17	1.02	0.45	

In the case of arsenic, perhaps from gallium arsenide, being dissolved into germanium the germanium atom which is replaced can be returned to the germanium, but one must also specify what is to be done with the vacant arsenic site; we have been left with a nonstoichiometric gallium arsenide crystal unless, as in the preceding subsection, we also dissolve a gallium, but then there is no doping. One alternative is to fill the arsenic site with a germanium atom. In this case, we simultaneously dope the gallium arsenide p type and the germanium n type and the energy we calculate is the sum of the energies required to dope the two systems. This is the case which is treated here.

For the particular interchange we are discussing, we may directly add the energies of substitution $E_{\mathrm{GeGe}}(\mathrm{As}_{\mathrm{Ge}})+E_{\mathrm{GaAs}}(\mathrm{Ge}_{\mathrm{As}})=1.53$ eV. This process leaves a free arsenic and a free germanium atom before and after the interchange so they can be ignored. We should note, however, that in our substitution of the arsenic for germanium, we placed, by construction, the extra electron in the valence band. This would be appropriate if the germanium were p type, but if we are interested in the doping of otherwise intrinsic material (or further doping n-type germanium), we should move the electron to the conduction band, costing the gap energy for germanium, 0.76 eV. Thus the total energy for the interchange, which dopes the Ge n type and the GaAs p type, is the sum $1.53+0.76=2.29$ eV.

We might instead wish to ask for the energy required to insert an arsenic atom into germanium, doping it n type, from a clump of arsenic on the germanium surface. We might do this by removing an arsenic atom from the arsenic metal, taking a cohesive energy of 2.96 eV, which we many obtain from a list for all elements given by Kittel.[27] We substitute this for a germanium atom, costing $E_{\mathrm{Ge}}(\mathrm{As}_{\mathrm{Ge}})=-1.62$ eV, but we then require 0.76 eV to raise the extra electron to the conduction band of the germanium. Finally, we return the substituted germanium atom to the germanium, gaining the cohesive energy per atom of germanium of 4.60 eV, for a total cost in energy of 3.74 eV per dopant atom. Similarly, we could substitute a germanium atom from pure germanium for an arsenic atom in gallium arsenide, placing the resulting free arsenic atom in a pure arsenic crystal costing an energy of 0.19 eV. These two doping energies depend upon a use of empirical tables of the cohesive energy of the elements, but our theoretical values for cohesion are close enough to experiment that the combination of theoretical and experimental values should not cause problems.

The calculation of desired doping energies is so straightforward from our tables, and it is so important in any application to decide what the process is which is being considered, that we have not produced a table of these doping energies.

ACKNOWLEDGMENTS

This work was supported, in part, by U.S. Office of Naval Research (ONR) Contract No. N00014-85-C-0135.

---

*Permanent address: Department of Applied Physics, Stanford University, Stanford, CA 94305.

[1]F. A. Trumbore, Bell Syst. Tech. J. 39, 205 (1960).
[2]G. B. Stringfellow, J. Phys. Chem. Solids 33, 665 (1972); 34, 1749 (1973).
[3]Ching-Hua Su and R. F. Brebrick, J. Phys. Chem. Solids 46, 963 (1985).
[4]K. Weiser, J. Phys. Chem. Solids 7, 118 (1958).
[5]J. A. Van Vechten, Phys. Rev. B 7, 1479 (1973).
[6]J. L. Martins and A. Zunger, Phys. Rev. B 30, 6217 (1984).
[7]D. Vanderbilt and J. D. Joannopoulos, Solid. State Commun. 35, 535 (1980).
[8]G. A. Baraff and M. Schlüter, Phys. Rev. B 30, 1853 (1984).
[9]M. Scheffler, J. P. Vigneron, and G. B. Bachelet, Phys. Rev. B 31, 1327 (1985).
[10]G. A. Baraff and M. Schlüter, Phys. Rev. Lett. 35, 1327 (1985).
[11]W. A. Harrison, Phys. Rev. B 27, 3592 (1983).
[12]E. A. Kraut and W. A. Harrison, J. Vac. Sci. Technol. B 2, 734 (1984).
[13]E. A. Kraut and W. A. Harrison, J. Vac. Sci. Technol. B 2, 1267 (1985).
[14]J. B. Mann, *Atomic Structure Calculations, I: Hartree-Fock Energy Results for Elements Hydrogen to Lawrencium* (National Technical Information Service, Springfield, VA, 1967).
[15]W. A. Harrison, Phys. Rev. B 25, 5835 (1981).
[16]W. A. Harrison, *Electronic Structure and the Properties of Solids* (Freeman, New York, 1980).
[17]R. Enderlein and W. A. Harrison, Phys. Rev. B 30, 1867 (1984).
[18]C. K. Shih, W. E. Spicer, W. A. Harrison, and A. Sher, Phys. Rev. B 31, 1139 (1985).
[19]G. B. Bachelet and M. Scheffler, in *Proceedings of the 17th International Conference on the Physics of Semiconductors, San Francisco, 1984*, edited by D. J. Chadi and W. A. Harrison (Springer, New York, 1985), p. 755.
[20]A. Erbil, W. Weber, G. S. Cargill III, and R. F. Boehme, Phys. Rev. B 34, 1392 (1986).
[21]M. Scheffler (private communication), based on the method described by M. Scheffler, J. P. Vigneron, and G. B. Bachelet, Phys. Rev. Lett. 49, 1765 (1982).
[22]F. Sette, S. J. Pearton, J. M. Poate, J. E. Rowe, and J. Stöhr, Phys. Rev. Lett. 56, 2637 (1986).
[23]S. Froyen and A. Zunger (private communication).
[24]J. C. Mikkelsen and J. B. Boyce, Phys. Rev. B 28, 7130 (1983).
[25]J. A. Van Vechten, J. Electrochem. Soc. 122, 423 (1975).
[26]R. W. Grant, J. R. Waldrop, S. P. Kowalczyk, and E. A. Kraut, J. Vac. Sci. Technol. B 3, 1295 (1985).
[27]C. Kittel, *Introduction to Solid State Physics*, 5th ed (Wiley, New York, 1976), p. 100.

Dipoles at polar heterojunction interfaces

R. W. Grant and W. A. Harrison[a)]
Rockwell International Science Center, Thousand Oaks, California 91360

(Received 3 February 1988; accepted 21 April 1988)

The Ge/GaAs heterojunction valence band discontinuity (ΔE_v) is observed to depend on crystallographic orientation. We explore theoretically the effect of interface geometry on ΔE_v. Interface geometries with unphysical charge accumulation are excluded. Allowed geometries with the same minimum sums of independent bond energies occur with positive, negative, and zero interface dipole giving a statistical average of zero dipole. Interbond interactions (metallization) yield different energies for geometries with unequal dipoles. Metallization energies are calculated for the smallest interface cells needed to sample positive, negative, and zero dipoles. A statistical average of the interface cells at the Ge/GaAs growth temperature predicts a dipole shift for each crystallographic orientation. The relative ordering of the predicted polar interface ΔE_v's agrees with experiment [i.e., $\Delta E_v(\overline{1}\overline{1}\overline{1})\text{As} > \Delta E_v(100) > \Delta E_v(111)\text{Ga}$] while the range of values from the model calculation is about a factor of 2 smaller than is experimentally observed.

I. INTRODUCTION

We seek an understanding of the heterojunction band lineup variation with crystal orientation, discovered experimentally earlier for the (110), (111), and (100) interfaces between Ge and GaAs.[1] Any attempt at such an understanding must consider, as we previously showed,[2] that the polar interfaces cannot be planar without producing charge accumulation. The resulting potential gradients extending indefinitely into the solid would have divergent energy, except that free carriers would inevitably be generated to neutralize the charge. The corresponding interface energy would still be very large due to the formation of carrier pairs. No such charged interfaces are expected nor is there any experimental evidence for them.

The real polar interface must avoid surface charges by substituting atoms near the interface to produce a neutral transition layer. For example, at an arsenic terminated (100) interface, a half-layer of extra gallium atoms could be substituted for germanium in the first germanium layer.[2] This would produce a dipole shift of $\pi e^2/2\epsilon a$ (+ 0.37 eV), but would eliminate charge accumulation. At first, one might think that placing these gallium atoms in the germanium layer would cost significant energy because Ga is very insoluble in Ge. However, that is not the case for the (100) interface. Kraut and Harrison[3] have shown that the strong insolubility of Ga in Ge arises because bonds of intermediate polarity are formed (it costs 0.25 eV of bond formation energy per intermediate-polarity bond formed). However, the planar (100) interface already has two intermediate-polarity bonds (GeAs bonds) for every surface atom. A gallium half-plane can be added such that it will eliminate one-half of these and add back an equal number of GaGe bonds, so the energy is essentially unchanged. Thus, the bond energy for this geometry, with no charge accumulation but a sizable dipole, is the same as for the geometry with charge accumulation which we ruled out.

In fact, we shall see that there are also geometries with the same number of intermediate-polarity bonds, and therefore, the same energy in the bond-orbital approximation,[4] which have no dipole or have dipole of opposite sign. In this approximation, we would expect a thermal distribution of such geometries which would lead, with positive and negative dipoles having the same energy, to an average dipole of zero. There would be a negligible number of geometries with more intermediate-polarity bonds because of the 0.25 eV excess energy for each intermediate bond formed. A more careful analysis of the geometries with the same number of intermediate bonds will show slight differences in the energies for geometries with different dipoles and the effect of these differences will be explored.

In order to restrict the total number of geometries which need considering, we perform our energy and statistical calculations by using geometries repeated in a periodic array with a small interface cell. We shall find that we may obtain the full range of experimentally observed dipoles, all with the same interface energy in the bond-orbital approximation, by using a square primitive cell containing four atoms in each (100) plane for (100) interfaces; one or two compositionally graded interface transition planes are required. For (111) interfaces, again with no net charge allowed at the interface, we shall need cells of eight atoms per plane, and again one or two transition planes [in contrast to the (100) interface, it costs bond formation energy to eliminate charge accumulation by compositionally grading an abrupt (111) interface]. Within this limitation, we select all possible geometries which have the same, and minimum, energy in the bond-orbital approximation, proceed to a more accurate calculation of their energies, and calculate the statistical distribution of these geometries to obtain the dipole.

In all, 28 different geometries for the (100) interface and 144 geometries for the (111) interface are considered. This is a rather small number of geometries, corresponding to the rather small cell, but hopefully should be adequate. If the cell was made larger and larger, the statistics would approach those of the real interface.

 0734-211X/88/041295-07$01.00 © 1988 American Vacuum Society

II. THE ENERGY OF THE INTERFACE

A. The bond-orbital approximation

In the bond-orbital approximation, the interface energy is written as the sum of bond formation energies, $E_b = -2(V_2^2 + V_3^2)^{1/2}$, where the covalent energy $V_2 = -3.22\hbar/md^2 = -4.09$ eV (d is the bond length and is assumed constant for all bonds considered here) and the polar energy $V_3 = (\epsilon_{hA} - \epsilon_{hB})/2$ depends on the hybrid energies (ϵ_h) of the two atoms that form the bond. The hybrid energy for a given atom depends upon s- and p-term values (ϵ_s and ϵ_p, respectively), as $\epsilon_h = (\epsilon_s + 3\epsilon_p)/4$.

We begin with the (100) interface which is somewhat simpler than the (111) interface. We consider an interface cell consisting of four atoms per plane and having a thickness of five planes, as shown in Fig. 1(a). The first plane (left-hand side) is pure Ge, indicated by a zero below, while the fifth plane (right-hand side) is an As plane in GaAs with a +4 below indicating that all 4 atoms are As. There are four ways to eliminate charge accumulation for this (100) interface. The four associated nuclear charge distributions are labeled A → D in Fig. 1(a). Case A was described above and has a half-Ge and half-Ga composition on plane 2 (indicated by −2) with plane 3 being all As and plane 4 all Ga. These charge distributions were obtained by considering a Ge–Ge homojunction, then removing a single proton from each nucleus to become gallium and adding one to each nucleus to become arsenic. Integrating Poisson's equation from the germanium, as illustrated in Fig. 1(a) (case A), gives a shift of $\pi e^2/2a$. These nuclear changes make the bonds polar, but the effect of bonds to the right cancels that of bonds to the left and the net dipole is unaffected by these polar bonds. The net dipole shift across the junction, however, is equivalent to an applied potential difference and is reduced by a factor of the dielectric constant $\epsilon = 10.9$. The oscillating potential (ϕ) in the GaAs contains a dipole such that an electron has higher electrostatic energy on the germanium side by $\pi e^2/2a\epsilon = 0.37$ eV, which we regard as a positive dipole. The valence band maximum (E_v) of GaAs lies below E_v of Ge and thus a positive dipole will increase ΔE_v. Case C has an equal magnitude but opposite sign dipole shift, while cases B and D have no net dipole shift.

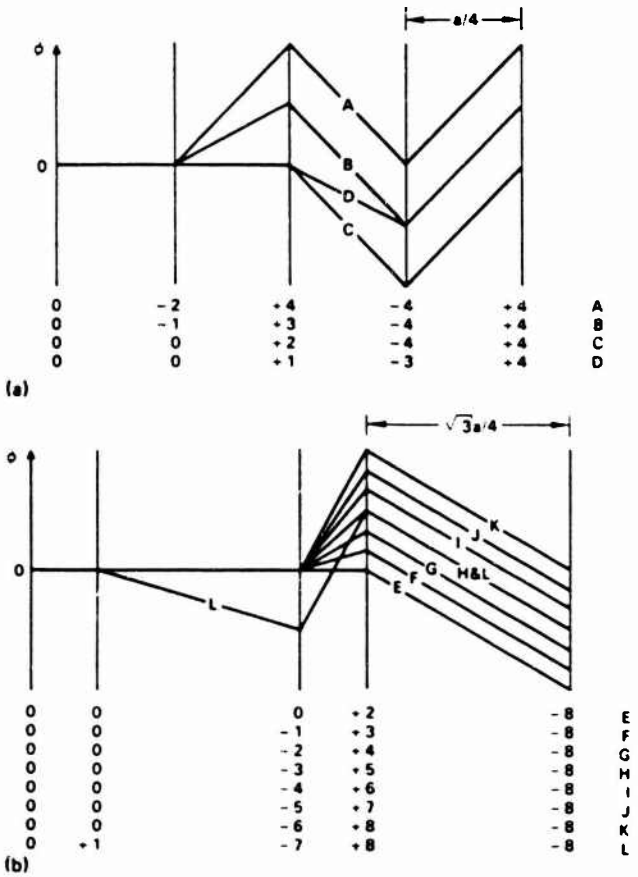

FIG. 1. Nuclear charge distributions and associated potential variations that eliminate charge accumulation for (a) (100) and (b) (111)Ga interfaces.

Returning to case A, there are six possible arrangements of two gallium and two germanium atoms in the two-by-two (100) primitive cell, all have the same energy in the bond-orbital approximation and all have the same dipole shift. Three of these arrangements are shown in Fig. 2. The interface is viewed along the (001) direction from Ge toward GaAs. Atoms in the five interface planes are indicated by circles of decreasing size as one goes from the Ge to the GaAs. To shorten the notation needed to specify a given interface, only the net nuclear charge on planes 2, 3, and 4 is given. The three missing atom arrangements are obtained by permuting the Ga and Ge atoms on plane 2 in Fig. 2. To compare the total bond formation energy (ΣE_b) of two interface cells, it is necessary to keep the atomic composition of the cells constant. This is done by adding a Ge–Ge atom pair and subtracting a Ga–As atom pair as needed (or vice versa). The Ge atoms can be imagined to be obtained from a step on the Ge surface which requires breaking four Ge–Ge bonds per Ge–Ge atom pair and the Ga–As atoms are added to a step on the GaAs surface, which requires formation of four Ga–As bonds per Ga–As atom pair. The interface composition for the 28 possible atom arrangements associated with the charge distributions specified in Fig. 1(a) were determined. After adjusting the interface cells to have equal compositions (4 Ga, 10 Ge, and 6 As atoms), the corresponding bond distribution for the 28 possible arrangements was 16 Ge–Ge, 4 Ge–Ga, 4 Ge–As, and 16 Ga–As bonds. Because in all cases the bond distribution is identical, ΣE_b for all interface cells with the minimum number of intermediate polarity bonds is equal.

The charge distributions required to eliminate charge accumulation for the (111)Ga interface [Ge epitaxial layer on

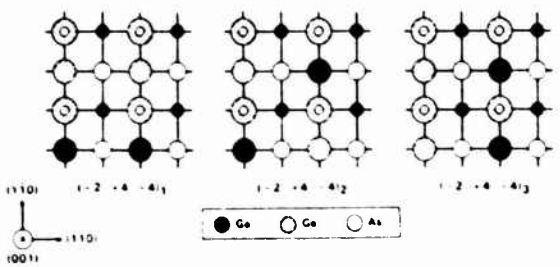

FIG. 2. Three possible atom arrangements associated with a (−2, +4, −4) nuclear charge distribution which eliminate charge accumulation for a (100) interface, have equal bond formation energy sums, but different metallization energy sums.

(111)Ga face of GaAs substrate] are given in Fig. 1(b) and are labeled E through L. The (111)Ga interface specifies the structure where a Ga atom in bulk GaAs has one bond directed toward the Ge layer and three back bonds to As atoms. The dipole shifts associated with cases E through L are -0.37, $-\frac{2}{3}(0.37)$, $-\frac{1}{3}(0.37)$, 0, $+\frac{1}{3}(0.37)$, $+\frac{2}{3}(0.37)$, $+0.37$, and 0 eV, respectively. The unit cell considered for the (111) interface contains eight atoms per plane and is again five planes in thickness. This cell is shown in Fig. 3, where the interface is viewed from Ge toward GaAs along a (111) direction. Again, the nuclear charge distribution on planes 2, 3, and 4 is used to specify a specific interface cell and as an example, the atomic arrangement associated with the $(0,-1,+3)$ distribution has been shown in Fig. 3.

For the (111)Ga interface, there are 144 possible atom arrangements. The interface composition was adjusted to 12 Ga, 22 Ge, and 6 As atoms to facilitate comparison of ΣE_b. In all cases, the bond distribution was 38 Ge–Ge, 6 Ge–Ga, 6 Ge–As, and 30 Ga–As bonds, so that ΣE_b is identical for these 144 possible atom arrangements. Similar results were obtained for the $\bar{1}\bar{1}\bar{1}$ As interface.

To summarize this section, within the bond-orbital approximation, it is found that interface geometries are favored which maximize the number of polar (Ga–As) bonds, minimize the number of intermediate polarity bonds and avoid formation of Ga–Ga or As–As bonds. However, since al these geometries have the same ΣE_b, a thermal distribution of such geometries should have an average zero dipole.

B. Effect of metallization

A key approximation of the bond orbital model is the neglect of coupling between a bond orbital and its environment, an effect termed metallization.[5] The coupling between a bond orbital and a neighboring antibond orbital, arising from the coupling V_1 (the metallic energy) of two hybrids sharing an atom, will lower the bond energy and raise the antibond energy. Because only the bond orbitals are occupied, the system energy is lowered. This gain is called metallization.

The combinations of bonds and neighboring antibonds is different for different geometries and thus the metallization energy must differ. There is uncertainty in the values of the parameters we use, but any choice with V_3 for Ge–As and Ge–Ga bonds one-half as large as that for Ga–As bonds and with V_1 for germanium equal to the average of that for gallium and arsenic will lead to the same qualitative result. We should not be misled by the fact that we subtract rather large sums of terms to obtain small differences, since there is exact cancellation of many terms. We shall carry out the numerical evaluation with Hartree–Fock and Herman–Skillman term values, which give significantly different values for individual contributions to the energy, but give very similar total energy differences.

To facilitate this calculation which follows Ref. 5, it is useful to associate a metallization energy with a specific group of three atoms found at the Ge/GaAs interface. The group consists of an atom M and two nearest neighbors L and N. We label parameters for the L–M bond and antibond by x, so that its polar energy is $V_{3x} = (\epsilon_{h\mathrm{L}} - \epsilon_{h\mathrm{M}})/2$ and its polarity is $\alpha_{px} = V_{3x}(V_2^2 + V_{3x}^2)^{-1/2}$. Similarly, the N–M bond and antibond are labeled by y. The coupling of the L–M bond to the N–M antibond is[5] $(1+\alpha_{px})^{1/2}(1-\alpha_{py})^{1/2} V_1(\mathrm{M})/2$ with $V_1 = (\epsilon_s - \epsilon_p)/4$ evaluated for atom M. The shift of the x bond energy due to coupling with the y antibond is

$$\delta\epsilon_{bx} = \frac{V_1(\mathrm{M})^2}{4}\left[\frac{(1+\alpha_{px})(1-\alpha_{py})}{V_{3x} - V_{3y} - (V_2^2 + V_{3x}^2)^{1/2} - (V_2^2 + V_{3y}^2)^{1/2}}\right]. \tag{1}$$

The shift $\delta\epsilon_{by}$ of the y bond energy due to coupling with the x antibond is the same, but with all V_3's and α_p's changed in sign. Combining $\delta\epsilon_{bx}$ and $\delta\epsilon_{by}$, and accounting for two electrons/bond gives the metallization energy associated with atom M that has L and N nearest neighbor atoms,

$$\delta\epsilon(\mathrm{LMN}) = 2(\delta\epsilon_{bx} + \delta\epsilon_{by}). \tag{2}$$

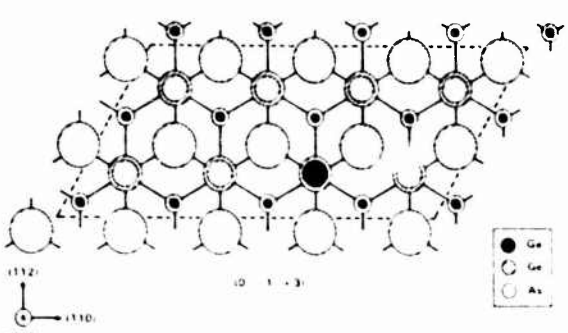

FIG. 3. A $(0,-1,+3)$ nuclear charge distribution that eliminates charge accumulation for a (111)Ga interface and shows cell (dashed lines) used in (111) interface calculations.

If Ga–Ga and As–As bonds are excluded from the Ge/GaAs interface region due to the associated unfavorable bond formation energies and if the number of Ga–As bonds is maximized, there are eleven possible LMN atom combinations that can exist. These eleven possibilities are enumerated in Table I; $\delta\epsilon(\mathrm{LMN})$ has been evaluated by using both Hartree–Fock and (Herman–Skillman) term values: $\epsilon_s(\mathrm{Ga}) = -11.55(-11.37)$ eV, $\epsilon_p(\mathrm{Ga}) = -5.67(-4.90)$ eV, $\epsilon_s(\mathrm{Ge}) = -15.15(-14.38)$ eV, $\epsilon_p(\mathrm{Ge}) = -7.33(-6.36)$ eV, $\epsilon_s(\mathrm{As}) = -18.91(-17.33)$ eV, and $\epsilon_p(\mathrm{As}) = -8.98(-7.91)$ eV; only the Hartree–Fock results are shown.

With the values of $\delta\epsilon(\mathrm{LMN})$ given in Table I, we can calculate a metallization energy (E_{met}) for a specific five atom cluster consisting of a central atom and its four nearest neighbors. For example, the cluster which has a central Ge atom with two Ge and two As nearest neighbors has a metallization energy of $\delta\epsilon(\mathrm{GeGeGe}) + 4\delta\epsilon(\mathrm{AsGeGe}) + \delta\epsilon(\mathrm{AsGeAs})$, where values of $\delta\epsilon$ are found in Table I. If Ga–Ga and As–As bonds are excluded and the number of Ga–As bonds is maximized, there are only 15 possible 5

TABLE I. Metallization energy $\delta\epsilon$(LMN) associated with atom M that has L and N nearest neighbor atoms.

LMN	$\delta\epsilon(\mathrm{LMN})_{\mathrm{H\text{-}F}}$ (eV)
As–Ge–As	−0.4216
As–Ge–Ge	−0.4830
Ge–Ge–Ge	−0.4672
Ge–Ge–Ga	−0.4825
Ga–Ge–Ga	−0.4229
Ge–Ga–As	−0.2249
As–Ga–As	−0.1826
Ge–Ga–Ge	−0.2391
Ga–As–Ga	−0.5207
Ga–As–Ge	−0.6391
Ge–As–Ge	−0.6799

atom clusters that can exist in the Ge/GaAs interface region. These 15 possibilities are listed in Table II, where the notation M[iL,$(4-i)$N] refers to a cluster that has M as the central atom with iL atoms and $(4-i)$N atoms tetrahedrally coordinated as nearest neighbors. Only values of E_{met} calculated with Hartree–Fock term values are given in Table II.

To determine the metallization energy associated with a specific interface cell, it is only necessary to determine the cluster distribution in the cell and sum the appropriate terms in Table II. This has been done for the (100), (111)Ga, and $(\bar{1}\bar{1}\bar{1})$ As interface cells. As an example, the cluster distributions for the (100) interface cells are given in Table III. Also given in Table III are the differences in the sums of E_{met} (with zero specifying the lowest energy geometry) calculated for both Hartree–Fock and Herman–Skillman term values, $\Delta(\mathrm{H}-\mathrm{F})$ and $\Delta(\mathrm{H}-\mathrm{S})$, respectively; the dipole associated with each cell is δ_{K} and the statistical weight (g_{K}) is the number of ways to obtain each geometry within the interface cell. Table IV summarizes $\Delta(\mathrm{H}-\mathrm{F})$, $\Delta(\mathrm{H}-\mathrm{S})$, δ_{K}, and g_{K} for the (111)Ga and $(\bar{1}\bar{1}\bar{1})$As interfaces.

The expected value of dipole shift at a given absolute temperature $\delta(T)$, was evaluated by statistically averaging δ_{K} by using a Boltzmann factor, where the population of a given geometry (n_{K}) was specified by

$$n_{\mathrm{K}}/n = g_{\mathrm{K}} \exp(-\Delta_{\mathrm{K}}/kT)/\Sigma_{\mathrm{K}}\, g_{\mathrm{K}} \exp(-\Delta_{\mathrm{K}}/kT) \quad (3)$$

and n is the total population number. The resulting $\delta(T) = \Sigma_{\mathrm{K}} n_{\mathrm{K}} \delta_{\mathrm{K}}/n$ are given in Fig. 4. For both Hartree–Fock and Herman–Skillman term values, a near-zero δ is predicted at all T for (111)Ga interfaces. For (100), a large positive ($+0.37$ eV) δ is predicted at $T=0$ K, which decreases rapidly as one approaches room temperature. The δ for $(\bar{1}\bar{1}\bar{1})$As interfaces is predicted to increase from 0 at $T=0$ K to a maximum well above room temperature.

TABLE II. Metallization energies E_{met} associated with clusters expected at the Ge/GaAs interface.

Cluster	E_{met}(H-F) (eV)
Ge(4Ge)	−2.8034
Ge(3Ge,1As)	−2.8506
Ge(2Ge,2As)	−2.8207
Ge(1Ge,3As)	−2.7138
Ge(3Ge,1Ga)	−2.8493
Ge(2Ge,2Ga)	−2.8202
Ge(1Ge,3Ga)	−2.7162
Ga(4As)	−1.0955
Ga(3As,1Ge)	−1.2226
Ga(2As,2Ge)	−1.3214
Ga(1As,3Ge)	−1.3921
As(4Ga)	−3.1243
As(3Ga,1Ge)	−3.4796
As(2Ga,2Ge)	−3.7572
As(1Ga,3Ge)	−3.9571

III. DISCUSSION

We now compare the calculated $\delta(T)$ with experimental results. In Table V, the Ge3d to Ga3d core level binding energy difference (ΔE_B) is reproduced from Ref. 1 for the polar (100), (111)Ga, and $(\bar{1}\bar{1}\bar{1})$As and nonpolar (110) Ge/GaAs heterojunction interfaces. The initial GaAs substrate (and associated low-energy electron diffraction pattern) prior to Ge epitaxial layer growth is specified at the top of the table. As noted in Ref. 1, a change in the Ge3d–Ga3d core binding energy difference [$\delta(\Delta E_B)$] indicates a change in the valence band discontinuity $\delta(\Delta E_v)$ and thus, the presence of an interface dipole. Because E_v of GaAs lies below E_v of Ge, $\delta(\Delta E_B) = -\delta(\Delta E_v)$.

As noted in Fig. 4, the predicted interface dipole for the (111)Ga interface is almost zero at all T. We will arbitrarily assume zero dipole for the Ge/GaAs(111) heterojunction and reference $\delta(\Delta E_v)$ to this interface. If we assume that thermal equilibrium is established at the Ge/GaAs heterojunction growth temperature ($T_G \approx 613$ K),[6] the predicted dipole contributions to ΔE_v for the polar Ge/GaAs heterojunctions are shown in Table V; δ_{HF} and δ_{HS} refer to predictions based on Hartree–Fock and Herman–Skillman term values (at 613 K), respectively. Although two different (by 0.05 eV) values of ΔE_v were measured for (100) interfaces prepared with different experimental conditions, the model calculation does not distinguish different polar faces for the (100) interface.

For the ideal nonpolar (110) interface (last column of Table V), one would anticipate a zero dipole as no interface compositional grading is needed to eliminate charge accumulation. Experimentally however, a positive dipole relative to the (111)Ga interface is observed. This suggests a possibility that the experimental interface may not be ideal. Without supporting evidence, we note that a (110) interface with equal numbers of (111)Ga and $(\bar{1}\bar{1}\bar{1})$As facets can be formed without cost of E_b to yield a dipole of the observed sign.

Returning to the polar Ge/GaAs interfaces, earlier work has indicated that ΔE_v for the (111)Ga interface is smaller than for the $(\bar{1}\bar{1}\bar{1})$As interface.[7] Also, ΔE_v has been measured for several Ge/GaAs (100) interfaces and found to be independent of initial GaAs surface reconstruction and stoichiometry.[8] From the results given in Table V, we note that the relative ordering of the predicted ΔE_v's agrees with experiment [i.e., $\Delta E_v(\bar{1}\bar{1}\bar{1})\mathrm{As} > \Delta E_v(100) > \Delta E_v(111)\mathrm{Ga}$],

TABLE III. Metallization energy variation in (100) cells of identical composition and bond formation energy. Number of occurrences of each cluster type (central atoms with 4 neighbors in parenthesis) in an interface cell are indicated in rows 1–15. Metallization energies are given relative to the $(-2,+4,-4)_2$ geometry, which for Hartree–Fock term values had ΣE_{met}(H–F) = −53.2530 eV. For each geometry, δ_K is the dipole shift and g_K is the statistical weight.

	$(-2,+4,-4)_1$	$(-2,+4,-4)_2$	$(-2,+4,-4)_3$	$(-1,+3,-4)$	$(0,+2,-4)_1$	$(0,+2,-4)_2$	$(0,+2,-4)_3$	$(0,+1,-3)$
Ge(4Ge)	4	4	6	4	4	4	6	4
Ge(3Ge,1As)	...	...	...	2	4	4	...	2
Ge(2Ge,2As)	2	2	2	1	...	...	2	1
Ge(1Ge,3As)	...	...	...	...	...	...	...	...
Ge(3Ge,1Ga)	4	4	...	2	...	...	...	2
Ge(2Ge,2Ga)	...	...	2	1	2	2	2	1
Ge(1Ge,3Ga)	...	...	...	...	...	...	...	...
Ga(4As)	2	2	2	1	2	...	...	1
Ga(3As,1Ge)	...	...	...	2	...	4	...	2
Ga(2As,2Ge)	2	2	2	1	2	...	...	1
Ga(1As,3Ge)	...	...	...	...	...	...	...	...
As(4Ga)	4	2	2	3	4	4	4	3
As(3Ga,1Ge)	...	4	4	2	...	...	...	2
As(2Ga,2Ge)	2	...	...	1	2	2	2	1
As(1Ga,3Ge)	...	...	...	...	...	...	...	...
Δ(H–F)(eV)	0.1554	0	0.1500	0.0473	0.1512	0.0946	0.2488	0.0473
Δ(H–S)(eV)	0.1164	0	0.1190	0.0257	0.1100	0.0514	0.1768	0.0257
δ_K (eV)	+0.37	+0.37	+0.37	0	−0.37	−0.37	−0.37	0
g_K	2	2	2	8	2	2	2	8

TABLE IV. Metallization energy variation, cell dipole shift, and statistical weight for (111)Ga and $(\bar{1}\bar{1}\bar{1})$As interface geometries.

(111)Ga	$(0,0,+2)_1$	$(0,0,+2)_2$	$(0,0,+2)_3$	$(0,-1,+3)$	$(0,-2,4)$	$(0,-3,+5)$	$(0,-4,+6)$	$(0,-5,+7)$	$(0,-6,+8)_1$	$(0,-6,+8)_2$	$(0,-6,+8)_3$	$(+1,-7,+8)$
Δ(H-F)(eV)	0.3885	0.3114	0.4656	0.1554	0.1548	0	0.1548	0.1542	0.3853	0.3076	0.4630	0.3095
Δ(H-S)(eV)	0.2912	0.2285	0.3539	0.1164	0.1209	0	0.1209	0.1254	0.3135	0.2553	0.3717	0.2419
δ_n (eV)	−0.37	−0.37	−0.37	−2(0.37)/3	−0.37/3	0	+0.37/3	+2(0.37)/3	+0.37	+0.37	+0.37	0
g_n	16	8	4	8	4	8	4	8	16	8	4	56
$(\bar{1}\bar{1}\bar{1})$As	$(0,0,-2)_1$	$(0,0,-2)_2$	$(0,0,-2)_3$	$(0,+1,-3)$	$(0,+2,-4)$	$(0,+3,-5)$	$(0,+4,-6)$	$(0,+5,-7)$	$(0,-6,8)_1$	$(0,+6,-8)_2$	$(0,+6,-8)_3$	$(-1,+7,-8)$
Δ(H-F)(eV)	0.1411	0.0661	0.2161	0.0566	0.1033	0	0.1033	0.1500	0.3748	0.3465	0.4031	0.2063
Δ(H-S)(eV)	0.1465	0.0870	0.2060	0.0586	0.0888	0	0.0888	0.1190	0.2973	0.2680	0.3266	0.1775
δ_n (eV)	+0.37	+0.37	+0.37	+2(0.37)/3	+0.37/3	0	−0.37/3	−2(0.37)/3	−0.37	−0.37	−0.37	0
g_n	16	8	4	8	4	8	4	8	16	8	4	56

TABLE V. Initial GaAs substrate surface, experimentally measured Ge3*d*-Ga3*d* binding energy differences (ΔE_B) for several Ge/GaAs heterojunction interfaces, experimentally determined variation in ΔE_v relative to the (111)Ga interface [$\delta(\Delta E_v)$] and calculated dipole shifts in ΔE_v at the growth temperature (613 K) by using Hartree–Fock (δ_{HF}) and Herman–Skillman (δ_{HS}) term values.

Substrate surface	(111)Ga (2×2)	(100)Ga $c(8\times2)$	(100)As ···	$(\bar{1}\bar{1}\bar{1})$As (1×1)	(110) (1×1)
ΔE_B(eV)	10.27(1)	10.22(1)	10.17(1)	10.11(1)	10.20(1)
	10.31(1)			10.10(1)	10.21(1)
$\delta(\Delta E_v)$(eV)	0	+0.07	+0.12	+0.185	+0.085
δ_{HF} (eV)	0.000	+0.070		+0.108	0
δ_{HS} (eV)	−0.005	+0.038		+0.078	0

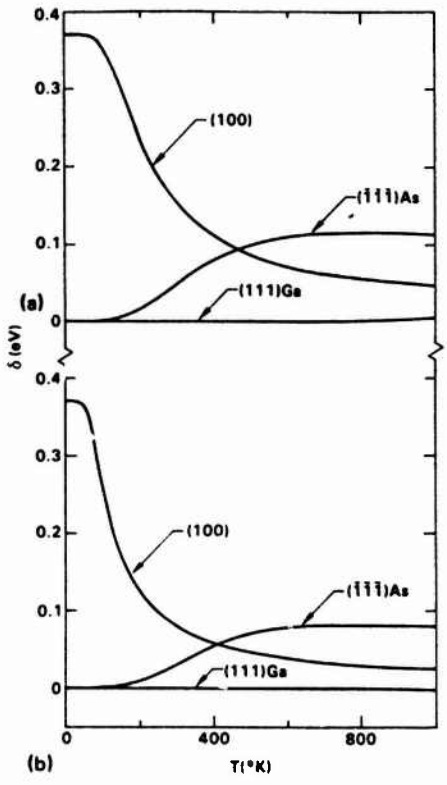

FIG. 4. Predicted dipole shifts vs equilibrium temperature for (100), (111)Ga, and ($\overline{111}$)As interfaces. Calculations based on (a) Hartree–Fock and (b) Herman–Skillman term values.

while the range of δ from the model calculation is about a factor of 2 smaller than is experimentally observed. The agreement between experiment and the model calculation suggests that the model offers a plausible explanation for the origin of the crystallographic orientation dependence of ΔE_v for polar Ge/GaAs heterojunction interfaces.

ACKNOWLEDGMENTS

Discussions with J. R. Waldrop and E. A. Kraut are greatly appreciated. This work was partially supported by the Office of Naval Research Contract No. N00014-85-C-0135.

[a] Permanent address: Stanford University, Stanford, California 94305.
[1] R. W. Grant, J. R. Waldrop, and E. A. Kraut, Phys. Rev. Lett. **40**, 656 (1978).
[2] W. A. Harrison, E. A. Kraut, J. R. Waldrop, and R. W. Grant, Phys. Rev. B **18**, 4402 (1978).
[3] E. A. Kraut and W. A. Harrison, J. Vac. Sci. Technol. B **3**, 1267 (1985).
[4] W. A. Harrison, Phys. Rev. B **24**, 5835 (1981).
[5] W. A. Harrison, Phys. Rev. B **27**, 3592 (1983).
[6] J. R. Waldrop, E. A. Kraut, S. P. Kowalczyk, and R. W. Grant, Surf. Sci. **132**, 513 (1983).
[7] F. F. Fang and W. E. Howard, J. Appl. Phys. **35**, 612 (1964).
[8] A. D. Katnani, P. Chiaradia, H. W. Sang, Jr., and R. S. Bauer, J. Vac. Sci. Technol. B **2**, 471 (1984).

GaAs/InP and InAs/InP heterojunction band offsets measured by x-ray photoemission spectroscopy

J. R. Waldrop, R. W. Grant, and E. A. Kraut
Rockwell International Science Center, Thousand Oaks, California 91360

(Received 7 February 1989; accepted 3 April 1989)

X-ray photoemission spectroscopy (XPS) has been used to measure the unstrained valence-band offset ΔE_v for the $x = 0$ and $x = 1$ end points of the $In_xGa_{1-x}As/InP$ (100) heterojunction system. Although the GaAs/InP (100) and InAs/InP (100) pseudomorphic interfaces investigated are strained because of lattice mismatch, the ΔE_v values obtained by the XPS measurement analysis used are interpreted as characteristic of an unstrained interface. Strain-free values of ΔE_v(GaAs/InP) = 0.19 eV and ΔE_v(InAs/InP) = 0.31 eV are reported. A linear interpolation of these $x = 0$ and $x = 1$ unstrained values gives $\Delta E_v(In_{0.53}Ga_{0.47}As/InP) = 0.25$ eV ($\Delta E_c/\Delta E_v = 58/42$) for the lattice-matched interface.

I. INTRODUCTION

The $In_xGa_{1-x}As/InP$ heterojunction system has attracted considerable interest for electronic device applications. Accurate knowledge of the band offsets, that is, the conduction- and valence-band discontinuities at the interface, is necessary for device design and modeling. Because most present devices use the lattice-matched (unstrained) interface at $x = 0.53$, band offset measurements have emphasized the $In_{0.53}Ga_{0.47}As/InP$ heterojunction. Published values for the valence-band offset ΔE_v at $x = 0.53$, as determined by a variety of electrical and optical techniques with samples prepared by several growth methods, have a rather large range of 0.0 to 0.38 eV.[1-7]

In this paper we use x-ray photoemission spectroscopy (XPS) to measure ΔE_v at the $x = 0$ and $x = 1$ end points of the $In_xGa_{1-x}As/InP$ (100) system. Three types of interface samples were prepared by molecular-beam epitaxial (MBE) growth within the XPS system: GaAs/InP (thin pseudomorphic GaAs layer grown on InP substrate, ~3.7% lattice mismatch), InP/GaAs (~3.8%), and InAs/InP (~3.2%). Although these pseudomorphic interfaces are strained owing to the lattice mismatch, we argue that the ΔE_v values obtained by the XPS analysis method described in this paper can be interpreted as being characteristic of an unstrained (relaxed) interface. These XPS strain-free ΔE_v values (a) allow a direct comparison to predictive models for ΔE_v that do not include strain effects, and (b) provide a reference ΔE_v for calculated strain corrections. A linear interpolation between the $x = 0$ and $x = 1$ XPS unstrained ΔE_v values is used to obtain a value for the $x = 0.53$ interface of $\Delta E_v(In_{0.53}Ga_{0.47}As/InP) = 0.25$ eV ($\Delta E_c/\Delta E_v = 58/42$).

II. EXPERIMENTAL

A. Sample preparation

Figure 1(a) shows schematic cross sections of representative sample structures. The interface analyzed by XPS is beneath the thin uppermost layer. The five samples with GaAs/InP and InAs/InP interfaces have InP substrates and the two with InP/GaAs interfaces have GaAs substrates, all of which are ~10×10 mm pieces of (100) oriented bulk material. One InAs/InP sample had a ~ 2μm InP buffer layer grown on the bulk substrate by metalorganic chemical vapor deposition (MOCVD) in addition to a MBE buffer layer; one GaAs/InP sample had the thin GaAs layer grown directly on a similar MOCVD InP buffer layer; and one InP/GaAs sample had no buffer layer. To prepare the bulk substrates, a piece was etched in 4:1:1 H_2SO_4:H_2O_2:H_2O solution (~3 min InP, ~30 s GaAs), quenched, dried with N_2, mounted on Mo plate with In, and immediately put into the XPS ultrahigh vacuum (10^{-10} Torr range base pressure) sample preparation chamber. The two MOCVD buffer layer samples were similarly mounted but not etched. The thin, < 10 Å thick, native oxide surface layer was removed from the substrates prior to MBE growth by momentary heating (~450 °C InP, ~575 °C GaAs) in a ~10^{-5} Torr

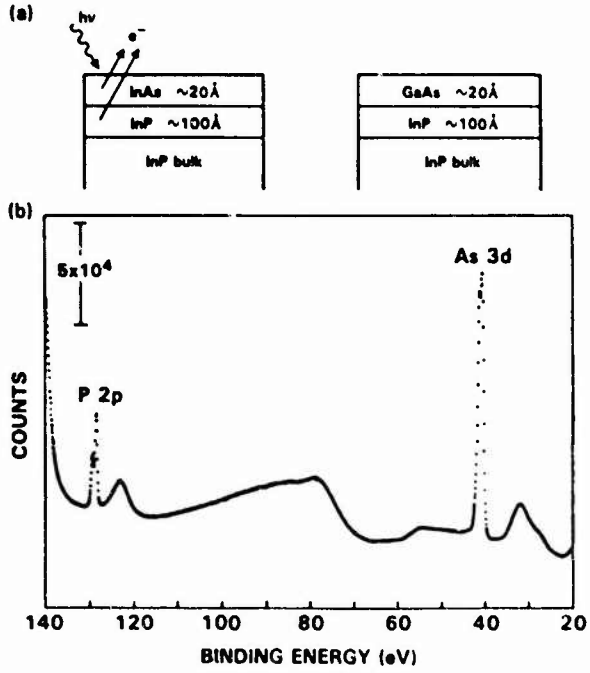

FIG. 1. (a) Sample structures for InAs/InP and GaAs/InP (100) heterojunctions. (b) XPS binding energy spectrum of a InAs/InP (100) sample in the region of the P 2*p* and As 3*d* core levels.

 0734-211X/89/040815-05$01.00 © 1989 American Vacuum Society

overpressure of the corresponding group V element (the GaAs substrate used for the one InP/GaAs sample without a buffer layer was heated in vacuum). The differences in substrate preparation or structure noted for three of the seven samples did not cause any apparent variation in ΔE_v.

The GaAs, InAs, and InP layers were grown at ~0.5–1 Å/s rates in $\sim 10^{-5}$ Torr overpressure of As_4 or P_2. The As_4 source was a small quartz oven filled with elemental As; the P_2 source was InP wrapped in resistively heated Ta wire; the In and Ga sources were *W* wire baskets. The thickness *t* of the thin top layer (listed in Table I) was measured from the intensity attenuation of a substrate XPS core level. Growth temperatures were between ~400–500 °C. Epitaxy of the thin top layer was assessed by using low-energy electron diffraction (LEED) after growth. Analysis of LEED patterns from representative samples indicated that the top layer had a lattice constant parallel to the substrate consistent with essentially pseudomorphic growth.

At the initial stage of MBE growth the heated substrate is always exposed to the group V element (P or As) prior to the group III element (In or Ga). We examined by XPS the surface of InP after exposure (at the MBE growth temperature) to As_4 and the surface of GaAs similarly exposed to P_2. In each instance, a limited surface chemical exchange reaction between the group V elements takes place: 1–2 monolayers of InAs are formed on the InP surface and 1–2 monolayers of GaP are formed on the GaAs surface (such a surface reaction between As and InP has been previously described[8]). Thus, the interfaces of MBE grown GaAs/InP and InP/GaAs heterojunctions are intrinsically nonabrupt on a scale on 1–2 monolayers. The InAs/InP interface appears to be atomically abrupt because the InAs growth simply proceeds on the InAs formed by the initial surface reaction between As and InP.

B. Measurement of unstrained ΔE_v at strained interfaces

The XPS system is based on a HP5950 angle-resolved electron spectrometer, which has a monochromatic Al $K\alpha$ x-ray source ($h\nu = 1486.6$ eV). The effective photoelectron escape depth λ for the photoelectron kinetic energies analyzed and the emission angle of the experiment is ~16 Å. Photoelectrons from each side of a heterojunction interface located a distance on the order of λ from the sample surface [Fig. 1(a)] will be detected in the same XPS binding energy spectrum. Thus, in Fig. 1(b) the XPS spectrum for a InAs/InP sample over a binding energy range of 20 to 140 eV contains both the As 3*d* core level peak from the thin InAs top layer and the P 2*p* core level peak from the underlying InP.

Figure 2(a) has schematic energy band diagrams of the GaAs/InP and InAs/InP interfaces in the absence of strain effects, where E_c and E_v are conduction-band minima and valence-band maxima, respectively, and ΔE_{CL} is a binding energy difference between core levels selected from each side of the interface (P 2*p* for InP and As 3*d* for GaAs and InAs). Thus, for the InAs/InP interface, $\Delta E_{CL} = (E^{InP}_{P\,2p} - E^{InAs}_{As\,3d})$. Hence, by inspection of the band diagram, $\Delta E_v(\text{InAs/InP}) = \Delta E_{CL}(\text{InAs/InP}) + (E^{InAs}_{As\,3d} - E^{InAs}_{v}) - (E^{InP}_{P\,2p} - E^{InP}_{v})$. Similarly, $\Delta E_v(\text{GaAs/InP}) = \Delta E_{CL}(\text{GaAs/InP}) + (E^{GaAs}_{As\,3d} - E^{GaAs}_{v}) - (E^{InP}_{P\,2p} - E^{InP}_{v})$, where $\Delta E_{CL}(\text{GaAs/InP}) = (E^{InP}_{P\,2p} - E^{GaAs}_{As\,3d})$. The two $(\Delta E_{CL} - \Delta E_v)$ terms in the ΔE_v expressions are core level to valence-band maximum binding energy differences which are obtained by separate XPS measurements on pure unstrained bulk material. A $(E_{CL} - E_v)$ value may depend on strain; however, because we wish to obtain a ΔE_v characteristic of an unstrained interface, any strain dependence does not affect the analysis. Thus, of the three quantities needed for the XPS measurement of an unstrained ΔE_v, only ΔE_{CL} is directly associated with the heterojunction. The primary assumption we make (discussed below) is that ΔE_{CL} is independent of strain.

Values of $(E^{GaAs}_{As\,3d} - E^{GaAs}_{v}) = 40.74 \pm 0.03$ eV and $(E^{InAs}_{As\,3d} - E^{InAs}_{v}) = 40.72 \pm 0.03$ eV have been previously measured by XPS for GaAs and InAs, respectively.[9] The measurement of $(E^{InP}_{P\,2p} - E^{InP}_{v}) = 128.24 \pm 0.03$ eV for

TABLE I. XPS measured unstrained valence-band offset ΔE_v values for pseudomorpnic InAs/InP, GaAs/InP, and InP/GaAs heterojunction interfaces.

Interface	ΔE_{CL} (eV)	ΔE_v (eV)	t (Å)
InAs/InP	87.84	0.32	42
	87.83	0.31	19
	87.82	0.30	23
GaAs/InP	87.71	0.21	18
	87.67	0.17	27
InP/GaAs	87.71	0.21	22
	87.70	0.20	26

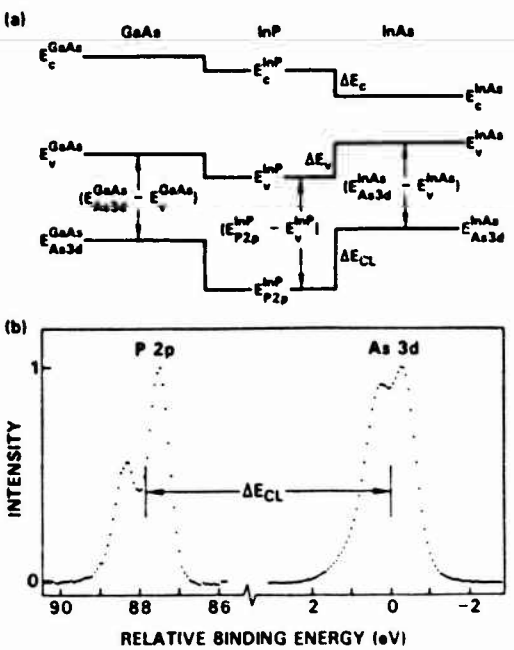

FIG. 2. (a) Schematic energy band diagrams of the InAs/InP and GaAs/InP interfaces in the absence of strain effects. (b) Measurement of $\Delta E_{CL} = (E^{InP}_{P\,2p} - E^{InAs}_{As\,3d})$ (data from Fig. 1).

InP is described in the next section. Substitution of these bulk values into the expressions for ΔE_v yields:

$$\Delta E_v(\text{InAs/InP}) = \Delta E_{CL}(\text{InAs/InP}) - 87.52\ \text{eV}, \quad (1)$$

and

$$\Delta E_v(\text{GaAs/InP}) = \Delta E_{CL}(\text{GaAs/InP}) - 87.50\ \text{eV}. \quad (2)$$

Equations (1) and (2) purposely include bulk $(E_{CL} - E_v)$ values because our principal aim is to measure unstrained ΔE_v values by considering the possible effect of strain solely on ΔE_{CL}. A ΔE_v value obtained from use of Eqs. (1) and (2) departs from the true strain-free value only to the degree that strain may cause a shift in the corresponding value of ΔE_{CL}. Although the $(E_{CL} - E_v)$ values are generally a function of strain, we emphasize that any strain shifts are irrelevant in our present approach to obtaining an unstrained ΔE_v value. For an analysis of XPS heterojunction data where $(E_{CL} - E_v)$ values are corrected for strain to obtain Si/Ge strained ΔE_v values, see Ref. 10.

The precision measurement of ΔE_{CL} is illustrated in Fig. 2(b), where the core level peaks from the InAs/InP spectrum in Fig. 1(b) have been analyzed. A background function that is proportional to the integrated peak intensity is subtracted from each core level peak. The peak binding energy is measured at the half-width point at half-height. The peak width and height are determined consistently by a computerized procedure in which a third order least-squares fit is made to segments at the sides and top of the discrete peak data. In this example, $\Delta E_{CL} = 87.83$ eV. The uncertainty in the ΔE_{CL} measurement is estimated to be ± 0.02 eV. Because of the additional uncertainties related to the $(E_{CL} - E_v)$ values the ΔE_v uncertainty associated with Eqs. (1) and (2) is ± 0.05 eV.

C. Measurement of $(E^{InP}_{P\,2p} - E^{InP}_v)$

Figure 3(a) is a -10 to 140 eV XPS binding energy spectrum from clean InP (100). Similar data were obtained from two samples of bulk material. The position of E_v was found by using a procedure described in detail elsewhere.[11] In brief, a theoretical valence-band density of states (VBDOS) for InP,[12] on an energy scale where $E_v = 0$ eV is precisely defined, is broadened by convolution with the experimentally determined XPS spectrometer resolution function. The broadened theoretical VBDOS function, where E_v has remained at zero energy, is least-squares fitted to the experimental data in the XPS VBDOS spectrum near E_v. This fitting procedure effectively transfers the position of E_v from the theoretical VBDOS function to the XPS data. Figure 3(b) shows the good fit obtained between the broadened theoretical VBDOS (line) and the XPS valence-band data of Fig. 3(a) plotted on an energy scale where $E_v = 0$ eV. The fit is over an interval that ends at an energy E_{max} below E_v (in this example, $E_{max} = 1.22$ eV).

Figure 4 shows the results of the valence-band fitting procedure applied to the data for the two InP samples, where the P 2p core level to valence-band energy $(E^{InP}_{P\,2p} - E^{InP}_v)$ is plotted as a function of E_{max}. The error bar for each value of $(E^{InP}_{P\,2p} - E^{InP}_v)$ indicates the 95% confidence interval of the fit. A value of $(E^{InP}_{P\,2p} - E^{InP}_v) = 128.24$ eV was obtained by taking the average of the $(E^{InP}_{P\,2p} - E^{InP}_v)$ values for $E_{max} > 0.7$ eV, a range over which the fit error bars are relatively small. An uncertainty of ± 0.03 eV (dashed lines) includes most of the $(E^{InP}_{P\,2p} - E^{InP}_v)$ values.

III. RESULTS AND DISCUSSION

Table I contains the ΔE_{CL} values measured for the pseudomorphic InAs/InP, GaAs/InP, and InP/GaAs samples.

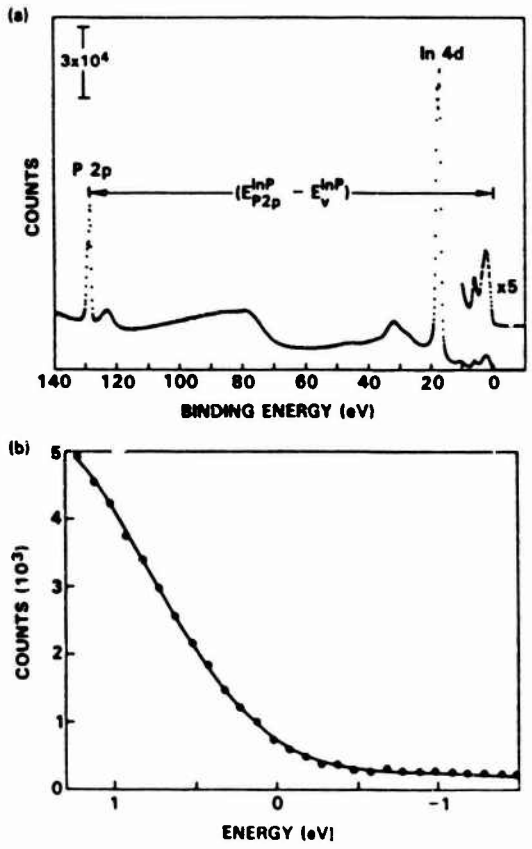

FIG. 3. (a) Representative -10 to 140 eV XPS binding energy spectrum for InP (100). (b) Fit of the broadened theoretical valence-band density of states (line) to the XPS valence band data shown in (a).

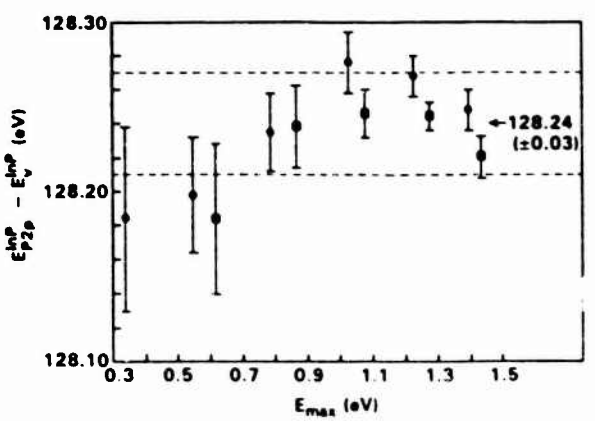

FIG. 4. P 2p core level to valence band maximum binding energy difference for two InP (100) samples as a function of the end point E_{max} of the valence-band fitting interval.

Also listed in Table I are the corresponding unstrained ΔE_v values for each heterojunction as obtained from Eqs. (1) and (2).

As mentioned above, strain can influence the strain-free ΔE_v value obtained from use of Eqs. (1) and (2) only through an effect on ΔE_{CL}. The strain associated with these (100) XPS samples occurs in the pseudomorphically grown thin top layer because its lattice constant parallel to the interface expands (or contracts) to accommodate the lattice constant of the thick substrate. This strain has two components, a hydrostatic strain associated with the volume change of the overlayer unit cell, and a shear (uniaxial and biaxial) strain associated with the tetragonal distortion of the overlayer. The uniaxial strain is perpendicular to the interface plane while the biaxial strain is parallel.

We have attempted to experimentally investigate the possibility of a strain-induced energy shift in a core-level peak from the thin pseudomorphic layer with respect to a core-level peak from the unstrained substrate by comparing ΔE_{CL}(GaAs/InP) and ΔE_{CL}(InP/GaAs) $[\Delta E_{CL} = E^{InP}_{P\,2p} - E^{GaAs}_{As\,3d}]$. The GaAs/InP interface is under tensile hydrostatic and compressive uniaxial strains (possible shift of the As 3*d* core level) while the InP/GaAs interface is under compressive hydrostatic and tensile uniaxial strains (possible shift of the P 2*p* core level). Within experimental error, the ΔE_{CL}(GaAs/InP) values and the ΔE_{CL}(InP/GaAs) values are equal (see Table I). This equality is achieved because either (a) the net strain shift of the As 3*d* core-level binding energy at ~41 eV is identical in magnitude and of opposite sign as the corresponding strain shift of the P 2*p* core level at ~129 eV, or (b) the magnitude of both shifts is insignificant. We have assumed the latter for our present analysis to thus suggest the lack of significant strain-induced core-level binding energy shifts in relation to the GaAs/InP, InP/GaAs, and InAs/InP ΔE_{CL} measurements. In other words, in the XPS measurement method we are using the unstrained ΔE_v is the sum of three quantities, of which the effect of strain on only one needs to be considered: the core-level binding energy difference ΔE_{CL}. Our analysis of the XPS data yields strain-free ΔE_v values under the critical assumption that ΔE_{CL} is not significantly affected by the level of strain present in our pseudomorphic heterojunction samples. Consequently, we regard the ΔE_v values in Table I as valence band offsets in the absence of strain.

The solid line in Fig. 5 is the linear interpolation of ΔE_v ($In_xGa_{1-x}As$/InP) vs x based on the average XPS measured unstrained ΔE_v values at the $x = 0$ and $x = 1$ end points: $\Delta E_v(GaAs/InP)_{avg} = 0.19$ eV and $\Delta E_v(InAs/InP)_{avg} = 0.31$ eV. We thus find a value of $\Delta E_v(In_{0.53}Ga_{0.47}As/InP) = 0.25$ eV, or $\Delta E_c/\Delta E_v = 58/42$, for the lattice-matched interface at $x = 0.53$. Our value is in fair agreement with $x = 0.53$ results, based on optical measurements, of Brunemeier *et al.*[3] where $\Delta E_c/\Delta E_v \simeq 65/35$ was found and of Temkin *et al.*[4] where $\Delta E_c/\Delta E_v > 50/50$ was found. We also note, from Table I, that $\Delta E_v(InP/GaAs)_{avg} = 0.21$ eV, which thus demonstrates the absence of a growth sequence dependence for unstrained GaAs–InP (100) ΔE_v values.

The nature of the strain contribution to ΔE_v at lattice mismatched heterojunction interfaces can be accounted for

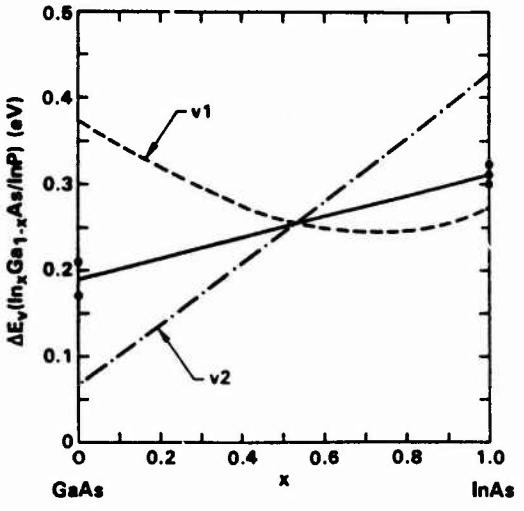

FIG. 5. Linear interpolation of unstrained ΔE_v($In_xGa_{1-x}As$/InP) based on the XPS measured values at $x = 0$ and $x = 1$ (solid line). The $In_xGa_{1-x}As$ strain-split valence bands $v1$ (heavy hole) and $v2$ (light hole) are calculated for perfect pseudomorphic growth of a thin overlayer on InP. ΔE_v for the lattice-matched $x = 0.53$ interface is 0.25 eV ($\Delta E_c/\Delta E_v = 58/42$).

by application of deformation potential models. At present it does not appear possible to quantitatively model the effect of hydrostatic strain on the XPS measured ΔE_{CL} values with an accuracy comparable to our experimental uncertainty. We note that the valence-band hydrostatic deformation potential a_v is typically an order of magnitude smaller than the conduction band deformation potential a_c.[13,14] This relationship suggests that core-level hydrostatic deformation potentials may plausibly be considered small, in which case the effect of strain on XPS core-level binding energies is negligible. It is possible that a refined analysis of hydrostatic strain effects on core levels might produce corrections to the XPS ΔE_{CL} energies measured across lattice mismatched interfaces to thus yield more accurate strain-free values. However, for the interfaces considered here the growth sequence ΔE_{CL} equivalence at GaAs–InP interfaces demonstrates that any substantial correction to the As 3*d* core level at the GaAs/InP interface (GaAs in tension) would be essentially equal and opposite to that for the As 3*d* core level at the InAs/InP interface (InAs in compression). Because the interpolated ΔE_v value for the lattice-matched $In_{0.53}Ga_{0.47}As/InP$ interface is very near $x = 0.5$, such equal and opposite sign corrections at the $x = 0$ and at $x = 1$ end points would thus not significantly change the $\Delta E_v(x = 0.53)$ value obtained from our present interpolation.

We now estimate the strained ΔE_v for the pseudomorphic interfaces. Calculations for the strained Si/Ge (100) interface indicate that the average energy of the three upper valence bands at Γ is relatively insensitive to hydrostatic strain.[15] This result indicates that valence-band shifts owing to hydrostatic strain are considerably less significant than

uniaxial strain induced shifts, as discussed further below. For GaAs, the experimental and theoretical a_v values range from ~ 1.6 to $+0.7$ eV.[13,14] A value of $|a_v| = 1$ eV would shift the GaAs average valence-band energy by 0.04 eV at a pseudomorphic GaAs/InP (100) interface. Because there is uncertainty as to the sign of a_v(GaAs), and because the calculated a_v(InAs) is smaller than a_v(GaAs),[13] we shall ignore any hydrostatic strain contribution to ΔE_v.

The effect of uniaxial strain on valence band energies is marked. We have calculated the uniaxial strain-induced splitting of the two highest energy valence bands $v1$ (heavy hole) and $v2$ (light hole) at Γ for pseudomorphic $In_xGa_{1-x}As$/InP interfaces by using the approach given in Refs. 15 and 16. It was assumed that the lattice constant of the $In_xGa_{1-x}As$ layer parallel to the interface matched that of InP. The spin-orbit splitting constants required were from Ref. 17. Values for other GaAs and InAs materials constants needed were from the tabulation in Ref. 18; a linear interpolation was used to obtain values for $In_xGa_{1-x}As$. The results of the uniaxial strain calculation are plotted in Fig. 5 (a similar calculation that used slightly different parameter values but with essentially identical results was recently reported[19]). This correction is based on a model in which uniaxial strain does not affect the average valence-band energy. An alternate viewpoint that involves charge transfer (neutral point) heterojunction models is discussed in Refs. 13 and 20.

In summary, XPS has been used to measure unstrained valence band offsets at pseudomorphic InAs/InP, GaAs/InP, and InP/GaAs heterojunction interfaces. A linear interpolation between unstrained ΔE_v(GaAs/InP) = 0.19 eV and ΔE_v(InAs/InP) = 0.31 eV values gives $\Delta E_v(In_{0.53}Ga_{0.47}As/InP) = 0.25$ eV ($\Delta E_c / E_v = 58/42$).

ACKNOWLEDGMENTS

The authors thank Prof. W. Harrison for helpful discussions. This work was supported by the Office of Naval Research under Contract No. N00014-85-C-0135.

[1] S. R. Forrest and O. K. Kim, J. Appl. Phys. **52**, 5838 (1981).
[2] Y. Guldner, J. P. Vieren, P. Voisin, M. Voos, M. Razeghi, and M. A. Poisson, Appl. Phys. Lett. **40**, 877 (1982).
[3] P. E. Brunemeier, D. G. Deppe, and N. Holonyak, Jr., Appl. Phys. Lett. **46**, 755 (1985).
[4] H. Temkin, M. B. Panish, P. M. Petroff, R. A. Hamm, J. M. Vandenberg, and S. Sumski, Appl. Phys. Lett. **47**, 394 (1985).
[5] K. Steiner, R. Schmitt, R. Zuleeg, L. M. F. Kaufmann, and K. Heime, Surf. Sci. **174**, 331 (1986).
[6] M. S. Skolnick, P. R. Tapster, S. J. Bass, A. D. Pitt, N. Apsley, and S. P. Aldred, Semicond. Sci. Technol. **1**, 29 (1986).
[7] D. V. Lang, M. B. Panish, F. Capasso, J. Allam, R. A. Hamm, A. M. Sergent, and W. T. Tsang, Appl. Phys. Lett. **50**, 736 (1987).
[8] J. M. Moison, M. Bensoussan, and F. Houzay, Phys. Rev. B **34**, 2018 (1986).
[9] J. R. Waldrop, R. W. Grant, and E. A. Kraut, J. Vac. Sci. Technol. B **5**, 1209 (1987); and references therein.
[10] G. P. Schwartz, M. S. Hybertsen, J. Bevk, R. G. Nuzzo, J. P. Mannaerts, and G. J. Gualtieri, Phys. Rev. B **39**, 1235 (1989).
[11] E. A. Kraut, R. W. Grant, J. R. Waldrop, and S. P. Kowalczyk, Phys. Rev. B **28**, 1965 (1983).
[12] J. R. Chelikowsky and M. L. Cohen, Phys. Rev. B **14**, 556 (1976).
[13] M. Cardona and N. E. Christensen, Phys. Rev. B **35**, 6182 (1987).
[14] D. D. Nolte, W. Walukiewicz, and E. E. Haller, Phys. Rev. Lett. **59**, 501 (1987).
[15] C. G. Van de Walle and R. M. Martin, Phys. Rev. B **34**, 5621 (1986).
[16] F. H. Pollak and M. Cardona, Phys. Rev. **172**, 816 (1968).
[17] O. Berolo and J. C. Woolley, in *Proceedings of the 11th International Conference on the Physics of Semiconductors*, Warsaw 1972 (Elsevier, NY, 1972), p. 1420.
[18] S. Adachi, J. Appl. Phys. **53**, 8775 (1982).
[19] R. People, Appl. Phys. Lett. **50**, 1604 (1987).
[20] J. Menendez, A. Pinczuk, D. J. Werder, S. K. Sputz, R. C. Miller, D. L. Sivco, and A. Y. Cho, Phys. Rev. **36**, 8165 (1987).

Measurement of GaAs/InP and InAs/InP heterojunction band offsets by x-ray photoemission spectroscopy

J. R. Waldrop, R. W. Grant, and E. A. Kraut
Rockwell International Science Center, Thousand Oaks, California 91360

(Received 28 December 1988; accepted for publication 2 March 1989)

The unstrained valence-band offset ΔE_v for the $x = 0$ and $x = 1$ end points of the $In_xGa_{1-x}As/InP$ (100) heterojunction system has been measured by x-ray photoemission spectroscopy (XPS). Although the GaAs/InP and InAs/InP interfaces are strained because of lattice mismatch, the ΔE_v values obtained by the XPS measurement method used are characteristic of an unstrained interface. Values of ΔE_v (GaAs/InP) = 0.19 eV and ΔE_v (InAs/InP) = 0.31 eV are observed. A linear interpolation between the $x = 0$ and $x = 1$ values gives ΔE_v ($In_{0.53}Ga_{0.47}As/InP$) = 0.25 eV for the $x = 0.53$ lattice-matched interface ($\Delta E_c / \Delta E_v = 58/42$).

There is substantial interest in the $In_xGa_{1-x}As/InP$ heterojunction system for devices, especially with regard to optoelectronic applications. Accurate knowledge of the band offsets is required for device design and modeling. Because particular importance is attached to the lattice-matched interface at $x = 0.53$, band offset measurements have concentrated on the $In_{0.53}Ga_{0.47}As/InP$ heterojunction. Literature values of the valence-band offset ΔE_v for $x = 0.53$, as determined by electrical and optical techniques, range from 0.0 to 0.38 eV.[1-7]

We report x-ray photoemission spectroscopy (XPS) ΔE_v measurements for the $x = 0$ and $x = 1$ end points of the $In_xGa_{1-x}As/InP$ (100) system. Three types of interface samples were prepared by molecular beam epitaxy growths within the XPS system: GaAs/InP (GaAs grown on InP), InP/GaAs, and InAs/InP. Although the pseudomorphic GaAs/InP and InAs/InP interfaces are lattice mismatched by 3.7% and 3.2%, respectively, and are thus strained, we argue that the ΔE_v values obtained by the XPS method used can be interpreted as representative of an unstrained (relaxed) interface. This measurement characteristic (a) permits a direct comparison of the results to the many predictive models for ΔE_v that do not include strain effects and (b) provides a reference ΔE_v for strain corrections. A calculated correction is made to the XPS ΔE_v values to account for the splitting of the valence bands by uniaxial strain. A linear interpolation between the $x = 0$ and $x = 1$ XPS measurements is used to arrive at a value for the $x = 0.53$ interface of ΔE_v ($In_{0.53}Ga_{0.47}As/InP$) = 0.25 eV.

The XPS system consists of a HP5950 electron spectrometer ($h\nu = 1486.6$ eV monochromatic Al $K\alpha$ x-ray source) coupled to an ultrahigh vacuum sample preparation chamber (base pressure 10^{-10} Torr range). The inset in Fig. 1 shows an example of the sample structure, in this instance, InAs/InP. The interface analyzed by XPS is directly beneath the thin upper layer. The five samples with GaAs/InP and InAs/InP interfaces have InP(100) substrates and the two with InP/GaAs interfaces have GaAs(100) substrates. One GaAs/InP sample and one InAs/InP sample had an ~ 2 μm InP epitaxial buffer layer grown by metalorganic chemical vapor deposition. The thin native oxide surface layer was removed from the substrates by momentary heating.

The GaAs, InAs, and InP layers were grown at $\sim$0.5–1 Å/s rates in $\sim 10^{-5}$ Torr overpressure of As_4 or P_2. The top layers were $\sim$20–40 Å in thickness t, as listed in Table I. Growth temperatures were between $\sim$400 and 500 °C. Epitaxy was confirmed by using low-energy electron diffraction (LEED). Analysis of representative LEED patterns indicated that the thin top layers had an in-plane lattice constant consistent with essentially pseudomorphic growth. The sample-to-sample differences in preparation conditions or structure did not cause any apparent variation in ΔE_v.

The effective XPS photoelectron escape depth is $\lambda = \sim 16$ Å. Photoelectrons from each side of a heterojunction interface located on the order of λ from the sample surface will be detected in the same XPS spectrum. Thus, in Fig. 1, the XPS spectrum for the InAs/InP sample over a binding energy range of 20 to 140 eV contains both the As 3d core level peak from InAs and the P 2p core level peak from InP.

Figure 2(a) is a schematic energy-band diagram that depicts the InAs/InP heterojunction interface region in the absence of strain effects, where E_c and E_v are the conduction-band minimum and valence-band maximum, respec-

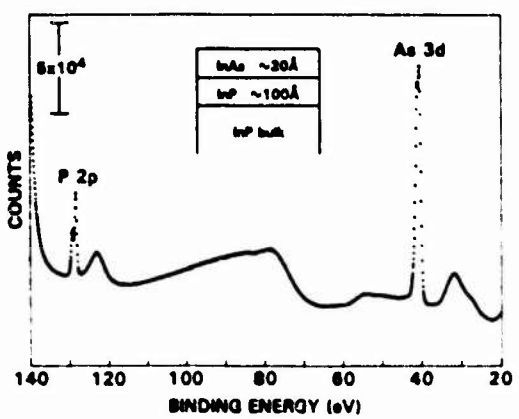

FIG. 1. XPS binding energy spectrum of an InAs/InP(100) sample in the region of the P2p and As3d core levels. Inset shows the sample structure.

 0003-6951/89/191878-03$01.00 © 1989 American Institute of Physics

TABLE I. XPS measured unstrained valence-band offset ΔE_v values for pseudomorphic GaAs/InP and InAs/InP heterojunction interfaces.

Interface	ΔE_{CL} (eV)	ΔE_v (eV)	t (Å)
InAs/InP(100)	87.84	0.32	42
	87.83	0.31	19
	87.82	0.30	23
GaAs/InP(100)	87.71	0.21	18
	87.67	0.17	27
InP/GaAs(100)	87.71	0.21	22
	87.70	0.20	26

tively, and $\Delta E_{CL} = (E^{InP}_{P\,2p} - E^{InAs}_{As\,3d})$ is the binding energy difference across the interface between the P 2p core level in InP and the As 3d core level in InAs. Hence, by inspection of the band diagram, $\Delta E_v(\text{InAs/InP}) = \Delta E_{CL} + (E^{InAs}_{As\,3d} - E^{InAs}_{v}) - (E^{InP}_{P\,2p} - E^{InP}_{v})$. The $(E_{CL} - E_v)$ terms are core level to valence-band maximum binding energy differences which are obtained by separate XPS measurements on pure unstrained bulk material. Thus, of the three quantities used to measure ΔE_v by XPS only ΔE_{CL} pertains to the heterojunction. Similarly, $\Delta E_v(\text{GaAs/InP}) = \Delta E_{CL} + (E^{GaAs}_{As\,3d} - E^{GaAs}_{v}) - (E^{InP}_{P\,2p} - E^{InP}_{v})$, where $\Delta E_{CL} = (E^{InP}_{P\,2p} - E^{GaAs}_{As\,3d})$. Values of $(E^{GaAs}_{As\,3d} - E^{GaAs}_{v}) = 40.74 \pm 0.03$ eV for GaAs and $(E^{InAs}_{As\,3d} - E^{InAs}_{v}) = 40.72 \pm 0.03$ eV for InAs have been previously measured by XPS.[8] By using the same measurement method,[9] we have found $(E^{InP}_{P\,2p} - E^{InP}_{v}) = 128.24 \pm 0.03$ eV for InP. Substitution of these values into the expressions for ΔE_v gives

$$\Delta E_v(\text{InAs/InP}) = \Delta E_{CL} - 87.52\ \text{eV} \quad (1)$$

and

$$\Delta E_v(\text{GaAs/InP}) = \Delta E_{CL} - 87.50\ \text{eV}. \quad (2)$$

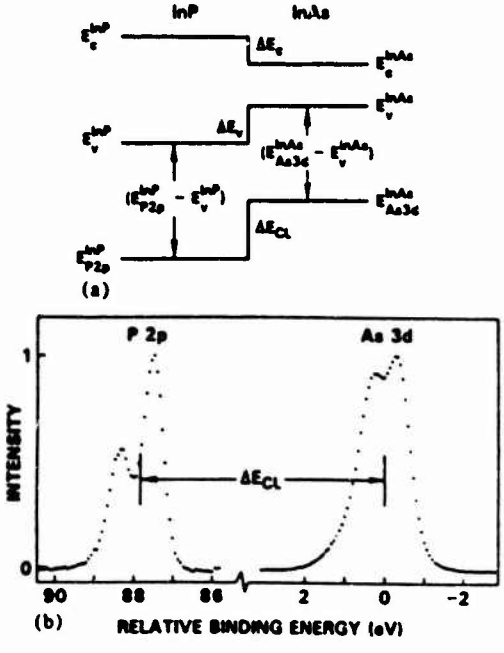

FIG 2. (a) Schematic energy-band diagram of the InAs/InP interface in the absence of strain effects. (b) Measurement of $\Delta E_{CL} = (E^{InP}_{P\,2p} - E^{InAs}_{As\,3d})$ (data from Fig. 1).

The measurement of ΔE_{CL} is illustrated in Fig. 2(b), where the core level peaks from the spectrum in Fig. 1 have been analyzed. A background function has been subtracted from each peak. The peak energy is measured at the half-width point at half-height by using a computerized algorithm in which third-order least-squares fits are made to segments at the sides and top of the peak data. In this example, $\Delta E_{CL} = 87.83$ eV. The estimated measurement uncertainty in ΔE_{CL} is ± 0.02 eV. The ΔE_v measurement uncertainty is ± 0.05 eV because of the uncertainties associated with the $(E_{CL} - E_v)$ values. Table I contains the ΔE_{CL} values measured for all the samples and the corresponding values of ΔE_v obtained from Eqs. (1) and (2) (the $In_xGa_{1-x}As$ valence band lies above that of InP).

The ΔE_v value obtained by using Eqs. (1) and (2) is influenced by strain only through an effect on ΔE_{CL}. We have attempted to experimentally ascertain the possibility of such core level energy shifts owing to strain by comparing ΔE_{CL}(GaAs/InP) and ΔE_{CL}(InP/GaAs). The GaAs/InP interface is subject to tensile hydrostatic and compressive uniaxial strains (possible As 3d shift), while the InP/GaAs interface is subject to compressive hydrostatic and tensile uniaxial strains (possible P 2p shift). Within experimental error ΔE_{CL}(GaAs/InP) and ΔE_{CL}(InP/GaAs) are equal. For these interfaces this result would obtain only if (a) the net strain shift of the As 3d core level binding energy at ~ 41 eV is of identical magnitude and opposite sign as the corresponding strain shift of the P 2p core level at ~ 129 eV, or (b) both shifts are insignificant. We have assumed the latter and use the constancy of ΔE_{CL} with growth direction as evidence of no significant strain effect in relation to the GaAs/InP, InP/GaAs, and InAs/InP ΔE_{CL} measurements (this conclusion is discussed further below). Consequently, we regard the ΔE_v values in Table I as valence-band offsets in the absence of strain.

In Fig. 3, the solid line is the linear interpolation of ΔE_v

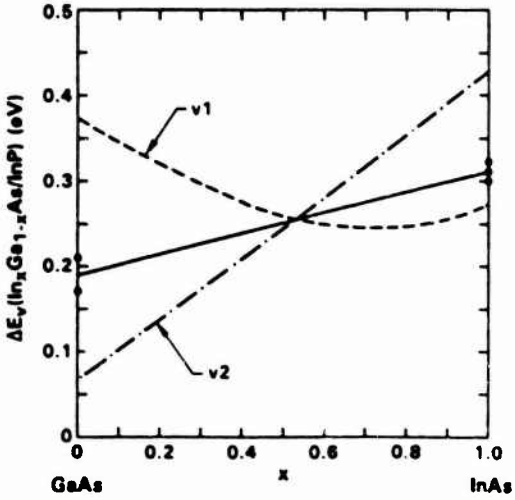

FIG. 3 Linear interpolation of $\Delta E_v(In_xGa_{1-x}As/InP)(100)$ based on the XPS measured unstrained values at $x = 0$ and $x = 1$ (solid line). The $In_xGa_{1-x}As$ strain split valence bands $v1$ (heavy hole) and $v2$ (light hole) are calculated for perfect pseudomorphic growth of a thin overlayer on InP. ΔE_v for the lattice-matched $x = 0.53$ interface is 0.25 eV ($\Delta E_{v1}/\Delta E_{v2} = 58/42$).

($In_xGa_{1-x}As/InP$) vs x based on the average XPS measured unstrained ΔE_v values at the end points: $\Delta E_v(GaAs/InP)_{avg} = 0.19$ eV and $\Delta E_v(InAs/InP)_{avg} = 0.31$ eV. Also, because the ΔE_v range between $x = 0$ and $x = 1$ is rather small, 0.12 eV, a departure from linearity can be expected to be small in magnitude. We thus find that the lattice-matched $x = 0.53$ interface has $\Delta E_v(In_{0.53}Ga_{0.47}As/InP) = 0.25$ eV, or $\Delta E_c/\Delta E_v = 58/42$. Our result is in fair accord with the $x = 0.53$ measurements, based on optical techniques, of Brunemeier *et al.*[3] where $\Delta E_c/\Delta E_v \cong 65/35$ was found and of Temkin *et al.*[4] where $\Delta E_c/\Delta E_v > 50/50$ was found. From Table I it is seen that $\Delta E_v(InP/GaAs)_{avg} = 0.21$ eV; thus, there is no ΔE_v growth sequence dependence at the GaAs/InP(100) interface.

The effect of the strain contribution to ΔE_v at $In_xGa_{1-x}As/InP$ interfaces owing to lattice mismatch can be accounted for by use of deformation potential models. Calculations for the strained Si/Ge(100) interface indicate that the average energy of the three highest energy valence bands at Γ is relatively insensitive to hydrostatic (volume change related) strain.[10] Also, the experimental and theoretical valence-band hydrostatic deformation potential a_v values for GaAs range from about -1.6 to $+0.7$ eV.[11,12] A value of $|a_v| = 1$ eV would shift the GaAs valence bands by 0.04 eV at a pseudomorphic GaAs/InP(100) interface. Because there is uncertainty as to the sign of the $a_v(GaAs)$, and because the calculated $a_v(InAs)$ is less than $a_v(GaAs)$,[11] we will ignore any hydrostatic strain contribution to ΔE_v. We also note that a_v is typically an order of magnitude smaller than the conduction-band deformation potential a_c.[11,12] This relationship suggests that the hydrostatic deformation potential for core levels should also be small, which suggests that the effect of strain on the XPS measured core level binding energy should be negligible compared to experimental uncertainty. A refined model for core level hydrostatic strain shifts may possibly produce corrections for XPS ΔE_{CL} energies at lattice-mismatched interfaces that would yield more accurate strain-free values. For the interfaces considered here, however, the growth sequence ΔE_{CL} equivalence at GaAs/InP interfaces shows that any substantial correction to the As 3*d* core level at the GaAs/InP interface (GaAs in tension) would be essentially equal and opposite to that for the As 3*d* core level at the InAs/InP interface (InAs in compression). Because the interpolated ΔE_v value for the lattice-matched $In_{0.53}Ga_{0.47}As/InP$ interface is very near $x = 0.5$, such equal and opposite corrections at $x = 0$ and $x = 1$ would not significantly affect the ΔE_v value obtained from our present interpolation.

The effect of uniaxial strain on valence-band energies is marked. We have calculated the uniaxial strain induced splitting of the upper two valence bands $v1$ (heavy hole) and $v2$ (light hole) at Γ for pseudomorphic $In_xGa_{1-x}As/InP$ interfaces by using the approach in Refs. 10 and 13. It was assumed that the $In_xGa_{1-x}As$ layer was strained to match the InP lattice constant. The spin orbit splitting constants needed were from Ref. 14. Other materials constants for GaAs and InAs were from the tabulation in Ref. 15; a linear interpolation was used to obtain values for $In_xGa_{1-x}As$. The calculation results are plotted in Fig. 3 (a similar calculation that used slightly different parameter values with essentially identical results was recently reported[16]).

In summary, XPS has been used to measure values of the unstrained valence-band offsets at InAs/InP, GaAs/InP, and InP/GaAs heterojunction interfaces. A linear interpolation between the $\Delta E_v(GaAs/InP) = 0.19$ eV and $\Delta E_v(InAs/InP) = 0.31$ eV results gives $\Delta E_v(In_{0.53}Ga_{0.47}As/InP) = 0.25$ eV.

The authors thank Professor W. Harrison for helpful discussions. This work was supported by the Office of Naval Research contract No. N00014-85-C-0135.

[1] S. R. Forrest and O. K. Kim, J. Appl. Phys. **52**, 5838 (1981).
[2] Y. Guldner, J. P. Vieren, P. Voisin, M. Voos, M. Razeghi, and M. A. Poisson, Appl. Phys. Lett. **40**, 877 (1982).
[3] P. E. Brunemeier, D. G. Deppe, and N. Holonyak, Jr., Appl. Phys. Lett. **46**, 755 (1985).
[4] H. Temkin, M. B. Panish, P. M. Petroff, R. A. Hamm, J. M. Vandenberg, and S. Sumski, Appl. Phys. Lett. **47**, 394 (1985).
[5] K. Steiner, R. Schmitt, R. Zuleeg, L. M. F. Kaufmann, and K. Heime, Surf. Sci. **174**, 331 (1986).
[6] M. S. Skolnick, P. R. Tapster, S. J. Bass, A. D. Pitt, N. Apsley, and S. P. Aldred, Semicond. Sci. Technol. **1**, 29 (1986).
[7] D. V. Lang, M. B. Panish, F. Capasso, J. Allam, R. A. Hamm, A. M. Sergent, and W. T. Tsang, Appl. Phys. Lett. **50**, 736 (1987).
[8] J. R. Waldrop, R. W. Grant, and E. A. Kraut, J. Vac. Sci. Technol. B **5**, 1209 (1987), and references therein.
[9] E. A. Kraut, R. W. Grant, J. R. Waldrop, and S. P. Kowalczyk, Phys. Rev. B **28**, 1965 (1983).
[10] C. G. Van de Walle and R. M. Martin, Phys. Rev. B **34**, 5621 (1986).
[11] M. Cardona and N. E. Christensen, Phys. Rev. B **35**, 6182 (1987).
[12] D. D. Nolte, W. Walukiewicz, and E. E. Haller, Phys. Rev. Lett. **59**, 501 (1987).
[13] F. H. Pollak and M. Cardona, Phys. Rev. **172**, 816 (1968).
[14] O. Berolo and J. C. Woolley, in *Proceedings of the 11th International Conference on the Physics of Semiconductors, Warsaw 1972* (Elsevier, New York, 1972), p. 1420.
[15] S. Adachi, J. Appl. Phys. **53**, 8775 (1982).
[16] R. People, Appl. Phys. Lett. **50**, 1604 (1987).

Relative core level deformation potentials in strained layer heterojunctions

R. W. Grant, J. R. Waldrop, E. A. Kraut, and W. A. Harrison[a)]
Rockwell International Science Center, Thousand Oaks, California 91360

(Received 31 January 1990; accepted 28 March 1990)

Accurate determination of the valence-band discontinuity (ΔE_v) at a pseudomorphic heterojunction interface from x-ray photoemission spectroscopy (XPS) core level measurements requires knowledge of hydrostatic core level to valence-band centroid binding energy shifts. These shifts can be calculated theoretically. Experiments are reported which measure relative core level deformation potentials in strained layer heterojunctions to test the accuracy of the calculated binding energy shifts. The measurements and calculations are not in good agreement; caution is suggested in deriving ΔE_v at pseudomorphic heterojunction interfaces by combining calculated deformation potentials with XPS data until this discrepancy is resolved.

I. INTRODUCTION

The use of pseudomorphic semiconductor layers in device structures has attracted much recent interest because the designer is offered an important new parameter (strain) with which to alter material electronic properties. Among the properties affected by strain are the heterojunction band discontinuities. The x-ray photoemission spectroscopy (XPS) technique for measuring band discontinuities[1] has been used successfully for lattice-matched heterojunctions. This technique relies on accurate knowledge of core level (E_{CL}) to valence-band maximum (E_v) binding energy (E_B) differences in the two semiconductors that form the heterojunction. The extension of XPS methods to measure band discontinuities at pseudomorphic heterojunction interfaces is a nontrivial task as has been recently emphasized.[2] One must either experimentally determine $E_{CL} - E_v$ binding energy differences for the strained semiconductor[3] or calculate the effect of strain on measured $E_{CL} - E_v$ values in unstrained materials. The limiting factor of the latter approach is the accuracy with which $E_{CL} - E_v$ binding energy differences can be calculated. We report results for two different types of relative core level deformation potential experiments in strained Ge and GaAs layers that test this accuracy. In one type of experiment the relative shifts between core level binding energies within a given atom are measured (intra-atomic shift); the second type of experiment measures relative core level E_B shifts in two elementally distinct atoms (interatomic shift). The comparison between experimental and theoretical results suggests that important issues involving hydrostatic effects remain to be resolved before calculated $E_{CL} - E_v$ values can be combined with XPS core level measurements for high accuracy band discontinuity measurements in strained layer heterojunctions.

II. EXPERIMENTAL

A. XPS measurement of ΔE_v

Figure 1 briefly summarizes the use of XPS to measure a heterojunction valence-band discontinuity (ΔE_v). The E_B is defined as zero at the Fermi energy (E_F). Semiconductors A and B are assumed to be unstrained and semiconductor B is thin enough (~ 20 Å) so that photoelectrons from core levels in both semiconductors (E^A_{CL} and E^B_{CL}) can be observed in the XPS spectrum of the heterojunction. If the ($E_{CL} - E_v$) binding energy differences have been determined for both bulk semiconductors,[4] a measurement of the core level E_B difference $\Delta E_{CL} = E^B_{CL} - E^A_{CL}$ can be used to determine $\Delta E_v = (E^B_{CL} - E^B_v) - (E^A_{CL} - E^A_v) - \Delta E_{CL}$.

If semiconductor B is strained so as to form a pseudomorphic layer (B′) on semiconductor A, the schematic energy level diagram is assumed to be modified as shown on the right of Fig. 1. For a thin pseudomorphic layer of semiconductor B′ on substrate A it is usually assumed that all the strain is accommodated in B′ and the volume change ($\Delta V/V$) in B′ is predicted by elasticity theory. On a low index heterojunction plane, the strain can be decomposed into a hydrostatic component and a volume-conserving uniaxial shear component. The uniaxial component removes the E_v degeneracy (calculations reported in Ref. 2 suggest that similar effects on the core level can be ignored) as shown schematically by the dotted lines in Fig. 1. The uniaxial deformation potentials associated with this splitting are well known experimentally for most common semiconductors.

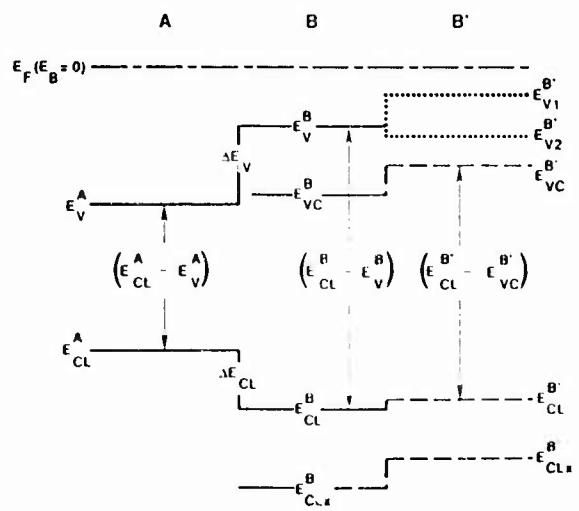

FIG. 1. Schematic energy band diagram that illustrates the use of XPS for band offset measurements at a lattice matched heterojunction B/A and the assumed effect of strain on energy levels if semiconductor B is a pseudomorphic layer B′.

 0734-211X/90/040736-05$01.00 © 1990 American Vacuum Society

The uniaxial strain component removes the valence-band degeneracy but does not shift the centroid of the upper three valence bands.[5] In Fig. 1 this valence-band centroid energy is labeled E_{vc} (the third spin-orbit split off valence band (E_{v3}) is not shown in the figure for simplicity). Only hydrostatic (volume change) strain shifts the ($E_{CL} - E_{vc}$) as noted schematically by the dashed line in Fig. 1. The ΔE_v for a pseudomorphic heterojunction is therefore determined by both uniaxial and hydrostatic contributions. Although valence-band shifts and splitting due to uniaxial strain can be quite large, uniaxial valence-band deformation potentials are generally available and the associated energy variations can be calculated with reasonable certainty. The key to interpreting XPS core level E_B measurements on strained layer heterojunctions to obtain ΔE_v is thus accurate knowledge of hydrostatic ($E_{CL} - E_{vc}$) deformation potentials and consequently uniaxial strain effects will not be considered further here.

The first reported calculation of ($E_{CL} - E_{vc}$) deformation potentials was performed by using a self-consistent linear combination of muffin-tin orbitals (LMTO) method and the local density approximation (LDA).[2] Results for Si and Ge suggest substantial effects (0.1–0.2 eV) with the possibility that core levels may have different hydrostatic deformation potentials that depend on orbital character and binding energy. The shift of a core level is given by a deformation potential multiplied by $\Delta V/V$. If two core levels have different deformation potentials, the difference in these deformation potentials is the relative core level E_B deformation potential which when multiplied by $\Delta V/V$ can be measured as an E_B difference between the two core levels in a strained and unstrained layer. In Sec. III, experiments are described that measure 3*d*, 3*p*, and 3*s* intra-atomic relative core level E_B deformation potentials in strained Ge and As3*d*–Ga3*d* interatomic relative core level E_B deformation potentials in strained GaAs. These measurements should provide useful tests of the theoretically calculated ($E_{CL} - E_{vc}$) deformation potentials which as noted above are a key to determining ΔE_v at pseudomorphic heterojunction interfaces.

B. Sample preparation and analysis

Three strained layer samples were prepared for the relative core level deformation potential measurements. These samples were Ge grown epitaxially on InAs (110) [Ge/InAs (110)], Ge/GaP (100) and GaAs/InAs (110). The strained layers were thin enough to permit estimation of overlayer thickness by attenuation of substrate photoelectron peak intensities and to minimize layer relaxation due to dislocation formation. X-ray diffraction was used to confirm that all substrate materials were aligned within 1.25° of the specified orientation.

Bulk InAs, GaP, and GaAs substrate material was etched in 3:1:1 H_2SO_4:H_2O_2:H_2O solution, quenched in H_2O, dried with N_2, mounted on a Mo platen with In, and immediately put into the XPS ultrahigh vacuum (10^{-10} Torr range base pressure) sample preparation chamber. The thin (< 10 Å) native oxide surface layer was removed from the substrate by momentary heating. InAs and GaAs were heated in $\sim 5\times10^{-6}$ Torr As_4 at ~500 and 575 °C, respectively; the GaP was heated in vacuum to ~570 °C. A Ge(110) surface was also studied. This sample was etched in 3:5:3 HF:HNO_3: acetic acid, dipped in HF, dried with N_2, and mounted as described above. The Ge (110) surface was cleaned by sputtering with 2 keV Ar^+ while annealing at ~630 °C.

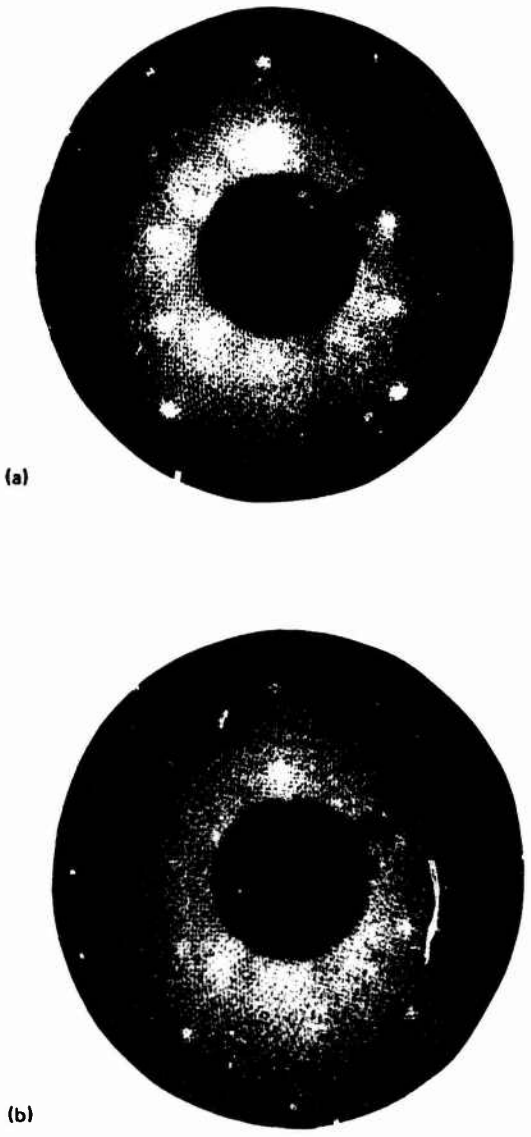

FIG. 2. LEED pictures for (a) InAs (110), 97 eV, and (b) Ge/InAs (110), 100 eV.

The epitaxial layers were grown at 0.1–0.2 Å/s. Epitaxial Ge on InAs and GaP was grown at ~325 and 430 °C, respectively. The GaAs/InAs sample was prepared at ~475 °C growth temperature in a 5×10^{-6} Torr overpressure of As_4. The Ge and Ga sources were W wire baskets while the As_4 source was a small quartz oven filled with elemental As.

The pseudomorphic nature of the epitaxial layer was measured by low-energy electron diffraction (LEED) with a Princeton Research Instruments Model RVL 6-120 LEED system. Knowledge of the strained condition of the thin overlayers is critical for the interpretation of the relative core level deformation potential measurements. Examples of LEED measurements on an InAs (110) substrate and Ge/InAs (110) strained layer are shown in Fig. 2. It is estimated from the diffraction spot size that the accuracy to

TABLE I. Layer thickness, in-plane lattice constant, linewidths, and core level binding energy differences for Ge layers.

Sample	t (Å)	$a_{\parallel}$ (Å)	Γ(Ge3d) (eV)[b]	Γ(Ge3$p_{3/2}$) (eV)[b]	Γ(Ge3s) (eV)[b]	$E_{3s}^{Ge} - E_{3d}^{Ge}$ (eV)[b]	$E_{3s}^{Ge} - E_{3p_{3/2}}^{Ge}$ (eV)[b]
Ge/InAs (110)	20	6.06	1.28	2.58	2.46	151.82	59.67
Ge/GaP (100)	25	5.52	1.25	2.59	2.41	151.81	59.64
Ge (110) (Bulk)	···	5.66[a]	1.22	2.53	2.41	151.84	59.66

[a] Literature value.
[b] Uncertainly ± 0.02 eV.

which the overlayer in-plane lattice constant ($a_{\parallel}$) could be determined was <0.1 Å.

The XPS system used for the core-level E_B measurements was a HP5950 electron spectrometer which has a monochromatic Al $K\alpha$ x-ray source (1486.6 eV). The effective photoelectron escape depth for the photoelectron kinetic energies analyzed and the emission angle of the experiment is ~16 Å. To determine core level peak positions from the room temperature XPS data, a background function that is proportional to the integrated peak intensity was subtracted from each peak. In those cases (Ge/InAs, GaAs/InAs) where weak substrate peaks overlapped the strained overlayer peaks, a reference substrate spectrum (normalized to a substrate peak intensity) was first subtracted from the data to remove the substrate contribution. To analyze the Ge3$p_{3/2}$ peak position, the spin-orbit split Ge3$p_{1/2}$ peak intensity was removed by a subtraction procedure[6] following the background subtraction. All peak binding energies were measured at the half-width point of the half height.

III. RESULTS

A. Strained Ge overlayers

Two strained Ge overlayers were analyzed to measure the intra-atomic relative Ge3d, Ge3$p_{3/2}$, and Ge3s core level deformation potentials by comparing the differences in 3s-3d, 3s-3$p_{3/2}$, and 3$p_{3/2}$-3d binding energies present in the strained layer and the bulk Ge (110) sample. Referring to Fig. 1, this difference in core level binding energies between strained and unstrained material is $(E_{CL,x}^{B'} - E_{CL}^{B'}) - (E_{CL,x}^{B} - E_{CL}^{B})$. A fully strained Ge/InAs (110) sample would have a predicted $\Delta V/V$ of +0.12 based on elasticity theory while a Ge/GaP (110) layer would have $\Delta V/V = -0.05$. The in-plane lattice constants of these strained layers as determined by LEED are given in Table I; to within experimental error the Ge layers appear to be fully strained. The Ge overlayer thicknesses are also listed.

Figure 3 shows XPS spectra of the Ge/InAs (110) experiment. From top the bottom the spectra are: (a) bulk InAs (110), (b) the Ge/InAs (110) sample, (c) spectrum (b) after subtraction of a normalized InAs spectrum (a), and (d) bulk Ge (110). As an example of the data analysis described in Sec. II. B, the 3s, 3$p_{3/2}$, and 3d peaks in spectrum d are shown on expanded energy scales in Fig. 4. The peak widths (Γ) and E_B differences $[(E_{3s}^{Ge} - E_{3d}^{Ge}), (E_{3s}^{Ge} - E_{3p_{3/2}}^{Ge})]$ for both Ge/InAs (110) and Ge (110) are given in Table I.

Figure 5(a) shows XPS data for the Ge/GaP (100) sample. Following data analysis the peaks corresponding to those shown in Fig. 4 are presented in Fig. 5(b). The results of this data analysis are also given in Table I.

The results shown in Table I indicate that to within experimental error there is no significant dependence of intra-atomic relative core level E_B deformation potentials on either orbital character or relative binding energy at least for the 3s, 3$p_{3/2}$, and 3d core levels of Ge studied here. Although

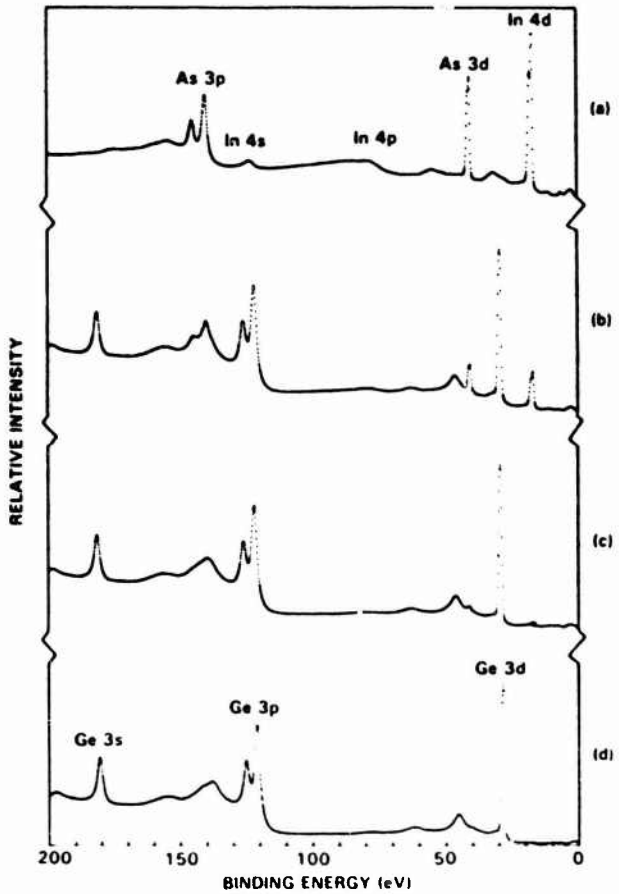

FIG. 3. XPS spectra of (a) InAs (110), (b) Ge/InAs (110), (c) spectrum b after subtraction of normalized InAs (110) substrate spectrum and (d) Ge (110).

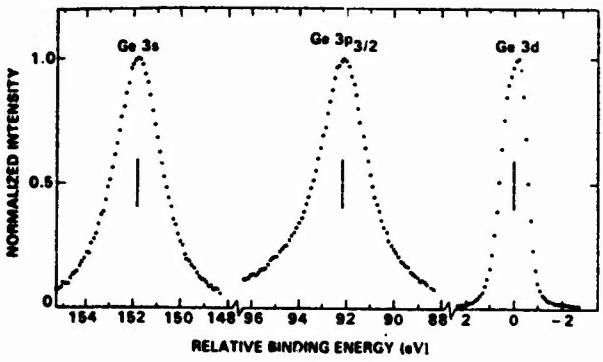

FIG. 4. XPS spectra of Ge3*d*, Ge$3p_{3/2}$, and Ge3*s* peaks in spectrum 3c after background and Ge$3p_{1/2}$ peak subtraction.

the core level line widths appear to be slightly broader (0.06 eV maximum) for the strained layers, this additional width is not sufficient to mask effects of 0.1 eV or more.

B. Strained GaAs overlayer

A strained layer of GaAs on InAs (110) was also analyzed to determine interatomic relative core level deformation potentials in a binary compound. The purpose of this experiment was to measure core level differences between two elementally different atoms in a condition of equal strain, in contrast to the experiments discussed in Sec. III. A. Figure 6 shows XPS spectra for the GaAs/InAs (110) experiment. The spectra from top to bottom are: (a) bulk InAs (110), (b) the GaAs/InAs (110) sample, (c) spectrum b after subtraction of a normalized InAs spectrum in (a), and (d) bulk GaAs (110).

To obtain peak positions and line widths of the spectra in

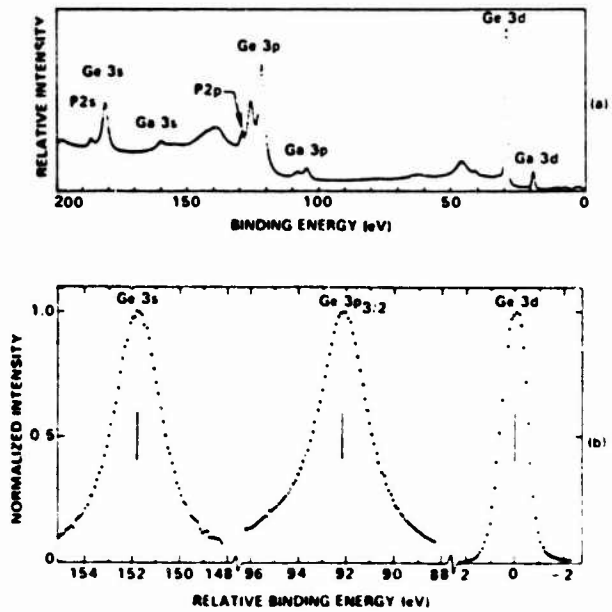

FIG. 5. XPS spectra of (a) Ge/GaP (100) and (b) the Ge3*d*, Ge$3p_{3/2}$, and Ge3*s* peaks in spectrum 5a after background and Ge$3p_{1/2}$ peak subtraction.

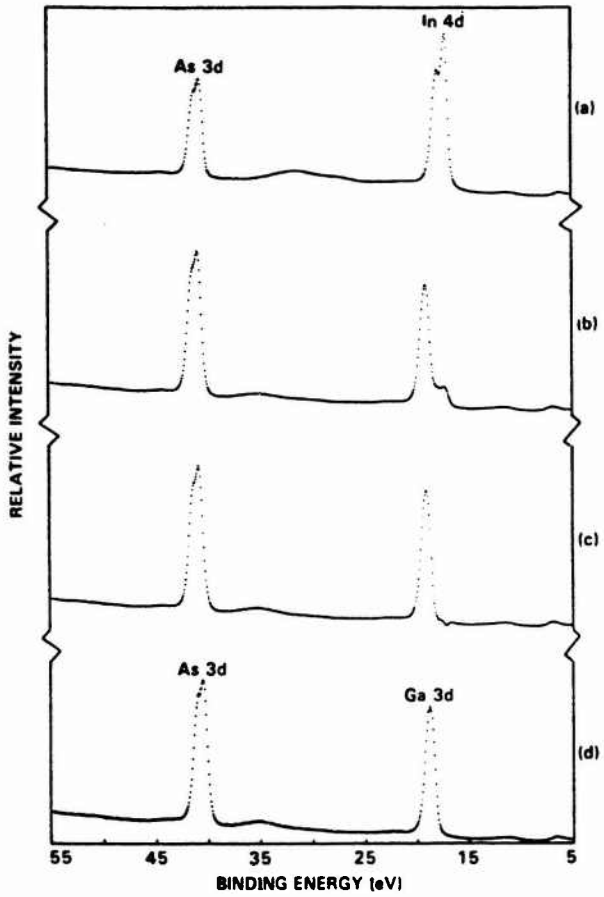

FIG. 6. XPS spectra of (a) InAs (110), (b) GaAs/InAs (110), (c) spectrum b after subtraction of normalized InAs (110) substrate spectrum and (d) GaAs (110).

Figs. 6(c) and 6(d), the data were analyzed as before. The E_B results along with the measured GaAs layer thickness and in-plane lattice constant are given in Table II. To within experimental error the GaAs layer appears to be fully strained. An ideally strained GaAs/InAs (110) sample would have a predicted $\Delta V/V$ of $+0.11$ based on elasticity theory.

The results shown in Table II indicate that interatomic relative core level E_B deformation potentials for Ga3*d* and As3*d* core levels in a strained GaAs (110) layer are equal to within experimental error; the observed linewidths are also equal.

IV. DISCUSSION

Two types of relative core level deformation potential measurements have been performed: one to measure shifts between core level binding energies in a given atom, the other to measure shifts between core level binding energies in different atoms. In both cases no relative core level E_B shifts were observed to within experimental error.

Christensen[7] has found from self-consistent LMTO/LDA calculations that the shifts with volume of all core term values within a given atom (e.g., the Ga2*s*, 3*s*, and 3*d* levels) are very nearly the same. This is in agreement with the strained Ge layer results if all core term values and bind-

TABLE II. Layer thickness, in-plane lattice constant, line widths, and core level binding energy differences for GaAs layers.

Sample	t (Å)	$a_{\parallel}$ (Å)	Γ(As3d) (eV)[b]	Γ(Ga3d) (eV)[b]	$E^{GaAs}_{As3d} - E^{GaAs}_{Ga3d}$ (eV)[b]
GaAs/InAs (110)	25	6.17	1.36	1.02	21.94
GaAs (110) (Bulk)	···	5.65[a]	1.37	1.05	21.95

[a] Literature value.
[b] Uncertainty ± 0.02 eV.

ing energies are assumed to shift equally. We have also estimated the shift of core levels due to the formation of core bands by using a technique developed by Straub and Harrison.[8] These shifts depended only on eigenvalue and atomic volume and were largest for the shallowest eigenvalue. For the Ge3d level the atomic term value is $\epsilon_{3d} = -44.63$ eV[9] (electronic relaxation effects [10] shift the absolute value of the core level binding energy significantly but we assume that these shifts are constant for all core levels on a single atom in agreement with our experiment.) The shift of the Ge3d core level is given by [Eqs. (24) and (25) of Ref. 8] $\delta\epsilon_{3d} = (32/3)(-\epsilon_{3d})(\mu r_0)^5 \exp(-4\mu r_0)$ where μ is obtained from $\epsilon_{3d} = -\hbar^2\mu^2/2m$ and r_0 is the atomic sphere radius. The shift with volume is obtained by taking the derivative of $\delta\epsilon_{3d}$ with respect to r_0 to give $(V\partial\delta\epsilon_{3d})/\partial V = (5-4\mu r_0)\,\delta\epsilon_{3d}/3 = -0.93\times10^{-3}$ eV which is negligible. These estimates, theoretical calculations,[7,11] and our experiments argue that intra-atomic relative core level shifts on a single atom are negligible.

In contrast to the small relative core term value shifts with volume within a given atom, LMTO calculations by Christensen[7] indicate rather large relative shifts of cation and anion core term values for binary compounds. In particular, he finds the volume derivative for the Ga3d-As3d term value difference in GaAs to be $V\partial[\epsilon_{3d}(\mathrm{Ga}) - \epsilon_{3d}(\mathrm{As})]/\partial V = 1.8$ eV. Such large shifts are not surprising. One might expect for example, changes in the charge transfer between atoms to produce relative shifts in the electrostatic potential at the two nuclei. For the strained GaAs/InAs (110) experiment reported in Sec. III. B with $\Delta V/V = +0.11$, an increase in core level E_B splitting of $1.8\times0.11 = 0.2$ eV would be predicted from Christensen's calculations. Such a large increase is clearly not observed in the experimental data (Table II). The origin of this discrepancy is unclear. One possibility is that despite the LEED measurements, the GaAs/InAs (110) sample was not fully strained. Another possibility is that effects beyond the LMTO/density-functional theory have approximately canceled the calculated relative core level deformation potential difference. For example, the magnitude of a volume dependence of electronic relaxation on neighboring atoms[10] is one possibility that needs investigation.

In summary, two types of experiments have been devised to compare calculated relative core term value deformation potentials with measured relative core level E_B deformation potentials. The experimental approach is quite general and could be applied to a wide variety of material systems. In one type of experiment the intra-atomic relative core level deformation potentials for core levels within a given atom were determined. No measurable relative core level binding energy shifts with strain were observed consistent with theoretical core term value calculations. In a second type of experiment, interatomic relative core level deformation potentials were measured for Ga3d and As3d core levels in a strained GaAs layer. The initial comparison between calculation and measurement in this case is not in good agreement. Until this discrepancy is resolved, caution is suggested when deriving band discontinuities by combining calculated deformation potentials with XPS data on strained layer heterojunctions.

ACKNOWLEDGMENTS

We greatly appreciate the x-ray diffraction analyses performed by M. D. Lind. This work was partially supported by ONR Contract No. N00014-85-C-0135.

[a] Permanent address, Stanford University, Stanford, CA 94305.

[1] R. W. Grant, J. R. Waldrop, and E. A. Kraut, Phys. Rev. Lett. **40**, 656 (1978); J. Vac. Sci. Technol. **15**, 1451 (1978).
[2] G. P. Schwartz, M. S. Hybertsen, J. Beuk, R. G. Nuzzo, J. P. Mannaerts, and G. J. Gualtieri, Phys. Rev. B **39**, 1235 (1989).
[3] E. T. Yu, E. T. Croke, T. C. McGill, and R. H. Miles, Appl. Phys. Lett. **56**, 569 (1990).
[4] E. A. Kraut, R. W. Grant, J. R. Waldrop, and S. P. Kowalczyk, Phys. Rev. B **28**, 1965 (1983).
[5] F. H. Pollak and M. Cardona, Phys. Rev. **172**, 816 (1968).
[6] K. D. Bringans, M. A. Olmstead, R. I. G. Uhrberg, and R. Z. Bachrach, Phys. Rev. B **36**, 9569 (1987).
[7] N. E. Christensen (private communication).
[8] G. K. Straub and W. A. Harrison, Phys. Rev. B **31**, 7668 (1985).
[9] J. B. Mann, Atomic Structure Calculations, I. Hartree-Fock Energy Results for Elements Hydrogen to Lawrencium, Distributed by Clearing House for Technical Information, Springfield, VA 22151.
[10] See e.g., D. A. Shirley, in *Photoemission in Solids I, Topics in Applied Physics*, edited by M. Cardona and L. Ley (Springer, New York, 1978), Vol. 26, p. 165.
[11] J. E. Bernard and A. Zunger, Phys. Rev. B **36**, 3199 (1987).

Measurement of AlAs/InP and InP/$In_{0.52}Al_{0.48}As$ heterojunction band offsets by x-ray photoemission spectroscopy

J. R. Waldrop, E. A. Kraut, C. W. Farley, and R. W. Grant
Rockwell International Science Center, Thousand Oaks, California 91360

(Received 30 January 1990; accepted 18 April 1990)

X-ray photoemission spectroscopy (XPS) has been used to measure the valence band offsets at the $x = 0$ and $x = 0.52$ points of the $In_xAl_{1-x}As$/InP(100) heterojunction system. For the lattice-matched interface we determine a value of $\Delta E_v(InP/In_{0.52}Al_{0.48}As) = 0.16$ eV (staggered band alignment). Although the pseudomorphic AlAs/InP(100) interface investigated is strained, the $\Delta E_v(AlAs/InP) = -0.27$ eV (nested band alignment) value obtained by the XPS analysis method used is interpreted as being characteristic of an unstrained interface.

I. INTRODUCTION

The $In_xAl_{1-x}As$/InP heterojunction system is of interest for possible device applications.[1] Accurate knowledge of the valence and conduction band offsets at the interface is required for device design and modeling. Two experimental measurements for the $x = 0.52$ lattice-matched interface are available, each of which used an optical method, that report a staggered band alignment where the InP valence band lies below the $In_{0.52}Al_{0.48}As$ valence band by 0.40 or 0.29 eV,[2,3] respectively.

In this paper we use x-ray photoemission spectroscopy (XPS) to measure ΔE_v at the $x = 0$ and $x = 0.52$ points of the $In_xAl_{1-x}As$/InP(100) system. Two kinds of interfaces were prepared by molecular beam epitaxy (MBE) within the XPS system: AlAs/InP (thin pseudomorphic AlAs layer grown on InP substrate); and InP/$In_{0.52}Al_{0.48}As$ (thin InP layer grown on $In_{0.52}Al_{0.48}As$ substrate). Although the AlAs/InP interface is strained owing to lattice mismatch we have used an XPS data analysis in which the measured ΔE_v is interpreted as being characteristic of an unstrained (relaxed) interface. For the AlAs/InP interface we obtain an unstrained ΔE_v of -0.27 eV (nested band alignment). With the InP/$In_{0.52}Al_{0.48}As$ interface, we measure $\Delta E_v = 0.16$ eV (staggered band alignment).

II. EXPERIMENTAL

A. Sample preparation

The insets in Figs. 1 and 2 show schematically the AlAs/InP and InP/$In_{0.52}Al_{0.48}As$ sample structures. XPS analyzes the interface beneath the thin uppermost layer. All MBE layer growths for the AlAs/InP samples were made within the XPS system. $In_{0.52}Al_{0.48}As$ layers for the InP/$In_{0.52}Al_{0.48}As$ samples were grown on InP substrates in a dedicated MBE system and transferred in air to the XPS system. The surface of the $In_{0.52}Al_{0.48}As$ was protected from oxidation and contamination during the transfer by an elemental arsenic cap; the InP top layer was grown in the XPS system.

Three of the AlAs/InP samples had a ~100 Å InP MBE buffer layer while the other two had AlAs grown directly onto an InP bulk substrate (this difference in sample structure did not cause any apparent variation in the measured ΔE_v). To prepare the bulk substrates, an InP piece is etched in 4:1:1 H_2SO_4:H_2O_2:H_2O solution for ~3 min, quenched in H_2O, dried with N_2, mounted on a Mo plate with In, and immediately placed into the ultrahigh vacuum (10^{-10} Torr range base pressure) XPS sample preparation chamber. The < 10 Å thick native oxide layer is removed from the InP substrate prior to MBE growth by momentary heating at ~450 °C in a ~10^{-5} Torr P_2 overpressure. The As cap was removed from the $In_{0.52}Al_{0.48}As$ substrates to reveal a clean surface by heating at ~450 °C for ~30 s.

The AlAs and InP layers were grown at ~0.5–1 Å/s rates in a ~10^{-5} Torr overpressure of As_4 and P_2, respectively. The As_4 source is a small quartz oven filled with elemental As; the P_2 source is InP wrapped in resistively heated Ta wire; and the Al and In sources are W wire baskets. The thickness t of the top layers (listed in Tables I and II) was measured from the intensity decrease of a substrate XPS core level. Epitaxy of the layers was confirmed by using low-energy electron diffraction (LEED). Analysis of LEED patterns from representative AlAs/InP samples indicated that the AlAs had a lattice constant parallel to the InP substrate consistent with pseudomorphic growth.

Attempts were made to form InP/AlAs samples by grow-

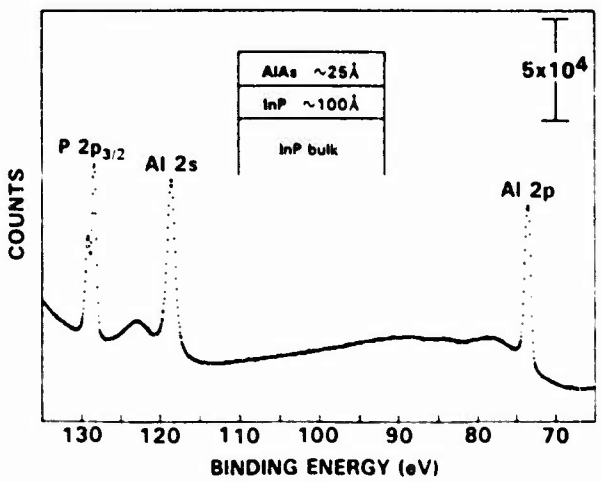

FIG. 1. XPS binding energy spectrum of an AlAs/InP(100) sample in the region of P 2*p* and Al 2*p* core levels. Sample structure shown in inset.

 0734-211X/90/040768-05$01.00 © 1990 American Vacuum Society

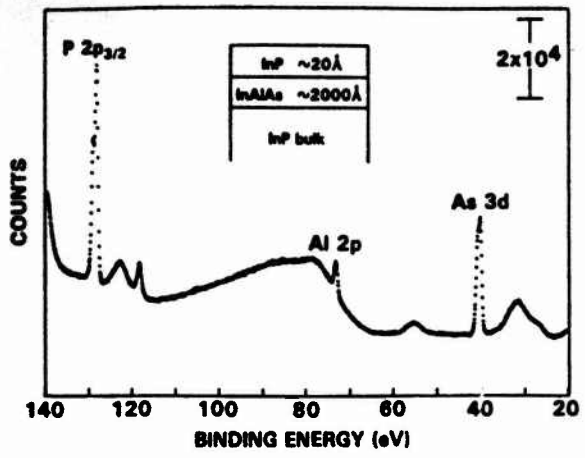

FIG. 2. XPS binding energy spectrum of an InP/$In_{0.52}Al_{0.48}As$(100) sample in the region of the P 2*p* and As 3*d* core levels. Sample structure shown in inset.

ing InP onto a thick AlAs layer (the AlAs was grown on GaAs bulk substrate) under conditions similar to those used for the AlAs/InP samples. A uniform epitaxial thin InP layer could not be achieved because the InP evidently grew as three-dimensional islands.

B. Measurement of ΔE_v

The XPS system is based on a HP5950 angle-resolved electron spectrometer that includes a monochromatic Al $K\alpha$ x-ray source ($h\nu = 1486.6$ eV). The effective photoelectron escape depth λ for the experimental configuration is ~16 Å. Photoelectrons originating from each side of a heterojunction interface that is located on the order of λ from a sample surface will therefore appear in the same XPS binding energy spectrum. Thus, the 65–135 eV XPS spectrum in Fig. 1 for an AlAs/InP sample includes both the Al 2*p* core level peak from the thin top layer and the P 2*p* core level peak from the InP below. Similarly, the 20–140 eV spectrum in Fig. 2 for a InP/$In_{0.52}Al_{0.48}As$ sample contains both a P 2*p* core level peak and an As 3*d* core level peak.

The schematic energy band diagrams of the AlAs/InP (in the absence of strain effects) and the lattice-matched InP/$In_{0.52}Al_{0.48}As$ interfaces are given in Figs. 3(a) and 4(a), respectively, where E_c is a conduction-band minimum, E_v is a valence-band maximum, and ΔE_{CL} is a binding energy difference between two core levels selected from each side of the interface. For these interfaces we use $\Delta E_{CL}(\text{AlAs/InP}) = (E^{\text{InP}}_{\text{P }2p3/2} - E^{\text{AlAs}}_{\text{Al }2p})$ and $\Delta E_{CL}(\text{InP/In}_{0.52}\text{Al}_{0.48}\text{As}) = (E^{\text{InP}}_{\text{P }2p3/2} - E^{\text{InAlAs}}_{\text{As }3d})$ (with $In_{0.52}Al_{0.48}As$ the As 3*d* core level is used in place of the Al 2*p* because the former has greater intensity). Hence, by inspection of the respective band diagrams:

$$\Delta E_v(\text{AlAs/InP}) = \Delta E_{CL}(\text{AlAs/InP}) + (E^{\text{AlAs}}_{\text{Al }2p} - E^{\text{AlAs}}_{v}) - (E^{\text{InP}}_{\text{P }2p3/2} - E^{\text{InP}}_{v}) \quad (1)$$

and

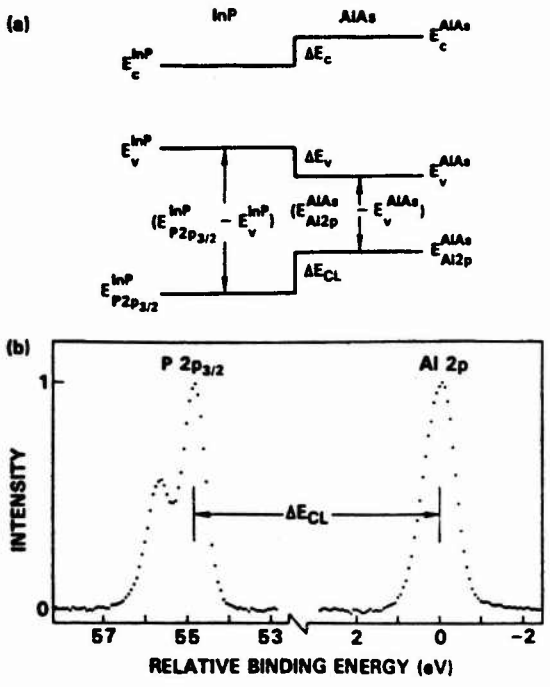

FIG. 3. (a) Schematic energy band diagram of the AlAs/InP interface in the absence of strain effects. (b) Measurement of $\Delta E_{CL}(\text{AlAs/InP}) = (E^{\text{InP}}_{\text{P }2p3/2} - E^{\text{AlAs}}_{\text{Al }2p})$ (data from Fig. 1).

$$\Delta E_v(\text{InP/In}_{0.52}\text{Al}_{0.48}\text{As}) = \Delta E_{CL}(\text{InP/In}_{0.52}\text{Al}_{0.48}\text{As}) + (E^{\text{InAlAs}}_{\text{As }3d} - E^{\text{InAlAs}}_{v}) - (E^{\text{InP}}_{\text{P }2p3/2} - E^{\text{InP}}_{v}). \quad (2)$$

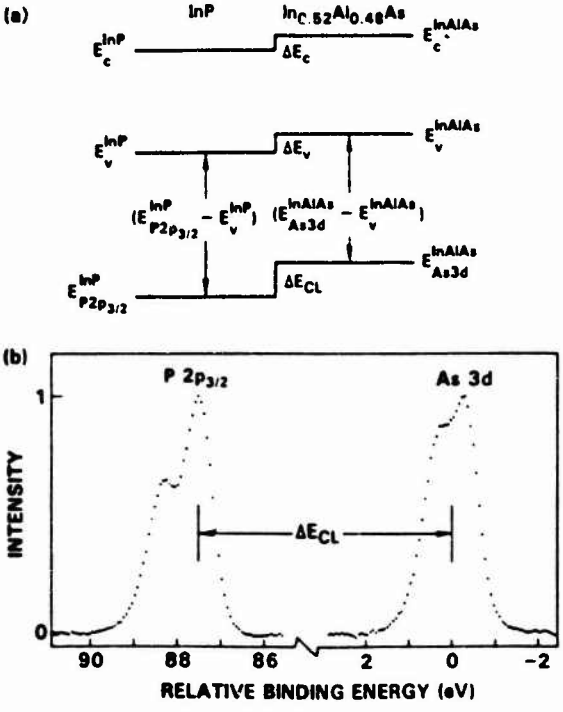

FIG. 4. (a) Schematic energy band diagram of the InP/$In_{0.52}Al_{0.48}As$ interface. (b) Measurement of $\Delta E_{CL}(\text{InP/In}_{0.52}\text{Al}_{0.48}\text{As}) = (E^{\text{InP}}_{\text{P }2p3/2} - E^{\text{InAlAs}}_{\text{As }3d})$ (data from Fig. 2).

We define ΔE_v negative when the InP valence band lies above that of the opposite semiconductor.

The two $(E_{CL} - E_v)$ terms that appear in each ΔE_v expression are core level to valence-band maximum binding energy differences that are obtained by independent XPS measurements on pure unstrained bulk material. Thus, of the three quantities required for the XPS determination of an unstrained ΔE_v only ΔE_{CL} is directly measured for a particular heterojunction.

Values of $(E^{AlAs}_{Al\,2p} - E^{AlAs}_v) = 72.70 \pm 0.04$ eV and $(E^{InP}_{P\,2p3/2} - E^{InP}_v) = 127.74 \pm 0.03$ eV have been measured by XPS for AlAs[4] and InP.[5] The measurement of $(E^{InAlAs}_{As\,3d} - E^{InAlAs}_v) = 40.43 \pm 0.03$ eV for $In_{0.52}Al_{0.48}As$ is described in the next section. Substitution of these material constants into Eqs. (1) and (2) gives

$$\Delta E_v(\text{AlAs/InP}) = \Delta E_{CL}(\text{AlAs/InP}) - 55.04\ \text{eV} \quad (3)$$

and

$$\Delta E_v(\text{InP/In}_{0.52}\text{Al}_{0.48}\text{As}) = \Delta E_{CL}(\text{InP/In}_{0.52}\text{Al}_{0.48}\text{As}) - 87.31\ \text{eV}. \quad (4)$$

Equations (3) and (4) are strictly valid only for unstrained heterojunctions such as $InP/In_{0.52}Al_{0.48}As$ owing to the use of $(E_{CL} - E_v)$ values obtained from unstrained material. Because the AlAs/InP interface is strained, the primary assumption we must make to obtain an unstrained AlAs/InP ΔE_v value is that ΔE_{CL} is independent of strain. Although the $(E_{CL} - E_v)$ values can generally be affected by strain, we emphasize that the unstrained XPS ΔE_v value we obtain for the AlAs/InP interface through use of the unstrained $(E^{InP}_{P\,2p3/2} - E^{InP}_v)$ value departs from the actual strain-free value by an amount determined solely by any strain shift in ΔE_{CL}.

The precision measurement of ΔE_{CL} is illustrated in Figs. 3(b) and 4(b) for the core level peaks in the corresponding AlAs/InP and $InP/In_{0.52}Al_{0.48}As$ spectra in Figs. 1 and 2. With the AlAs/InP data, the Al $2p$ peak is in the energy region of the In $4p$ peak and the P $2p$ peak is near the As $3p$ peak. The latter interference also occurs in the $InP/In_{0.52}Al_{0.48}As$ data in addition to In $4d$ loss peaks near the As $3d$ peak. Normalized reference spectra from clean InP and AlAs were used to subtract such interference from the heterojunction data. Following removal of these interfering peaks, a background function that is proportional to the integrated peak intensity is subtracted from each core level peak. The peak width and height of the Al $2p$ and As $3d$ core levels are found by using a computerized procedure in which a third order polynomial is least-squares fit to segments at the sides and top of the discrete peak data. The peak binding energy is measured at the half-width point at half-height. Because the P $2p_{3/2}$ and P $2p_{1/2}$ components of the P $2p$ peak are nearly resolved we used a nonlinear least-square fit routine in which the peak components are modeled with a Gaussian–Lorentzian product function [defined by Eqs. (1) and (2) of Ref. 6] to find the center of the P $2p_{3/2}$ peak. The uncertainty in the ΔE_{CL} measurement is estimated to be ± 0.02 eV; because of the additional uncertainties of the $(E_{CL} - E_v)$ values the ΔE_v uncertainty associated with Eqs. (3) and (4) is ± 0.05 eV.

C. Measurement of $(E^{InAlAs}_{As\,3d} - E^{InAlAs}_v)$

Figure 5 shows a -5 to 80 eV binding energy spectrum from a clean $In_{0.52}Al_{0.48}As(100)$ surface that includes the valence band. Similar data were acquired from two samples of epitaxial material. The position of E_v was located by using a method described in detail elsewhere.[7] In brief, a theoretical valence band density of state (VBDOS) for the semiconductor, with an energy scale where $E_v = 0$ is exactly defined, is convolved with the experimentally determined XPS spectrometer resolution function. The broadened theoretical VBDOS, where E_v has remained at zero energy, is least-squares fitted to the XPS VBDOS data in the region near E_v. This fitting procedure thus effectively transfers the position of E_v from the theoretical VBDOS to the experimental data. Because a theoretical $In_{0.52}Al_{0.48}As$ VBDOS was unavailable, we tried both an InAs[8] and a GaAs[8] VBDOS (it was previously found that a theoretical GaAs VBDOS gives a good fit to experimental AlAs VBDOS data because the shapes of the XPS valence band data for AlAs and GaAs are similar near E_v).[4] Figure 6 is an example of the good fit obtained between the broadened theoretical GaAs VBDOS and the $In_{0.52}Al_{0.48}As$ XPS valence band data plotted on an energy scale where $E_v = 0$ eV. The fit is over an interval that terminates at an energy E_{max} below E_v ($E_{max} = 1$ eV in Fig. 6).

Figure 7 (upper panel) gives the results of the valence band fitting procedure that used the GaAs VBDOS for the two $In_{0.52}Al_{0.48}As$ samples, where the As $3d$ core level to valence-band energy $(E^{InAlAs}_{As\,3d} - E^{InAlAs}_v)$ is plotted versus E_{max}. The error bars indicate the 95% confidence interval of the fit. A value of $(E^{InAlAs}_{As3d} - E^{InAlAs}_v) = 40.43$ eV is assigned because an uncertainty of ± 0.03 eV includes most of the $(E^{InAlAs}_{As3d} - E^{InAlAs}_v)$ values. Interestingly, this value for $(E^{InAlAs}_{As3d} - E^{InAlAs}_v)$ is, within experimental error, the average of the $(E^{InAs}_{As\,3d} - E^{InAs}_v) = 40.72 \pm 0.03$ eV and $(E^{AlAs}_{As\,3d} - E^{AlAs}_v) = 40.16 \pm 0.04$ eV values previously measured for InAs and AlAs.[4] We also measured $(E^{InAlAs}_{Al\,2p} - E^{InAlAs}_{As\,3d}) = 32.64 \pm 0.01$ eV. The corresponding value of $(E^{InAlAs}_{Al\,2p} - E^{InAlAs}_v)$ is thus 73.07 ± 0.03 eV.

The lower panel of Fig. 7 shows the fit results based on the

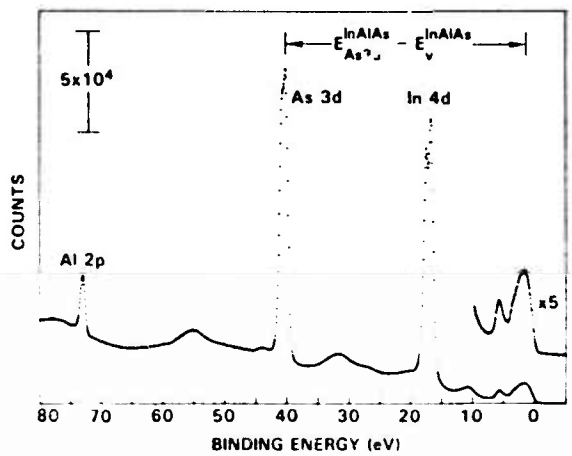

FIG. 5. Representative -5 to 80 eV XPS binding energy spectrum for $In_{0.52}Al_{0.48}As(100)$.

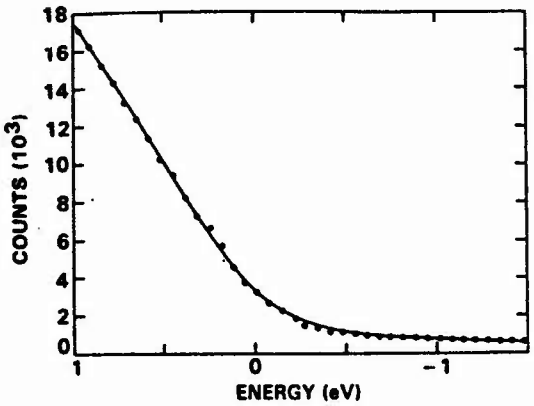

FIG. 6. Fit of the broadened GaAs theoretical valence-band density of states (line) to the $In_{0.52}Al_{0.48}As$ valence band data.

InAs theoretical VBDOS; the error bars are significantly larger than in the upper panel and there is a 0.2 eV increase in $(E^{InAlAs}_{As\,3d} - E^{InAlAs}_{v})$ over the E_{max} range. Thus, the $In_{0.52}Al_{0.48}As$ VBDOS near E_v is very similar in shape to that of AlAs and rather dissimilar to that of InAs.

III. RESULTS AND DISCUSSION

Table I lists the ΔE_{CL} and corresponding unstrained ΔE_v values for the five pseudomorphic AlAs/InP samples. The average ΔE_v(AlAs/InP) value is -0.27 eV. Table II lists the ΔE_{CL} and corresponding ΔE_v values for the three $InP/In_{0.52}Al_{0.48}As$ samples. The average $\Delta E_v(InP/In_{0.52}Al_{0.48}As)$ value is 0.16 eV. Thus, based on the 1.44 eV band gap of $In_{0.52}Al_{0.48}As$,[9] the $InP/In_{0.52}Al_{0.48}As$ band alignment is staggered with $\Delta E_c = 0.25$ eV.

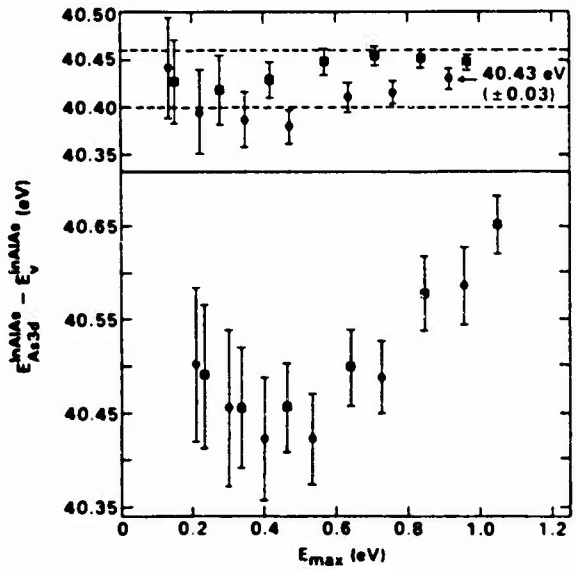

FIG. 7. (upper panel) As 3*d* core level to valence band maximum binding energy difference for two $In_{0.52}Al_{0.48}As(100)$ samples as a function of the end point E_{max} of the fitting interval based on GaAs theoretical valence band density of states. (lower panel) Same as above except based on InAs theoretical valence band density of states.

TABLE I. XPS measured unstrained valence-band offset ΔE_v for the pseudomorphic AlAs/InP(100) heterojunction interface. $\Delta E_{CL} = (E^{InP}_{P\,2p3/2} - E^{AlAs}_{Al\,2p})$. Average ΔE_v(AlAs/InP) = -0.27 eV.

ΔE_{CL} (eV)	ΔE_v (eV)	t (Å)
55.75	−0.29	33
55.76	−0.28	24
55.76	−0.28	42
55.77	−0.27	21
55.81	−0.23	23

As remarked above, strain can affect the unstrained ΔE_v(AlAs/InP) value obtained from Eq. (3) only by causing a shift in ΔE_{CL}(AlAs/InP). The strain in the AlAs/InP samples occurs because the parallel lattice constant of the thin pseudomorphic AlAs layer has expanded to match that of the InP substrate (-3.5% mismatch). This strain has two components: a hydrostatic strain owing to the $\Delta V/V = 0.04$ volume change and a uniaxial strain owing to tetragonal distortion of the AlAs. A recently reported calculation[10] suggested that XPS core level binding energy shifts from uniaxial strain, which in principal may occur, can be ignored when measuring a ΔE_{CL}. Neither theoretical nor experimental absolute hydrostatic core level deformation potentials for semiconductors are presently available. Consequently, we have assumed that the As 3*d* hydrostatic core level deformation potential for AlAs is small, such that ΔE_{CL}(AlAs/InP) is not significantly affected in comparison to the experimental uncertainty by the level of strain in the AlAs/InP interface. The ΔE_v(AlAs/InP) values in Table I are thus considered to be offsets in the absence of strain.

The solid line in Fig. 8 is an interpolation for $\Delta E_v(In_xAl_{1-x}As/InP)$ versus x based on the XPS unstrained ΔE_v values at $x = 0$ and $x = 1$ and the direct measurement at $x = 0.52$. The ΔE_v(InAs/InP) = 0.46 eV value is from previous ΔE_{CL} data[11] in conjunction with a redetermined[5] $(E^{InP}_{P\,2p3/2} - E^{InP}_{v})$ value for InP. The $x = 0.52$ direct measurement of 0.16 eV is, for this heterojunction system, in reasonable agreement with the 0.11 eV $x = 0.52$ value obtained from a linear interpolation between the end points.

We now estimate the strain correction to the $\Delta E_v(In_xAl_{1-x}As/InP)$ interpolation in Fig. 8. The theoretical AlAs valence-band hydrostatic deformation potential a_v values range from -1.2 to $+0.4$ eV.[12] A value of $|a_v| = 1$ eV would shift the energy centroid of the upper three AlAs valence bands by 0.04 eV at a pseudomorphic

TABLE II. XPS measured valence-band ΔE_v for the lattice-matched $InP/In_{0.52}Al_{0.48}As(100)$ heterojunction interface $\Delta E_{CL} = (E^{InP}_{P\,2p3/2} - E^{InAlAs}_{As\,3d})$. Average $\Delta E_v(InP/In_{0.52}Al_{0.48}As) = 0.16$ eV.

ΔE_{CL} (eV)	ΔE_v (eV)	t (Å)
87.47	0.16	21
87.47	0.16	30
87.48	0.17	21

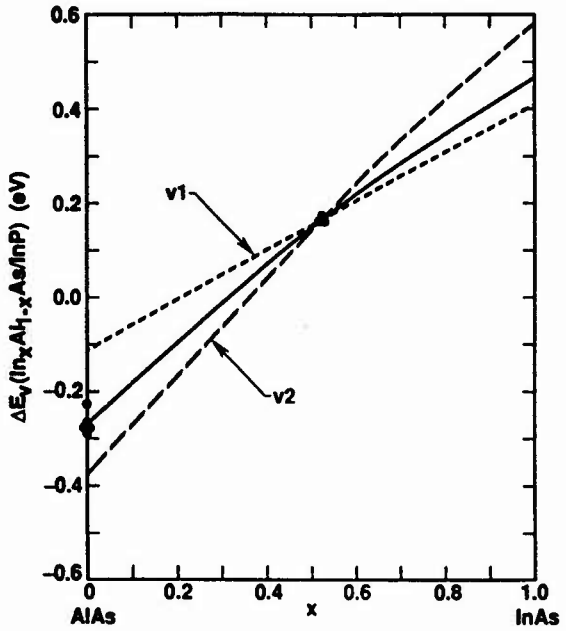

FIG. 8. Interpolation of unstrained $\Delta E_v(In_xAl_{1-x}As/InP)$ based on XPS measured values at $x=0$, $x=0.52$, and $x=1$ (solid line). The $In_xAl_{1-x}As$ strain split $v1$ (heavy hole) and $v2$ (light hole) bands are calculated for perfect pseudomorphic growth of a thin layer on InP. ΔE_v is negative when InP valence band lies above $In_xAl_{1-x}As$ valence band.

AlAs/InP(100) interface. Because a_v(AlAs) is of uncertain sign and because the theoretical a_v(InAs) is smaller than a_v(AlAs), the hydrostatic correction to $\Delta E_v(In_xAl_{1-x}As/InP)$ will be ignored. Uniaxial strain, on the other hand, has a marked effect on valence band energies. We calculated the splitting of the upper two energy bands $v1$ (heavy hole) and $v2$ (light hole) at Γ for thin pseudomorphic $\Delta E_v(In_xAl_{1-x}As/InP)$ interfaces by using the method in Refs. 13 and 14. It was assumed that the $In_xAl_{1-x}As$ parallel lattice constant matched InP. Necessary $In_xAl_{1-x}As$ materials constants were obtained by linear interpolation of the corresponding AlAs and InAs constants.[15,16] The results of the uniaxial strain calculation are plotted in Fig. 8.

In summary, XPS has been used to measure the unstrained ΔE_v at the AlAs/InP(100) interface and the ΔE_v at the lattice-matched $InP/In_{0.52}Al_{0.48}As(100)$ interface. An unstrained ΔE_v value of -0.27 eV is obtained for the AlAs/InP interface (nested band alignment). A value of $\Delta E_v(InP/In_{0.52}Al_{0.48}As) = 0.16$ eV is obtained for the lattice-matched interface (staggered band alignment).

ACKNOWLEDGMENT

This work was supported by the Office of Naval Research under Contract No. N00014-85-C-0135.

[1] C. M. Hanson and H. H. Wieder, J. Vac. Sci. Technol. B 5, 971 (1987).
[2] E. J. Caine, S. Subbanna, H. Kroemer, J. L. Merz, and A. Y. Cho, Appl. Phys. Lett. 45, 1123 (1984).
[3] L. Aina, M. Mattingly, and L. Stecker, Appl. Phys. Lett 53, 1620 (1988).
[4] J. R. Waldrop, R. W. Grant, and E. A. Kraut, J. Vac. Sci. Technol. B 5, 1209 (1987).
[5] J. R. Waldrop, E. A. Kraut, and R. W. Grant (to be published).
[6] I. Kojima and M. Kurahashi, J. Electron Spectrosc. Relat. Phenom. 42, 177 (1987).
[7] E. A. Kraut, R. W. Grant, J. R. Waldrop, and S. P. Kowalczyk, Phys. Rev. B 28, 1965 (1983).
[8] J. R. Chelikowsky and M. L. Cohen, Phys. Rev. B 14, 556 (1976).
[9] D. Oertel, D. Bimberg, R. K. Bauer, and K. W. Carey, Appl. Phys. Lett. 55, 140 (1989).
[10] G. P. Schwartz, M. S. Hybertsen, J. Bevk, R. G. Nuzzo, J. P. Mannaerts, and G. P. Gualtieri, Phys. Rev. B 39, 1235 (1989).
[11] J. R. Waldrop, R. W. Grant, and E. A. Kraut, J. Vac. Sci. Technol. B 7, 815 (1989).
[12] M. Cardona and N. E. Christensen, Phys. Rev. B 35, 6182 (1987).
[13] F. H. Pollak and M. Cardona, Phys. Rev. 172, 816 (1968).
[14] C. G. Van de Walle and R. M. Martin, Phys. Rev. B 34, 5621 (1986).
[15] S. Adachi, J. Appl. Phys. 53, 8775 (1982).
[16] S. Adachi, J. Appl. Phys. 58, R1 (1985).

Formation and Schottky barrier height of metal contacts to β-SiC

J. R. Waldrop and R. W. Grant
Rockwell International Science Center, Thousand Oaks, California 91360

(Received 28 August 1989; accepted for publication 29 November 1989)

Formation of Schottky barrier contacts to *n*-type β-SiC(100) was systematically investigated for several metals with various physical and chemical properties. The metals (Pd, Au, Co, Ti, Ag, Tb, and Al) were deposited onto oxygen terminated ($\sim$1 monolayer) surfaces. Metal/β-SiC interface chemistry and Schottky barrier height ϕ_B during contact formation were obtained by x-ray photoemission spectroscopy; the corresponding electrical properties of thick contacts were characterized by capacitance-voltage and current-voltage methods. The metal/β-SiC interface is unreactive at room temperature. X-ray photoemission spectroscopy and electrical measurements demonstrate that these metal contacts exhibit a wide range of ϕ_B, 0.95–0.16 eV; within this range an individual contact ϕ_B value depends strongly on the metal work function in general accord with the Schottky–Mott limit.

SiC has attracted increased recent interest for high temperature semiconductor device applications, principally owing to the availability of the cubic (β) polytype in the form of thin films epitaxially grown on Si substrates. Metal/SiC contacts, whose electrical properties are dominated by the associated Schottky barrier height ϕ_B, are an essential element in the design and operation of many SiC-based devices. Studies of contacts to hexagonal (α) SiC for a limited number of metals (Au, Ag, and Al) have indicated that ϕ_B has a narrow range and is independent of the metal work function.[1–3] The as-deposited electrical properties of only a few metals to β-SiC have been reported. Of these, Au and Pt form high (>1 eV) ϕ_B contacts[4–6] while Al forms an ohmic contact[5,7,8] with unspecified ϕ_B.

In this letter we report on a systematic investigation of Schottky barrier contact formation to *n*-type β-SiC(100) for several metals chosen to include a wide variety of physical and chemical properties. The metals (Pd, Au, Co, Ti, Ag, Tb, and Al) were deposited at room temperature onto oxygen terminated ($\sim$1 monolayer) surfaces of similar SiC material. The metal/β-SiC interface chemistry and ϕ_B during contact formation were obtained by x-ray photoemission spectroscopy (XPS); the thick metal contact electrical properties were characterized by capacitance-voltage (*C-V*) and current-voltage (*I-V*) methods.

The metal/β-SiC interfaces were prepared and initially characterized in an ultrahigh vacuum (10^{-10} Torr range base pressure) XPS system comprised of a computerized HP 5950 electron spectrometer ($h\nu = 1486.6$ eV monochromatic Al $K\alpha$ x-ray source, $\sim$16 Å photoelectron effective escape depth) and a custom sample preparation chamber. Absolute XPS core level binding energies, which were measured at the half-width point of the background subtracted peak half-height, were obtained by reference to the Au $4f_{7/2}$ peak at 84.00 eV. A HP 4275A capacitance meter, HP 4140B pA/voltage source, and Tektronix 577 curve tracer were used for electrical measurements. *C-V* data were taken at 1 MHz in 0.1 eV increments to a reverse bias of -2 V.

The β-SiC(100) material was a $\sim$10-μm-thick *n*-type epilayer grown on an n^+-Si(100) substrate wafer by chemical vapor deposition.[9] A doping concentration of $\sim 10^{16}$ cm^{-3} was derived from the *C-V* data. All samples are pieces of the same wafer. To prepare a surface, a sample was serially placed in solutions of detergent, 5:1:1 NH_4OH:H_2O_2:H_2O, 5:1:1 HCl:H_2O_2:H_2O, HF, heated K_2CO_3, dilute HCl, and HF (the latter four steps are similar to those used in Ref. 4). After the etch sequence the sample was mounted on a Mo plate with In and immediately placed into the XPS system. Volatile compounds were removed by briefly heating to 600 °C.

XPS analysis of the SiC surface chemistry that results from the preparation procedure, based on the intensities and line shapes of the O 1*s*, C 1*s*, and Si 2*p* core levels, indicates the presence of $\sim$1 monolayer of O bonded primarily as SiO_x (the Si 2*p* peak has a small component at $\sim$0.5 eV higher binding energy with respect to the principal SiC peak that we attribute to O bonding). A similar conclusion concerning O bonding on β-SiC(100) surfaces has been reported.[10,11] The surface also consistently exhibits a 1×1 low-energy electron diffraction pattern similar to a pattern observed[11,12] for O-covered β-SiC(100) surfaces. The sharp SiC diffraction spots had satellite spots associated with the monolayer oxide that were incommensurate with the SiC lattice spacing. Our starting surface for the metal depositions most likely has close to the minimum amount of O that can be simply achieved without either ion sputter cleaning or heating to a very high temperature, procedures which may introduce complications for device applications. Temperatures above $\sim$1000 °C are generally required to thermally clean the β-SiC surface of all O.[12,13]

Metals were deposited onto room-temperature SiC surfaces by evaporation from W wire basket sources. The thickness of an initial thin metal deposit was $\sim$10–20 Å, as measured by the attenuation of the underlying SiC C 1*s* core level intensity. Following XPS analysis of interface formation (by using the C 1*s*, Si 2*p*, and appropriate metal core levels) an additional thick metal overlayer >2000 Å was deposited. Circular 2.54×10^{-2} cm diam contacts were defined by photolithography and chemical etching. Electrical data were thus obtained from the same interfaces characterized by XPS.

The C 1*s* core level data in Fig. 1 demonstrate how XPS was used to measure the interface Fermi energy E_F and ϕ_B for the various thin metal overlayers. The inset in Fig. 1

 0003-6951/90/060557-03$02.00 © 1990 American Institute of Physics

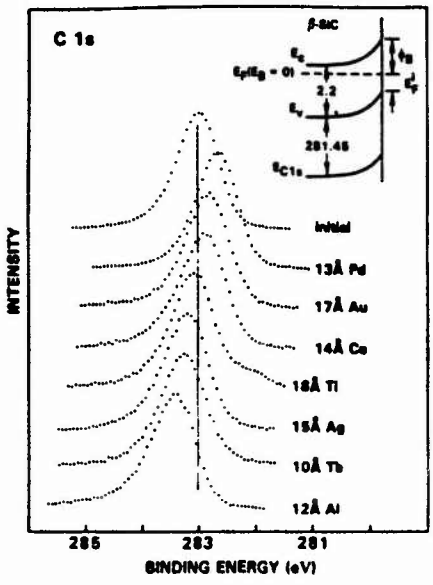

FIG. 1. XPS C 1s core level spectra for various thin metal overlayers deposited onto β-SiC(100) surfaces. Inset shows relationship between the C 1s binding energy and ϕ_B.

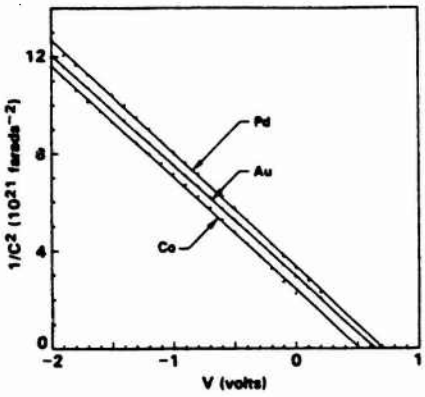

FIG. 2. Representative C-V data for Pd, Au, and Co contacts. Line is least squares fit extrapolation to V_r.

shows the relationship between the C 1s binding energy measured in SiC at an interface (E_{C1s}), and both E_F^i and ϕ_B (the photoelectron escape depth is much less than the band-bending distance). Thus $E_F^i = E_{C1s} - (E_{C1s} - E_v)$, where $(E_{C1s} - E_v)$ is the constant C 1s to valence-band maximum binding energy difference in β-SiC (note that the XPS binding energy E_B scale is zero at the sample Fermi energy E_F). We measured $(E_{C1s} - E_v) = 281.45 \pm 0.1$ eV by using XPS valence-band data obtained from a surface before metal deposition; the position of E_v was determined by a linear extrapolation of the valence-band leading edge to zero intensity (we assume that the presence of the O monolayer has a negligible effect on the valence-band data near E_v). The uppermost peak in Fig. 1 at a binding energy of $E_{C1s} = 283.03$ eV, marked by the vertical reference line, is for a representative initial SiC surface (etched and thermally cycled) which thus corresponds to an $E_F^i = 1.58$ eV (the average E_F^i for the initial surfaces of seven samples is 1.63 eV).

The second peak in Fig. 1 is for 13 Å Pd deposited onto the initial surface associated with the first peak (peak heights in Fig. 1 are normalized). A decrease in C 1s binding energy to 282.70 eV occurs during Schottky barrier formation, which thus corresponds to a decrease in E_F^i to 1.25 eV and an increase in band bending. The XPS measured Schottky barrier height is $\phi_B^{XPS} = 2.2 - E_F^i$ eV, where 2.2 eV is the band gap[14,15] of β-SiC. The remaining C 1s peaks in Fig. 1 are for Au, Co, Ti, Ag, Tb, and Al overlayers of indicated thickness deposited onto the other SiC samples. There is a marked variation in E_{C1s} for the various metals. By referring to the inset in Fig. 1 when comparing these E_{C1s} values, a negative binding energy difference represents a positive ϕ_B difference; that is, $\Delta\phi_B = -\Delta E_{C1s}$. Table I lists the binding energy of each SiC C 1s peak and the corresponding ϕ_B^{XPS} value. The measurement uncertainty in the metal-to-metal change in ϕ_B based on E_{C1s} differences is estimated as ± 0.02 eV; the uncertainty in relating the C 1s binding energy scale to the ϕ_B scale is larger, ± 0.1 eV, because of the additional uncertainties associated with the $(E_{C1s} - E_v)$ and β-SiC band-gap constants. The ϕ_B^{XPS} values range from 0.95 eV (Pd) to 0.16 eV (Al), a span of 0.79 eV. The Si 2p core level peak had similar sample-to-sample relative binding energy shifts with metal deposition as the C 1s peak.

TABLE I. Schottky barrier height of various metal contacts to β-SiC.

Metal	C 1s (eV)	ϕ_B^{XPS} (eV)	ϕ_B^{CV} (eV)	ϕ_m* (eV)
Pd	282.70	0.95	0.92	5.12
Au	282.87	0.78	0.87	5.1
Co	282.96	0.69	0.73	5.0
Ti	283.12	0.53	· · ·	4.33
Ag	283.25	0.40	· · ·	4.26
Tb	283.30	0.35	· · ·	3.0
Al	283.49	0.16	· · ·	4.28

*Reference 17.

For all the metals, the C 1s and Si 2p core level line shapes and half-widths were essentially unchanged after the thin overlayer deposition; no new peak components indicative of an interface reaction were observed (the small low binding energy peak component on the C 1s peak for the Ti deposition is because of an interaction between Ti and the vacuum chamber ambient). These metal/β-SiC interfaces thus appear to be abrupt and chemically inert. The metals investigated encompass a wide range of chemical properties, especially with respect to oxide formation. When reactions between either Tb, Al, or Ti and SiO_2 in which Si is reduced and an oxide of the form Tb_2O_3 are considered, for example, the respective bulk heats of formation predict, by a substantial margin, that such a reaction is favorable. The absence of SiO_x reduction in the presence of these reactive metals at room temperature thus indicates that the monolayer of oxide observed prior to metal deposition is chemically inert, possibly because latent reactions are kinetically limited.

Figure 2 shows representative C-V data for Pd, Au, and Co contacts (C-V data could not be obtained for contacts of the other metals because of large reverse bias currents). The data were analyzed by using the conventional model[16] where

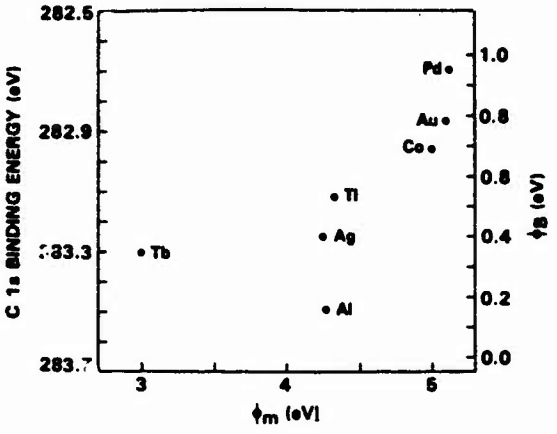

FIG. 3. Plot of XPS C 1s binding energy in β-SiC with thin metal overlayers (Table I) and corresponding ϕ_B vs the work function ϕ_m of contact.

the intercept V_i (determined by a least-squares fit extrapolation) on the voltage axis of the $1/C^2$ vs V plot is related to ϕ_B^{CV} by additive terms. For $10^{16}\,cm^{-3}$ n-type β-SiC, a calculation gave $\phi_B^{CV} = V_i + 0.21$ eV. The Pd, Au, and Co ϕ_B^{CV} values, listed in Table I, are in good agreement with the ϕ_B^{XPS} values.

A curve tracer evaluation of the I-V characteristics showed the Pd, Au, and Co contacts to be rectifying and the Ti, Ag, Tb, and Al contacts to be ohmic-like (that is, an essentially linear I-V curve for both forward and reverse bias). A more detailed examination of the I-V curves for Pd, Au, and Co by using $\log I$ vs V plots showed a significant departure from ideal forward bias Schottky barrier transport behavior owing to excessive leakage currents at low bias and large (>1.4) ideality factors at high bias that precluded a quantitative analysis for ϕ_B. The origin of this nonideal I-V behavior is uncertain. Qualitatively, however, the I-V analysis indicated $\phi_B(\text{Pd}) > \phi_B(\text{Au}) > \phi_B(\text{Co})$. Thus, the I-V data are consistent with both the XPS and C-V data.

Figure 3 shows the C 1s binding energy values and the corresponding ϕ_B^{XPS} values in Table I plotted against the work function[17] ϕ_m of the contact. There is a strong correlation between ϕ_B and ϕ_m; high work function metals have high barriers and low work function metals have low barriers (Al forms a nearly ideal ohmic contact). Thus, E_F^i is relatively unpinned at these metal/β-SiC interfaces, which implies a low concentration of interface electronic states. The electron affinity χ of SiC is about 4 eV.[15] The plot in Fig. 3 suggests that, excepting Tb, the mechanism for Schottky barrier formation to β-SiC yields ϕ_B values in reasonable accord with the Schottky–Mott limit of $\phi_B = \phi_m - \chi$.

In summary, for a variety of Schottky barrier contacts (Pd, Au, Co, Ti, Ag, Tb, and Al) to oxygen terminated (~ 1 monolayer) n-type β-SiC(100) surfaces the metal/β-SiC interface is chemically unreactive at room temperature. XPS and electrical characterization measurements demonstrate that metal contacts to β-SiC exhibit a wide range of ϕ_B, 0.95–0.16 eV. The ϕ_B values depend strongly on the ϕ_m of the contact metal. For device applications, high work function metals are appropriate for Schottky barrier contacts and low work function metals for ohmic contacts.

The authors thank L. G. Matus of the NASA Lewis Research Center for kindly supplying the β-SiC material. This work was supported by the Office of Naval Research, contract No. N00014-85-C-0135.

[1] C. A. Mead and W. G. Spitzer, Phys. Rev. A 134, 713 (1964).
[2] S. H. Hagen, J. Appl. Phys. 39, 1458 (1968).
[3] S. Y. Wu and R. B. Campbell, Solid-State Electron. 17, 683 (1974).
[4] S. Yoshida, K. Sasaki, E. Sakuma, S. Misawa, and S. Gonda, Appl. Phys. Lett. 46, 766 (1985).
[5] J. A. Edmond, J. Ryu, J. T. Glass, and R. F. Davis, J. Electrochem. Soc. 135, 359 (1988).
[6] D. E. Ioannou, N. A. Papanicolaou and J. P. E. Nordquist, IEEE Trans. Electron Devices ED-34, 1094 (1987).
[7] S. Yoshida, H. Daimon, M. Yamanaka, E. Sakuma, E. Misawa, and K. Endo, Appl. Phys. Lett. 46, 766 (1985).
[8] H. Daimon, M. Yamanaka, E. Sakuma, S. Misawa, and S. Yoshida, Jpn. J. Appl. Phys. 25, L592 (1986).
[9] β-SiC material supplied by L. G. Matus of the NASA Lewis Research Center, Cleveland, OH.
[10] R. Kaplan, J. Appl. Phys. 56, 1636 (1984).
[11] M. Dayan, J. Vac. Sci. Technol. A 3, 361 (1985).
[12] S. Hasegawa, S. Nakamura, N. Kawamoto, H. Kishibe, and Y. Mizokawa, Surf. Sci. 206, L851 (1988).
[13] V. M. Bermudez, J. Appl. Phys. 63, 4951 (1988).
[14] R. Dalven, J. Phys. Chem. Solids 13, 163 (1960).
[15] H. R. Philipp and E. A. Taft, in *Silicon Carbide—A High Temperature Semiconductor*, edited by J. R. O'Connor and J. Smiltens (Pergamon, New York, 1960), p. 366.
[16] A. M. Goodman, J. Appl. Phys. 34, 329 (1963).
[17] H. B. Michaelson, J. Appl. Phys. 48, 4729 (1977).

Measurement of InP/$In_{0.53}Ga_{0.47}As$ and $In_{0.53}Ga_{0.47}As$/$In_{0.52}Al_{0.48}As$ heterojunction band offsets by x-ray photoemission spectroscopy

J. R. Waldrop, E. A. Kraut, C. W. Farley, and R. W. Grant
Rockwell International Science Center, Thousand Oaks, California 91360

(Received 30 July 1990; accepted for publication 10 September 1990)

X-ray photoemission spectroscopy (XPS) has been used to measure the valence-band offset ΔE_v for the lattice-matched InP/$In_{0.53}Ga_{0.47}As$ and $In_{0.53}Ga_{0.47}As$/$In_{0.52}Al_{0.48}As$ heterojunction interfaces. The heterojunctions were formed by molecular-beam epitaxy. We obtain values of ΔE_v(InP/$In_{0.53}Ga_{0.47}As$) = 0.34 eV ($\Delta E_c/\Delta E_v = 43/57$) and ΔE_v($In_{0.53}Ga_{0.47}As$/$In_{0.52}Al_{0.48}As$) = 0.22 eV ($\Delta E_c/\Delta E_v = 68/32$) for the respective interfaces. By combining these measurements with available XPS ΔE_v(InP/$In_{0.52}Al_{0.48}As$) data we find that band offset transitivity is satisfied. Accordingly, the band offsets for heterojunction pairs formed from InP, $In_{0.53}Ga_{0.47}As$, and $In_{0.52}Al_{0.48}As$ are not influenced by interface specific effects.

I. INTRODUCTION

Heterojunction devices based on the lattice-matched semiconductors $In_{0.53}Ga_{0.47}As$, $In_{0.52}Al_{0.48}As$, and InP are of considerable interest. In particular, devices that use $In_{0.53}Ga_{0.47}As$/InP or $In_{0.52}Al_{0.48}As$/$In_{0.53}Ga_{0.47}As$ heterojunction interfaces are being developed for a wide variety of optoelectronic and high-speed electronic applications. The band gaps of $In_{0.53}Ga_{0.47}As$, $In_{0.52}Al_{0.48}As$, and InP are 0.75, 1.44, and 1.35 eV, respectively.[1-3] How the band-gap difference ΔE_g at an interface (0.60 eV for $In_{0.53}Ga_{0.47}As$/InP, 0.69 eV for $In_{0.52}Al_{0.48}As$/$In_{0.53}Ga_{0.47}As$) is distributed between a conduction-band offset ΔE_c and a valence-band offset ΔE_v, where $\Delta E_g = \Delta E_v + \Delta E_c$, is central to the operation of most heterojunction devices.

A large number of In Ga As/InP interface investigations have been made by current-voltage (I-V), capacitance-voltage (C-V), and optical methods to measure either ΔE , ΔE , or ΔE /ΔE .[4-10] Expressed in terms of ΔE the In Ga As/InP results range from 0.0 to 0.4 eV. For the In Al As/In Ga As interface several C-V and I-V measurements[4-7] of ΔE and an optical measurement of ΔE /ΔE have been reported. These literature In Al As/In Ga As ΔE values lie in a remarkably narrow 0.50–0.55-eV range.

In this paper we use x-ray photoemission spectroscopy (XPS) to measure directly ΔE at InP/In Ga As (InP grown on In Ga As) and In Ga As/In Al As heterojunction interfaces grown by molecular-beam epitaxy (MBE). The results are combined with available XPS data for the InP/In Al As interface to test the ΔE transitivity of the heterojunction pairs formed between In Ga As, In Al As, and InP. A transitivity test assesses the influence of interface specific effects on the band offsets.

II. EXPERIMENT

A. Sample preparation

The insets in Figs. 1 and 2 show schematic cross sections of the InP/In Ga As and In Ga As/In Al As sample structures. XPS analyzes the heterojunction interface underneath the thin top layer of the sample. The In Ga As/In Al As samples and the In Ga As layers for the InP/In Ga As samples were prepared by epitaxial growth on (100)-oriented bulk InP substrates in a Varian GEN II MBE system with subsequent transfer in air to the XPS system. A thick cap of condensed elemental As protected the sample surface[11] from oxidation and contamination during the transfer process. The cap was desorbed in the custom ultrahigh vacuum (10^{-10} Torr range base pressure) XPS sample preparation chamber by heating to ~450 °C for ~30 s. A characteristic low-energy electron diffraction (LEED) pattern was observed from the clean decapped surface of each sample.

The InP/In Ga As samples were completed by growing a thin MBE InP layer on In Ga As within the XPS system. Growth was in a ~10^{-5} Torr P overpressure at a substrate temperature of ~400 °C. InP wrapped in resistively heated Ta wire provided the P ; a W basket is the In source. The thickness t (listed in Table I) of the InP for the four samples prepared was measured from the intensity de-

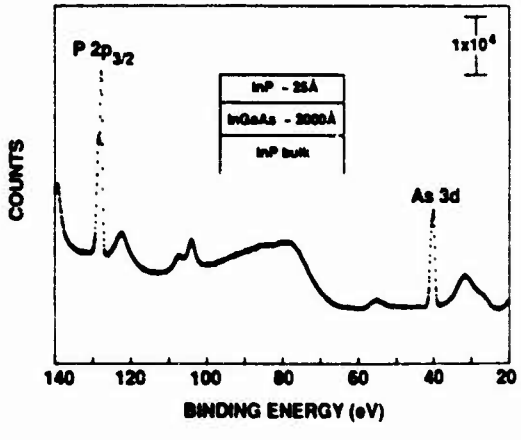

FIG. 1. XPS binding energy spectrum of an InP In Ga As (100) sample in the region of the P 2p and As 3d core levels. Sample structure shown in inset.

 0021-8979/91/010372-07$03.00 © 1991 American Institute of Physics

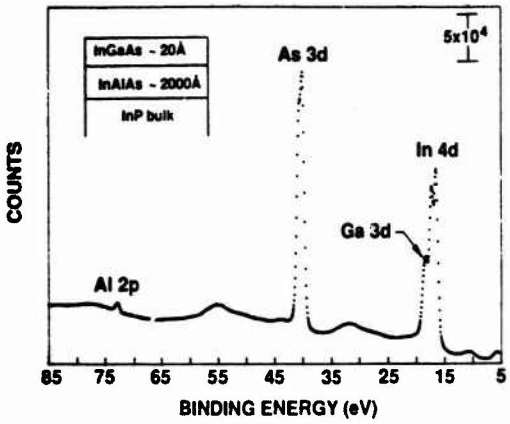

FIG. 2. XPS binding energy spectrum of an In Ga As/In Al As sample in the region of the Al 2*p* and Ga 3*d* core levels. Sample structure shown in inset.

crease of the As 3*d* core level in the substrate. Epitaxy of the InP layer was confirmed by LEED.

Two In Ga As/In Al As samples were used from each of two different MBE growth runs. The $In_{0.53}Ga_{0.47}As$ top layers were 20 Å thick for both growths. Both the In Ga As and the In Al As layers were grown at a substrate temperature of 520 °C with 1×10^{17} cm^{-3} Si dopant concentration.

B. Measurement of ΔE_v

The XPS system is based on a HP5950 angle-resolved electron spectrometer that includes a monochromatic Al $K\alpha$ x-ray source ($h\nu = 1486.6$ eV) and computerized data collection and analysis. Briefly, the x rays irradiate a sample to cause ejection of photoelectrons having kinetic energy E_K. These photoelectrons are energy analyzed and counted in channels on a binding energy E_B scale where $E_B = h\nu - E_K$ ($E_B \equiv 0$ eV at the sample Fermi energy). Particular care is taken to insure an accurate eV/channel calibration of the E_B scale. An XPS spectrum contains peaks associated with the outer core levels of the atoms that compose the sample surface region; each core level has a characteristic binding energy E_{CL}. The effective photoelectron escape depth λ for our experimental configuration is ~16 Å. Photoelectrons originating from each side of a heterojunction interface that is located on the order of λ from a sample surface will therefore be detected in the same XPS photoelectron binding energy spectrum. Thus, the 20–140-eV XPS binding energy spectrum in Fig. 1 for an $InP/In_{0.53}Ga_{0.47}As$ sample contains both a P 2*p* core-level peak from the thin InP top layer and an As 3*d* core-level peak from the underlying thick $In_{0.53}Ga_{0.47}As$ (other prominent peaks are In 4*p* at ~80 eV, Ga 3*p* at ~105 eV, In 4*s* at ~125 eV, As 3*p* at ~140 eV, and In 4*d* loss peaks at ~30 eV). Similarly, the 5–85-eV spectrum in Fig. 2 for an $In_{0.53}Ga_{0.47}As/In_{0.52}Al_{0.48}As$ sample contains both Ga 3*d* and Al 2*p* core-level peaks.

Schematic energy-band diagrams of the $InP/In_{0.53}Ga_{0.47}As$ and In Ga As/In Al As interfaces are shown in Figs. 3(a) and 4(a), respectively, where E_c is a conduction-band minimum, E_v is a valence-band maximum, and ΔE_{CL} is a binding energy difference between two core levels selected from opposite sides of the interface. For these heterojunctions we have used

$$\Delta E_{CL}\ (\mathrm{InP/In_{0.53}Ga_{0.47}As}) = (E_{P2p_{3/2}}^{InP} - E_{As3d}^{InGaAs})$$

and

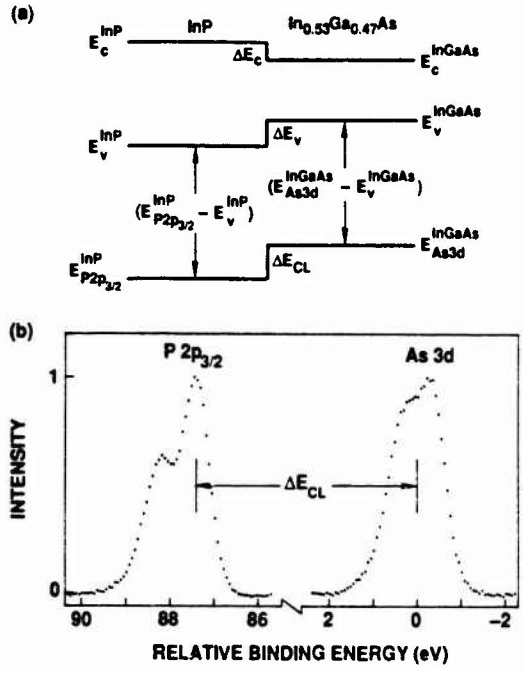

FIG. 3. (a) Schematic energy-band diagram of the $InP/In_{0.53}Ga_{0.47}As$ interface. (b) Measurement of $\Delta E_{CL} = (E_{P2p_{3/2}}^{InP} - E_{As3d}^{InGaAs})$ (data from Fig. 1).

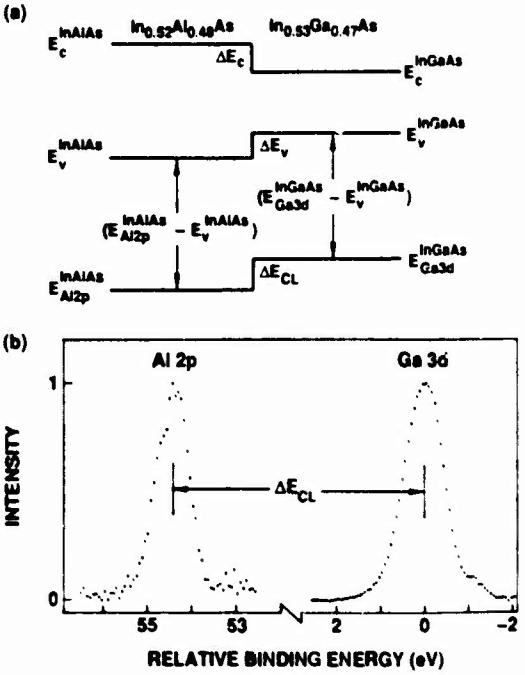

FIG. 4. (a) Schematic energy-band diagram of the In Ga As/In Al As interface. (b) Measurement of $\Delta E_{CL} = (E_{Al2p}^{InAlAs} - E_{Ga3d}^{InGaAs})$ (data from Fig. 2).

$$\Delta E_{v,1}(\mathrm{In_{0.53}Ga_{0.47}As/In_{0.52}Al_{0.48}As}) = (E^{\mathrm{InAlAs}}_{\mathrm{Al}\,2p} - E^{\mathrm{InGaAs}}_{\mathrm{Ga}\,3d}).$$

By inspection of the interface-band diagrams it can be seen that

$$\Delta E\,(\mathrm{InP/In_{1-x}Ga_xAs}) = \Delta E_{v,1}(\mathrm{InP/In_{0.53}Ga_{0.47}As}) + (E_v^{\mathrm{InGaAs}} - E^{\mathrm{InGaAs}}) - (E_v^{\mathrm{InP}} - E^{\mathrm{InP}}) \quad (1)$$

and

$$\Delta E\,(\mathrm{In_{1-x}Ga_xAs/In_{1-y}Al_yAs}) = \Delta E_{v,1}(\mathrm{In_{1-x}Ga_xAs/In_{0.52}Al_{0.48}As}) + (E^{\mathrm{InGaAs}}_{\mathrm{Ga}\,3d} - E^{\mathrm{InGaAs}}) - (E^{\mathrm{InAlAs}}_{\mathrm{Al}\,2p} - E^{\mathrm{InAlAs}}). \quad (2)$$

The two $(E_{Ga\,3d} - E_v)$ terms that appear on the right-hand side of Eqs. (1) and (2), which are core level to valence band maximum binding energy differences, are bulk constants obtained by independent XPS measurements on the pure material. Thus, of the three quantities required for the XPS determination of ΔE only $\Delta E_{v,1}$ is measured for an individual heterojunction (additional details concerning the XPS measurement method are available elsewhere [24]).

A value of $(E^{\mathrm{InAlAs}}_{\mathrm{Al}\,2p} - E^{\mathrm{InAlAs}}_v) = 73.07 \pm 0.03$ eV has been measured for $\mathrm{In_{0.52}Al_{0.48}As}$.[25] Measurements which have determined $(E^{\mathrm{InGaAs}}_{\mathrm{As}\,3d} - E^{\mathrm{InGaAs}}_v) = 40.69 \pm 0.03$ eV, $(E^{\mathrm{InGaAs}}_{\mathrm{Ga}\,3d} - E^{\mathrm{InGaAs}}_v) = 18.87 \pm 0.03$ eV, and $(E^{\mathrm{InP}}_{\mathrm{P}\,2p_{3/2}} - E^{\mathrm{InP}}_v) = 127.74 \pm 0.03$ eV are described in Appendices A and B. Substitution of these material constants into Eqs. (1) and (2) gives

$$\Delta E_v(\mathrm{InP/In_{0.53}Ga_{0.47}As}) = \Delta E_{CL}(\mathrm{InP/In_{0.53}Ga_{0.47}As}) - 87.05 \text{ eV} \quad (3)$$

and

$$\Delta E_v(\mathrm{In_{0.53}Ga_{0.47}As/In_{0.52}Al_{0.48}As}) = \Delta E_{CL}(\mathrm{In_{0.53}Ga_{0.47}As/In_{0.52}Al_{0.48}As}) - 54.20 \text{ eV}. \quad (4)$$

The precision measurement of $\Delta E_{v,1}$ for each heterojunction is illustrated in Figs. 3(b) and 4(b) by using the core-level peaks in the corresponding InP/In$_{1-x}$Ga$_x$As and In$_{1-x}$Ga$_x$As/In$_{1-y}$Al$_y$As spectra in Figs. 1 and 2. For $\Delta E_{v,1}$ (InP/In$_{1-x}$Ga$_x$As), a background function that is proportional to the integrated peak intensity (from low to high binding energy) is first subtracted from each peak. The As $3d$ peak height and the width at half-height are found by using a computerized procedure in which a third-order polynomial is least-squares fit to segments at the top and sides of the discrete peak data. The corresponding As $3d$ peak binding energy is measured at the midpoint of the peak width at half-height. Because the $2p_{3/2}$ and $2p_{1/2}$ components of the P $2p$ peak are nearly resolved we used a nonlinear least-square-fit analysis where the peak shape of each component is modeled with a Gaussian–Lorentzian product function [defined by Eqs. (1) and (2) of Ref. 26] to determine the center of the P $2p_{3/2}$ peak. Measurement of $\Delta E_{v,1}$ (In$_{1-x}$Ga$_x$As/In$_{1-y}$Al$_y$As) is complicated by significant overlap between the Ga $3d$ and In $4d$ peaks and by the very broad In $4p$ peak underneath the narrow Al $2p$ peak. A normalized reference spectrum from clean InAs was used to subtract both of these interfering In peaks from the heterojunction spectrum, after which the Ga $3d$ and Al $2p$ peak energies were determined by the same procedure used for the As $3d$ peak. The $\Delta E_{v,1}$ measurement uncertainty is estimated to be ± 0.02 eV; owing to the additional uncertainties associated with the $(E_{Ga\,3d} - E_v)$ values the ΔE uncertainty is ± 0.05 eV.

III. RESULTS AND DISCUSSION

A. InP/In$_{0.53}$Ga$_{0.47}$As ΔE_v

Table I lists the $\Delta E_{v,1}$ and corresponding ΔE values measured for the four InP/In$_{1-x}$Ga$_x$As samples. The average ΔE (InP/In$_{1-x}$Ga$_x$As) value is 0.34 eV, with a very narrow 0.02-eV range in values. From $\Delta E = \Delta E - 0.34$ eV we obtain $\Delta E = 0.26$ eV and $\Delta E/\Delta E = 43/57$. The present measurement agrees with the admittance spectroscopy measurement of Lang *et al.* ($\Delta E = 0.346$ eV) and the optical studies of Westland *et al.* ($\Delta E/\Delta E = 45/55$).[27] Our result is also in good accord with several previous measurements that give ΔE values of 0.20 to 0.23 eV.[3,14] A comparison between the two measurements[3] which obtained ΔE at a single In$_{1-x}$Ga$_x$As/InP interface and our InP/In$_{1-x}$Ga$_x$As value indicates that any growth sequence effect on the band offsets is small.

The unstrained valence-band offsets measured by XPS at the $x = 0$ and $x = 1$ end points of the In$_{1-x}$Ga$_x$As/InP system, as given in Appendix B, are ΔE (GaAs/InP) $= 0.34$ eV and ΔE (InAs/InP) $= 0.46$ eV, respectively (the unstrained offset is defined as the offset that would obtain if the interface were fully relaxed). Our measurement at $x = 0.53$ is equal to the $x = 0$ value of 0.34 eV rather than the 0.40-eV value obtained by a linear interpolation between the end points. While somewhat small in terms of absolute energy, the percent deviation (bowing) is quite large. This bowing is in contrast to that of the common-anion Al$_{1-x}$Ga$_x$As/GaAs system in which the offsets are essentially linear with x and the nearly linear behavior of the In$_{1-x}$Al$_x$As/InP system. However, these heterojunction systems have offsets that change by >0.4 eV with composition. Thus, although many alloy systems may have offsets that are approximately linear with composition, a departure from linearity may be relatively large when the offset difference between the end points is small.

TABLE I. XPS measured valence-band offset ΔE_v for InP/In$_{1-x}$Ga$_x$As (100) heterojunction interfaces. ΔE (InP/In$_{0.53}$Ga$_{0.47}$As) = 0.34 eV.

$\Delta E_{v,1}$ (eV)	ΔE_v (eV)	$\Delta E_v/\Delta E_c$
87.38	0.33	48/52
87.39	0.34	50/50
87.40	0.35	51/49
87.40	0.35	51/49

B. $In_{0.53}Ga_{0.47}As/In_{0.52}Al_{0.48}As$ ΔE_v

Table II lists the ΔE_{CL} and corresponding ΔE_v values measured for the four $In_{0.53}Ga_{0.47}As/In_{0.52}Al_{0.48}As$ samples. The average ΔE_v ($In_{0.53}Ga_{0.47}As/In_{0.52}Al_{0.48}As$) value is 0.22 eV, with a small range in values of 0.03 eV. Thus, $\Delta E_c = \Delta E_g - 0.22 = 0.47$ eV and $\Delta E_c/\Delta E_v = 68/32$.

Our value for ΔE_c based on measuring ΔE_v is slightly lower but in agreement within experimental error with several direct ΔE_c measurements[17,18,20–22] that cluster at 0.50–0.52 eV. The XPS ΔE_v measurement is therefore consistent with the ΔE_c obtained by other methods. Three of the ΔE_c results[17,18,21] involved characterization of a single $In_{0.52}Al_{0.48}As/In_{0.53}Ga_{0.47}As$ interface; thus, a comparison with our $In_{0.53}Ga_{0.47}As/In_{0.52}Al_{0.48}As$ value demonstrates the absence of a growth sequence effect for this heterojunction.

C. Transitivity of $In_{0.53}Ga_{0.47}As$, $In_{0.52}Al_{0.48}As$, and InP heterojunction offsets

If three heterojunction interfaces are formed from a group of three semiconductors A, B, and C, ΔE_v is transitive if $\Delta E_v(A/C) = \Delta E_v(A/B) + \Delta E_v(B/C)$; that is, summation with appropriate signs of any two offsets will yield the third. Transitivity is satisfied when the band offsets are determined solely by the bulk properties of the semiconductors. Failure of transitivity suggests that specific interface effects are significantly contributing to the band offset at one or more of the heterojunctions.

Transitivity for heterojunctions formed from $In_{1-x}Ga_xAs$, $In_{1-x}Al_xAs$, and InP can be tested by using our InP/$In_{1-x}Ga_xAs$ and $In_{1-x}Ga_xAs/In_{1-x}Al_xAs$ offsets in conjunction with a recent XPS measurement[23] of $\Delta E_v(InP/In_{1-x}Al_xAs) = 0.16 \pm 0.05$ eV. Thus,

$$\begin{aligned}\Delta E_v&(InP/In_{1-x}Ga_xAs)\\ &- \Delta E_v(In_{1-x}Ga_xAs/In_{1-x}Al_xAs)\\ &- \Delta E_v(InP/In_{1-x}Al_xAs)\\ &= 0.34 - 0.22 - 0.16\\ &= -0.04 \pm 0.09 \text{ eV}.\end{aligned}$$

Consequently, within the experimental uncertainty these interfaces are transitive.

The transitivity test uncertainty can be sizably reduced by using the XPS ΔE_{CL} data for each interface, where the individual uncertainty is ± 0.02 eV, in place of the corresponding ΔE_v value.[28] When each ΔE_v is expressed as in Eq. (1) and summed the $(E_{CL} - E_v)$ constants cancel to reduce the transitivity test to the sum of three ΔE_{CL} values. For proper cancellation it is necessary that the same core level be used in both of the ΔE_{CL} terms associated with a common semiconductor. The ΔE_{CL}-based transitivity test for these heterojunctions is somewhat complicated because we used the $In_{0.53}Ga_{0.47}As$ As $3d$ level for ΔE_{CL} (InP/$In_{0.53}Ga_{0.47}As$) but the $In_{0.53}Ga_{0.47}As$ Ga $3d$ level was required for ΔE_{CL} ($In_{0.53}Ga_{0.47}As/In_{0.52}Al_{0.48}As$). Similarly, the $In_{0.52}Al_{0.48}As$ Al $2p$ level was used for ΔE_{CL} ($In_{0.53}Ga_{0.47}As/In_{0.52}Al_{0.48}As$) but the $In_{0.52}Al_{0.48}As$ As $3d$ level was used[25] for ΔE_{CL} ($InP/In_{0.52}Al_{0.48}As$). This difficulty can be resolved by subtracting the bulk $(E^{InGaAs}_{As\,3d} - E^{InGaAs}_{Ga\,3d}) = 21.82 \pm 0.01$ eV binding energy difference (Appendix A) from ΔE_{CL} ($In_{0.53}Ga_{0.47}As/In_{0.52}Al_{0.48}As$) and the bulk $(E^{InAlAs}_{Al\,2p} - E^{InAlAs}_{As\,3d}) = 32.64 \pm 0.01$ eV difference[25] from ΔE_{CL} ($InP/In_{0.52}Al_{0.48}As$). By combining these bulk core-level constants, the average of the ΔE_{CL} values in Tables I and II, and

$$\Delta E_{CL}(InP/In_{0.52}Al_{0.48}As) = (E^{InP}_{P\,2p_{3/2}} - E^{InAlAs}_{As\,3d}) = 87.47 \pm 0.02 \text{ eV}$$

(Ref. 25), the transitivity test becomes

$$\begin{aligned}&(E^{InP}_{P\,2p_{3/2}} - E^{InGaAs}_{As\,3d}) - (E^{InAlAs}_{Al\,2p} - E^{InGaAs}_{Ga\,3d})\\ &+ (E^{InGaAs}_{As\,3d} - E^{InGaAs}_{Ga\,3d}) - (E^{InP}_{P\,2p_{3/2}} - E^{InAlAs}_{As\,3d})\\ &+ (E^{InAlAs}_{Al\,2p} - E^{InAlAs}_{As\,3d})\\ &= 87.39 - 54.42 + 21.82 - 87.47 + 32.64\\ &= -0.04 \pm 0.04 \text{ eV}.\end{aligned}$$

Thus, this refined test also indicates transitivity but with the experimental uncertainty reduced to ± 0.04 eV.

TABLE II. XPS measured valence-band offset ΔE_v for $In_{1-x}Ga_xAs/In_{1-x}Al_xAs$ (100) heterojunction interfaces. ΔE_v ($E_{CL} - E_v$). Average ΔE_v ($In_{1-x}Ga_xAs/In_{1-x}Al_xAs$) = 0.22 eV.

ΔE_{CL} (eV)	ΔE_v (eV)	Growth No.
54.41	0.21	1
54.44	0.24	1
54.42	0.22	2
54.42	0.22	2

IV. SUMMARY

XPS has been used to measure the valence-band offset for the lattice-matched $InP/In_{0.53}Ga_{0.47}As$ and $In_{0.53}Ga_{0.47}As/In_{0.52}Al_{0.48}As$ heterojunction interfaces. Values of ΔE_v ($InP/In_{0.53}Ga_{0.47}As$) = 0.34 eV ($\Delta E_c/\Delta E_v = 43/57$) and ΔE_v ($In_{0.53}Ga_{0.47}As/In_{0.52}Al_{0.48}As$) = 0.22 eV ($\Delta E_c/\Delta E_v = 68/32$) are obtained for the respective interfaces. The band offsets for heterojunction pairs formed from InP, $In_{0.53}Ga_{0.47}As$, and $In_{0.52}Al_{0.48}As$ are found to satisfy transitivity. Accordingly, the band offsets for interfaces formed between these semiconductors are not influenced by interface specific effects.

ACKNOWLEDGMENT

This work was supported by the Office of Naval Research under Contract No. N00014-85-C-0135.

APPENDIX A: MEASUREMENT OF $(E^{InGaAs}_{As\,3d} - E^{InGaAs}_{v})$

Figure 5 shows a -5 to 50 eV XPS binding energy spectrum for a clean $In_{1-x}Ga_xAs$ (100) surface that includes the As $3d$ core level and the valence-band region. Such data were acquired from two different samples. The

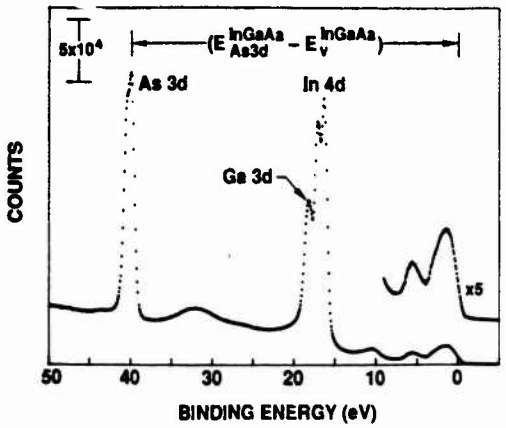

FIG. 5. Representative 5 to 50 eV XPS binding energy spectrum for In Ga As (100).

position of E_F in the XPS data was found through use of a method described in detail elsewhere.[7] Briefly, a theoretical valence-band density of states (VBDOS) for the semiconductor, defined on an energy scale where E_F is located at zero energy, is convolved with the experimentally determined XPS spectrometer resolution function. This broadened theoretical VBDOS, where E_F has remained at zero energy, is least-squares fitted to the XPS VBDOS data in the region near E_F. The fitting procedure transfers the position of E_F from the theoretical VBDOS to the XPS spectrum; the energy of the core level of interest is measured with respect to E_F. For a reliable result the broadened theoretical VBDOS and the data should closely overlap over the range of the fit.

The data were fit to three different theoretical VBDOS: In Ga As (based on molecular coherent-potential approximation calculations), GaAs, and InAs (the latter two based on nonlocal pseudopotential calculations). The best fits were obtained with the GaAs VBDOS. Figure 6 is an example of the good fit between the broadened GaAs VBDOS and the In Ga As XPS valance-band data of Fig. 5 plotted on a binding energy scale where $E_F = 0$ eV. The fit is over a range that terminates at an energy E_{max} below E_F ($E_{max} = 1$ eV in Fig. 6). Figure 7 (upper panel) gives the results for the two In Ga As samples when the fitting procedure was used with the GaAs VBDOS. The As 3*d* core level to valence-band energy ($E^{\ln GaAs}_{As\,3d} - E^{\ln GaAs}_{v}$) is plotted versus E_{max}; the error bars indicate the 95% confidence interval of the nonlinear fit. A value of ($E^{\ln GaAs}_{As\,3d} - E^{\ln GaAs}_{v}$) = 40.69 eV is assigned because an uncertainty of ± 0.03 eV includes all the ($E^{\ln GaAs}_{As\,3d} - E^{\ln GaAs}_{v}$) values for E_{max} near E_F. We also measured ($E^{\ln GaAs}_{In\,4d} - E^{\ln GaAs}_{v}$) = 21.82 ± 0.01 eV. The corresponding value of ($E^{\ln GaAs}_{In\,4d} - E^{\ln GaAs}_{As\,3d}$) is thus 18.87 ± 0.03 eV.

The essentially constant ($E^{\ln GaAs}_{As\,3d} - E^{\ln GaAs}_{v}$) over the E_{max} range shown in the upper panel of Fig. 7 indicates a good match between the shape of the broadened theoretical GaAs VBDOS and the In Ga As XPS data for this energy interval. In contrast, the lower panel in Fig. 7 shows the ($E^{\ln GaAs}_{As\,3d} - E^{\ln GaAs}_{v}$) vs E_{max} results when the In Ga As VBDOS (triangles) and InAs VBDOS (diamonds) are used

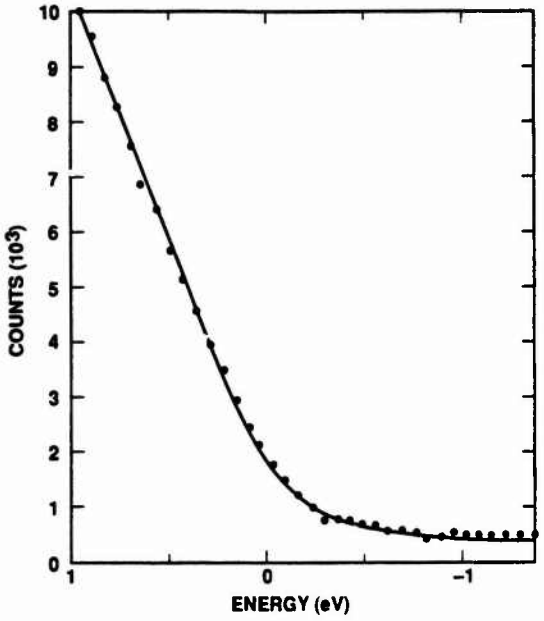

FIG. 6. Fit of broadened GaAs theoretical VBDOS (line) to the In Ga As valence-band data of Fig. 5.

for the same data represented by the closed circles in the upper panel. The relatively large increase in ($E^{\ln GaAs}_{As\,3d} - E^{\ln GaAs}_{v}$) with E_{max} and examination of the fits reveals a poor correspondence between the data and both the broadened InAs VBDOS and broadened $In_{0.5}Ga_{0.5}As$ VBDOS. Thus, the shape of the $In_{0.53}Ga_{0.47}As$ VBDOS near E_v is similar to that of GaAs and rather dissimilar to that of InAs.

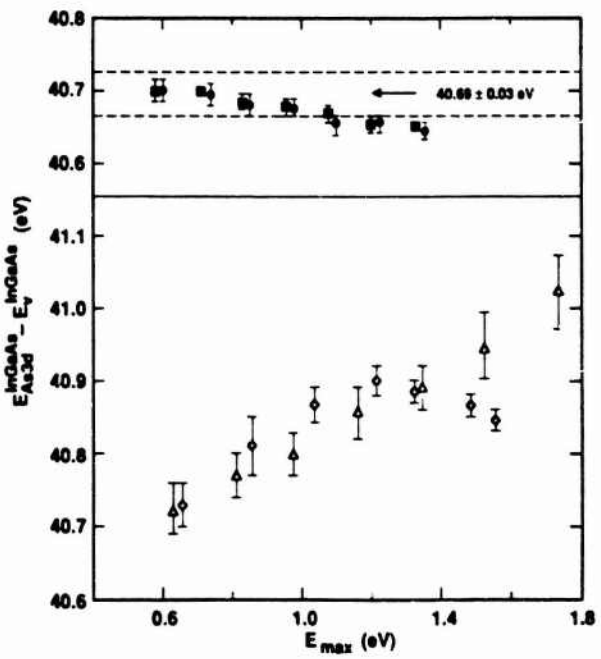

FIG. 7. (Upper panel) As 3*d* core level to valence-band maximum binding energy difference for two $In_{0.53}Ga_{0.47}As$ (100) samples as a function of the end point E_{max} of the fitting interval based on the GaAs theoretical VBDOS. (Lower panel) Same as above when the closed circle data are fit to the theoretical $In_{0.5}Ga_{0.5}As$ VBDOS (triangles) and to the theoretical InAs VBDOS (diamonds).

APPENDIX B: REEVALUATION OF $(E_{P\,2p}^{InP} - E_v^{InP})$

Our previous XPS measurement of $(E_{P\,2p}^{InP} - E^{InP})$ was based on data from two InP (100) samples.[33] These two samples had an azimuthal rotation of the crystal surface that differed by 90° relative to the photoelectron emission direction analyzed by the XPS spectrometer. Although the two (100) data sets gave results in good agreement, for low values of E_{max} the apparent $(E_{P\,2p}^{InP} - E^{InP})$ value was decreasing rather than remaining constant. This deviation was attributed to the greater statistical uncertainty that may occur for small E_{max} values. We have investigated this deviation in greater detail and have found the same apparent decrease in $(E_{P\,2p}^{InP} - E^{InP})$ at low E_{max} with new InP (100) data. Based on these results and the analysis of data recently taken for InP (110) and (111) surfaces that is presented below, we have concluded that a previously unrecognized surface state exists on the InP (100) surface. This state contributes substantial intensity to the XPS VBDOS spectrum in the binding energy region extending a few tenths of an eV around E_v. Our XPS data taken at different azimuthal angles on the (100) surface is consistent with a surface state that has approximately axial orbital symmetry with respect to the surface normal. Because of this (100) InP surface state the value of $(E_{P\,2p}^{InP} - E^{InP})$ and, as a consequence, the XPS measured band offsets (for GaAs/InP and InAs/InP) obtained by use of this quantity need reevaluation.

Figure 8 shows a -10 to 140 eV binding energy spectrum for a clean InP (110) surface. Similar data were collected for another InP (110) sample where the azimuthal angle was rotated by 90° and for a (111) sample. The method described in Appendix A was used to find E_v and the P $2p$ core-level binding energy was determined as described in Sec. II B. Figure 9 indicates the good fit obtained between a broadened theoretical InP VBDOS and the valence-band data of Fig. 8. Figure 10 shows $(E_{P\,2p}^{InP} - E^{InP})$ vs E_{max}; there is good agreement between, and very little variation of, $(E_{P\,2p}^{InP} - E^{InP})$ for both orientations. A value of $(E_{P\,2p}^{InP} - E^{InP}) = 127.74 \pm 0.03$ eV is assigned because the uncertainty includes all the (110) data versus E_{max} and the (111) data for E_{max} near E_v. Our previous measurement

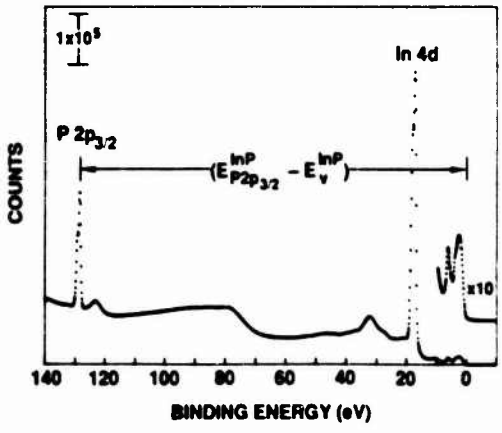

FIG. 8. Representative -10 to 140 eV binding energy spectrum for InP (110).

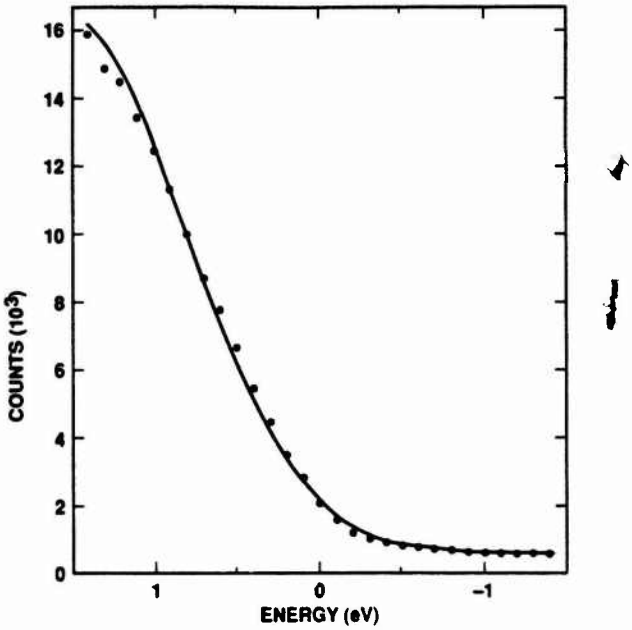

FIG. 9. Fit of the broadened InP theoretical VBDOS to the InP valence-band data of Fig. 8.

of $(E_{P\,2p}^{InP} - E^{InP})$ based on (100) samples was referenced to the midpoint of the P $2p$ envelope half-width at half-height; the new $(E_{P\,2p}^{InP} - E^{InP})$ value is 0.16 eV smaller than the old value when compared at this reference point. Thus, we believe that a (100) surface state significantly influenced the prior analysis of the InP (100) valence-band data with respect to determining the bulk value of $(E_{P\,2p}^{InP} - E^{InP})$.

The redetermined $(E_{P\,2p}^{InP} - E^{InP})$ value necessitates reevaluation of our previously reported unstrained ΔE (InAs/InP) and ΔE (GaAs/InP) results. In Ref. 33, Eqs. (1) and (2) become

$$\Delta E\ (\text{InAs/InP}) = \Delta E_{v,v}\ (\text{InAs/InP}) - 87.02\ \text{eV}$$

and

$$\Delta E\ (\text{GaAs/InP}) = \Delta E_{v,v}\ (\text{GaAs/InP}) - 87.00\ \text{eV},$$

respectively. The average $\Delta E_{v,v}$ values for these interfaces are $\Delta E_{v,v}$ (InAs/InP) = 87.48 eV and $\Delta E_{v,v}$ (GaAs/InP)

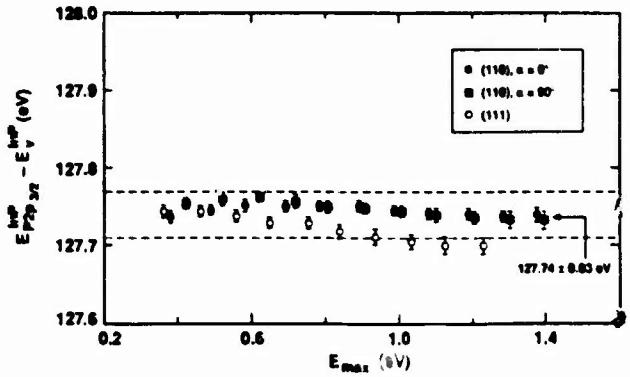

FIG. 10. P $2p$ core-level to valence-band maximum binding energy difference for InP (100) and (111) samples as a function of E_{max}.

= 87.34 eV, where the data were reanalyzed to provide binding energy differences with respect to the P $2p_{3/2}$ component of the P $2p$ core level in InP. Thus, the values for the unstrained offsets become ΔE_v (InAs/InP) = 0.46 eV and ΔE_v (GaAs/InP) = 0.34 eV.

R. E. Nahory, M. A. Pollack, J. W. D. Johnson, and R. L. Barns, Appl. Phys. Lett. **33**, 659 (1978).
D. Oertel, D. Bimberg, R. K. Bauer, and K. W. Carey, Appl. Phys. Lett. **55**, 140 (1989).
S. Adachi, J. Appl. Phys. **53**, 8775 (1982).
S. R. Forrest and O. K. Kim, J. Appl. Phys. **52**, 5838 (1981).
Y. Guldner, J. P. Vieren, P. Voisin, M. Voos, M. Razeghi, and M. A. Poisson, Appl. Phys. Lett. **40**, 877 (1982).
H. Temkin, M. B. Panish, P. M. Petroff, R. A. Hamm, J. M. Vandenberg, and S. Sumski, Appl. Phys. Lett. **47**, 394 (1985).
P. E. Brunemeier, D. G. Deppe, and J. N. Holonyak, Appl. Phys. Lett. **46**, 755 (1985).
M. S. Skolnick, P. R. Tapster, S. J. Bass, A. D. Pitt, N. Apsley, and S. P. Aldred, Semicond. Sci. Technol. **1**, 29 (1986).
R. Sauer, T. D. Harris, and W. T. Tsang, Phys. Rev. B **34**, 9023 (1986).
D. V. Lang, M. B. Panish, F. Capasso, J. Allam, R. A. Hamm, A. M. Sergent, and W. T. Tsang, Appl. Phys. Lett. **50**, 736 (1987).
D. J. Westland, A. M. Fox, A. C. Maciel, J. F. Ryan, M. D. Scott, J. I. Davies, and J. R. Riffat, Appl. Phys. Lett. **50**, 839 (1987).
K. Stemer, R. Schmitt, R. Zuleeg, F. M. T. Kaufmann, K. Heime, F. Kuphal, and J. Wolter, Surf. Sci. **174**, 331 (1986).
M. Ogawa, M. Miyoshi, S. Shimizu, F. Murakami, and F. Miyoshi, Jpn. J. Appl. Phys. **27**, L1334 (1988).
D. Grutzmacher, R. Meyer, M. Zachau, P. Helgesen, A. Ziemer, K. Wolter, H. Jurgensen, F. Koch, and P. Balk, J. Cryst. Growth **93**, 382 (1988).
[15] M. A. Hasse, N. Pan, and G. E. Stillman, Appl. Phys. Lett. **54**, 1457 (1989).
[16] K. Uomi, S. Sasaki, T. Tsuchiya, and N. Chinone, J. Appl. Phys. **67**, 904 (1990).
[17] D. V. Morgan, K. Board, C. E. C. Wood, and L. F. Eastman, Phys. Status Solidi A **72**, 251 (1982).
[18] R. People, K. W. Wecht, K. Alavi, and A. Y. Cho, Appl. Phys. Lett. **43**, 118 (1983).
[19] Y. Sugiyama, T. Inata, T. Fujii, Y. Nakata, S. Muto, and S. Hiyamizu, Jpn. J. Appl. Phys. **25**, L648 (1986).
[20] C. K. Peng, T. Won, C. W. Litton, and H. Morkoç, IEEE Electron Dev. Lett. **9**, 331 (1988).
[21] P. Z. Lee, C. L. Lin, J. C. Ho, L. G. Meiners, and H. H. Wieder, J. Appl. Phys. **67**, 4377 (1990).
[22] D. F. Welch, G. W. Wicks, and L. F. Eastman, J. Appl. Phys. **55**, 3176 (1984).
[23] S. P. Kowalczyk, D. L. Miller, J. R. Waldrop, P. G. Newman, and R. W. Grant, J. Vac. Sci. Technol. **19**, 255 (1981).
[24] J. R. Waldrop, R. W. Grant, S. P. Kowalczyk, and E. A. Kraut, J. Vac. Sci. Technol. A **3**, 835 (1985).
[25] J. R. Waldrop, E. A. Kraut, C. W. Farley, and R. W. Grant, J. Vac. Sci. Technol. B **8**, 768 (1990).
[26] I. Kojima and M. Kurahashi, J. Electron Spectrosc. Relat. Phenom. **42**, 177 (1987).
[27] J. M. Langer, C. Delerue, M. Lannoo, and H. Heinrich, Phys. Rev. B **38**, 7723 (1988).
[28] J. R. Waldrop and R. W. Grant, Phys. Rev. Lett. **43**, 1686 (1979).
[29] E. A. Kraut, R. W. Grant, J. R. Waldrop, and S. P. Kowalczyk, Phys. Rev. B **28**, 1965 (1983).
[30] R. J. Lempert, K. C. Hass, and H. Ehrenreich, Phys. Rev. B **36**, 1111 (1987).
[31] J. R. Chelikowsky and M. L. Cohen, Phys. Rev. B **14**, 556 (1976).
[32] J. R. Waldrop, R. W. Grant, and E. A. Kraut, J. Vac. Sci. Technol. B **7**, 815 (1989).
[33] J. R. Waldrop, R. W. Grant, and E. A. Kraut, Appl. Phys. Lett. **54**, 1878 (1989).